ProQuest LLC.
789 East Eisenhower Parkway
P.O. Box 1346
Ann Arbor, MI 48106 – 1346

EVALUATION OF MODERN CONTROL SYSTEM DESIGN TECHNIQUES FOR A MULTIVARIABLE ELECTRO-HYDRAULIC SYSTEM

Roger Roddis

A Thesis Submitted in Partial Fulfilment of the Requirements of Sheffield Hallam University for the Degree of Master of Philosophy

May 2000

Contents

Evaluation of Modern Control System Design Techniques for a Multivariable Electro-Hydraulic System

by

Roger Roddis

A Thesis Submitted in Partial Fulfilment of the Requirements of Sheffield Hallam University for the Degree of Master of Philosophy.

Abstract

An experimental apparatus has been developed with the object of providing a test plant, based on commercially available electro-hydraulic components, for the investigation of multivariable control system design methodologies. A mathematical model has been produced for this experimental plant and a preliminary analysis of the plant carried out.

A selection of controller design techniques has been investigated. Designs have been produced for two state feedback controllers in which the feedback coefficients were based on LQR theory, one of which used a full order estimator based on a Kalman Filter, the other using a reduced order observer whose poles were chosen arbitrarily. In addition, forward path compensators have been developed using the Characteristic Locus and the H^{∞}/Mixed Sensitivity methods. These controller designs were based on computations and simulations utilising Matlab and a selection of its control engineering toolboxes and Simulink. The completed designs were implemented in digital form and tested on the actual plant.

A series of tests were carried out to assess the robustness of the various controllers in the presence of plant uncertainty. The physical plant was modified and the controllers based on the nominal plant model used in conjunction with this modified plant. As a design technique which enabled robustness issues to be addressed explicitly, the H^{∞} approach was used to improve the robustness of the original H^{∞} controller.

Acknowledgements

I would like to thank Professor Richard Wynne, firstly for agreeing to my taking time out from my full-time post to carry out this research and secondly for acting as my Director of Studies and supporting the work reported here. I would also like to thank Dr Ken Dutton for the clarity and wisdom of the many helpful comments he has made during the course of the work and Mr David Wardman for his enthusiasm in initiating the work and the many occasions on which he has helped overcome impasses of a technical and sometimes of a psychological nature.

Finally, I would like to thank Mr Len Evans, without whose mechanical and hydraulic expertise the beam and carriage apparatus may never have been built, and Mr Steven Brandon for creating the 3D model from which the drawings of the apparatus were produced.

Nomenclature

$\mathbf{A}$	Plant State-Space Description
$\mathbf{B}$	Plant State-Space Description
$\mathbf{C}$	Plant State-Space Description
$\mathbf{D}$	Plant State-Space Description
$\mathbf{A}_{cp}$	Compensator State-Space Description
$\mathbf{B}_{cp}$	Compensator State-Space Description
$\mathbf{C}_{cp}$	Compensator State-Space Description
$\mathbf{D}_{cp}$	Compensator State-Space Description
$\mathbf{A}_e$	Estimator State Space Description
$\mathbf{B}_e$	Estimator State Space Description
$\mathbf{C}_e$	Estimator State Space Description
$\mathbf{D}_e$	Estimator State Space Description
$\mathbf{e}$	Error Vector (= **y**-**r**)
E	Expectation
g	Gravitational Acceleration
$\mathbf{G}(s)$	Plant Transfer Function Matrix
$\mathbf{G}_n(s)$	Nominal Plant Transfer Function Matrix
$\overline{\mathbf{G}}(s)$	Closed Loop (with UNF) Plant Transfer Function Matrix
J	Quadratic Cost Function
$\mathbf{K}(s)$	Compensator Transfer Function Matrix
l	Bound on Perturbation Magnitude
$\mathbf{L}$	Plant Model Perturbation (Uncertainty)
$\mathbf{P}$	(Unique Positive-semidefinite) Solution of ARE for LQR
$q_i(s)$	Eigenvalues or Characteristic Loci of $\mathbf{Q}(s)$
$\mathbf{Q}$	Cost Function Weighting Matrix, (Unique Positive-semidefinite) Solution of ARE for Kalman Filter
$\mathbf{Q}(s)$	Transfer Function of Compensator plus Plant,
$\mathbf{r}$	Reference Input Vector
$\mathbf{R}$	Cost Function Weighting Matrix
$\mathbf{T}$	Signal Sampling Interval
$\mathbf{u}$	Plant Input Vector
$\mathbf{x}$	State Vector
$\hat{\mathbf{x}}$	Estimate of State Vector
$\tilde{\mathbf{x}}$	State Estimate Error (= $\mathbf{x} - \hat{\mathbf{x}}$)
$\mathbf{v}$	Compensator Input Vector
$\mathbf{V}$	Measurement Noise Covariance
w	Scalar Weighting Function
$\mathbf{w}$	Augmented Plant Input Vector
$\mathbf{W}$	Weighting Function, Process Noise Covariance
$\mathbf{W}(s)$	Diagonalising Matrix Operator
$\mathbf{y}$	Plant Output Vector
$\mathbf{z}$	Augmented Plant Output Vector
γ	Variable of Iteration for H^∞ Controller Synthesis
γ_{opt}	Optimal Value of γ
Δ	Normalised Plant Model Perturbation
λ_i	Eigenvalues of a Constant Matrix
μ_i	Eigenvalues of a Constant Matrix

1970s

Iss. — 12/11

Ret - 12/11

ν_i Eigenvalues of a Constant Matrix

ω Angular Frequency

1 Introduction

1.1 Historical Background

Developments in control engineering during the Second World War brought together engineers and mathematicians with results which included Bode's original work on stability[1] and developments in the theory of stochastic processes based on the earlier work of Wiener[2]. There followed a return to the time domain and the study of the system differential equations, often in state space form. This was called 'modern' control theory to distinguish it from the 'classical' control based on the frequency domain and largely the product of Nyquist[3], Bode and others working with the complex variable.

The new theory, with its emphasis on linear algebra and numerical methods, was suitable for the solution of design problems using digital computers and stimulated much work from 1960 onwards on multivariable systems and more recently on system robustness. This research has necessarily adopted a mathematical perspective and consequently the results are given in a mathematical form often inaccessible to the practising control engineer. In addition, the evaluation of controller parameters based on these theoretical results requires extensive use of numerical methods and for all practical purposes they are only available to engineers using purpose designed software on digital computers. The emergence of these numerical methods and the digital computer has also led to to the availability of relatively fast and easy system simulation, whereas previously the engineer requiring a simulation of controller designs before implementation was essentially restricted to the use of analogue computers.

Prior to the development of modern control methods, a development that was in part a response to multivariable control problems emerging in the process control and aerospace industries, the control engineer had relatively few tools with which to produce controllers for multi-input, multi-output (MIMO) systems. Typically these systems manifested interaction between the desired input-output pairs such that changes in one input impacted on more than one output. Frequency response methods existed for designing single loop (SISO) controllers but the presence of interaction in the MIMO system meant that there was no guarantee that separate SISO controllers for each control loop in the system would give satisfactory or even stable performance when combined.

Coughanowr and Koppel[4] give an example of a distillation tower which has five interacting inputs and outputs. By use of simple controllers such as flow controls this was reduced to a system with two interacting control loops but the authors conclude that a satisfactory controller design required past experience and "when new and different applications arise considerable difficulty may be involved in obtaining satisfactory process control".

A multivariable controller design problem from the aerospace industry was posed by Povejsil and Fuchs[5]. Their method of solution involved managing interaction by an iterative process of controller synthesis which involved applying control action to one of the control loops, assessing the effect on the complete system by evaluating its characteristic equation and repeating until a satisfactory design was produced. The resulting controller managed rather than eliminated interaction. Kinnen and Liu[6] produced a procedure for designing a multivariable controller using root loci. This gave a method of constraining interaction and achieving satisfactory performance but, whilst it proved practicable for two-input, two-output systems, its complexity increased considerably as the number of inputs and outputs increased. Both methods typically involved digital computation, the former for matrix manipulation, the latter for the transition from pole-zero form to time domain response.

The development of modern control with its emphasis on state space methods, together with the relative ease with which accurate linear models could be generated for aerospace applications, stimulated work on optimal control theory. One result of this was the development of controller design techniques based on quadratic performance indicators[7]. The resulting controllers, called Linear Quadratic Regulators (LQRs), implemented a state feedback law for which it was necessary to estimate all states not available by direct measurement. A deterministic estimator, or observer, was developed by Luenberger[8] which, by the separation principle that observer design and control law determination could be treated independently, was combined with the LQR to form a complete controller. A non-deterministic estimator, based on the Kalman filter[9], [10] which permitted the consideration of process and measurement noise as stochastic processes was also used in conjunction with the LQR to give the Linear Quadratic Gaussian (LQG) controller[11] .

This work on state feedback acquired a larger following in academic than in industrial circles for several reasons. The method was based on the assumption of a good plant model, which did not always exist for industrial processes, and a meaningful quadratic performance indicator was more elusive in, say, a process control application than in a spacecraft guidance system. Also, there were doubts about the robustness of the LQG controller and the design process was considered too sophisticated and too far removed from the classical approach on which control engineering practice was largely based. For these reasons there was a resurgence of interest in applying frequency domain methods to the multivariable control problem.

The obvious approach was to apply a decoupling compensator[12] to the plant and treat the resulting system as a combination of non-interacting SISO control loops. However, such a compensator would have to be based on an inverse of the plant across its effective frequency range and, as such, was impossible to find for all but exceptional applications. The Inverse Nyquist Array method of Rosenbrock[13] overcame this problem by finding simple compensators to produce a 'diagonally dominant' system such that separate SISO controllers for the essentially decoupled control loops would produce a satisfactory design. The Sequential Return Difference method[14] sought to investigate and accommodate interactions to produce a controller which gave satisfactory performance whilst tolerating interaction.

Work by Rosenbrock[15] and others seeking to generalise the concept of poles and zeros to the multivariable case resulted in the system matrix, a polynomial matrix in terms of which the poles and zeros of the system could be defined. This development included the use of the McMillan form of the transfer function matrix, a diagonal form from which transmission poles and zeros could be readily deduced. Similar efforts to generalise stability criteria resulted in multivariable descriptions of the Nyquist criterion based on the characteristic loci[16] of the system. This focus on characteristic loci resulted in the development of the Characteristic Locus method[17], which approximately diagonalised the system and used separate, non-interacting controllers to improve the stability margins of the characteristic loci.

A further development in the assessment of multivariable controller performance was the use of principal gains[18]. These are the singular values of the transfer function matrix and the maximum singular values can be used in conjunction with sensitivity or other

system functions to give worst case performance predictions with respect to, for example, tracking of reference inputs and noise rejection. H^∞ optimisation, originating in the work of Zames[19], enabled an optimal solution for the maximum singular values of selected system functions across the frequency range to be found and was largely developed to address problems of robustness in multivariable systems. Further developments led to the use of the structured singular value[20] which enabled a structured uncertainty description to be used in robustness analyses.

H^∞ optimisation as a controller design tool is still undergoing development. Kwakernaak[21], reviewing the application of H^∞ optimisation to robust control problems, concluded that the area is a rewarding one for research and that practising engineers are already familiar with the aspects of classical control theory contained in H^∞ design issues. Similarly, work on improving the robustness of LQG controllers is ongoing. One approach to their lack of robustness, due to the interference of the Kalman filter with the state feedback properties[22], has been by Loop Transfer Recovery (LTR)[23], which seeks to eliminate the effects of state estimation.

In a recent design exercise[24], twenty-one teams of control engineers based in various academic and commercial organisations throughout Europe worked on two benchmark multivariable control problems from the aeronautical field. Thirteen controller design methodologies were investigated, including H^∞ optimisation, LQG/LTR and classical control theory. One conclusion of the work was that "to some extent ..... modern techniques can be used to design controllers for realistic problems" in this field.

1.2 Research Objectives

The present work is concerned with the implemention and comparison of several methods of designing multivariable control systems from the original design stage through system simulation to controller implementation and evaluation. The work is motivated by a desire to aquire a better understanding of the methods investigated, to use them to produce controller designs for a multivariable electromechanical system and to implement and assess these designs. For the purposes of producing the designs considerable use has been made of Matlab[25] and a selection of its specialist control engineering toolboxes and hence a discussion of the design process necessarily involves indication of some of the many functions available in these toolboxes.

In order to form a basis for comparison of controller design methodologies, an electro-hydraulic experimental rig has been built which is based on further development of the well-known ball and beam problem. An experimental apparatus for the latter was produced by Wellstead et al.[26] in the Control Systems Centre at the University of Manchester Institute of Science and Technology. In their development of the experiment, the angle of tilt of a channel section beam, controlled by a moving coil actuator, produced the acceleration of a metal ball running along the inner edges of the upward facing channel. Transducers were devised to monitor the angle of beam tilt and the ball position, the object being to control the position of the ball along the beam. The ball and beam apparatus, by virtue of the double integrator contained in the ball dynamics, presents the control engineer with the problem of inherent instability (the system is unstable under unity negative feedback for all non-dynamic additional loop gains). Wellstead et al. solve the resulting control problem by a variety of techniques including the classical approach of introducing a forward path, phase lead compensator and the modern one of applying state feedback.

The experimental rig used in the present work was based on commercially available electro-hydraulic actuators so that its dynamics were relevant to industrial applications and the resulting design represented a coupled multivariable system, i.e. a system in which there is interaction between the various input-output pairs. For this reason the rig is a suitable vehicle for the investigation of design methodologies for multivariable systems.

To produce the controller designs, a subset of the available design methods was chosen, all resulting from modern developments in multivariable control system design. Adopting an approach based on the time domain, designs were produced using state feedback. Firstly, a design was developed utilising a full order estimator in conjunction with LQG theory. Subsequently a reduced order observer was produced by observer pole placement. From amongst the available frequency domain approaches, the Characteristic Locus method was chosen. Finally, it was considered desirable to apply a method which addresses the problem of robustness explicitly and for this an H^{∞} approach based on mixed sensitivity was adopted.

Comparisons of the above design methods were initially made on the basis of the best available plant model and the performances of the various controllers at simulation and

implementation stages were compared. In addition, it was considered that some assessment of control system robustness was desirable and for this the various controller designs were used with the plant after modification of its physical characteristics. In this way it was hoped to obtain a general indication as to how well the various designs would cope with plant perturbations.

2 The Beam and Carriage Apparatus

The 'standard' ball and beam experiment is an example of a double integrator problem in which the objective is to maintain the ball at a desired position along the beam. It is a single input, single output (SISO) system, there being no attempt to control the height of the ball. However, if each end of the beam rested on a hydraulic ram, then the horizontal and the vertical positions of the ball could be controlled. Since the rams would be used both to raise and lower the beam and to introduce a gradient down which the ball would roll, coupling would exist between the two variables to be controlled, ball height and horizontal ball position, i.e. either of the plant inputs on its own would effect a change in both outputs. A multi-input, multi-output (MIMO) system with square transfer function matrix would result with two inputs to control the extension of the two rams and two outputs representing the ball horizontal and vertical positions.

For the present work an experimental rig has been developed along these lines, but in which a carriage has replaced the ball, this carriage being floated on the beam using a virtually frictionless air bearing. Figs 2.1 and 2.2 show front and rear views of the rig with electrical connections omitted. Fig 2.3 gives a guide to the major components of the rig.

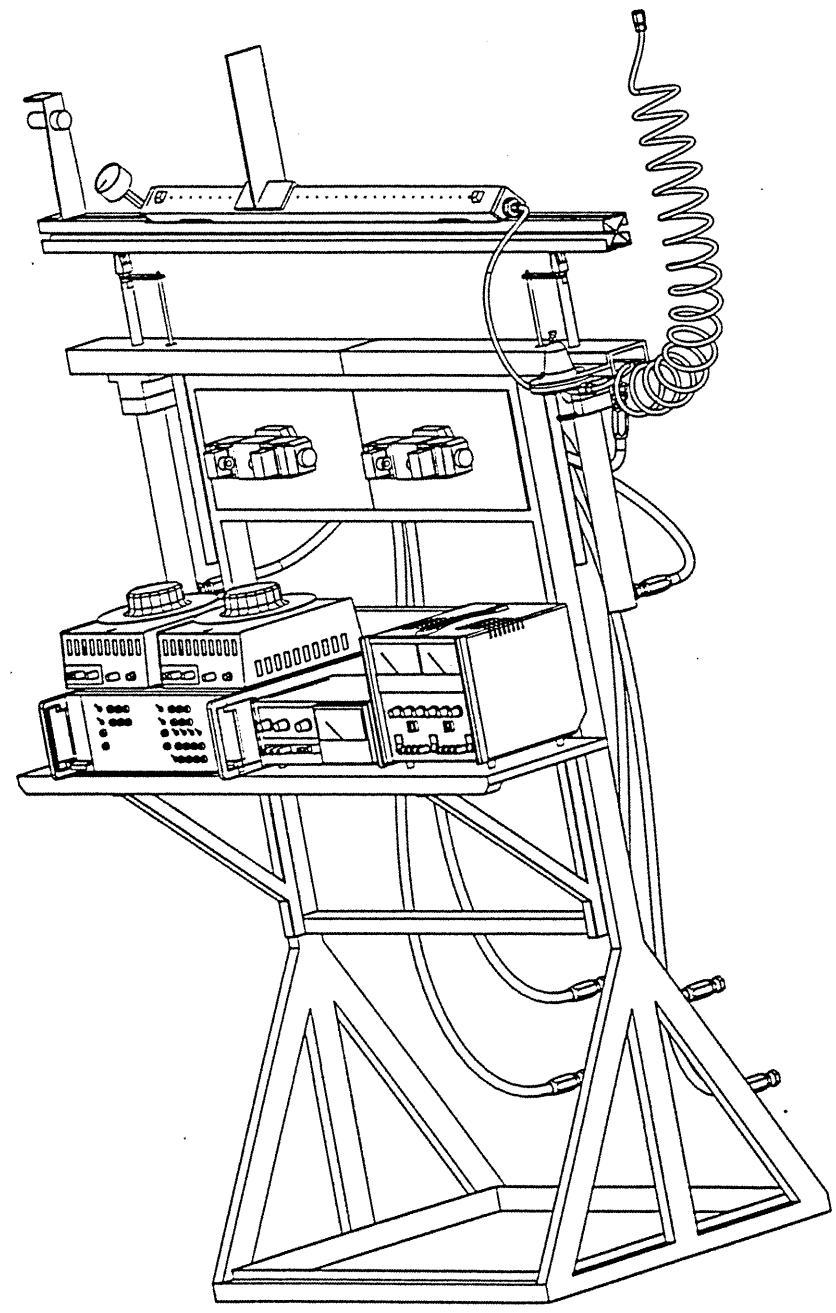

Fig 2.1 Front View of Beam and Carriage

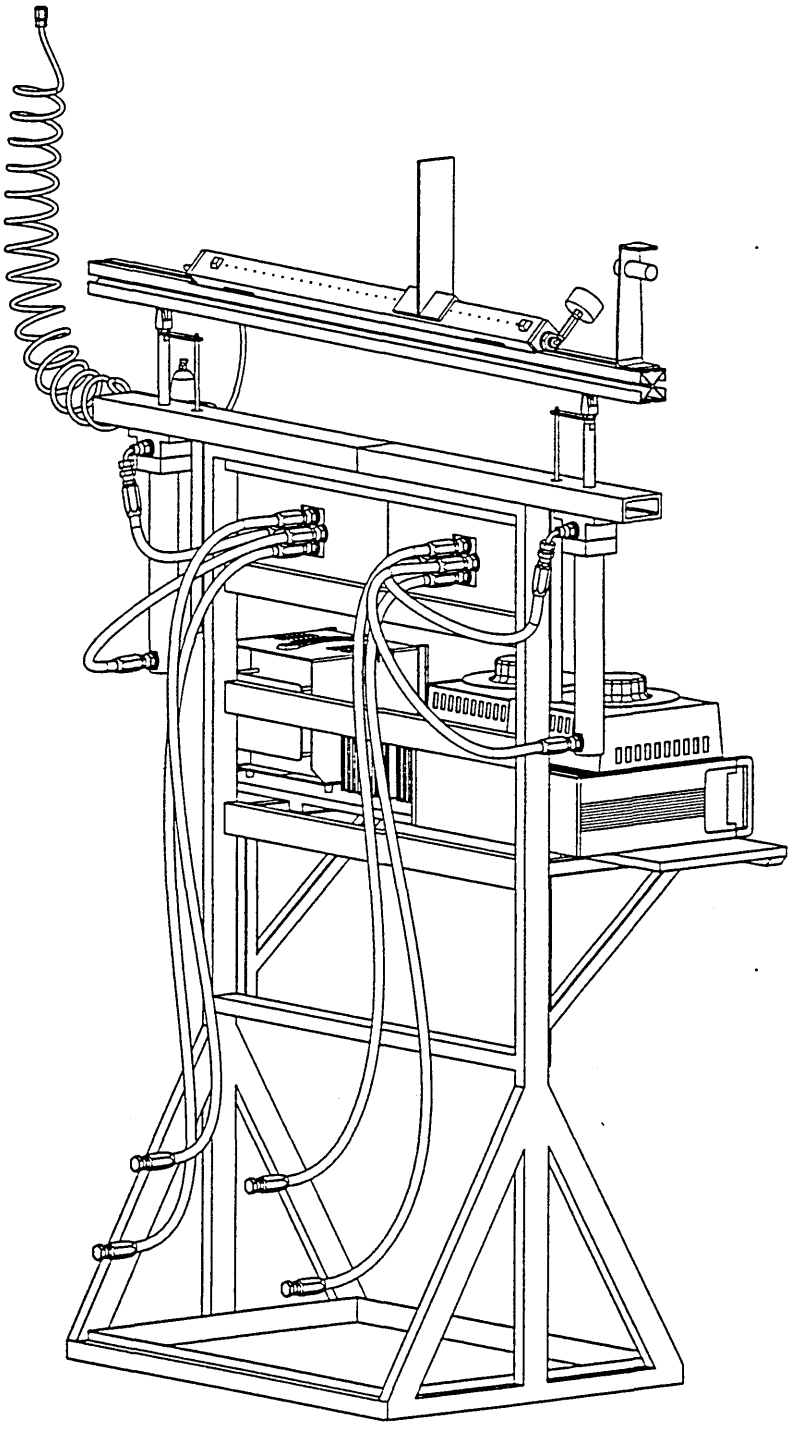

Fig 2.2 Rear View of Beam and Carriage

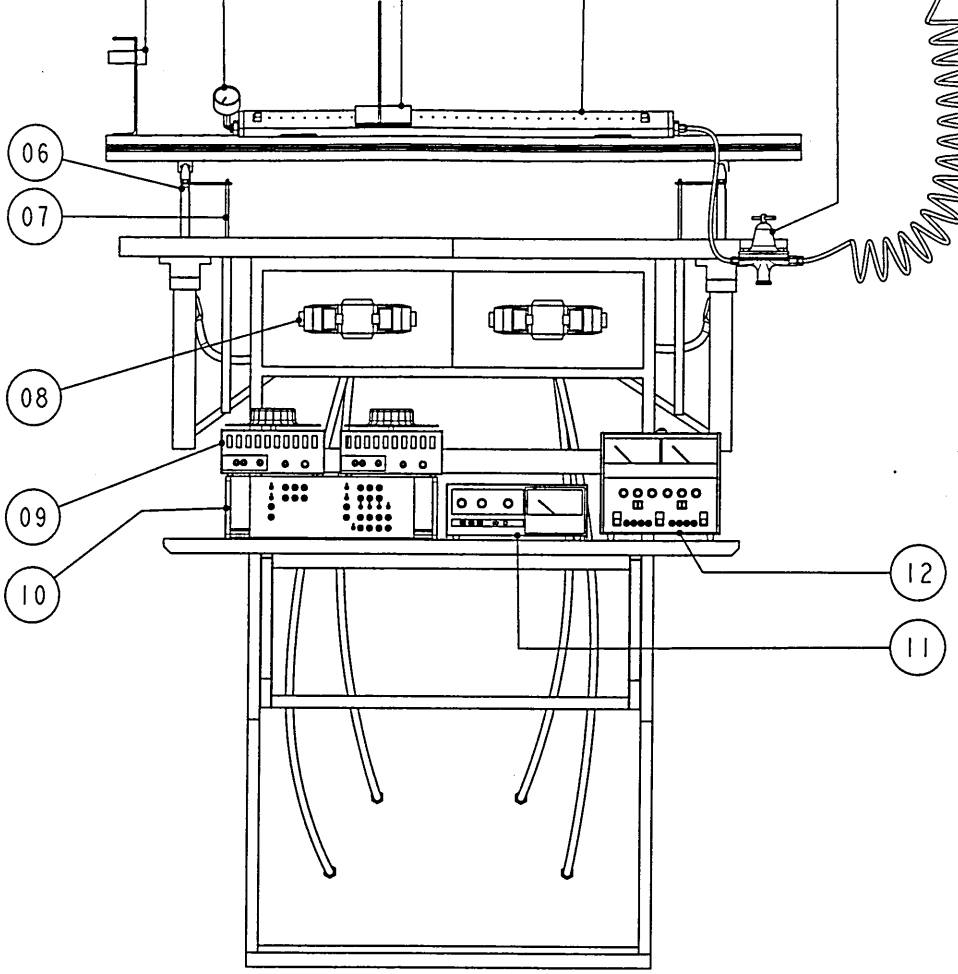

PART NO.	DESCRIPTION
11, 12	DC POWER SUPPLIES FOR TRANSDUCERS
10	POWER AMPLIFIERS
09	REFERENCE INPUT POTENTIOMETER
08	PROPORTIONAL VALVE
07	RESISTIVE TRANSDUCER
06	LEFT-HAND RAM
05	ULTRASONIC TRANSDUCER
04	AIR PRESSURE GAUGE
03	CARRIAGE
02	AIR BEARING
01	AIR PRESSURE REGULATOR

Fig 2.3 Principal Components of Beam and Carriage Assembly

This rig is shown schematically in Fig 2.4. The hydraulic rams have potentially high load capacity and consequently the beam and carriage are of a substantial construction, introducing realistic dynamics into the operation of the experimental equipment.

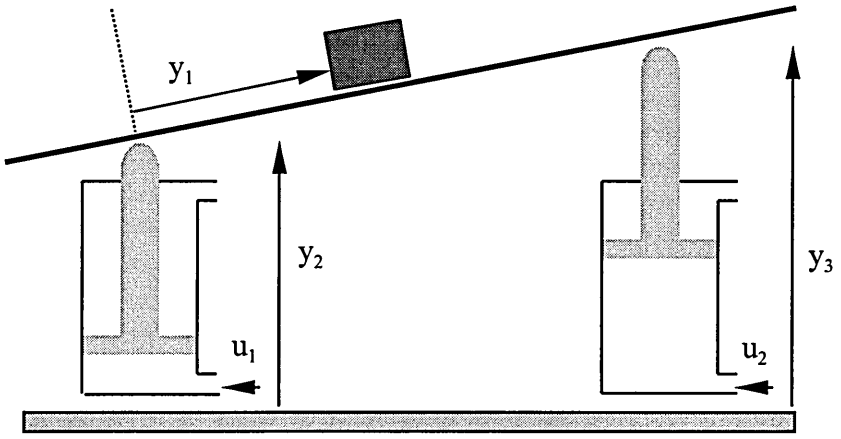

Fig 2.4 Carriage and Beam Schematic

The control of the hydraulic rams is effected via double solenoid, proportional direction control valves, each driving a double acting hydraulic cylinder. The input to the valves is provided by servoamplifiers with differential inputs so that a local servo can be implemented for each ram, the inputs to each servoamplifier being the control input and a (negative) feedback signal from a resistive transducer monitoring ram position. A third, ultrasonic, transducer was used to measure the position of the carriage along the beam. The signal flow diagram is shown in Fig 2.5.

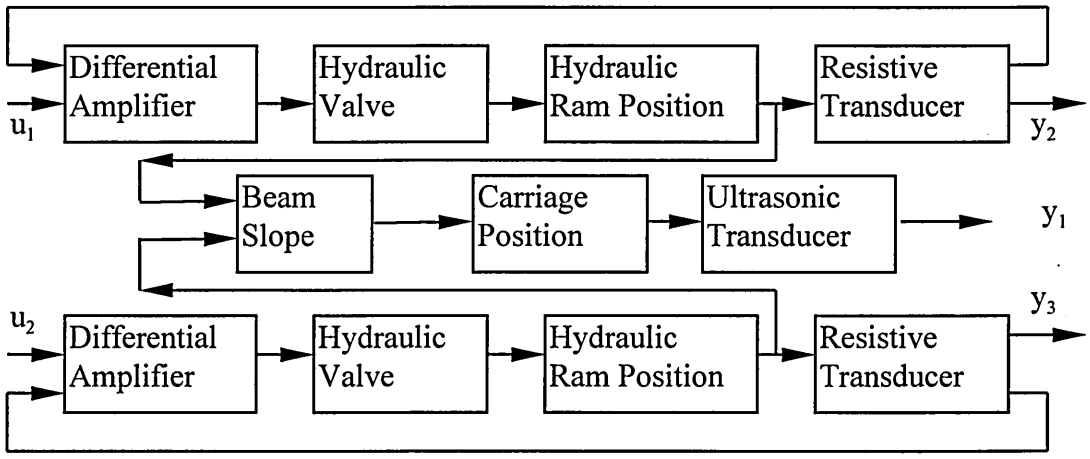

Fig 2.5 Signal Flow Schematic

In order to provide an approximation of carriage height, the heights of the two beam ends, y_2 and y_3, were averaged to produce the y_2 of the ultimate square system, y_1 being

the horizontal carriage position. In the steady state, the beam is horizontal and the carriage height is therefore given precisely under these conditions.

Table 2.1 lists the proprietary components used in the beam and carriage apparatus.

Component List	
Hydraulic Components:	**Power Amplifiers:**
Vickers Proportional Valves KDG4V3 7 Litres/min	Vickers EEA-PAM-523-A-30
	Transducers:
Vickers PVB10 Pump 30 Litres/min	Penny and Giles Resistive Transducers HLP190/F1V250/10K
	Amerace Ultrasonic Transducer
Sun Relief/Unloader Valve RVEA-LBN	PCUC30M72AV
Pall Filter HC960 FKP4H	

Table 2.1

The maximum stroke of each cylinder was 228mm, the cylinder bores 38mm and the piston rod diameter 20mm. The cylinders were mounted vertically with a horizontal separation of 1140mm. Two resistive transducers were used, one for each hydraulic piston, and the outputs were scaled to give ± 10V over the working piston stroke. The ultrasonic transducer was scaled to give 0 to 10V over the 708mm working range for carriage horizontal position. This unipolar voltage was rescaled to give a working range of ± 10V prior to input to the various controllers which were all based on the assumption of bipolar signals in the range ± 10V.

2.1 System Identification

In order to ensure repeatability of the system it was necessary to standardise the settings of various parameters. For determination of the plant model and subsequent normal running of the system, the air bearing inlet pressure was set at 0.1 bar, which gave virtually frictionless performance of the bearing even under low slope conditions. The servoamplifiers were set to minimum deadband and maximum gain on the piston outstroke. For the instroke, the amplifier gains were set lower to balance the maximum piston instroke and outstroke velocities (it being necessary to reduce the flow rate into the annular side of the piston). In this way, the system was made as linear as possible and the ram response as fast as possible.

2.1.1 The Symmetrical Model

The first attempt at establishing the nominal plant model was based on analysis of the carriage and a subjective comparison of actual ram response to step inputs with simulated responses of theoretical second order systems in order to obtain an approximate second order model.

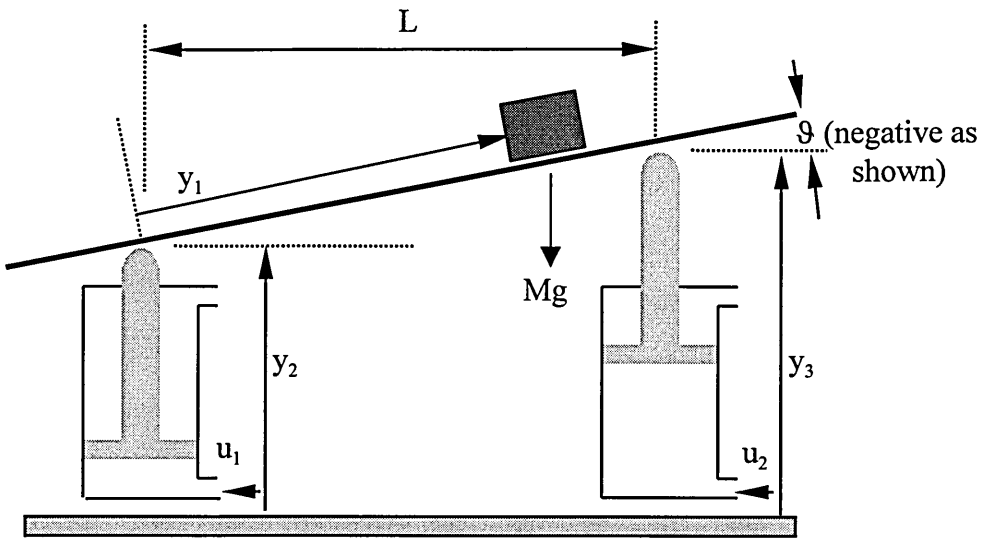

Fig 2.6 Beam and Carriage Line Diagram

Fig 2.6 shows the model for analysing frictionless movement of the carriage down a gradient. Simple analysis showed that, for θ small

$$\ddot{y}_1 = g\sin\theta \approx \frac{g}{L}(y_2 - y_3) \qquad (2.1)$$

where g is gravitational acceleration. Since the intention was to produce a model based on volts in and volts out, equation (2.1) was rescaled on the basis of scaling factors of 28.25 Vm^{-1} for the carriage transducer and 87.7 Vm^{-1} for the ram transducers to give the following equation of motion for the carriage scaled in volts:-

$$\ddot{y}_1 = 2.773(y_2 - y_3) \qquad (2.2)$$

Checks were made to establish the degree of correspondence between the time taken for the carriage to cover a fixed distance, l, of the beam and the theoretical time of

$\sqrt{\frac{2l}{2.773(y_2 - y_3)}}$ seconds for a range of relatively small beam slopes. These showed the amount of friction to be too small to affect measurements made by simple, manual timing methods.

Comparisons of actual and theoretical second order system responses to step inputs gave the following (volt to volt) equations of motion for the hydraulic rams:-

$$\ddot{y}_2 + 25\dot{y}_2 + 200y_2 = 200u_1 \tag{2.3}$$

$$\ddot{y}_3 + 25\dot{y}_3 + 200y_3 = 200u_2 \tag{2.4}$$

It was felt to be appropriate at this stage to limit the model for the hydraulic rams to second order to avoid generating an unnecessarily complex model for the complete system. If evidence of the need to do so were to arise at a later stage, attempts could be made to model the higher order dynamics of the hydraulic actuators as, for example, in [27].

Combining equations (2.2), (2.3) and (2.4) and defining system states $x_1 = y_1$, $x_2 = y_2$, $x_3 = y_3$, $x_4 = \dot{y}_1$, $x_5 = \dot{y}_2$, $x_6 = \dot{y}_3$, yields the state space description of the system, $\mathbf{G}(s) \overset{s}{=} \begin{bmatrix} \mathbf{A} & \mathbf{B} \\ \mathbf{C} & \mathbf{D} \end{bmatrix}$ (2.5)

(i.e. $\mathbf{G}(s) = \mathbf{C}(s\mathbf{I} - \mathbf{A})^{-1}\mathbf{B} + \mathbf{D}$)

where

$$\mathbf{A} = \begin{bmatrix} 0 & 0 & 0 & 1 & 0 & 0 \\ 0 & 0 & 0 & 0 & 1 & 0 \\ 0 & 0 & 0 & 0 & 0 & 1 \\ 0 & 2.773 & -2.773 & 0 & 0 & 0 \\ 0 & -200 & 0 & 0 & -25 & 0 \\ 0 & 0 & -200 & 0 & 0 & -25 \end{bmatrix} \tag{2.6}$$

$$\mathbf{B} = \begin{bmatrix} 0 & 0 \\ 0 & 0 \\ 0 & 0 \\ 0 & 0 \\ 200 & 0 \\ 0 & 200 \end{bmatrix} \tag{2.7}$$

$$\mathbf{C} = \begin{bmatrix} 1 & 0 & 0 & 0 & 0 & 0 \\ 0 & 0.5 & 0.5 & 0 & 0 & 0 \end{bmatrix} \tag{2.8}$$

$$\mathbf{D} = \begin{bmatrix} 0 & 0 \\ 0 & 0 \end{bmatrix} = \mathbf{0}_{2,2} \tag{2.9}$$

In the output equation, $\mathbf{y} = \mathbf{Cx} + \mathbf{Du}$, y_2 and y_3 have been averaged and y_2, the carriage height, redefined as this average.

2.1.2 The Non-Symmetrical Model

In an attempt to refine the plant model, further investigation of the two hydraulic ram systems was undertaken. For the two rams, frequency response data were gathered, relating ram displacements x_2 and x_3 to sinusoidal excitation at servoamplifier inputs u_1 and u_2 respectively. For this a Hewlett Packard HP35665A Dynamic Signal Analyzer was used to perform swept frequency response tests on each ram. The resulting complex frequency response data were imported into Matlab and the second order transfer function computed for each, using function *invfreqs* in Matlab's Signal Processing Toolbox [28]. Fig 2.7 shows the frequency response of the left hand ram to sinusoidal excitation of 5V amplitude produced by the HP DSA.

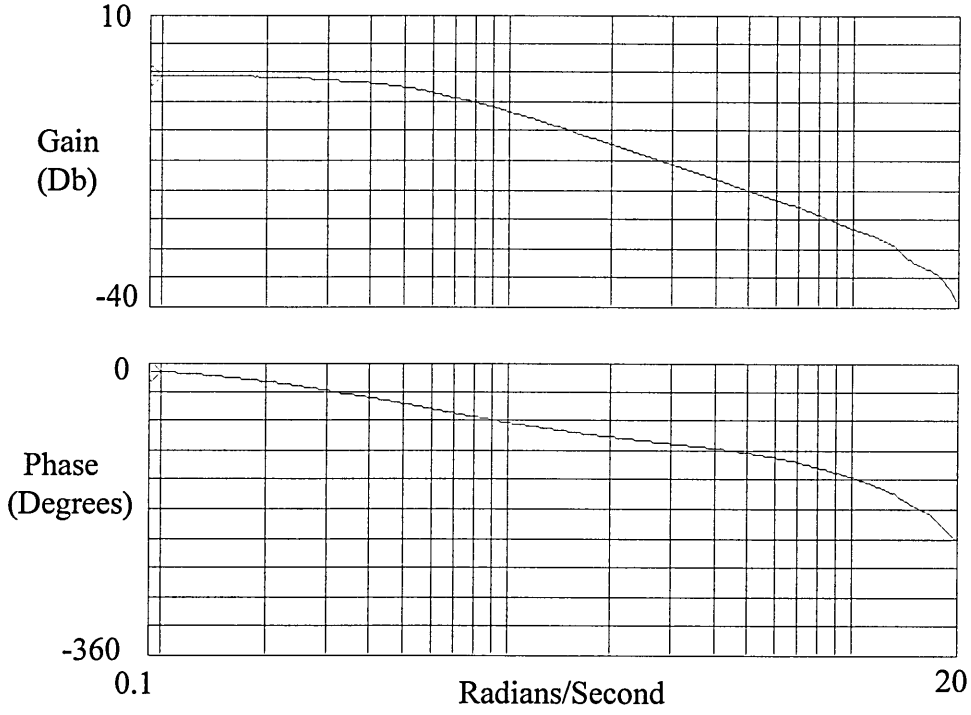

Fig 2.7 Frequency Response of Left-Hand Ram

The resulting transfer functions for left and right hand rams respectively were:-

$$\frac{y_2}{u_1} = \frac{179.4}{s^2 + 49.4s + 175.7} \tag{2.10}$$

$$\frac{y_3}{u_2} = \frac{205.6}{s^2 + 53.7s + 208.6} \tag{2.11}$$

The difference between the two rams' dynamics can be accounted for in terms of variations in the physical characteristics of the proportional valves, the valve amplifiers, the resistive transducers and the hydraulic cylinders themselves.

In order to check the repeatability of the parameters in (2.10) and (2.11), further frequency response tests were undertaken and the corresponding second order transfer functions computed. These tests were all carried out after allowing time for the hydraulic power source to warm the hydraulic oil to normal operating temperature. For each ram, two tests were undertaken at each of three excitation amplitudes, these being 1V, 2V and 3V respectively. Adopting the standard form, $\frac{k\omega_n^2}{s^2 + 2\varsigma\omega_n s + \omega_n^2}$, for the ram transfer functions, the maximum deviations of ω_n, ς and k from the values corresponding to (2.10) and (2.11) were 13%, 32% and 7% respectively. Most of these

variations were attributable to changes in the excitation levels, higher levels of excitation consistently producing higher values of ς and k. Further investigation showed that the variations in theoretical frequency response corresponding to these various transfer functions were small compared to the discrepancy between these theoretical frequency responses and the actual frequency responses obtained from the tests. Thus, the major source of error in transfer function approximation was due to the restriction of the transfer function to second order. However, it was considered that, since the ram dynamics were fast compared to the carriage dynamics, it was justifiable to proceed with the second order approximations with a view to limiting the beam and carriage model to sixth order.

The corresponding state space representation of the system is given by:-

$$\mathbf{A} = \begin{bmatrix} 0 & 0 & 0 & 1 & 0 & 0 \\ 0 & 0 & 0 & 0 & 1 & 0 \\ 0 & 0 & 0 & 0 & 0 & 1 \\ 0 & 2.773 & -2.773 & 0 & 0 & 0 \\ 0 & -175.7 & 0 & 0 & -49.4 & 0 \\ 0 & 0 & -208.6 & 0 & 0 & -53.7 \end{bmatrix} \tag{2.12}$$

$$\mathbf{B} = \begin{bmatrix} 0 & 0 \\ 0 & 0 \\ 0 & 0 \\ 0 & 0 \\ 179.4 & 0 \\ 0 & 205.6 \end{bmatrix} \tag{2.13}$$

$$\mathbf{C} = \begin{bmatrix} 1 & 0 & 0 & 0 & 0 & 0 \\ 0 & 0.5 & 0.5 & 0 & 0 & 0 \end{bmatrix} \tag{2.14}$$

$$\mathbf{D} = \mathbf{0}_{2,2} \tag{2.15}$$

2.2 Analysis of Plant Models

For purposes of analysis, both models are balanced in the sense that inputs and outputs are all of the same order of magnitude (viz $\pm$ 10V). For this reason it was thought unnecessary to scale the models and since they were already linear, notably by the

approximation of the carriage equation of motion, linear analysis was directly applicable.

2.2.1 Poles, Zeros and Stability

System zeros and poles are the zeros and poles of the 'internal model' of the plant based on the system matrix, $\mathbf{P}(s)$,[29] where

$$\mathbf{P}(s) = \begin{bmatrix} s\mathbf{I} - \mathbf{A} & -\mathbf{B} \\ \mathbf{C} & \mathbf{D} \end{bmatrix} \tag{2.16}$$

The system zeros for a square system are given by the roots of det($\mathbf{P}(s)$) and are all invariant, i.e. they are also present in the corresponding closed loop system formed by constant output or state feedback. System poles are the roots of det($s\mathbf{I}$-$\mathbf{A}$).

Transmission zeros and poles are the zeros and poles which appear in the transfer function matrix (TFM) of the system, $\mathbf{G}(s) = {}^{s}\begin{bmatrix} \mathbf{A} & \mathbf{B} \\ \mathbf{C} & \mathbf{D} \end{bmatrix}$, where $\mathbf{G}(s)$ is given by

$$\mathbf{G}(s) = \mathbf{C}(s\mathbf{I} - \mathbf{A})^{-1}\mathbf{B} + \mathbf{D}. \tag{2.17}$$

The zeros are all the zeros contained in the numerator terms of the McMillan form [30] of $\mathbf{G}(s)$, (a diagonal matrix containing all the zeros and poles of $\mathbf{G}(s)$), whilst the poles are all the zeros contained in the denominator terms (including repeated zeros in each case). Where system zeros cancel with system poles, these zeros and poles do not appear as transmission zeros and poles and such zeros are called decoupling zeros.

Use of Matlab's Symbolic Math Toolbox [31] established that there were no system zeros in either model (det($\mathbf{P}(s)$) being constant in each case) and therefore both state space descriptions are minimum realisations with all six system poles present in the TFM. These transmission poles (and the absence of transmission zeros) can be seen in the McMillan forms of the symmetrical and non-symmetrical models respectively,

Symmetrical Model:-

$$\mathbf{M}(s) = \begin{bmatrix} \dfrac{1}{s^2(s^2 + 25s + 200)} & 0 \\ 0 & \dfrac{110920}{s^2 + 25s + 200} \end{bmatrix} \tag{2.18}$$

Non-symmetrical Model:-

$$\mathbf{M}(s) = \begin{bmatrix} \dfrac{1}{s^2(s^2+49.4s+175.7)(s^2+53.7s+208.6)} & 0 \\ 0 & 102281 \end{bmatrix} \tag{2.19}$$

Obviously, there are two poles at the origin in each case.

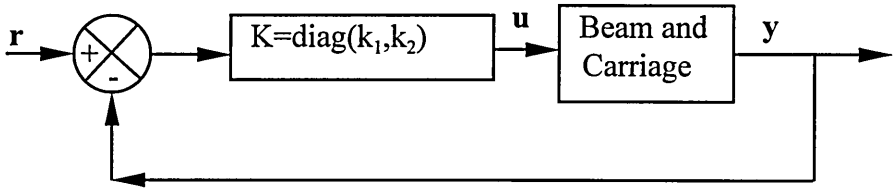

Fig 2.8 Closed Loop System with Diagonal Compensator

For the closed loop systems based on unity negative feedback (UNF) and a constant forward path compensator $\mathbf{K} = diag(k_1, k_2)$, as shown in Fig 2.8, the McMillan form for the symmetrical model is given by

$$\mathbf{M}(s) = \begin{bmatrix} \dfrac{1}{den1} & 0 \\ 0 & 110920k_1k_2 \end{bmatrix} \tag{2.20}$$

where

$$den1 = s^6 + 50s^5 + (1025+100k_2)s^4 + 2500(4+k_2)s^3 + [20000(2+k_2)+554.6k_1]s^2 + 13865k_1s + 110920k_1(1+k_2)$$

and for the nonsymmetrical model by

$$\mathbf{M}(s) = \begin{bmatrix} \dfrac{1}{den2} & 0 \\ 0 & 102281k_1k_2 \end{bmatrix} \tag{2.21}$$

where

$$den2 = s^6 + 103.1s^5 + (3037.1+102.8k_2)s^4 + (19739.9+5078.3k_2)s^3 + (36651.0+497.5k_1+18062.0k_2)s^2 + 26715.8k_1s + (103778.5+102281.0k_1)k_2.$$

For each closed loop system, k_1 and k_2 can be chosen such the system is not unstable and the small stable region in the gain space for each system can be seen in Figs 2.9 and 2.10.

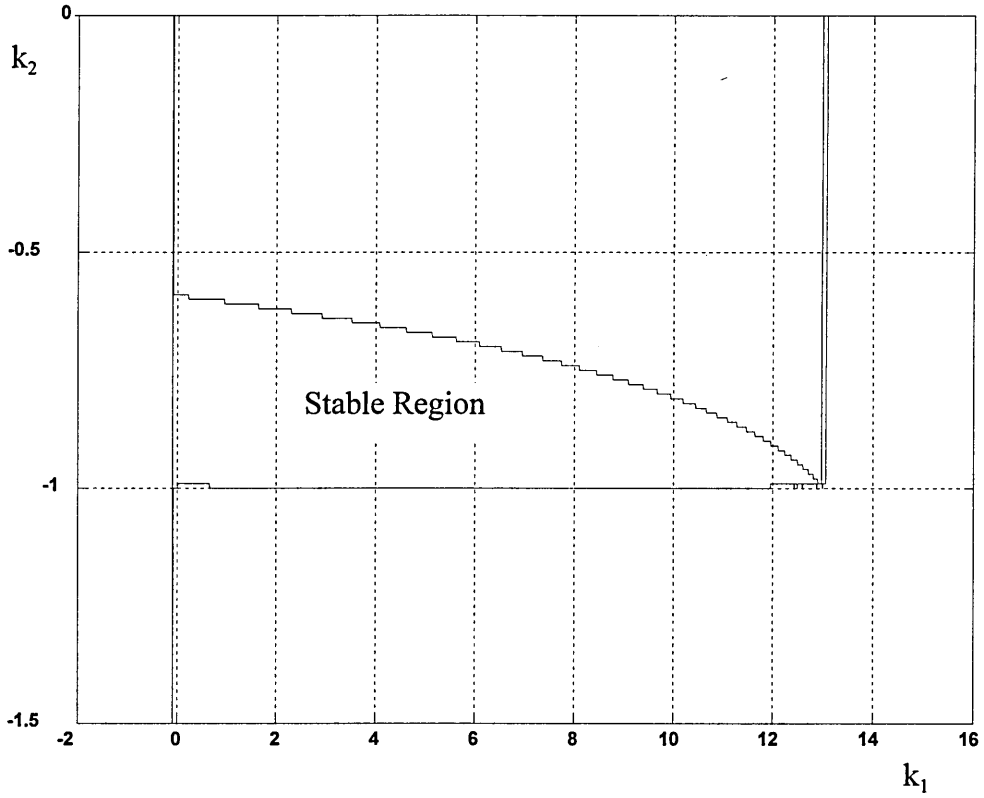

Fig 2.9 Gain Space for Symmetric Model

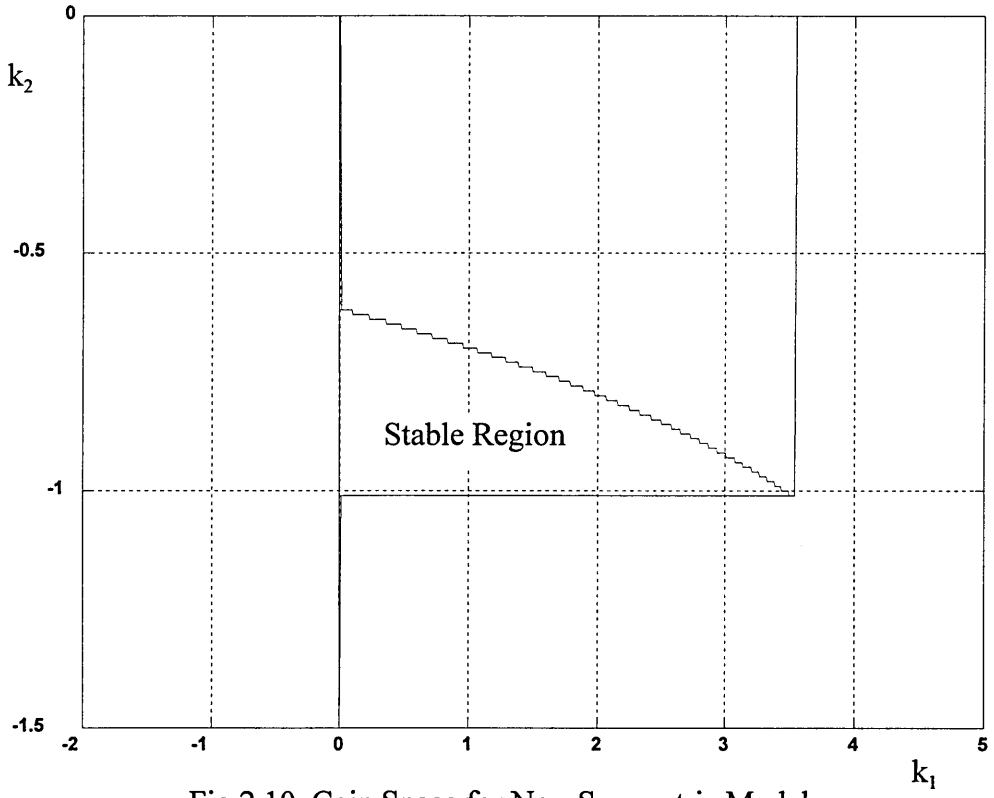

Fig 2.10 Gain Space for Non-Symmetric Model

These show that both systems would be unstable with a unity compensator ($\mathbf{K} = \mathbf{I}$) but would be stable with $\mathbf{K} = diag(1,-0.8)$, for instance. If system $\mathbf{G}(s)$ is said to be inherently unstable when no stable closed loop system exists for any choice of constant forward path gain matrix, $\mathbf{K}$ (i.e. for all non-dynamic $\mathbf{K}$), then neither system is inherently unstable. However, according to classical control criteria, the SISO system (ball and beam), with $\mathbf{G}(s) = \dfrac{k}{s^2(s^2 + as + b)}$, is inherently unstable by the above definition. It seems that the 'mixing' of terms in the closed loop system due to interaction in the MIMO system has introduced additional terms in the characteristic polynomial such that the system can potentially be stabilised by a constant compensator. However, the scope for improving dynamic performance is very limited and the total elimination of both interaction and steady state error impossible with such a simple compensator. As an example of this, Figs 2.11 and 2.12 show the simulated closed loop step response of the symmetric and non-symmetric models respectively with a constant forward path compensator, $\mathbf{K} = diag(1,-0.8)$.

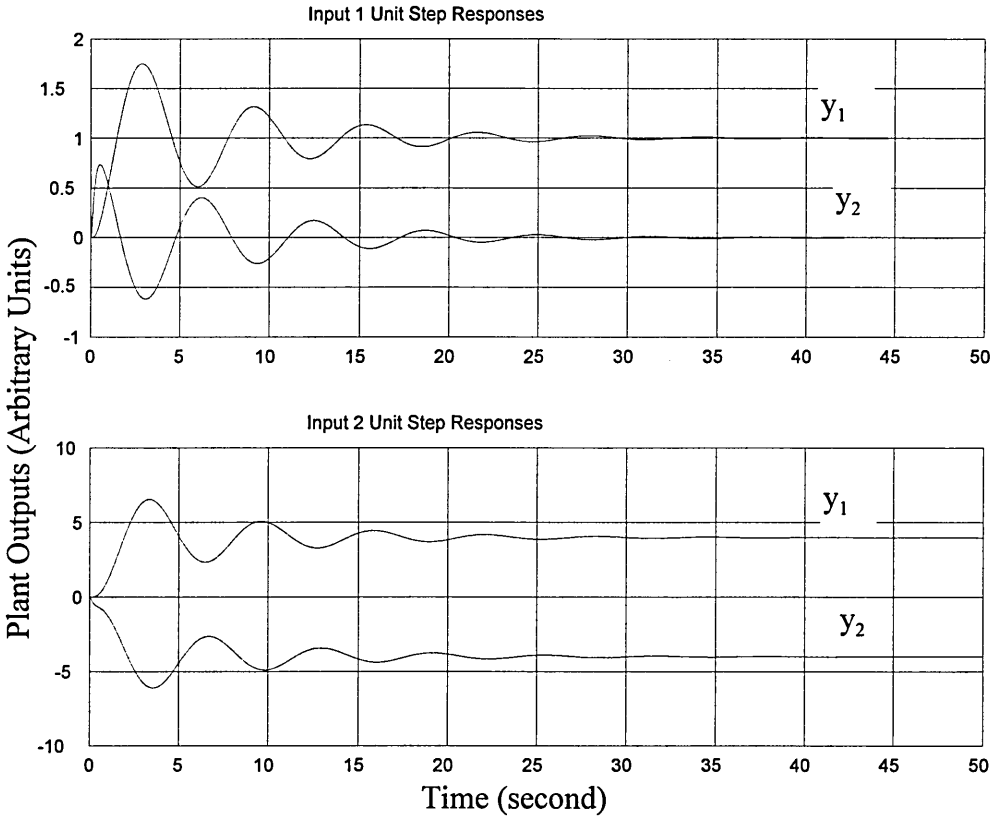

Fig 2.11 Step Response of Symmetric Model

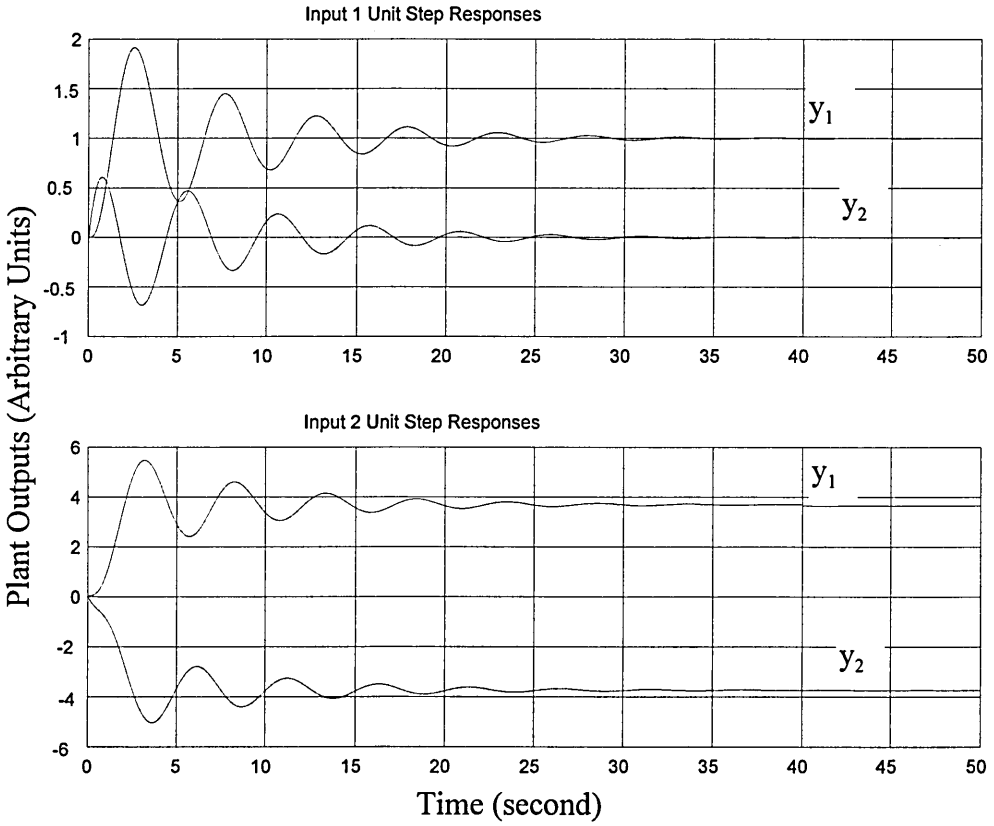

Fig 2.12 Step Response of Non-Symmetric Model

It can be seen that there is no steady state error on y_1 and zero steady state output on y_2 in response to a step input on r_1. Examination of the closed loop system TFM shows that this would be true for all 2-input, 2-output systems with pure integrators in the first row of G(s) and no pure integrators in the second row.

2.2.2 Controllability and Observability

Since the state space descriptions of the two models are minimum realisations, they possess no decoupling zeros (and hence no hidden modes) and are both controllable and observable. The pair (**A**, **B**) and hence the system (**A**, **B**, **C**, **D**) is controllable if all states can be controlled by suitable choice of input vector, **u**. This is the case if $\left[\mathbf{B} \quad \mathbf{AB} \quad \mathbf{A}^2\mathbf{B} \quad \ldots \quad \mathbf{A}^{n-1}\mathbf{B}\right]$ is full rank[32] (i.e. has rank n where **A** is $n \times n$).

The pair (**A**, **C**) is observable if all states can be inferred from a full knowledge of system inputs and outputs, **u** and **y**. The pair (**A**, **C**) and hence the system (**A**, **B**, **C**, **D**) is observable if $\begin{bmatrix} \mathbf{C} \\ \mathbf{CA} \\ \mathbf{CA}^2 \\ \vdots \\ \mathbf{CA}^{n-1} \end{bmatrix}$ has rank n[33].

If a system is uncontrollable, states which contribute to the system outputs cannot be controlled by any combination of system inputs and therefore the outputs are not under the full control of the inputs. Unobservable systems have states which do not contribute to the system outputs and hence cannot be inferred from observations of plant inputs and outputs. It is not possible to construct full state estimators or observers for such systems.

2.2.3 Frequency Response of the Systems

A knowledge of the frequency response of the system is essential when applying controller design methods based on the frequency domain. Figs 2.13 to Fig 2.16 show the bode plots of the four elements of the open loop TFM for the symmetric model, Figs 2.17 to 2.20, those for the non-symmetric model.

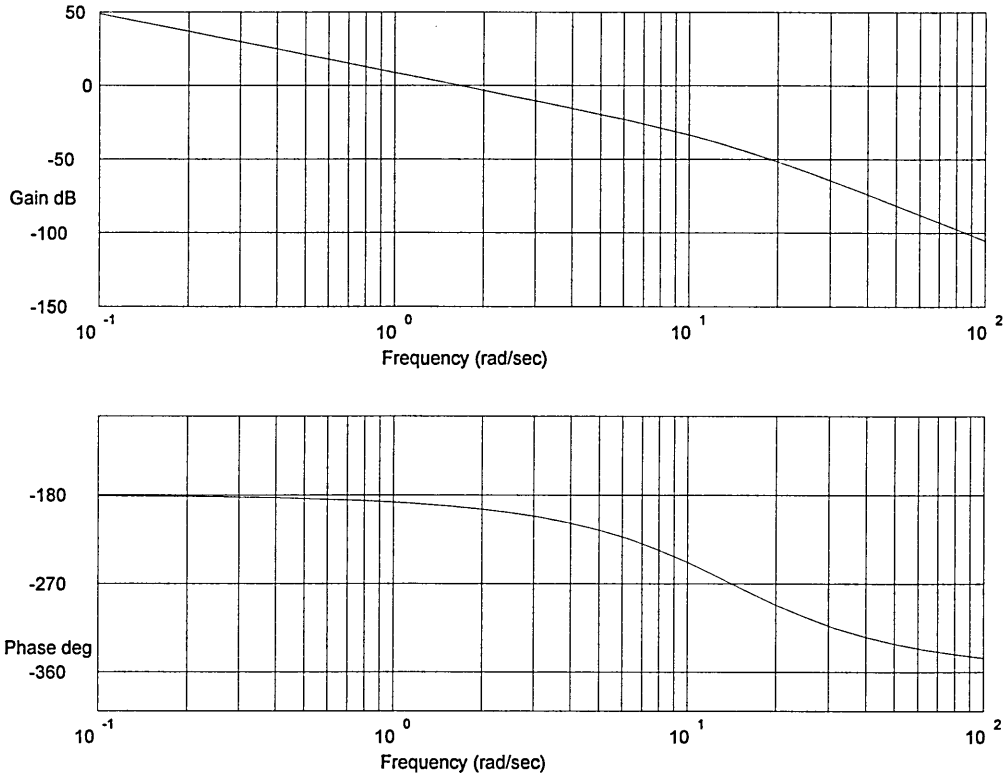

Fig 2.13 Bode Plot of $g_{11}(s)$ for Symmetric Model

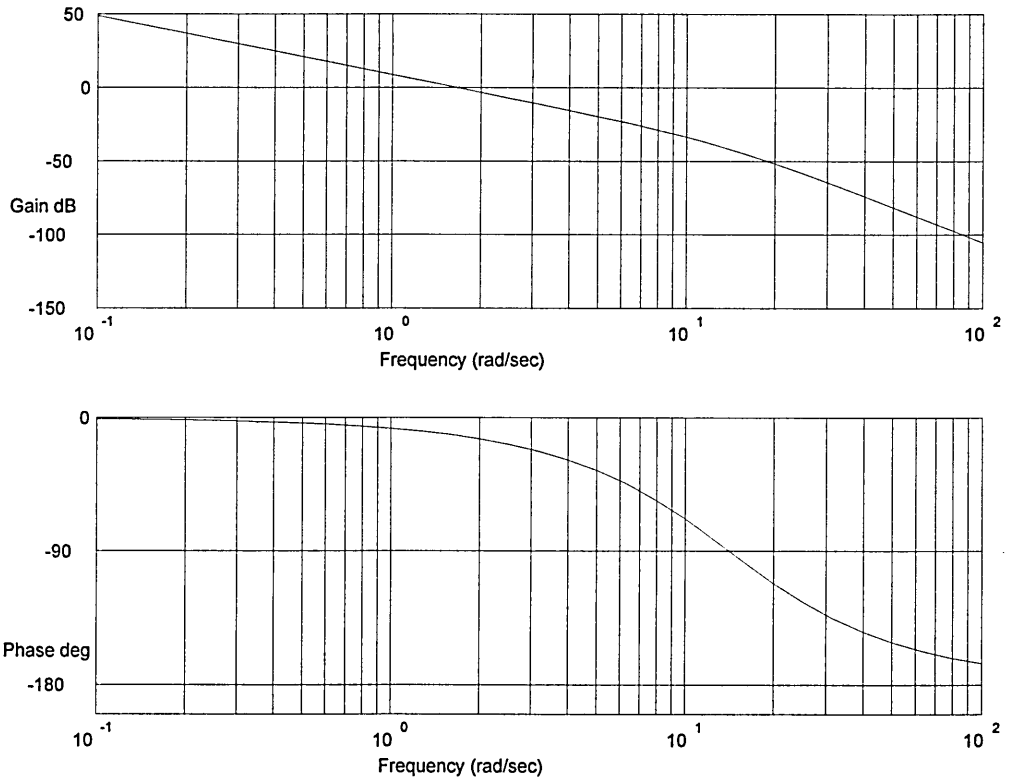

Fig 2.14 Bode Plot of $g_{12}(s)$ for Symmetric Model

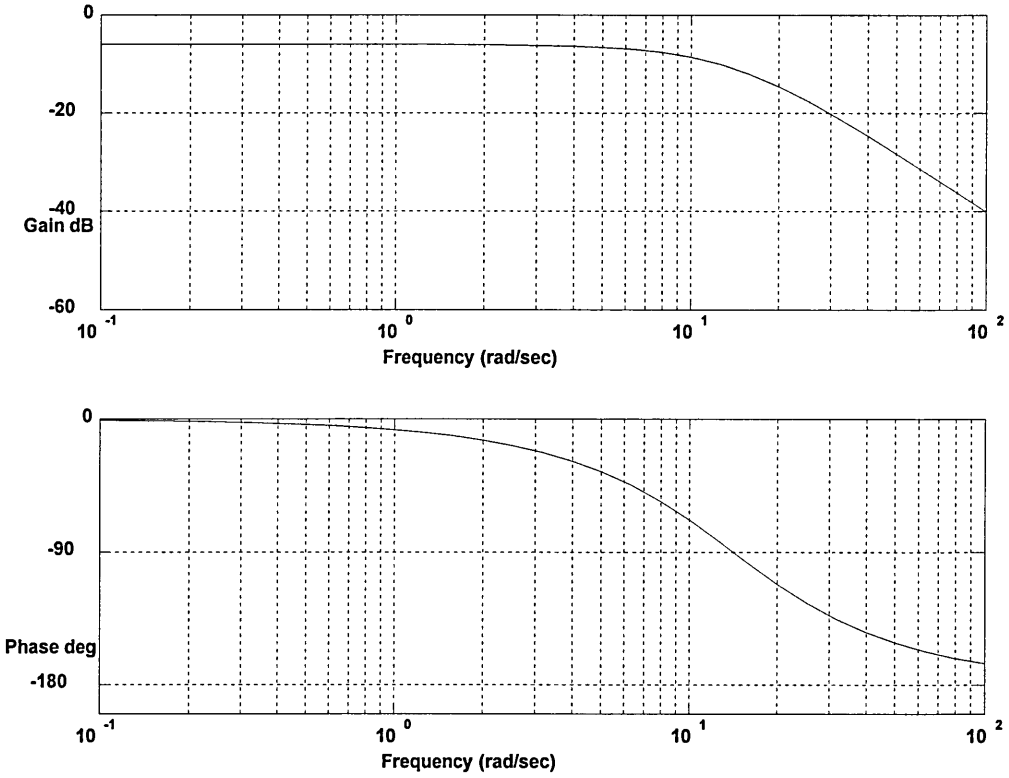

Fig 2.15 Bode Plot of $g_{21}(s)$ for Symmetric Model

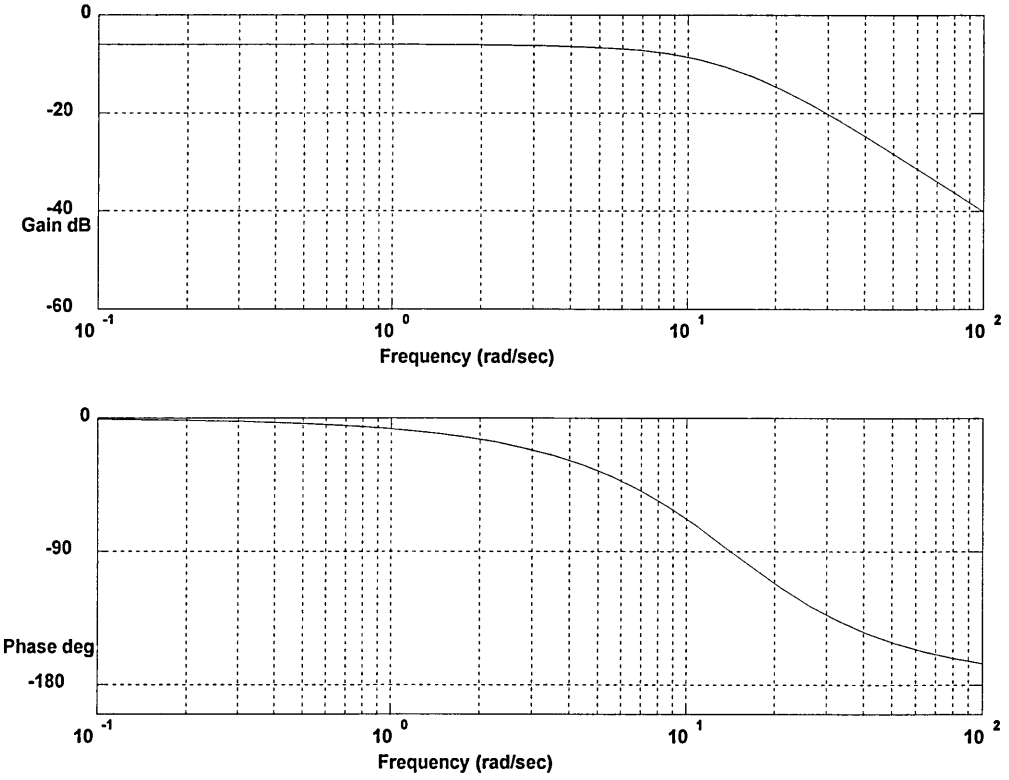

Fig 2.16 Bode Plot of $g_{22}(s)$ for Symmetric Model

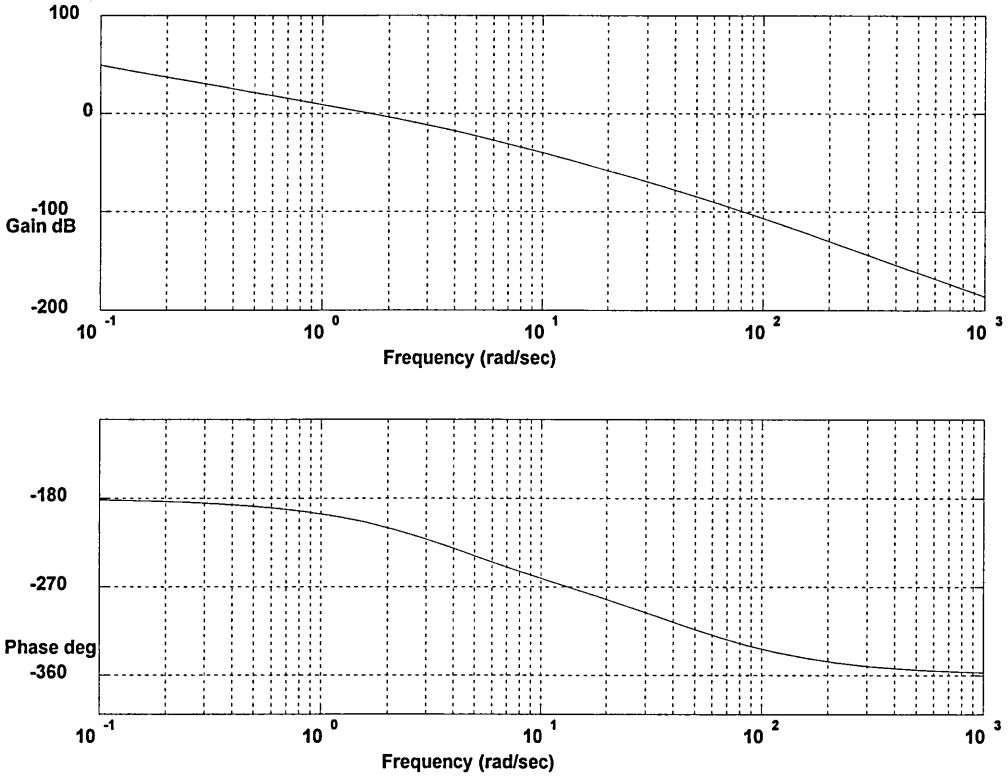

Fig 2.17 Bode Plot of $g_{11}(s)$ for Non-Symmetric Model

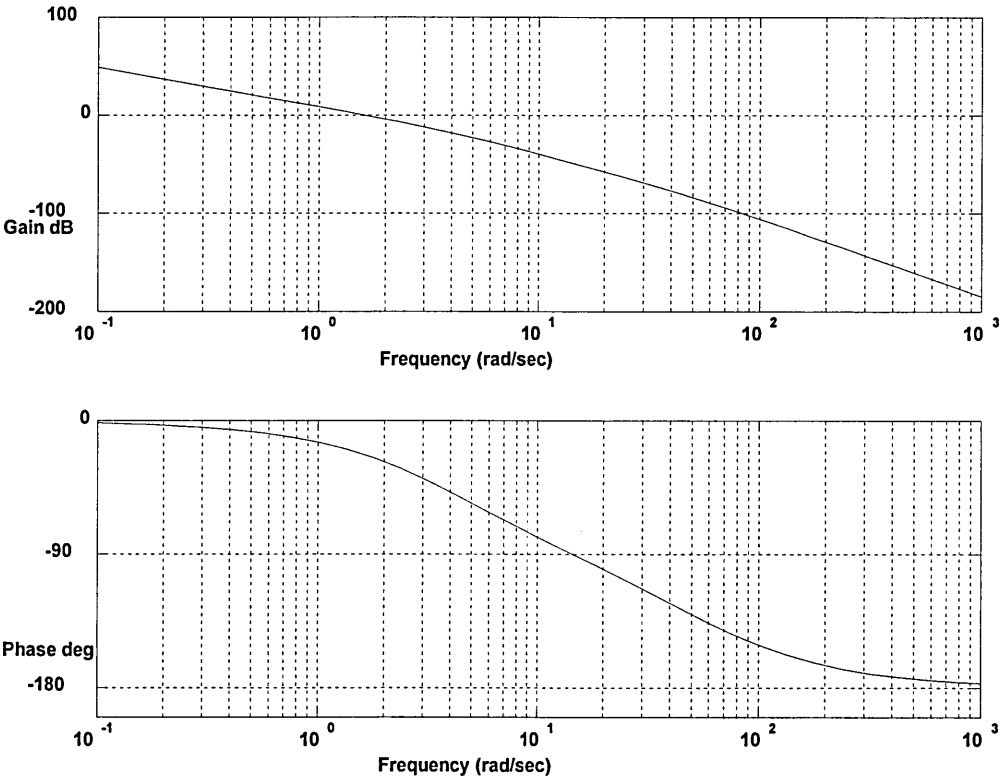

Fig 2.18 Bode Plot of $g_{12}(s)$ for Non-Symmetric Model

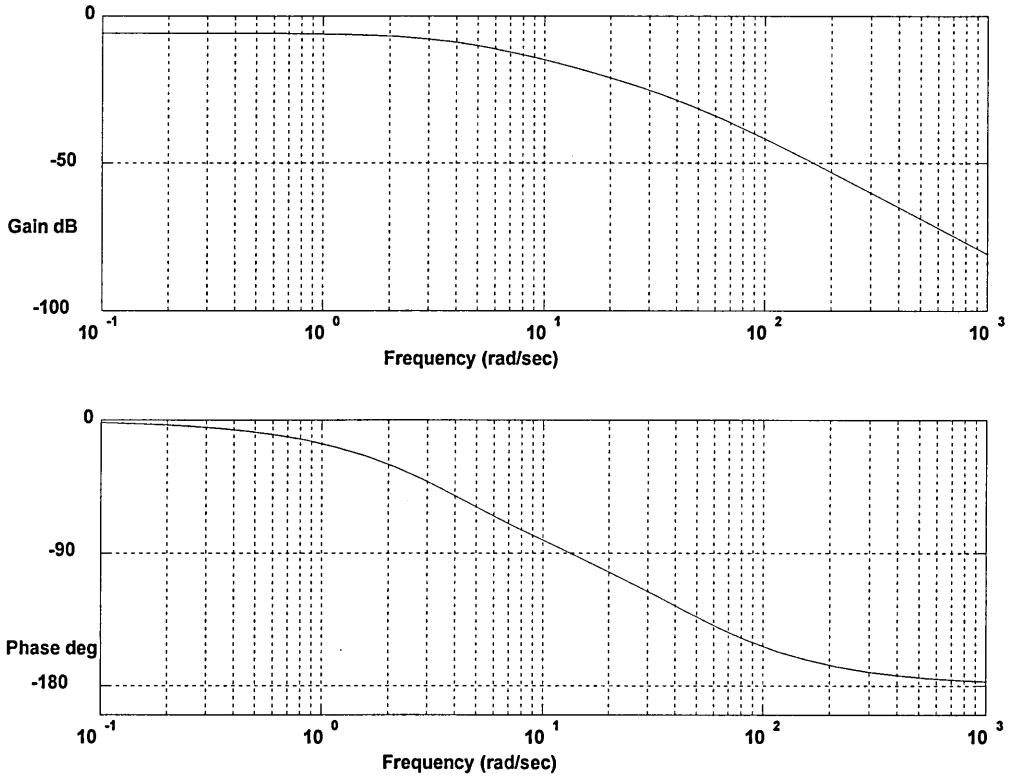

Fig 2.19 Bode Plot of $g_{21}(s)$ for Non-Symmetric Model

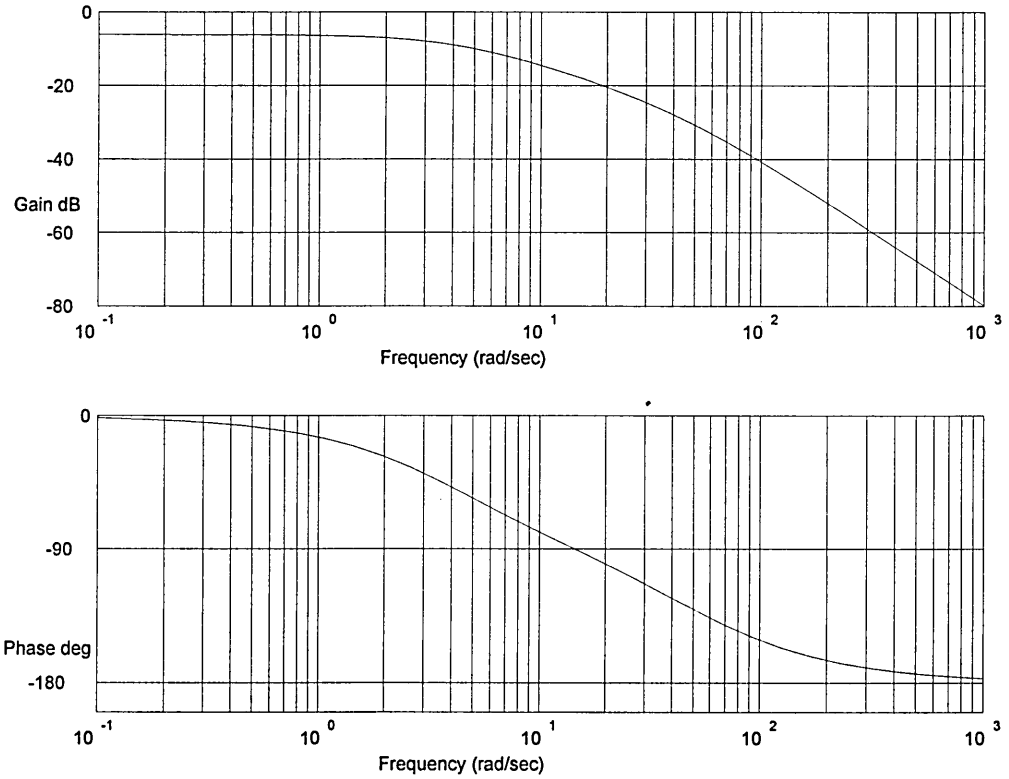

Fig 2.20 Bode Plot of $g_{22}(s)$ for Non-Symmetric Model

The TFM, $\mathbf{G}(s)$, can be written

$$\mathbf{y} = \begin{bmatrix} g_{11}(s) & g_{12}(s) \\ g_{21}(s) & g_{22}(s) \end{bmatrix} \mathbf{u} \tag{2.22}$$

$g_{11}(s)$ and $g_{12}(s)$, relating to horizontal carriage position, contain the dynamics of both carriage and rams whilst $g_{21}(s)$ and $g_{22}(s)$, relating to beam height, contain only ram dynamics. The 180° phase shift at zero frequency in $g_{11}(s)$ is due to the double integrator in carriage dynamics. This phase shift is cancelled in $g_{12}(s)$ by the negative effect of increases in u_2 on y_1.

From the gain plots it can be seen that for the symmetrical model, $g_{11}(s)$ and $g_{12}(s)$ have a crossover frequency of about 2 rs^{-1} and $g_{21}(s)$ and $g_{22}(s)$ are 3 dB down at about 10 rs^{-1}. Corresponding figures for the non-symmetrical model are 2 rs^{-1} and 4 rs^{-1}.

2.2.4 A Simple Decoupler

The TFM for the symmetrical model is given by

$$\mathbf{G}_{sym}(s) = \begin{bmatrix} \dfrac{554.6}{s^2(s^2+25s+200)} & \dfrac{-554.6}{s^2(s^2+25s+200)} \\ \dfrac{100}{s^2+25s+200} & \dfrac{100}{s^2+25s+200} \end{bmatrix} \tag{2.23}$$

and for the non-symmetrical model by

$$\mathbf{G}_{nsym}(s) = \begin{bmatrix} \dfrac{497.5}{s^2(s^2+49.4s+175.7)} & \dfrac{-570.1}{s^2(s^2+53.7s+208.6)} \\ \dfrac{89.7}{s^2+49.4s+175.7} & \dfrac{102.8}{s^2+53.7s+208.6} \end{bmatrix} \tag{2.24}$$

The symmetrical nature of (2.23) suggests the simple expedient of decoupling[12] the system by using a constant compensator of the form $\mathbf{K} = \begin{bmatrix} a & b \\ -a & b \end{bmatrix}$ such that $\mathbf{G}_{sym}(s)\mathbf{K}$ is diagonal. Fig 2.21 shows the gain space of $\mathbf{G}_{sym}(s)\mathbf{K}$ where $\mathbf{K} = \begin{bmatrix} 0.5 & 0.5 \\ -0.5 & 0.5 \end{bmatrix}$.

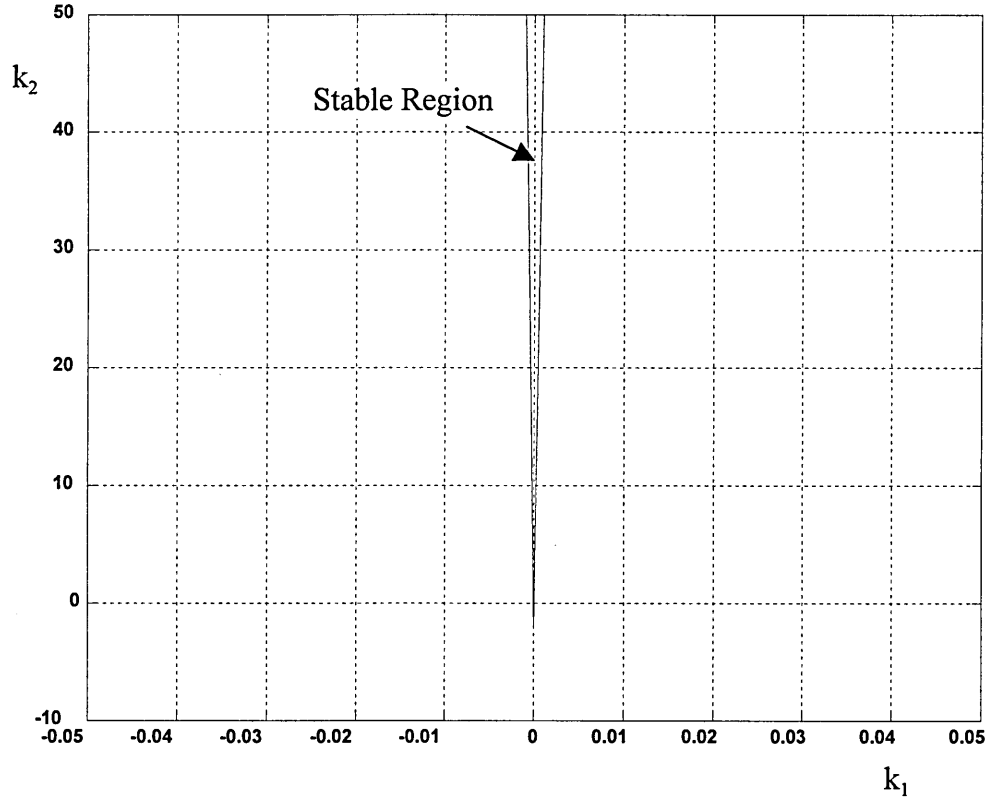

Fig 2.21 Gain Space of Symmetrical Model with Decoupler

Obviously this is of no practical value since for the gain matrix, $\mathbf{K}' = diag(k_1, k_2)$, k_1 is effectively zero and stability has been achieved by suppressing movement of the carriage along the beam. However, a dynamic compensator of the form $\mathbf{K}_d(s) = diag(\frac{s+1}{0.1s+1}, 1+\frac{5}{s})$ was tried with the decoupled system as shown in Fig 2.22.

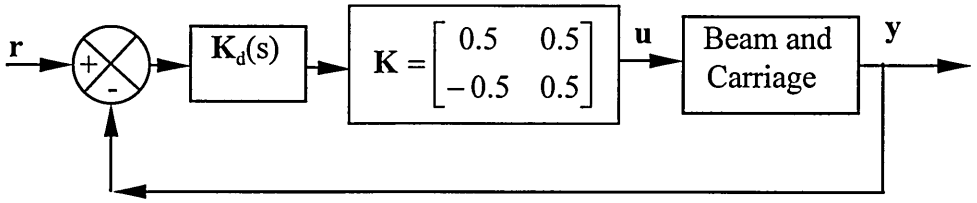

Fig 2.22 Decoupled System with Dynamic Compensator

This compensator introduced phase lead into the first control loop to give a positive phase margin and integral action into the second loop to eliminate steady state error. The resulting system was decoupled and stabilised, as shown by the simulated step

responses of Fig 2.23. For completeness, this two part compensator was applied to the non-symmetrical model. The resulting responses, Fig 2.24, show a more oscillatory response and, of course, some interaction, both dynamic and steady state.

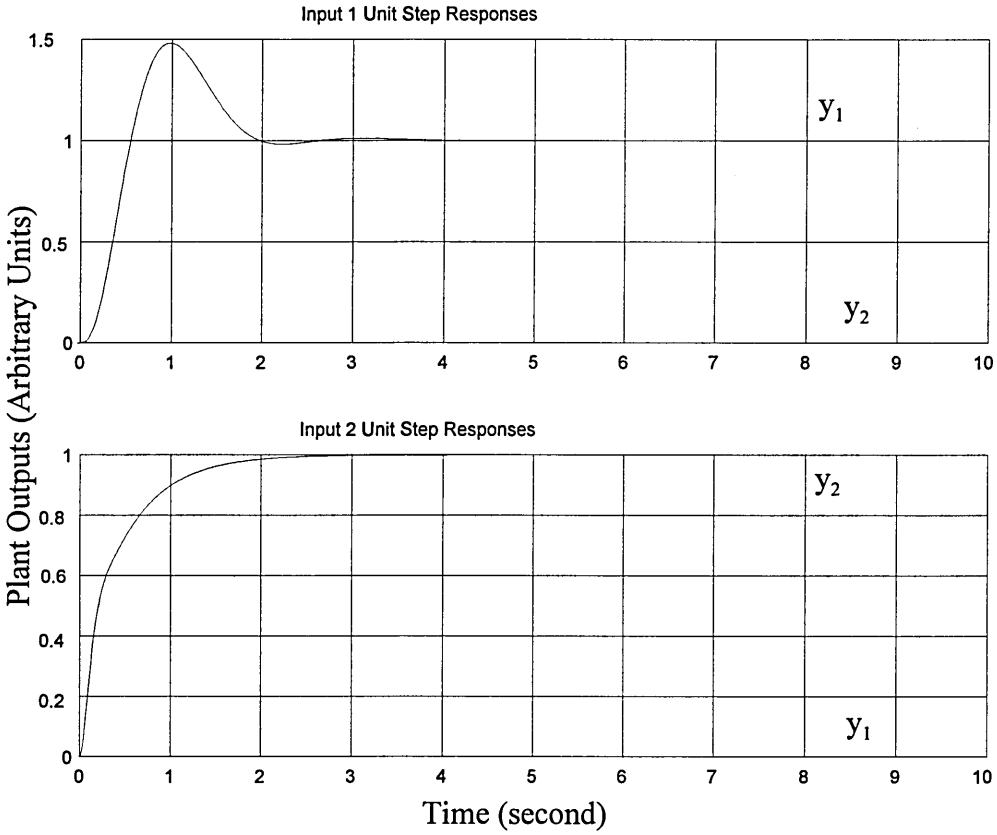

Fig 2.23 Step Response of Stabilised Symmetric Model with Decoupler

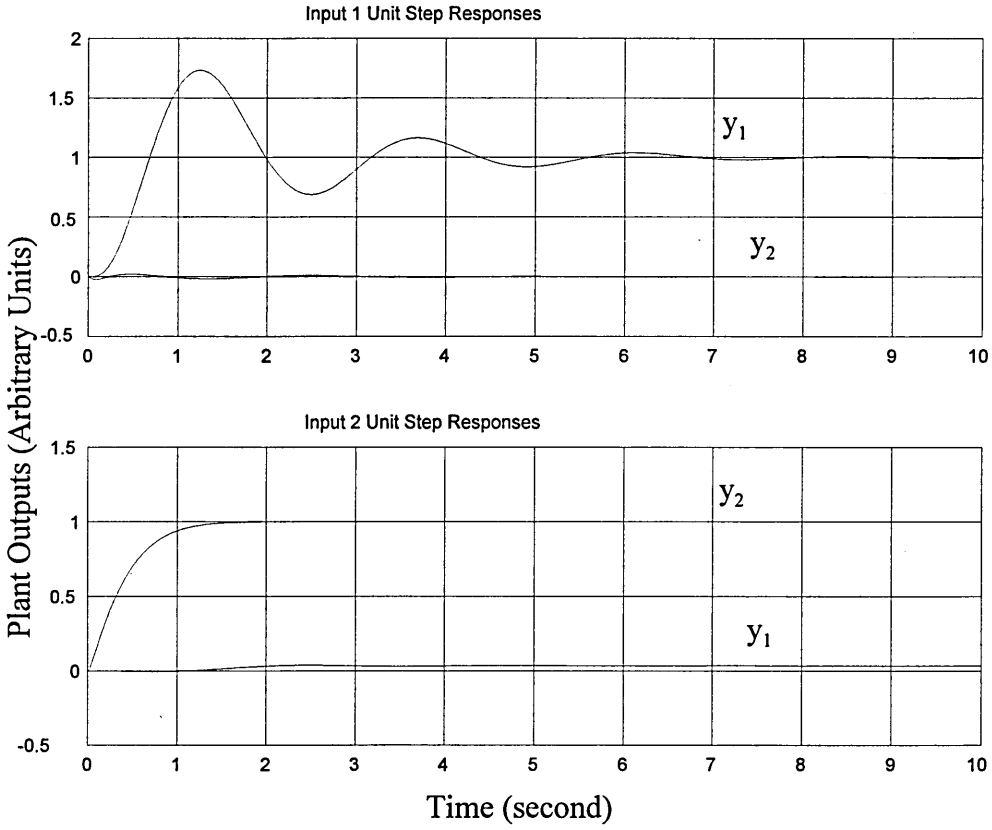

Fig 2.24 Step Response of Stabilised Non-Symmetric Model with Decoupler

In this study of the beam and carriage apparatus, two state space models have been created. The models are both minimum realisations and each has two poles at zero and no zeros. It has been shown that the symmetrical model can be completely decoupled using a constant precompensator and the resulting system stabilised and its steady state error eliminated using a dynamic compensator. The non-symmetrical model has been chosen for the application of the controller design methodologies which follow since it more clearly reflects variations in the operational characteristics of the engineering components used in the beam and carriage apparatus.

3 Theoretical Design Considerations

The development of modern control theory, with its emphasis on linear algebra and numerical methods, has given rise to much work on multivariable systems and system robustness. There are currently available many textbooks summarising these developments, a selection of which has been used extensively for the present work[34], [35], [36], [37].

The techniques which have been applied to the beam and carriage problem in the present work and which form the basis of the comparative study, all result from modern developments in multivariable control system design. Controller design techniques based on state feedback were chosen as an example of the time domain approach, the characteristic locus method was adopted as a method based on the frequency domain and the H^{∞}/mixed sensitivity approach was chosen as a technique for designing robust controllers.

3.1 State Feedback - A Time Domain Approach

For a linear, time-invariant system the objective is to place the closed loop poles at predetermined positions or to optimise the system in terms of some previously defined cost function. Where the cost function to be minimised is based on a quadratic function of the form[38]

$$J = \int_0^{\infty} (\mathbf{x}^T\mathbf{Q}\mathbf{x} + \mathbf{u}^T\mathbf{R}\mathbf{u})dt \qquad (3.1)$$

or[39]

$$J = \int_0^{\infty} (\mathbf{y}^T\mathbf{Q}\mathbf{y} + \mathbf{u}^T\mathbf{R}\mathbf{u})dt \qquad (3.2)$$

the problem is called the Linear Quadratic Regulator (LQR) problem. The cost function of (3.1) seeks to minimise system states and plant inputs whilst that of (3.2) seeks to minimise plant outputs and inputs.

The state vector is usually defined such that some states are available to the control system designer as measured outputs but higher order states will typically be

unavailable. In order to implement a full state feedback controller these states must be estimated.

The development of controller designs based on state feedback and state estimation made extensive use of Matlab's Control System Toolbox (CSTB) [40] and simulations of the resulting controllers were prepared using the associated simulation software, Simulink [41].

3.1.1 Determination of the State Feedback Coefficients

The object is to determine the state feedback matrix, **K**, shown in Fig 3.1, all system states being either measured or estimated.

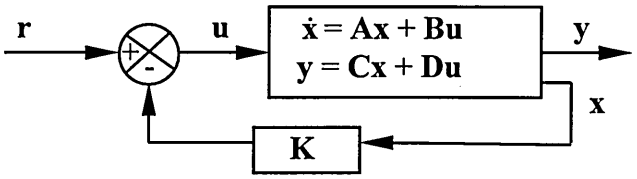

Fig 3.1 State Feedback

Closed-Loop Pole Placement

The plant's open loop poles are given by the eigenvalues of **A** which are the roots of the characteristic equation (CE)[42]

$$\det(s\mathbf{I} - \mathbf{A}) = 0 \tag{3.3}$$

For the closed-loop system shown in Fig 3.1[43]

$$\dot{\mathbf{x}} = (\mathbf{A} - \mathbf{BK})\mathbf{x} + \mathbf{Br} \tag{3.4}$$

and its poles are the eigenvalues of $(\mathbf{A} - \mathbf{BK})$. In simple cases the elements of **K** can be found by comparing the characteristic polynomial (CP), $\det(s\mathbf{I} - \mathbf{A} + \mathbf{BK})$, with the desired CP, $(s\text{-}p_1)(s\text{-}p_2)...(s\text{-}p_n)$ where the p_i are the desired closed-loop poles. Algorithms based on numerical methods are available for computing **K** and Matlab's CSTB functions *acker* and *place* are based on these. *Place* minimises the sensitivity of the eigenvalues to variations in the plant dynamics and is more reliable than *acker*[44].

LQR Design

For a linear time-invariant system the LQR design seeks to apply a control input vector, $\mathbf{u} = -\mathbf{K}\mathbf{x}$, in order to minimise a cost function of the form given in (3.1) or (3.2) whilst returning the plant to its original state from some arbitrary state. (Thus this is formulated as a regulator problem). For this problem it is assumed that $\mathbf{Q}$ and $\mathbf{R}$ are real and symmetric and that $\mathbf{Q}$ is positive-semidefinite ($\mathbf{x}^T\mathbf{Q}\mathbf{x} \geq 0$ for all real $\mathbf{x}$) and $\mathbf{R}$ is positive-definite ($\mathbf{u}^T\mathbf{R}\mathbf{u} > 0$ for all real $\mathbf{u} \neq \mathbf{0}$). $\mathbf{Q}$ and $\mathbf{R}$ are chosen to reflect the relative importance of $\mathbf{x}$ and $\mathbf{u}$ and their various components in the optimisation process.

This is a deterministic problem with optimal solution given by [45]

$$\mathbf{K} = \mathbf{R}^{-1}\mathbf{B}^T\mathbf{P} \tag{3.5}$$

where $\mathbf{P}$ is the solution of the algebraic Riccati equation (ARE)

$$\mathbf{A}^T\mathbf{P} + \mathbf{P}\mathbf{A} + \mathbf{Q} - \mathbf{P}\mathbf{B}\mathbf{R}^{-1}\mathbf{B}^T\mathbf{P} = \mathbf{0} \tag{3.6}$$

If ($\mathbf{A}$, $\mathbf{B}$) is controllable the resulting closed-loop system is asymptotically stable.

CSTB function *lqr* computes $\mathbf{K}$ (and also $\mathbf{P}$ and the closed-loop poles) for the cost function given by (3.1), *lqry* computes $\mathbf{K}$ for the cost function of (3.2).

3.1.2 State Estimation

For the deterministic problem where system noise is not considered, state estimators, often called observers[8], can be designed by selecting poles for the observer which are significantly faster (i.e. have significantly more negative real parts) than those of the plant. Alternatively, an optimisation problem may be formulated which seeks to minimise errors in the estimated states in the presence of process and measurement noise treated as stochastic processes. One such approach involves the use of a Kalman Filter [9], [10] which, when used in conjunction with state feedback based on LQR theory, is called a Linear Quadratic Gaussian (LQG) controller [11].

The above estimators estimate all the states of a plant, some of which may be available as measured outputs. It is possible to design a reduced order observer which estimates only the subset of unmeasured states.

Full order Estimators

Observer Design by Pole Placement

For the observer to effectively track the actual plant states it must be supplied with information concerning the discrepancy between actual plant and observer outputs, $\mathbf{y}-\hat{\mathbf{y}}$, and this is fed back to the observer via gain matrix, L, as shown in Fig 3.2[46].

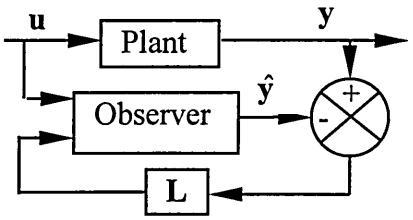

Fig 3.2 State Estimator

For the observer[46],

$$\dot{\hat{\mathbf{x}}} = \mathbf{A}\hat{\mathbf{x}} + \mathbf{B}\mathbf{u} + \mathbf{L}(\mathbf{y} - \hat{\mathbf{y}}) \tag{3.7}$$

$$\hat{\mathbf{y}} = \mathbf{C}\hat{\mathbf{x}} + \mathbf{D}\mathbf{u} \tag{3.8}$$

and if $\mathbf{D}=\mathbf{0}$

$$\dot{\hat{\mathbf{x}}} = (\mathbf{A} - \mathbf{LC})\hat{\mathbf{x}} + \begin{bmatrix}\mathbf{B} & \mathbf{L}\end{bmatrix}\begin{bmatrix}\mathbf{u}\\ \mathbf{y}\end{bmatrix} \tag{3.9}$$

Defining error vector $\tilde{\mathbf{x}} = \mathbf{x} - \hat{\mathbf{x}}$ gives

$$\dot{\tilde{\mathbf{x}}} = (\mathbf{A} - \mathbf{LC})\tilde{\mathbf{x}} \tag{3.10}$$

Thus, the dynamics of the error vector are determined by the eigenvalues of (**A-LC**) and for effective estimation these dynamics must be 'fast' compared to the plant dynamics. When eigenvalues have been chosen for (**A-LC**), **L** can be computed by a process similar to that by which **K** was computed for closed-loop pole placement. In fact, whereas *place*(**A**, **B**, **p**) returns **K** such that **p** is the vector of eigenvalues of (**A-BK**), *place*($\mathbf{A}^T$, $\mathbf{C}^T$, **p**) returns $\mathbf{L}^T$ such that **p** is the vector of eigenvalues of (**A-LC**).

The complete controller using full order observer and state feedback is shown in Fig 3.3.

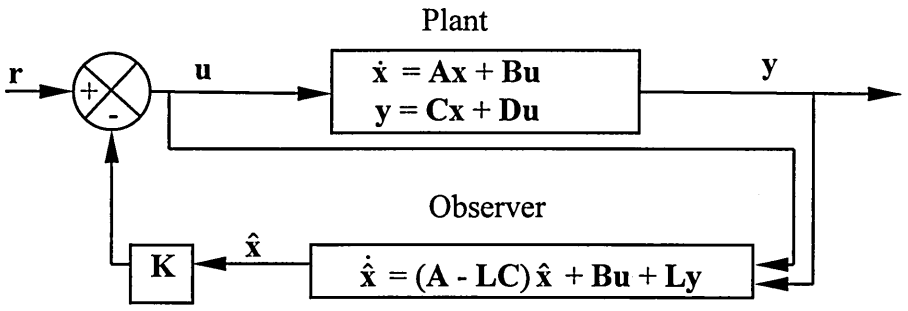

Fig 3.3 State Feedback with Observer

The LQG Controller

The object is to generate a control input $\mathbf{u} = -\mathbf{Kx}$ to minimise a quadratic cost function whilst returning the system to its initial state in the presence of process noise (plant disturbance) and measurement noise. This problem is formulated as a *regulator* problem: it is required to maintain the desired system output in the absence of a reference input.

The plant model is[47]

$$\dot{\mathbf{x}} = \mathbf{Ax} + \mathbf{Bu} + \mathbf{w}_d \tag{3.11}$$

$$\mathbf{y} = \mathbf{Cx} + \mathbf{Du} + \mathbf{w}_n \tag{3.12}$$

where $\mathbf{w}_d$ and $\mathbf{w}_n$ are uncorrelated, zero-mean Gaussian stochastic processes with constant covariance matrices, **W** and **V**, given by

$$\mathbf{W} = E\{\mathbf{w}_d.\mathbf{w}_d^{\mathrm{T}}\} \tag{3.13}$$

$$\mathbf{V} = E\{\mathbf{w}_n.\mathbf{w}_n^{\mathrm{T}}\} \tag{3.14}$$

The cost function is given by[47]

$$J = E\{\lim_{\tau\to\infty} \frac{1}{\tau} \int_0^{\tau} (\mathbf{x}^{\mathrm{T}}\mathbf{Q}\mathbf{x} + \mathbf{u}^{\mathrm{T}}\mathbf{R}\mathbf{u})dt\} \tag{3.15}$$

where **Q** and **R** are as described for the LQR problem.

The LQG problem separates into the dual problem:

(i) Design an LQR to produce optimal $\mathbf{u} = -\mathbf{Kx}$ as before

(ii) Design a Kalman Filter to provide optimal estimates of **x** in the presence of plant disturbance and measurement noise

Kalman Filter Design

It is required to determine estimator gain, **L**, in order to minimise $E\{(\mathbf{x}-\hat{\mathbf{x}})^{\mathrm{T}}(\mathbf{x}-\hat{\mathbf{x}})\}$. Consequently, the variance of the estimation error is minimised.

With **W** symmetric, positive-semidefinite, **V** symmetric, positive-definite and (**A**, **C**) observable, the solution is given by[48]

$$\dot{\hat{\mathbf{x}}} = (\mathbf{A}-\mathbf{LC})\hat{\mathbf{x}} + \begin{bmatrix}\mathbf{B} & \mathbf{L}\end{bmatrix}\begin{bmatrix}\mathbf{u}\\ \mathbf{y}\end{bmatrix} \tag{3.16}$$

where

$$\mathbf{L} = \mathbf{QC}^{\mathrm{T}}\mathbf{V}^{-1} \tag{3.17}$$

and **Q** is the solution of the ARE

$$\mathbf{QA}^{\mathrm{T}} + \mathbf{AQ} - \mathbf{QC}^{\mathrm{T}}\mathbf{V}^{-1}\mathbf{CQ} + \mathbf{W} = \mathbf{0} \tag{3.18}$$

The CSTB function *lqe* can be used to compute the Kalman gain matrix and, given this gain, *estim* can be used to return the Kalman estimator in state space form.

Reduced Order Observer Design

In order to implement a reduced order observer the states are partitioned into the measured states, $\mathbf{x}_a = \mathbf{y}$, and the states to be estimated, $\mathbf{x}_b$.

The partitioned state equations become

$$\begin{bmatrix}\dot{\mathbf{x}}_a\\ \dot{\mathbf{x}}_b\end{bmatrix} = \begin{bmatrix}\mathbf{A}_{aa} & \mathbf{A}_{ab}\\ \mathbf{A}_{ba} & \mathbf{A}_{bb}\end{bmatrix}\begin{bmatrix}\mathbf{x}_a\\ \mathbf{x}_b\end{bmatrix} + \begin{bmatrix}\mathbf{B}_a\\ \mathbf{B}_b\end{bmatrix}\mathbf{u} \tag{3.19}$$

$$\mathbf{y} = \begin{bmatrix}\mathbf{I} & \mathbf{0}\end{bmatrix}\begin{bmatrix}\mathbf{x}_a\\ \mathbf{x}_b\end{bmatrix} \tag{3.20}$$

The state equations for the unmeasured states may be written[49]

$$\dot{\mathbf{x}}_b = \mathbf{A}_{bb}\mathbf{x}_b + \begin{bmatrix}\mathbf{B}_b & \mathbf{A}_{ba}\end{bmatrix}\begin{bmatrix}\mathbf{u}\\ \mathbf{y}\end{bmatrix} \tag{3.21}$$

$$\dot{\mathbf{y}} - \begin{bmatrix} \mathbf{B}_a & \mathbf{A}_{aa} \end{bmatrix} \begin{bmatrix} \mathbf{u} \\ \mathbf{y} \end{bmatrix} = \mathbf{A}_{ab}\mathbf{x}_b \tag{3.22}$$

or

$$\dot{\mathbf{x}}_b = \mathbf{A}_{bb}\mathbf{x}_b + \begin{bmatrix} \mathbf{B}_b & \mathbf{A}_{ba} \end{bmatrix} \mathbf{v} \tag{3.23}$$

$$\mathbf{z} = \mathbf{A}_{ab}\mathbf{x}_b \tag{3.24}$$

Equations (3.23), (3.24) suggest that an observer can be built to estimate $\mathbf{x}_b$ which has notional inputs given by $\mathbf{v} = \begin{bmatrix} \mathbf{u} \\ \mathbf{y} \end{bmatrix}$ and notional outputs given by $\mathbf{z} = \dot{\mathbf{y}} - \begin{bmatrix} \mathbf{B}_a & \mathbf{A}_{aa} \end{bmatrix} \begin{bmatrix} \mathbf{u} \\ \mathbf{y} \end{bmatrix}$.

Based on observer gain, $\mathbf{L}$, the observer equation is

$$\dot{\hat{\mathbf{x}}}_b = \mathbf{A}_{bb}\hat{\mathbf{x}}_b + \begin{bmatrix} \mathbf{B}_b & \mathbf{A}_{ba} \end{bmatrix} \mathbf{v} + \mathbf{L}(\mathbf{z} - \mathbf{A}_{ab}\hat{\mathbf{x}}_b) \tag{3.25}$$

and

$$\dot{\tilde{\mathbf{x}}}_b = (\mathbf{A}_{bb} - \mathbf{L}\mathbf{A}_{ab})\tilde{\mathbf{x}}_b \tag{3.26}$$

The observer gain can be chosen such that the poles of $(\mathbf{A}_{bb} - \mathbf{L}\mathbf{A}_{ab})$ are fast compared to the plant poles.

The observer of (3.25) cannot be implemented because a measurement of $\dot{\mathbf{y}}$ is not available. If a new variable, $\mathbf{x}_c = \mathbf{x}_b - \mathbf{L}\mathbf{y}$ is defined then an observer for $\mathbf{x}_c$ can be built using[50]

$$\dot{\hat{\mathbf{x}}}_c = (\mathbf{A}_{bb} - \mathbf{L}\mathbf{A}_{ab})\hat{\mathbf{x}}_c + \begin{bmatrix} \mathbf{B}_b - \mathbf{L}\mathbf{B}_a & \mathbf{A}_{ba} - \mathbf{L}\mathbf{A}_{aa} + \mathbf{A}_{bb}\mathbf{L} - \mathbf{L}\mathbf{A}_{ab}\mathbf{L} \end{bmatrix} \begin{bmatrix} \mathbf{u} \\ \mathbf{y} \end{bmatrix} \tag{3.27}$$

and $\hat{\mathbf{x}}_b$ obtained from

$$\hat{\mathbf{x}}_b = \hat{\mathbf{x}}_c + \mathbf{L}\mathbf{y} \tag{3.28}$$

3.2 The Characteristic Locus Method - A Frequency Response Approach

The characteristic loci in general may be used for stability assessment of multivariable systems by summing the encirclements of the critical point in the Nyquist diagram made by each locus over the total number of loci[16]. This is due to the fact that the system $\mathbf{Q}(s)$ is stable (with UNF) if and only if $\det(\mathbf{I}+\mathbf{Q}(s))$ has no zeros in the RHP and

$$\det(\mathbf{I}+\mathbf{Q}(s)) = \prod_i (1+q_i(s)) \tag{3.29}$$

where $\mathbf{Q}(s)$ and $diag(q_i(s))$ are related by the similarity transformation $\mathbf{Q}(s) = \mathbf{W}(s).diag(q_i(s)).\mathbf{W}^{-1}(s)$. $\mathbf{W}(s)$, the matrix function which diagonalises $\mathbf{Q}(s)$, is made up (columnwise) of the frequency dependent eigenvectors of $\mathbf{Q}(s)$ and the $q_i(s)$ are the frequency dependent eigenvalues or characteristic loci of $\mathbf{Q}(s)$.

However, the characteristic locus method is a particular technique for producing solutions for multivariable control system design problems with respect to dynamic performance, steady state error and interaction.[17] The object is to diagonalise the multivariable control system over the system bandwidth by designing a series of compensators for each of the selected frequency bands (usually three), then applying dynamic compensation to achieve satisfactory performance.

For the present work on controller design by the characteristic locus method, extensive use was made of Matlab's Multivariable Frequency Domain Toolbox (MVFDTB) [51].

3.2.1 High Frequency Compensator

Firstly a constant compensator, $\mathbf{K}_h$, is designed in order to diagonalise the system in its upper frequency range. MVFDTB function *align* may be used to compute real matrix, $\mathbf{K}_h$, such that, at some target frequency, ω_h [52]

$$\mathbf{G}(j\omega_h)\mathbf{K}_h \approx diag(\lambda_i) \tag{3.30}$$

$\mathbf{K}_h$ is computed such that the diagonalising matrix for $\mathbf{G}(j\omega_h)\mathbf{K}_h$, given by $\mathbf{W}_h$ where $diag(\lambda_i) = \mathbf{W}_h^{-1}\mathbf{G}(j\omega_h)\mathbf{K}_h\mathbf{W}_h$, approximates the identity matrix (i.e. the eigenvectors of $\mathbf{G}(j\omega_h)\mathbf{K}_h$ are *aligned* with the standard basis vectors of the system) and thus $\mathbf{G}(j\omega_h)\mathbf{K}_h \approx diag(\lambda_i)$. *Align* also attempts to equalise the magnitudes of the characteristic values at ω_h and set them equal to unity, such that $|\lambda_1| = |\lambda_2| = \ldots = |\lambda_n|$.

(In this sense $\mathbf{K}_h$ can be taken as an approximation of $\mathbf{G}^{-1}(j\omega_h)$). The presumption is that $\mathbf{Q}_1(s) = \mathbf{G}(s)\mathbf{K}_h$ remains diagonal over a useful high frequency range.

3.2.2 Mid Frequency Compensator

Secondly, an Approximate Commutative Controller (ACC), $\mathbf{K}_m(s)$, is designed to give suitable dynamic performance in the mid-frequency range. This is a dynamic compensator which is computed such that[53]

$$\mathbf{K}_m(s) \approx \mathbf{W}_m diag(k_i(s))\mathbf{W}_m^{-1} \tag{3.31}$$

where, for some target frequency in the mid-frequency range, ω_m

$$\mathbf{Q}_1(j\omega_m) = \mathbf{W}_m diag(\mu_i)\mathbf{W}_m^{-1} \tag{3.32}$$

Thus $\mathbf{K}_m(j\omega_m)$ and $\mathbf{Q}_1(j\omega_m)$ approximately commute.

The forward path is now

$$\mathbf{Q}_2(s) = \mathbf{G}(s)\mathbf{K}_h\mathbf{K}_m(s) \tag{3.33}$$

and

$$\mathbf{Q}_2(j\omega_m) \approx \mathbf{W}_m diag(\mu_i k_i(j\omega_m))\mathbf{W}_m^{-1} \tag{3.34}$$

(3.34) shows that, for frequencies sufficiently close to ω_m where $\mathbf{Q}_1(s) \approx \mathbf{W}_m diag(q_i(s))\mathbf{W}_m^{-1}$, there is no interaction between the dynamic elements, $q_i(s)$, which are the characteristic loci of $\mathbf{Q}_1(s)$, and the $k_i(s)$, which are dynamic elements of the ACC. This lack of interaction persists for the closed-loop system formed by UNF since if $\mathbf{Q}(s) = \mathbf{W}diag(q_i)\mathbf{W}^{-1}$ then $(\mathbf{I}+\mathbf{Q}(s))^{-1}\mathbf{Q}(s) = \mathbf{W}diag(\frac{q_i}{1+q_i})\mathbf{W}^{-1}$.

Thus the $k_i(s)$ can be specified on SISO principles by treating $\mathbf{Q}_1(s)$ as n single loop systems, choosing each of the $k_i(s)$ to give the required performance when applied to the corresponding $q_i(s)$. The $k_i(s)$ are normally specified such that $\lim_{s\to\infty} k_i(s) = 1$, with the result that the diagonalisation of $\mathbf{Q}_1(s)$ at high frequencies is not disturbed. As in the first design stage, the presumption is that the decoupling of dynamic elements at the target frequency persists over a useful mid-frequency range.

The ACC may be designed using MVFDTB function *facc* given $\mathbf{Q}_1(j\omega_m)$ and $k_i(s)$, i = 1, 2, ..., *n*. Function *facc* returns real matrices **A** and **B** as approximations to $\mathbf{W}_m$ and $\mathbf{W}_m^{-1}$ which are computed as *align*($\mathbf{W}_m^{-1}$) and *align*($\mathbf{W}_m$) respectively. At this point $\mathbf{Q}_2(j\omega_m)$ is not necessarily diagonal. The less sensitive the eigenvectors of $\mathbf{Q}_1(j\omega)$ are to changes in frequency, the more diagonal $\mathbf{Q}_2(j\omega_m)$ will be, since for $\mathbf{W}_m \approx \mathbf{W}_h \approx \mathbf{I}$, $\mathbf{Q}_2(j\omega_m) \approx diag(\mu_i k_i(j\omega_m))$.

3.2.3 Low Frequency Compensator

The final stage of the characteristic locus design is to apply correction for steady state errors. This involves the design of a low frequency compensator, $\mathbf{K}_l(s)$, with dynamic components containing integral terms where necessary. $\mathbf{K}_l(s)$ may be designed as an ACC based on a target frequency in the low frequency range and specifying suitable dynamic compensation for the *n* control loops. Integral terms, $l_i(s)$, in the compensator correct steady state errors and also the large low frequency gains associated with them have the effect of removing interaction as follows:-

The final forward path gain is given by

$$\mathbf{Q}_3(s) = \mathbf{Q}_2(s)\mathbf{K}_l(s) \tag{3.35}$$

where $\mathbf{K}_l(s) = \mathbf{W}_l diag(l_i(s))\mathbf{W}_l^{-1}$ and $\mathbf{Q}_2(j\omega_l) \approx \mathbf{W}_l diag(\nu_i)\mathbf{W}_l^{-1}$.

For low frequencies

$$\mathbf{Q}_3(j\omega) \approx \mathbf{W}_l diag(\nu_i l_i(j\omega))\mathbf{W}_l^{-1} \tag{3.36}$$

and for the closed-loop system

$$\overline{\mathbf{Q}}_3(j\omega) \approx \mathbf{W}_l diag(\frac{\nu_i l_i(j\omega)}{1+\nu_i l_i(j\omega)})\mathbf{W}_l^{-1} \tag{3.37}$$

For $l_i(j\omega)$ sufficiently large $|\nu_i l_i(j\omega)| >> 1$ and $\overline{\mathbf{Q}}_3(j\omega) \approx \mathbf{I}$.

The complete controller is shown in Fig 3.4. Since the only dynamic components in the compensator are the diagonal components $k_i(s)$ and $l_i(s)$, the order of the compensator is given by the sum of the orders of these components.

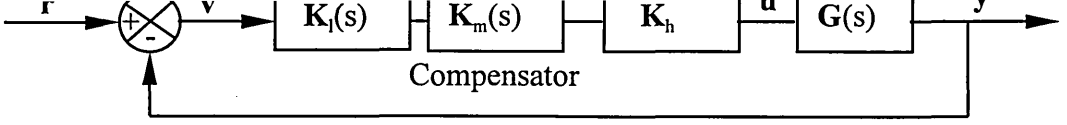

Fig 3.4 Characteristic Locus Controller

3.3 H^∞ Mixed Sensitivity - A Robust Approach

This approach is based on the minimisation of the magnitude of a mixed sensitivity function as measured using the H^∞ norm. The H^∞ norm is a measure of the maximum gain of an operator function and much work has been done on developing numerical methods for synthesising controllers which optimise the H^∞ norm of design based operator functions. [54]

The mixed sensitivity function or operator is chosen such that the resulting controller designs have satisfactory characteristics with respect to, for example, performance, robustness and disturbance rejection.

3.3.1 The H^∞ norm

The H^∞ norm may be used as a scalar measure of a stable transfer function matrix. The H^∞ norm of $\mathbf{G}(s)$ is defined as[55]

$$\|\mathbf{G}(s)\|_\infty = \sup|_\omega \bar{\sigma}(\mathbf{G}(j\omega)) \tag{3.38}$$

$\bar{\sigma}(\mathbf{G}(j\omega))$, the maximum singular value of $\mathbf{G}(j\omega)$, can be interpreted as the maximum gain of $\mathbf{G}(j\omega)$ taken over all directions of input vector $\mathbf{u}(\omega)$ [56].

i.e.

$$\bar{\sigma}(\mathbf{G}(j\omega)) = \max|_{\mathbf{u}(\omega)} \frac{\|\mathbf{y}(\omega)\|_2}{\|\mathbf{u}(\omega)\|_2} \tag{3.39}$$

where $\|.\|_2$ is the vector 2-norm defined by

$$\|\mathbf{a}\|_2 = \left[\sum_i a_i^2\right]^{1/2} \tag{3.40}$$

$\|\mathbf{G}(s)\|_\infty$ is therefore the maximum gain of $\mathbf{G}(s)$ taken over all directions and all frequencies of the input vector.

The H^{∞} norm may also be written in terms of vector time functions as[57]

$$\|\mathbf{G}(s)\|_{\infty} = \max \frac{\|\mathbf{y}(t)\|_2}{\|\mathbf{u}(t)\|_2} \tag{3.41}$$

where the 2-norm of vector time function $\mathbf{x}(t)$ is defined as

$$\|\mathbf{x}(t)\|_2 = \left[\int_0^{\infty} \sum_i |x_i(t)|^2 dt\right]^{1/2} \tag{3.42}$$

This interpretation of the H^{∞} norm is as a measure of the maximum gain for a set of 2-norm bounded input signals which represent all possible combinations of spectrum and vector direction. For this reason the norm is suitable for use with optimal control problems. In addition the H^{∞} norm conforms to the multiplicative property,

$\|\mathbf{G}_1(s).\mathbf{G}_2(s)\|_{\infty} \leq \|\mathbf{G}_1(s)\|_{\infty}.\|\mathbf{G}_2(s)\|_{\infty}$, which enables robust control designs based on this norm to formulate a sufficient condition for robust stability and avoid unnecessary conservatism since the condition is also necessary[58].

3.3.2 Sensitivity Functions

A generalised model for a single degree of freedom control system[59] is shown in Fig 3.5.

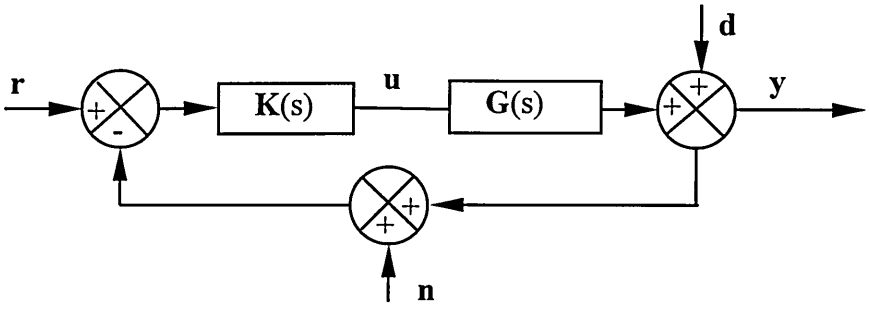

Fig 3.5 One Degree of Freedom System

This system has exogenous inputs consisting of reference input vector, **r**, plant disturbance (or process noise), **d**, and measurement noise, **n**, and has exogenous output, **y**.

The output for this system is given by[60]

$$\mathbf{y}(s) = (\mathbf{I} + \mathbf{GK}(s))^{-1}\mathbf{GKr}(s) + (\mathbf{I} + \mathbf{GK}(s))^{-1}\mathbf{d}(s) - (\mathbf{I} + \mathbf{GK}(s))^{-1}\mathbf{GKn}(s) \tag{3.43}$$

(For convenience terms such as $\mathbf{G}(s)\mathbf{K}(s)\mathbf{r}(s)$ are written $\mathbf{GKr}(s)$).

Here $(\mathbf{I} + \mathbf{GK}(s))^{-1}$ is the Sensitivity Function or Operator, $\mathbf{S}(s)$, and $(\mathbf{I} + \mathbf{GK}(s))^{-1}\mathbf{GK}(s)$ is the Complementary Sensitivity Function or Operator, $\mathbf{T}(s)$. Hence

$$\mathbf{y}(s) = \mathbf{Tr}(s) + \mathbf{Sd}(s) - \mathbf{Tn}(s) \tag{3.44}$$

and in addition

$$\mathbf{e}(s) = \mathbf{y}(s) - \mathbf{r}(s) = -\mathbf{Sr}(s) + \mathbf{Sd}(s) - \mathbf{Tn}(s) \tag{3.45}$$

$$\mathbf{u}(s) = \mathbf{KSr}(s) - \mathbf{KSd}(s) - \mathbf{KSn}(s) \tag{3.46}$$

(3.45) shows that in order to keep controller error low, $\mathbf{S}(s)$ must be kept low or, alternatively, (3.44) shows that $\mathbf{T}(s)$ must approach $\mathbf{I}$. It can also be seen that a low value of $\mathbf{S}(s)$ suppresses process noise, whilst a low value of $\mathbf{T}(s)$ suppresses measurement noise. Control effort, as measured by plant input, $\mathbf{u}$, is dependent on $\mathbf{KS}(s)$.

The two sensitivity functions are related via

$$\mathbf{S}(s) + \mathbf{T}(s) = \mathbf{I} \tag{3.47}$$

and, for strictly proper $\mathbf{GK}(s)$,

$$Lim_{s\to\infty}\mathbf{S}(s) = \mathbf{I} \tag{3.48}$$

$$Lim_{s\to\infty}\mathbf{T}(s) = \mathbf{0} \tag{3.49}$$

This poses a set of interesting controller design problems. It is desirable to keep $\mathbf{S}(s)$ low to minimise controller error and plant disturbance but this tends to elevate $\mathbf{T}(s)$ which aggravates measurement noise. In addition, as discussed in section 3.3.3, high values of $\mathbf{T}(s)$ lead to a lack of robustness and so are inadvisable where plant model uncertainty is significant.

The typical solution involves a trade-off between $\mathbf{S}(s)$ and $\mathbf{T}(s)$ across the frequency range. The reference inputs and plant disturbance are usually of low frequency so at low frequencies $\mathbf{S}(j\omega)$ is kept low, the bandwidth of the resulting system being conveniently defined in terms of this 'low' region of $\mathbf{S}(j\omega)$. Since measurement noise and plant uncertainty are generally more significant at higher frequencies (in the latter case due to neglected higher order dynamics), the elevated magnitude of $\mathbf{T}(j\omega)$ in the low frequency range is generally tolerable. Conversely, at higher frequencies it is desirable to constrain the magnitude of $\mathbf{T}(j\omega)$ to tolerate greater plant uncertainty and measurement noise, so here $\mathbf{S}(j\omega)$ is allowed to rise towards unity on the assumption that reference inputs and plant disturbance are not significant at these frequencies. In fact, as shown by (3.48), this rise in $\mathbf{S}(j\omega)$ is inevitable at high frequencies. Control effort can be constrained, if required, by limiting the magnitude of $\mathbf{KS}(s)$.

The mixed sensitivity approach described in section 3.3.4 represents a formal method for achieving this trade-off.

3.3.3 Robustness Criteria

The robustness of a control system is a measure of its ability to tolerate variations in the plant. The controller is designed on the basis of a nominal plant model but, owing to model uncertainty, the controller may be used with any of a set of possible plants and therefore some degree of robustness is required.

Model Uncertainty

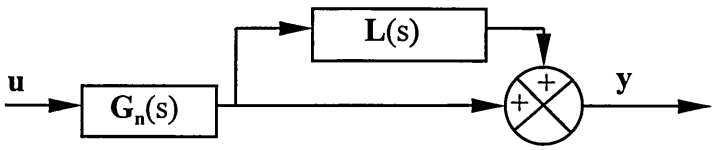

Fig 3.6 Unstructured Multiplicative Output Model Uncertainty

Restricting consideration of plant perturbation to unstructured uncertainty, where all the possible causes of plant variation from the nominal model are lumped into a single parameter, and using the mutiplicative output model[61] shown in Fig 3.6, the set of all possible plant models, $\mathbf{G}(s)$, is expressed in terms of the nominal plant model, $\mathbf{G}_n(s)$ by[62]

$$\mathbf{G}(s) = (\mathbf{I} + \mathbf{L}(s))\mathbf{G}_n(s) \tag{3.50}$$

Here the perturbation, $\mathbf{L}(s)$, is given by

$$\mathbf{L}(s) = l(s)\Delta(s) \tag{3.51}$$

where $l(s)$ is a real scalar and $\|\Delta(s)\|_\infty \leq 1$.

The closed-loop plant with controller is shown in Fig 3.7.

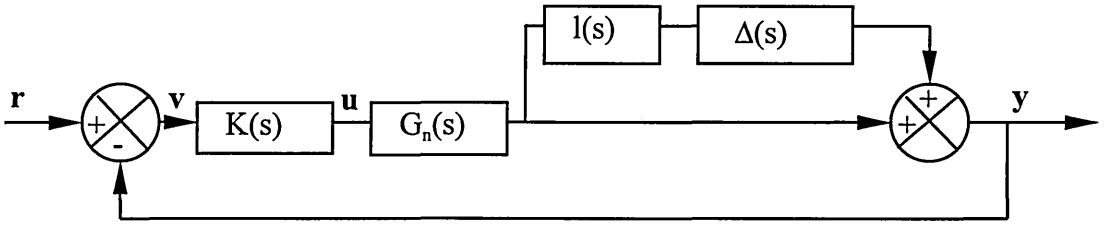

Fig 3.7 Controller with Model Uncertainty

The set of possible plants is given by all the possible $\Delta(s)$ such that $\|\Delta(s)\|_\infty \leq 1$, i.e. at any particular frequency the possible plant models are given by

$$\mathbf{G}(j\omega) = (\mathbf{I} + l(\omega)\Delta(j\omega))\mathbf{G}_n(j\omega) \tag{3.52}$$

for all $\Delta(j\omega)$ such that $\bar{\sigma}(\Delta(j\omega)) \leq 1$.

Robust Stability (RS)

A system is robustly stable if it is stable for all possible plant models. Provided that the system shown in Fig 3.7 is stable for the nominal plant it is stable if and only if [63]

$$\|\mathbf{T}_n(s)l(s)\|_\infty < 1 \tag{3.53}$$

where $\mathbf{T}_n(s)$ is the complementary sensitivity of the nominal system.

This can be written

$$\text{RS} \Leftrightarrow \bar{\sigma}(\mathbf{T}_n(j\omega)) < l^{-1}(\omega), \forall\omega \tag{3.54}$$

From (3.54) it can be seen that robust stability requires the imposition of an upper bound on $\mathbf{T}_n(j\omega)$ across the frequency range. In particular, increases in plant uncertainty as indicated by an increase in $l(\omega)$ impose increasing constraints on the magnitude of $\mathbf{T}_n(j\omega)$.

Robust Performance (RP)

It is common practice to use a performance specification which places an upper bound on the sensitivity function, $\mathbf{S}(s)$, in order to limit controller error. Using an H^∞ description of operator magnitude, the robust performance criterion can be written[64]

$$\text{RP} \Leftrightarrow \|\mathbf{S}(s)w(s)\|_\infty < 1 \tag{3.55}$$

for all possible plant models. $w(s)$ is a scalar weight chosen to reflect the relative urgency of suppressing $\mathbf{S}(s)$ at different frequencies over the operating range. In the case of the unstructured, multiplicative output uncertainty description

$$\text{RP} \Leftrightarrow \|\mathbf{S}(s)w(s)\|_\infty < 1 \text{ for all possible plant models}$$

$$\Leftarrow \|\mathbf{S}_n(s)w(s)\|_\infty + \|\mathbf{T}_n(s)l(s)\|_\infty < 1 \tag{3.56}$$

(3.56) gives a sufficient (but not necessary) condition for RP in terms of the nominal plant model and the uncertainty parameter, $l(s)$. This satisfies the RS criterion and the performance criterion for the nominal system by some margin.

The form of (3.56) provides the motivation for a mixed sensitivity approach to robust controller design.

3.3.4 Mixed Sensitivity and H^∞ Optimisation

The mixed sensitivity approach is motivated by a desire to achieve a balance between the different requirements of the controller over the operating frequency range. It is necessary to consider an augmented plant model with exogenous inputs, **w**, and weighted exogenous outputs, **z**. The augmented plant model used in the present work is shown in Fig 3.8.

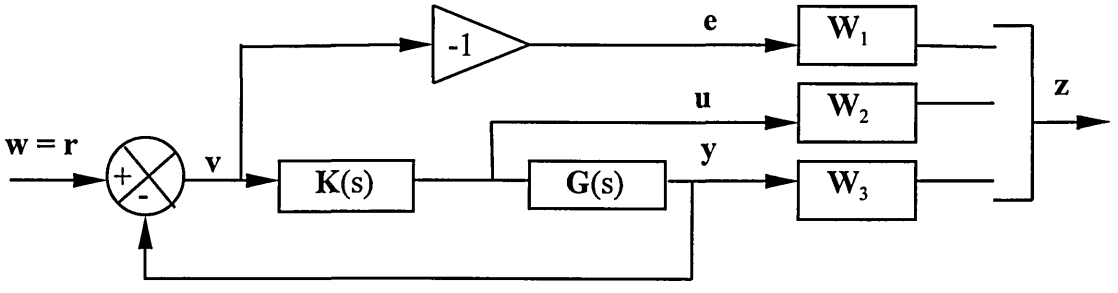

Fig 3.8 Augmented Plant Model with Controller

Process and measurement noise were not considered, but weighted forms of the error vector, **e**, the control input vector, **u**, and the plant outputs, **y**, were included in the augmented plant. Thus the inputs and outputs of the augmented plant become

$$\mathbf{w} = \mathbf{r} \tag{3.57}$$

and

$$\mathbf{z} = \begin{bmatrix} \mathbf{W}_1(s)\mathbf{e}(s) \\ \mathbf{W}_2(s)\mathbf{u}(s) \\ \mathbf{W}_3(s)\mathbf{y}(s) \end{bmatrix} \tag{3.58}$$

Using (3.44), (3.45) and (3.46), (3.58) may be written

$$\mathbf{z} = \begin{bmatrix} -\mathbf{W}_1\mathbf{S}(s) \\ \mathbf{W}_2\mathbf{K}\mathbf{S}(s) \\ \mathbf{W}_3\mathbf{T}(s) \end{bmatrix} \mathbf{w} \tag{3.59}$$

Here, $\begin{bmatrix} \mathbf{W}_1\mathbf{S}(s) \\ \mathbf{W}_2\mathbf{K}\mathbf{S}(s) \\ \mathbf{W}_3\mathbf{T}(s) \end{bmatrix} = \mathbf{T}_{zw}(s)$, the augmented transfer function from inputs **w** to outputs **z**, ignoring the sign in the $\mathbf{e}(s)$ component since magnitudes are being considered here.

The objective of the mixed sensitivity approach is to design a controller which minimises the magnitude of $\mathbf{T}_{zw}(s)$, measured in some way, for a choice of weighting functions which achieves suitable controller characteristics in terms of stability and performance, control effort and robustness. Obviously, the choice of weights is a central problem to controller design. As a starting point it is expedient to proceed on the basis of the results given in section 3.3.2, choosing $\mathbf{W}_1(s)$ high within the required system bandwidth to suppress the magnitude of $\mathbf{S}(s)$. $\mathbf{W}_3(s)$ is chosen to suppress $\mathbf{T}(s)$ in the upper frequency range where plant uncertainty may be significant (whilst bearing in mind the complementarity of $\mathbf{S}(s)$ and $\mathbf{T}(s)$). $\mathbf{W}_2(s)$ can be manipulated as necessary to achieve the desired level of control effort.

The H^∞ optimal control synthesis problem results when the H^∞ norm is used as a measure of the magnitude of $\mathbf{T}_{zw}(s)$. Much work has been done on the development of algorithms to solve the H^∞ optimal control problem. For the present work functions *hinf*

and *hinfopt* in Matlab's Robust Control Toolbox (RCTB) [65] were used. *Hinf* computes the 'central' controller of a family of controllers which satisfy the condition

$$\|\mathbf{T}_{zw}(s)\|_\infty < 1 \tag{3.60}$$

if such a family exists. This is the Standard H^∞ control problem. *Hinfopt* computes the unique controller which maximises γ such that

$$\gamma\|\mathbf{T}_{zw}(s)\|_\infty < 1 \tag{3.61}$$

(The inequality is written in this form because *hinfopt* provides the option of selecting a subset of the rows of $\mathbf{T}_{zw}(s)$ to be premultiplied by γ. For instance, the optimisation could be based on $\left\| \begin{matrix} \gamma \mathbf{W}_1\mathbf{S} \\ \mathbf{W}_2\mathbf{K}\mathbf{S} \\ \mathbf{W}_3\mathbf{T} \end{matrix} \right\|_\infty < 1$). This is called the H^∞ optimal control problem.

The RCTB also provides a function, *augtf*, which computes the generalised model of the augmented plant in a form suitable for H^∞ controller synthesis given the original plant model and the weighting functions. The generalised model takes the form of **P** in Fig 3.9.

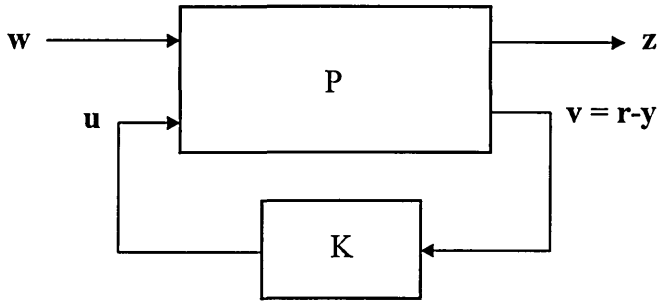

Fig 3.9 Generalised Model of Augmented System

In terms of this model, $\mathbf{T}_{zw}(s)$ is given by the lower linear fractional transformation of **P** and **K** as follows[66]:-

$$\mathbf{T}_{zw} = F_l(\mathbf{P},\mathbf{K}) = \mathbf{P}_{11} + \mathbf{P}_{12}\mathbf{K}(\mathbf{I} - \mathbf{P}_{22}\mathbf{K})^{-1}\mathbf{P}_{21} \tag{3.62}$$

where $\begin{bmatrix} \mathbf{z} \\ \mathbf{v} \end{bmatrix} = \begin{bmatrix} \mathbf{P}_{11} & \mathbf{P}_{12} \\ \mathbf{P}_{21} & \mathbf{P}_{22} \end{bmatrix} \begin{bmatrix} \mathbf{w} \\ \mathbf{u} \end{bmatrix}$.

Comparing (3.53) and (3.60) a correspondence between $\mathbf{W}_3(s)$ and $l(s)$ can be deduced.

From (3.60) it follows that

$$\bar{\sigma}(\mathbf{W}_3\mathbf{T}(j\omega)) < 1, \forall\omega \tag{3.63}$$

whilst from (3.53)

$$\bar{\sigma}(\mathbf{T}(j\omega))l(\omega) < 1, \forall\omega \tag{3.64}$$

In the case of SISO systems these reduce to $|W_3(j\omega)|.|T(j\omega)| < 1$ and $l(\omega)|T(j\omega)| < 1$ respectively and since $l(\omega) = \left|\frac{G(j\omega) - G_n(j\omega)}{G_n(j\omega)}\right|$, $|W_3(s)|$ is a direct measure of the multiplicative uncertainty of the plant model.

3.4 Model Reduction

The controller resulting from the synthesis of the H^∞ controller is of the same order as the augmented plant. In the present work that is typically 10^{th} or 12^{th} order depending on weight selection. Obviously, it is desirable to investigate ways of reducing this order whilst preserving the properties of the controller. Two methods of model reduction were attempted in this work, balanced residualisation and optimal Hankel minimum degree approximation.

3.4.1 Balanced Residualisation[67]

This approach involves discarding states associated with relatively small Hankel singular values. The controller model is first balanced by a similarity transform such that the controllability and observability gramians are equal and diagonal, the diagonal elements being the ordered (descending) Hankel values. These values correspond to states of the balanced sytem and their relative magnitudes reflect the importance of the associated states on input/output behaviour. Unimportant states are eliminated by residualisation, which is to say that if x_r is to be eliminated, $\dot{x}_r$ is set to zero and the resulting equation used to eliminate x_r from the system of state equations. CSTB function *balreal* balances the system and produces the diagonal gramian containing the

Hankel singular values. Inspection of these permits an assessment of the number of states to be discarded and CSTB function *modred* is used to eliminate these by residualisation.

3.4.2 Optimal Hankel Minimum Degree Approximation (OHMDA)[68]

For a system $\mathbf{K}(s)$ of order n, the OHMDA is system $\mathbf{K}_r(s)$ of order k such that

$$\left\|\mathbf{K}(s)-\mathbf{K}_r(s)\right\|_\infty \leq 2\sum_{i=k+1}^{n}\sigma_i \qquad (3.65)$$

where the σ_i are the ordered Hankel singular values. RCTB function *ohkapp* computes the OHMDA of a system given the order of the reduced model. The system does not need to be balanced before *ohkapp* is called.

3.5 Comparison of Design Methods

Of the three design methods chosen for the beam and carriage controller, the LQG controller would appear to be the most direct in the sense that, if statistical data for plant disturbance and measurement noise are available, the controller can be designed without recourse to iteration. However, it has been shown that LQG controller designs have no guaranteed stability margins [25] and may therefore result in unsatisfactory controllers for systems where plant perturbation is present. For control systems based on state feedback in which closed-loop plant and observer poles are chosen arbitrarily, a more iterative approach may be adopted. This permits an assessment of performance criteria for a range of possible designs, but no direct consideration of the resulting system robustness can be made at the design stage.

The characteristic locus method presents a more naturally iterative approach. The choice of frequency bands and single loop dynamic compensators at medium and low frequency are all subjective factors which influence the final design. As is the case for controllers based on state feedback, no explicit consideration of robustness can be incorporated into the controller design procedure.

The H^∞/mixed sensitivity approach enables robustness to be built into the system at the design stage. However, for this approach a choice of weighting is required for each element of the sensitivity operator chosen. This must take into account the required 'shape' of each sensitivity function with respect to frequency and the relative importance

of the different sensitivity functions. For this reason, significant iteration is again likely to be required in applying this method, but separate parameters exist for influencing controller error, control effort and robustness levels and this should theoretically facilitate the design of a controller which achieves a satisfactory compromise between these conflicting requirements.

4 Controller Designs Based on the Nominal Plant Model

It was considered appropriate to use the best available plant model as a basis for controller design. Thus the symmetrical model was discarded after early investigative work on LQG controller design and the nonsymmetrical model adopted for the work reported here. Controller designs based on state feedback were produced firstly in conjunction with LQG theory (state feedback via LQR theory, full order estimation by Kalman Filter) and secondly using a reduced order observer with observer pole placement in conjunction with LQR theory for state feedback. In addition to these, controller designs based on the Characteristic Locus Method and on H^{∞}/Mixed Sensitivity were developed.

The performance of all controller designs with the nominal plant model was simulated in continuous and discrete forms using step inputs for the components of the reference input vector, **r**. All satisfactory designs were then implemented on the beam and carriage apparatus.

4.1 Controller Implementation Details

Prior to use with the controller, the beam and carriage was set up in a standard manner. The output of the ultrasonic transducer monitoring horizontal carriage position was calibrated using the gain and offset potentiometers on the transducer to give outputs of 0V and 10V for the leftmost and rightmost positions of the carriage on the beam respectively. The bipolar voltage supply to the two resistive transducers was adjusted to $\pm$10V such that the output of each transducer was -10V and +10V when the corresponding ram was at its top and bottom position respectively. The power amplifiers for the hydraulic valves each had separate gain settings for piston advance and retract commands and a potentiometer setting for the valve deadband. The potentiometers were set to give maximum velocity for a given voltage command on the piston outstroke and a matching velocity on the piston instroke (where a reduced gain was required to reduce the flow rate into the annular side of the piston). The deadband on each amplifier/valve combination was set to minimum. Finally, the regulator for air pressure inside the beam was set to 0.1 bar.

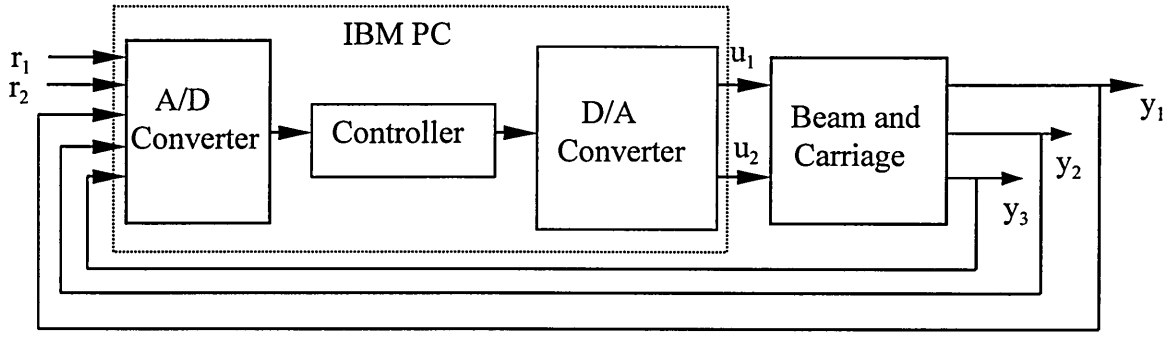

Fig 4.1 Controller Implementation

The general configuration of the controller and beam and carriage is shown in Fig 4.1. Here the controller took the form of an IBM PC compatible executing compiled code produced by the Borland Turbo Pascal V6.0[69] compiler. The computer interface for analog signals and the real time clock required for interval timing were provided by a Keithley DAC1601[70] data acquisition card. This provided 16 channels of analog input via a 12 bit A/D converter and 2 channels of analog output via a 12 bit D/A converter. A range setting of ± 10V was selected for all analog signals and the calibration of the converters verified. The maximum conversion rate of the A/D converter was 100 kHz.

Euler's method[71] was adopted for the controller discretisations used in both the discrete simulations and the actual implementation. For a continuous system in state space form given by

$$\dot{\mathbf{x}} = \mathbf{A}\mathbf{x} + \mathbf{B}\mathbf{u} \tag{4.1}$$

$$\mathbf{y} = \mathbf{C}\mathbf{x} + \mathbf{D}\mathbf{u} \tag{4.2}$$

Euler's method gives the difference equations

$$\mathbf{x}(k+1) = (\mathbf{I} + \mathbf{A}\mathrm{T})\mathbf{x}(k) + \mathbf{B}\mathrm{T}\mathbf{u}(k) \tag{4.3}$$

$$\mathbf{y}(k) = \mathbf{C}\mathbf{x}(k) + \mathbf{D}\mathbf{u}(k) \tag{4.4}$$

where T is the sampling interval. As can be seen from Fig 4.1, the IBM PC performed the task of closing the control loop in addition to implementing the controller.The PC also rescaled the ultrasonic transducer to ± 10V and averaged the output of the two resistive transducers for all but the ROE controller (for which all three outputs were required).

Pascal code was written for each of the controller implementations and the minimum sampling intervals determined by checking the maximum execution times for the program iterations. In each case a reliable sampling interval of 5ms of less was attainable. Discrete simulations showed that sampling rates of this order were sufficient to implement the controllers reported here by some margin, so recourse to more sophisticated disretisation methods than Euler was not made.

For the tests carried out on the rig, the reference inputs were supplied (in the range $\pm$ 10V by two potentiometers or, for the step tests, using step inputs applied individually to the controller inputs. A Gould DSO400 oscilloscope was used to capture the step inputs and the beam and carriage output responses. (For all but the ROO controller the outputs of the two vertical ram position transducers were averaged using a simple summing circuit to give output y_2). The captured traces were downloaded to an IBM PC via the DSO400's serial interface.

4.2 Controller Based on LQG Theory

Early LQG work based on the symmetric model [72] produced a controller for the beam and carriage, implemented on a set of analogue modellers, which resulted in a stable, essentially decoupled system. This work was repeated for the nonsymmetrical model and the controller implemented on a digital computer to enable comparison with the other digitally implemented controllers. As in the earlier work, **Q** and **R** were initially chosen as $\mathbf{I}_2$ for the LQR design and **W** and **V** as $0.001\mathbf{B}\mathbf{B}^T$ and $0.01\mathbf{I}_2$ respectively for the Kalman Filter design. The design was carried out using the user-written M-file *lqg* (see the M-file listings). This gave the coefficients of the feedback matrix, **K**, the coefficients of the state estimator in state-space form and the static decoupling matrix, which is the inverse of the DC gain matrix of plant plus state feedback.

The state feedback placed the plant poles at -49.44, -45.50, -4.99, -4.11, -1.30 ± 1.46j and the estimator poles were placed at -49.48, -45.54, -4.28, -3.91, -0.77 ± 0.80j. The resulting system, closed loop plant plus estimator, is 12^{th} order and its poles are given by the union of the above two sets. The slowest estimator pole was significantly faster than the slowest open loop plant pole at 0.0 but slower than the slowest closed loop plant poles at -1.30 ± 1.46j. Also, given that the open loop plant poles were at -49.48, -45.54, -4.22, -3.86, 0, 0, it is clear that the Kalman Filter could not accurately estimate the transient system states following the application of step changes in the reference input.

4.2.1 LQG Controller Simulations

Continuous and discrete simulations were carried out on the LQG design. Fig 4.2 shows the simulink model for the continuous simulation. This gives the plant outputs and inputs for unit steps on r_1 and r_2 at 2 and 6 seconds respectively and these are shown in Figs 4.3 to 4.6. These graphs indicate satisfactory performance of the controlled outputs with no steady state error, overshoot on y_1 of less than 10% and negligible dynamic interaction. The maximum plant input signal levels are only some 20% higher than the step inputs and unlikely to lead to plant saturation. Attempts were made to improve performance by manipulation of the **Q** and **R** matrices used in the LQR design process. Since plant input levels were considered satisfactory, **R** was held at $\mathbf{I}_2$ and only changes in the (diagonal) elements of **Q** were considered. The obvious choice was to increase q_{11} to constrain overshoot on the horizontal carriage position, y_1, ram height control being much better behaved. However, increases in q_{11}, whilst reducing the settling time of y_1, did this at the expense of increases in both plant inputs in response to step inputs on r_1 and had little effect on the level of overshoot of y_1. For these reasons it was considered that the initial values of **Q** and **R** achieved a satisfactory LQR design for the beam and carriage.

The Simulink model of the plant with discrete controller (i.e. with the estimator implemented in discrete form using Euler's method) is given in Fig 4.7. Saturation blocks were inserted to simulate the limits on signals in the actual plant (± 10V) resulting from the use of D/A and A/D converters to produce the control inputs and sample the plant outputs respectively. For this discrete model the reference inputs were scaled up to 8V steps in order to test the controller more severely, the saturation blocks being inserted to enable detection of instability arising from large signal levels and the resulting saturation. The plant outputs and inputs using a sampling interval of 0.02 seconds are shown in Figs 4.8 to 4.11. These indicate plant performance comparable to the continuous model. Simulations repeated for a variety of sampling intervals showed that stable performance of the model was sustained for values of T up to 0.04 seconds.

4.2.2 LQG Controller Implementation

Figs 4.12 to 4.15 show the actual plant outputs achieved for reference input steps of approximately 7V using a sampling interval of 4ms. From these Figs it can be seen that a significant cyclic drift is present on y_1 in the actual implementation and some

interaction between y_1 and r_2 is apparent. Stable behaviour of the actual plant was sustained for sampling intervals up to 35ms.

4.3 Controller Based on the Reduced Order Observer (ROO)

Work on the design of a reduced order observer for the beam and carriage has been reported elsewhere [73]. For the reduced order observer it was desirable to define as many states as possible as measured outputs. For this reason the plant outputs were redefined as the three measured variables corresponding to x_1, x_2 and x_3 such that $x_1 = y_1,\ x_2 = y_2, x_3 = y_3, x_4 = \dot{y}_1, x_5 = \dot{y}_2, x_6 = \dot{y}_3$. This involved redefining state matrix **C** as

$$\mathbf{C} = \begin{bmatrix} 1 & 0 & 0 & 0 & 0 & 0 \\ 0 & 1 & 0 & 0 & 0 & 0 \\ 0 & 0 & 1 & 0 & 0 & 0 \end{bmatrix} \tag{4.5}$$

resulting in a non-square system with two inputs and three outputs. This permitted partitioning of the state equations to give

$$\mathbf{x}_a = \begin{bmatrix} x_1 \\ x_2 \\ x_3 \end{bmatrix} = \begin{bmatrix} y_1 \\ y_2 \\ y_3 \end{bmatrix} \tag{4.6}$$

$$\mathbf{x}_b = \begin{bmatrix} \dot{x}_1 \\ \dot{x}_2 \\ \dot{x}_3 \end{bmatrix} \tag{4.7}$$

Here $\mathbf{x}_a$ contains the measured states whilst the components of $\mathbf{x}_b$ are the states to be estimated.

The state feedback was derived using LQR theory, as for the LQG controller, with unity weightings on each of the plant's outputs and inputs (in this case, $\mathbf{Q} = \mathbf{I}_3$, $\mathbf{R} = \mathbf{I}_2$). This resulted in closed loop poles at -49.31, -45.37, -5.95, -5.55, -1.15 ± 1.30j.

The observer design involved the arbitrary selection of the three observer poles, each required to be fast compared to the open loop plant poles. The M-file *redest* was used to obtain the observer parameters, the required observer poles being input to *redest* in the vector **p**. The state feedback matrix produced by the LQR design had relatively small coefficients in the fifth and sixth columns, the largest of these having a magnitude of

0.015 compared to the smallest coefficient magnitude in the first four columns of 0.32. For this reason states x_5 and x_6, the ram velocities, were discarded for purposes of state feedback and, since the state space description of the observer, ($\mathbf{A}_e$, $\mathbf{B}_e$, $\mathbf{C}_e$, $\mathbf{D}_e$) showed that these states were not required to provide the estimate of x_4, carriage velocity, the observer was simplified to give the first order observer, ($\mathbf{A}_{es}$, $\mathbf{B}_{es}$, C_{es}, $\mathbf{D}_{es}$), also calculated by *redest*. (This observer was further simplified by the fact that estimation of x_4 did not require use of the plant input, **u**). For this simplified observer it was only necessary to choose one pole.

4.3.1 ROO Controller Simulations

The Simulink model used to provide simulations of the controller based on the continuous, third order observer with unit step inputs at 2 and 6 seconds is shown in Fig 4.16. Saturation blocks of ± 1.5 have been added immediately before and after the plant, at the point of D/A and A/D conversions, to ensure that saturation due to unreasonably large signals is likely to be simulated in the model. The plant output and control input signals produced by this simulation model with observer poles at -10, -10 ± 10j are shown in Figs 4.17 to 4.21. These show system performance consistent with the LQG model. The 'bumps' on y_2 and y_3 in Figs 4.18 and 4.19 at 2 seconds are due to the redefinition of the plant outputs: obviously the left and right hand rams move up and down respectively to advance the carriage along the beam.

Fig 4.22 shows the Simulink model for the simplified, continuous controller using the first order observer and the resulting plant outputs and inputs with observer pole at -10 are shown in Figs 4.23 to 4.27. There is no noticeable loss in performance as a result of the controller simplification.

The Simulink model representing the controller with first order observer discretised by Euler's method is shown in Fig 4.28 and the corresponding plant outputs and inputs with a sampling interval of T = 0.02 seconds and 8V steps applied to r_1 at 2 seconds and r_2 at 6 seconds are shown in Figs 4.29 to 4.33. The 8V steps were again chosen to produce reasonably severe operating conditions in relation to the ± 10V saturation levels imposed on the model. Comparing Figs 4.29 to 4.33 with Figs 4.17 to 4.21, it can be seen that the discrete, simplified controller performs satisfactorily compared with the continuous, unsimplified one.

For the state observer, the faster the choice of pole, the higher the observer gain will be. This would cause rescaling of the observer equations to be necessary to avoid saturation if the the observer were implemented in analogue form but where it is implemented on a digital computer large values of the intermediate variables can be tolerated and the observer output will be no larger than for an observer with slower poles. However, faster poles would require faster signal sampling rates for the controller to perform satisfactorily as was borne out by further simulation work. Whilst the controller based on the discrete observer with pole at -10 gave stable simulated behaviour for sampling intervals up to 0.2 seconds, a controller based on an observer with pole at -500 required a sampling interval of not more than 0.004 seconds. Poles between these two required sampling intervals of between 0.2 and 0.004 seconds on a roughly proportional basis. Thus, available sampling rate at the implementation stage is a factor which must be borne in mind when selecting observer pole positions.

4.3.2 ROO Controller Implementation

The controller was again discretised by Euler's method and implemented on an IBM compatible PC using code compiled by Turbo Pascal. With this implementation sampling intervals down to 2ms were achievable. The first two plant outputs obtained in response to step inputs of approximately 7V at 2 and 6 seconds on r_1 and r_2 respectively are shown in Figs 4.34 to 4.37. Output y_3 is omitted since its behaviour is virtually identical to y_2 (although, of course, y_3 goes negative in response to a positive step on r_1). These graphs show that the controller performance predicted by simulations has essentially been achieved in practice with very little of the drift experienced with the LQG controller. The controller exhibited stable behaviour, though with progressive degradation of performance, using sampling intervals up to approximately 0.175 seconds.

4.4 The LQG Controller Revisited

The superior performance of the controller implementation based on the ROO to that produced by LQG design theory poses the following questions:-

(i) Why is the drift so pronounced (and at the implementation stage only) with the LQG controller?

(ii) Why is the sampling interval constraint much lower for the LQG controller, even though the slowest pole is much slower than that for the ROO?

The answer to (ii) is that the LQG controller's estimator also has significantly faster poles than the ROO. The dynamics of these are required to produce satisfactory state estimates.

To answer (i), attempts were made to manipulate the covariance matrices **W** and **V**, in order to produce faster estimator poles comparable to the ROO pole. This would seem to be especially desirable in view of the unfavourable comparison of the original LQG estimator poles with the open loop plant poles. The estimator poles become faster as process noise covariance, **W**, increases, thus allowing the estimated states to respond more quickly to this disturbance, and slower as measurement noise covariance, **V**, increases, for the opposite reason. As a check on the effect of estimator poles on the implementation of the LQG controller, **W** was changed from $0.001\mathbf{B}\mathbf{B}^T$ to $\mathbf{B}\mathbf{B}^T$ and **V** from $0.01\mathbf{I}_2$ to $0.0001\mathbf{I}_2$. The Kalman filter design now produced an estimator with slowest poles at $-5.83 \pm 9.89j$ and the plant outputs obtained from the implementation of this controller are shown in Figs 4.38 to 4.41. The drift is virtually eliminated by this controller since the controller is designed to react more quickly to plant disturbance (and also, undesirably, to measurement noise) and is therefore more responsive.

Dutton et al. [74] give a fuller interpretation of the effect of **W** and **V** on estimator poles. For systems with large measurement noise relative to process noise, the Kalman Filter gain is decreased to give less prominence to plant outputs and more to the plant prediction part of the estimator. Conversely, relatively uncertain plant behaviour results in a high filter gain to place more emphasis on measured outputs. Higher estimator gains are associated with faster estimator poles.

4.5 Controller Design by the Characteristic Locus (CL) Method

To implement the characteristic locus method it was necessary to choose a suitable working frequency range for the design process and three separate frequencies upon which the three stages of compensation were to be based. Referring to Figs. 2.17 to 2.20, a working frequency range of 0.01 to 100 rs^{-1} was chosen, encompassing the dynamic range of the model from virtually steady state to a gain of less than -40 dB. The multivariable frequency response (MVFR) matrix was created for a set of discrete

frequencies across this range using MVFDTB function *mv2fr*. The MVFR matrix consists of a set of component matrices corresponding to the set of frequencies selected, each component matrix being the gain matrix in complex form at a particular frequency. This matrix provides the basic data for the toolbox functions *align*, *feig* and *facc*, which align the eigenvectors of the system, calculate the characteristic loci and compute the parameters of the ACC respectively.

4.5.1 The High Frequency Compensator, $\mathbf{K}_h$

To design the high frequency compensator, a frequency corresponding to one of the component matrices in the MVFR matrix is chosen and the component matrix diagonalised by eigenvector alignment using MVFDTB function *align*. The presumption is that eigenvector alignment spreads over a useful frequency range and this can be checked by using function *fmisalg* to compute the resulting alignment for each component matrix in the working frequency range.

For the earlier work on the symmetrical model, perfect alignment across the whole frequency range was achieved (although *fmisalg* reported nonzero alignment at the target frequency itself - possibly a quirk of the numerical processing). This is to be expected since, as shown in section 2.2.4, perfect diagonalisation of this model is achievable using a constant, decoupling compensator. For the symmetrical model *align* returned a compensator given by

$$\mathbf{K}_h = \begin{bmatrix} 1107.8 & -5.9 \\ -1107.8 & -5.9 \end{bmatrix} \tag{4.8}$$

which compares with the decoupler, $\begin{bmatrix} 0.5 & 0.5 \\ -0.5 & 0.5 \end{bmatrix}$, suggested in 2.2.4. The particular values computed for $\mathbf{K}_h$ are due to the fact that align, in addition to diagonalising the system, tries to achieve $|\mathbf{G}(j\omega_h)\mathbf{K}_h| = \mathbf{I}$, where the notation $|\mathbf{Q}|$ is taken to mean

$$\begin{bmatrix} |q_{11}| & |q_{12}| & . & . \\ |q_{21}| & . & . & . \\ . & . & . & . \\ . & . & . & . \end{bmatrix}.$$

For the nonsymmetrical model, the frequency upon which the computation of $\mathbf{K}_h$ was based, ω_h, was chosen as 30 rs^{-1}, this being at the top of the model's dynamic range. The value returned for $\mathbf{K}_h$ was

$$\mathbf{K}_h = \begin{bmatrix} 83.84 & -10.16 \\ -77.53 & -9.39 \end{bmatrix} \qquad (4.9)$$

resulting in a maximum alignment error of 12.9^o.

The high frequency compensator for each model has a second column which is negative compared to the simple decoupling compensator. The alignment process can result in eigenvectors pointing in either direction along the basis vectors and in this case the negative second column of $\mathbf{K}_h$ results in a negative second column of the diagonalised $\mathbf{GK}_h$ leading to positive feedback in the second loop of a controller based on output feedback. In general, it is necessary to inspect the columns of $\mathbf{K}_h$ and adjust their signs where appropriate before proceeding to the next stage. In this case the sign of the second column of $\mathbf{K}_h$ was changed.

4.5.2 The Mid Frequency Compensator, $\mathbf{K}_m(s)$

This compensator was based on an ACC design for which a 'central' frequency and a dynamic compensator for each loop in the (approximately) diagonalised system was required to be chosen. Fig 4.42 shows the characteristic loci for the diagonalised model. Stability requirements alone indicate the need to introduce positive phase shift into the loop corresponding to the first characteristic locus, $q_1(s)$, so a lead-lag compensator of the form

$$\mathrm{K}_d(s) = \frac{s+a}{s+\alpha a} \qquad (4.10)$$

where $\alpha > 1$, was investigated for this loop, the second loop being left without compensation at this stage. The compensator of (4.10), having unity gain at high frequencies, has the advantage of not disturbing the alignment produced by $\mathbf{K}_h$ at these frequencies but in the present case some high frequency attenuation was required to avoid excessive control effort (as manifested by large magnitude of the plant input vector, $\mathbf{u}$) in response to steps on the reference inputs.

Using a dynamic compensator given by

$$\mathbf{K}_d(s) = diag\left(\frac{s+1}{50(s+10)},\ 1\right) \qquad (4.11)$$

a first order ACC was produced. (The ACC is the same order as $\mathbf{K}_d(s)$ since it was produced from $\mathbf{K}_d(s)$ by manipulation involving constant matrices only). The frequency upon which the ACC was based is 0.1 rs^{-1}.

The characteristic loci of the system with high and mid frequency compensators are shown in Fig 4.43. There is now a positive phase margin on $q_1(s)$ and the stability of the closed loop system using the two compensators is confirmed by Fig 4.44 which shows the plant outputs in response to unit steps on the reference inputs. Fig 4.45 shows the corresponding plant inputs. From Fig 4.45 it can be seen that the maximum control effort required in the first control loop is somewhat less than 2, which is acceptable in the context of a unit step input on the reference input of loop 1. However, in the second control loop, the control effort is of the order of 10V for a 1V reference input and is likely to lead to plant saturation. In addition, there is a steady state error in the second loop. These problems were attended to at the third stage of compensation.

The performance of the first control loop is rather unsatisfactory and does not compare well with the compensators based on state feedback. It was possible to reduce the overshoot and the settling time using a simple lead-lag compensator in this loop but only at the cost of excessive control effort. Second order compensation was also tried but this gave rise to problems which will be discussed in section 4.4.5.

4.5.3 The Low Frequency Compensator, $K_l(s)$

This compensator was based upon an ACC for which no compensation was introduced into the first loop and proportional plus integral compensation was introduced into the second to eliminate steady state error. The dynamic compensator upon which the ACC was based is

$$\mathbf{K}_d(s) = diag(1,\ 0.2 + \frac{0.5}{s}) \tag{4.12}$$

which resulted in a first order low frequency compensator. The frequency upon which this ACC was based was 0.01 rs^{-1}, representing essentially steady state conditions for the compensated plant.

4.5.4 CL Controller Simulations

The design and simulation of the continuous controller based on the characteristic locus method was carried out using the M-file *charloc*. The final compensator, based on the high, medium and low frequency compensators discussed above was second order and was given in state space form by

$$\mathbf{A}_k = \begin{bmatrix} 0 & 0 \\ -0.0015 & -10 \end{bmatrix} \tag{4.13}$$

$$\mathbf{B}_k = \begin{bmatrix} 0 & -1 \\ -1 & -0.0093 \end{bmatrix} \tag{4.14}$$

$$\mathbf{C}_k = \begin{bmatrix} -4.79 & 15.09 \\ -4.96 & -13.96 \end{bmatrix} \tag{4.15}$$

$$\mathbf{D}_k = \begin{bmatrix} 1.68 & 1.93 \\ -1.55 & 1.97 \end{bmatrix} \tag{4.16}$$

The plant outputs and inputs using this controller with step reference inputs were produced directly from *charloc* and are shown in Figs 4.46 and 4.47. The integral term in $\mathbf{K}_I(s)$ has eliminated the steady state error on y_2 and the attenuation introduced in the proportional term has eliminated overshoot in y_2 and reduced the control effort in the second loop to an acceptable level.

A Simulink model of the discretised characteristic locus controller is shown in Fig 4.48. The discretisation of the controller was carried out using Euler's method and ± 10V saturation blocks were again inserted to model any saturation resulting from the 8V steps on r_1 and r_2 at 0 and 5 seconds respectively. The plant outputs and inputs obtained from this model with a sampling interval of 0.01 seconds are shown in Figs 4.49 to 4.52. Overshoot on y_1 of the order of 90% was certainly excessive but, as explained earlier, attempts to find a viable compensator based on second order compensation in the first loop had proved unsuccessful. With the existing signal saturation levels of ± 10V, saturation occurred in y_1, u_1 and u_2 and the simulation includes the effect of this.

4.5.5 CL Controller Implementation

As for the previous controllers, the implementation was based on a compensator discretised using Euler's method. In this case the controller utilised a second order compensator inserted into the forward path. Figs 4.53 to 4.56 show plant outputs y_1 and y_2 obtained in response to step inputs of approximately 7V on the actual plant. The overshoot on y_1 is somewhat less than would be expected from the simulations but there is a low frequency drift similar to that which existed for the first LQG controller.

In an attempt to improve the performance of the system, a second order term was introduced for the first diagonal component of the mid frequency compensator to give

$$\mathbf{K}_d(s) = diag\left(\frac{(s+1)^2}{50(s+3)^2}, 1\right) \tag{4.17}$$

Trial simulations showed that this resulted in a much improved response in y_1 compared to simulations using the first order compensator and control effort was at a similar level. However, the implementation of the resulting third order compensator resulted in steady movement of the carriage to the right hand end of the beam, irrespective of the corresponding reference input. It was assumed that this was indicative of system instability and this assumption was supported by the fact that subsequent simulations showed that this compensator resulted in unstable behaviour when used in conjunction with the symmetrical beam and carriage model, whilst the previous, second order compensator was stable with both models. The inference is that the controller is very sensitive to plant model perturbation and hence that increasing the order of the mid frequency compensator, whilst improving performance with the nominal model, has resulted in a decrease in robustness sufficient to result in instability with the actual plant.

4.6 Controller Design by H^∞/Mixed Sensitivity

Central to the H^∞/mixed sensitivity controller design process are the choice of mixed sensitivity operator or function and the choice of weighting for each element of this function. It must also be decided whether to solve the standard H^∞ control problem using RCTB function *hinf* or the optimal control problem using *hinfopt*. In the latter case, it must be decided whether γ in (3.61) premultiplies all or a subset of the rows of the mixed sensitivity function before its optimal value is found by iteration.

For the present work, the mixed sensitivity function contained three elements: the sensitivity function **S**(s); **KS**(s), where **K**(s) is the forward path compensator's TFM; and the complementary sensitivity function **T**(s). Minimising the magnitude of suitably weighted forms of these functions, $\mathbf{W}_1\mathbf{S}$, $\mathbf{W}_2\mathbf{KS}$ and $\mathbf{W}_3\mathbf{T}$, allows constraints to be placed on controller error, ***y-r***, control effort, **u**, and controller robustness respectively. After some preliminary work it was decided to concentrate on the H^∞ optimal control problem with γ premultiplying all rows of the mixed sensitivity function, i.e. *hinfopt* was used to maximise γ where $\gamma \left\| \begin{matrix} \mathbf{W}_1\mathbf{S}(s) \\ \mathbf{W}_2\mathbf{KS}(s) \\ \mathbf{W}_3\mathbf{T}(s) \end{matrix} \right\|_\infty < 1$.

(Solving the standard H^{∞} control problem of finding a family of compensators, $\mathbf{K}(s)$, such that $\left\| \begin{matrix} \mathbf{W}_1\mathbf{S}(s) \\ \mathbf{W}_2\mathbf{KS}(s) \\ \mathbf{W}_3\mathbf{T}(s) \end{matrix} \right\|_{\infty} < 1$, it is necessary to specify weightings such that a compensator exists. If the magnitude of one or more weight is chosen too large, no compensator can satisfy this inequality. This is equivalent to the optimal control design process returning a value of γ less than one.).

4.6.1 Preliminary Weight Selection and Controller Design

Generally speaking, when selecting weights, good input tracking within the system bandwidth is of primary importance. To achieve this $\mathbf{W}_1$ must have high gain within the bandwidth to constrain sensitivity, **S**. However, at higher frequencies, where model uncertainty and measurement noise may be a problem, it is often desirable to limit **T** to achieve robustness and good noise rejection. Therefore, $\mathbf{W}_3$ may be required to be large at these frequencies. Since neither weight should interfere with the other, $\mathbf{W}_1$ should take the form of a low pass filter and $\mathbf{W}_3$ should be a high pass filter. Usually one or more lag-lead filters or first order lags are chosen for $\mathbf{W}_1$ and one or more lead-lag filters or differentiators for $\mathbf{W}_3$[75]. $\mathbf{W}_1$ would have high DC gain and its order and break frequencies chosen to give the required bandwidth with adequate roll-off rate and high frequency gain. $\mathbf{W}_3$ would normally be selected to give low DC gain within the required system bandwidth and higher gains at frequencies where model uncertainty and noise may be a problem. $\mathbf{W}_2$ should be chosen to limit the controller output to desired levels. For this a constant weight may be chosen or, where reference inputs with high frequency components such as step inputs are used, it may be chosen as a high pass filter to limit controller outputs at high frequency.

For the present work it was decided to operate within the bandwidth of the open loop plant as given by the Bode plots of Figs 2.17 to 2.20. The bandwidth of $g_{11}(s)$ and $g_{12}(s)$ can be seen from Figs 2.17 and 2.18 to be about 2 rs^{-1}, so the first element of $\mathbf{W}_1(s)$ was chosen to have a gain of 40 dB for $\omega < 2\,rs^{-1}$. Above this frequency, the gain was prescribed to fall at a rate of 40 dB/decade to a small final value such that **S**(s) was free to rise and **T**(s), governing robustness, was free to fall. Similarly, the second element of $\mathbf{W}_1(s)$ was determined by the bandwidth of $g_{21}(s)$ and $g_{22}(s)$ which can be seen from Figs 2.19 and 2.20 to be approximately 4 rs^{-1}, so the break frequency of this second element was 4 rs^{-1}. Thus the first weighting was given by

$$\mathbf{W}_1(s) = diag(\frac{(0.02s+1)^2}{0.01(0.5s+1)^2}, \frac{(0.01s+1)^2}{0.01(0.25s+1)^2}) \quad (4.18)$$

In order to select the third weight, $\mathbf{W}_3(s)$, a roll-off in $\mathbf{T}(s)$ of 40 dB/decade above 2 rs^{-1} for the carriage response and above 4 rs^{-1} for the response of the rams was prescribed and, accordingly, the weighting was chosen as

$$\mathbf{W}_3(s) = diag(\frac{s^2}{4}, \frac{s^2}{16}) \quad (4.19)$$

As a starting point, the second weight was chosen as

$$\mathbf{W}_2(s) = \mathbf{I}_2 \quad (4.20)$$

The H^∞ controller synthesis procedure is not directly applicable to plants with poles on the imaginary axis (the beam and carriage has two poles at zero). Following the procedure suggested by Chiang and Safonov [76], a special bilinear transform was applied to the plant prior to the controller synthesis and the transform applied in reverse to the resulting controller. In effect, the plant poles were moved 0.1 units to the right prior to the synthesis and the resulting controller poles moved left by the same amount.

For the weights above, the augmented plant and therefore the controller were tenth order. Application of CSTB function *balreal* indicated that a good fourth order approximation should exist (the first four elements of the diagonal gramian of the balanced system being large compared to the other elements). CSTB function *modred* was used to reduce the model by balanced residualisation and RCTB function *ohmkapp* to reduce it by optimal Hankel minimum degree approximation (OHMDA).

4.6.2 H^∞ Controller Simulation

The H^∞ controller design and the simulation of the continuous controller were carried out using the M-file *hinfinit*. Figs 4.57 and 4.58 show the plants outputs and inputs respectively produced by simulations of the continuous optimum H^∞ controller computed by RCTB function *hinfopt* using the above weightings and reduced to fourth order by balanced residualisation. The fourth order model reduced by OHMDA resulted in an unstable system. The simulated plant outputs using the full (tenth) order controller are shown for comparison in Fig 4.59. Fig 4.57 shows a very good response of y_1 to r_1, though the response of y_2 to r_2 is more oscillatory than would be expected (since the rams without compensation are not oscillatory) and there is substantial steady state error

in y_2. Dynamic coupling exists between y_2 and r_1 and this is more apparent in the reduced than in the full order compensator.

Fig 4.58 shows that the tight response of y_1 was achieved at the expense of unacceptably large control effort. The plant inputs, u_1 and u_2, peaked at almost five times the step input level of r_1 and this would lead to saturation in the implemented compensator for quite modest step commands. Control effort for y_2 was of the order of 1.75 times the step inputs.

The process of finding suitable weights for the controller design was a difficult one, partly due to interactions between each weight and performance indicators other than those which it was intended to constrain. For instance, attempts to constrain control effort by increasing $\mathbf{W}_2$ would normally result in deterioration in terms of controller error. For the present work, many combinations of weightings were investigated and it was at this stage that the decision to restrict the investigation to optimal H^∞ controller synthesis, with the parameter of iteration, γ, multiplying all rows of mixed sensitivity, was made. This invariably returned a controller (and the associated optimal γ_{opt}), which was not the case for standard H^∞ controller synthesis.

The actual value of γ_{opt} reflected the magnitude of the weights used for the controller synthesis and was not necessarily an indicator of plant performance. For instance, using the controller weights above, γ_{opt} was 0.0408 whereas when $\mathbf{W}_1$, $\mathbf{W}_2$ and $\mathbf{W}_3$ were all doubled, γ_{opt} was exactly halved. The H^∞ controller was unchanged by this doubling of the weights. Doubling $\mathbf{W}_1$, $\mathbf{W}_2$ and $\mathbf{W}_3$ separately reduced γ_{opt} to 0.0251, 0.0337 and 0.0386 respectively and here a different controller resulted in each case. These values of γ_{opt} would seem to indicate that the magnitude of mixed sensitivity was most sensitive to changes in the term involving sensitivity, **S**, and therefore that **S** was the most severely constrained indicator for this set of weights. Since γ_{opt} was less than one, the family of controllers satisfying the standard H^∞ controller synthesis inequality did not exist.

4.6.3 Design and Simulation of an Improved H^∞ Controller

As a result of a process of iteration through combinations of zero, first and second order weighting factors and assessment of the performance of the resulting controllers at the

simulation stage, a reasonable controller was obtained using first order weights as follows

$$\mathbf{W}_1(s) = diag(\frac{10}{10s+1}, \frac{10}{10s+1}) \tag{4.21}$$

$$\mathbf{W}_2(s) = diag(\frac{0.1(0.2s+1)}{0.002s+1}, \frac{0.1(0.2s+1)}{0.002s+1}) \tag{4.22}$$

$$\mathbf{W}_3(s) = diag(\frac{s}{10}, \frac{s}{10}) \tag{4.23}$$

This again gave a tenth order system but the gramian of the balanced system indicated that a good third order approximation should exist. Figs 4.60 and 4.61 show the simulated plant outputs and inputs respectively using the third order compensator model reduced by balanced residualisation. The third order controller reduced by OHMDA again gave unstable results.

In order to reduce the steady state error in y_2 shown by Fig 4.60, the second element of $\mathbf{W}_1(s)$ was increased to constrain the second element of $\mathbf{S}(s)$ more severely. This improved y_2 but resulted in a more sluggish response in y_1. Since there was scope for increasing control effort, the elements of $\mathbf{W}_2(s)$ were reduced to lessen the constraint on both elements of $\mathbf{KS}(s)$. The resulting plant outputs are shown in Figs 4.62 and 4.63 respectively, the controller again having been reduced to third order by balanced residualisation. This final choice of weights was

$$\mathbf{W}_1(s) = diag(\frac{10}{10s+1}, \frac{50}{10s+1}) \tag{4.24}$$

$$\mathbf{W}_2(s) = diag(\frac{0.05(0.2s+1)}{0.002s+1}, \frac{0.05(0.2s+1)}{0.002s+1}) \tag{4.25}$$

$$\mathbf{W}_3(s) = diag(\frac{s}{10}, \frac{s}{10}) \tag{4.26}$$

Using a version of this controller reduced to third order by OHMDA, a stable but highly oscillatory system resulted, as shown by Fig 4.64. For comparison, the plant ouputs were simulated using the tenth order compensator and these are shown in Fig 4.65. They can be seen to correspond closely with those for the compensator reduced by balanced residualisation.

Attempts to squeeze out steady state error further by increasing the constraint on the second element of $\mathbf{S}(s)$ led to unacceptably high levels of control effort in response to

steps on r_1. (This observation is based on simulations using the tenth order compensator since model reduction by balanced residualisation became inviable due to the generation of complex elements in the reduced compensator's state space description. The models reduced by OHMDA were again too oscillatory).

There are two points about the H^∞ controllers that may be made at this point. The first is that in almost all the simulations produced during this work the compensated system exhibited little or no interaction, i.e. the system was diagonalised. Presumably this is because any interaction implies steady state error and this is dealt with via the inclusion of sensitivity in the mixed sensitivity function. Secondly, the reduction of the compensator by balanced residualisation resulted in a model that was not strictly proper (i.e. $\mathbf{D} \neq \mathbf{0}$) even though the full order model was. This resulted in complications upon implementation which will be considered later.

For simulations using the H^∞ controller discretised by Euler's method, the Simulink model used for the characteristic locus controller and shown in Fig 4.48 was used again. The plant outputs and inputs produced by this model using the final H^∞ controller reduced by balanced residualisation and a sampling interval of 0.01 seconds are shown in Figs 4.66 to 4.69. It can be seen that a small amount of saturation on u_1 and u_2 resulted from the 8V steps applied on r_1 and r_2 at 0 and 5 seconds respectively, but that this has not had a serious effect on plant performance as compared to simulation with the continuous controller. Further simulations showed that performance of the discrete model began to deteriorate seriously for sampling intervals greater than 0.05 seconds.

4.6.4 H^∞ Controller Implementation

The discrete third order controller simulated above was implemented on an IBM PC with a sampling interval of 5ms and used in conjunction with the beam and carriage. The system was unstable in a non-oscillatory manner, the carriage moving to an extreme end of the beam and being held there by significant beam gradient. As explained above, the H^∞ compensator was not strictly proper after reduction to third order. It was decided to ignore the **D** matrix of the reduced model (i.e. to take $\mathbf{D} = \mathbf{0}$) as an unwanted by-product of the model approximation process and to implement the resulting strictly proper compensator. The plant outputs obtained by this implementation using step inputs of approximately 7V into the beam and carriage rig are shown in Figs 4.70 to 4.73. Overshoot on both y_1 and y_2 is greater than that exhibited in the simulations as is the interaction between y_1 and r_2. There is no apparent steady state error in y_1 or y_2.

The design and implementation of four controllers has been described in the foregoing. The performance of the LQG controller was changed considerably by varying the estimates of process and measurement noise. Relatively low process and high measurement noise estimates for the original LQG controller resulted in slower poles for the estimator and a slower response to step inputs as compared to the improved LQG controller with more conservative process noise and less conservative measurement noise predictions. A controller based on a reduced order observer was implemented which, by adopting an observer pole comparable to the slowest pole of the improved LQG controller, gave similar performance.

The controllers based on the Characteristic Locus and H^{∞} Optimisation approaches were less satisfactory. The process of finding suitable dynamic compensators for the former and performance weights for the latter was a difficult one, involving a high degree of iteration. However, the H^{∞} Optimisation design process does offer an explicit approach to the design of robust controllers.

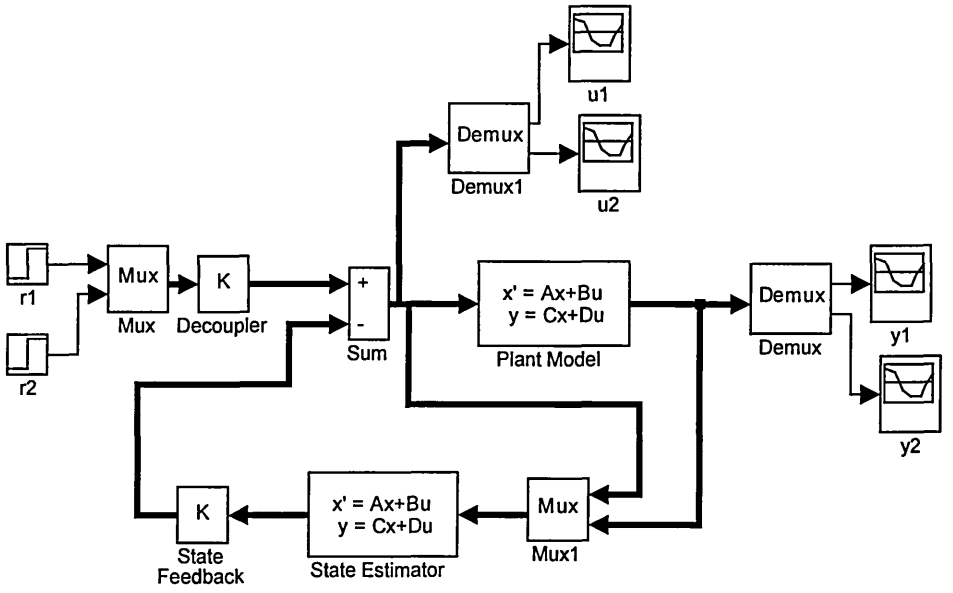

Fig 4.2 Simulink Model for Continuous LQG Controller

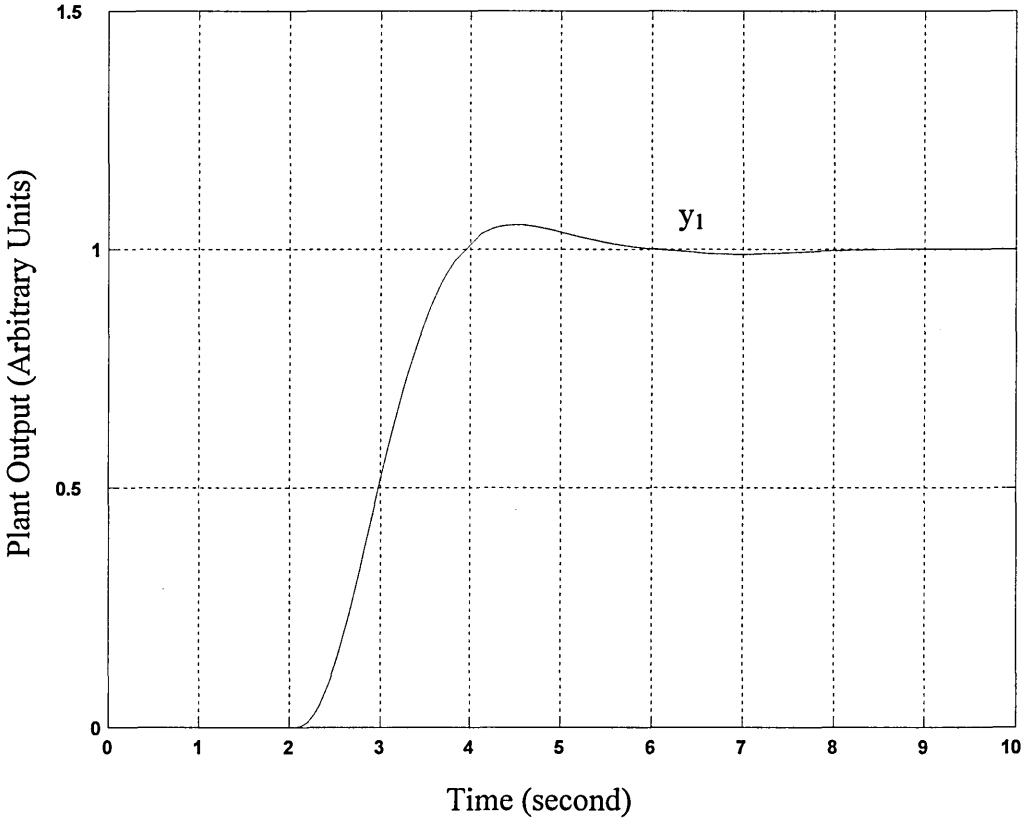

Fig 4.3 Continuous LQG Controller Simulation - Plant Output y_1

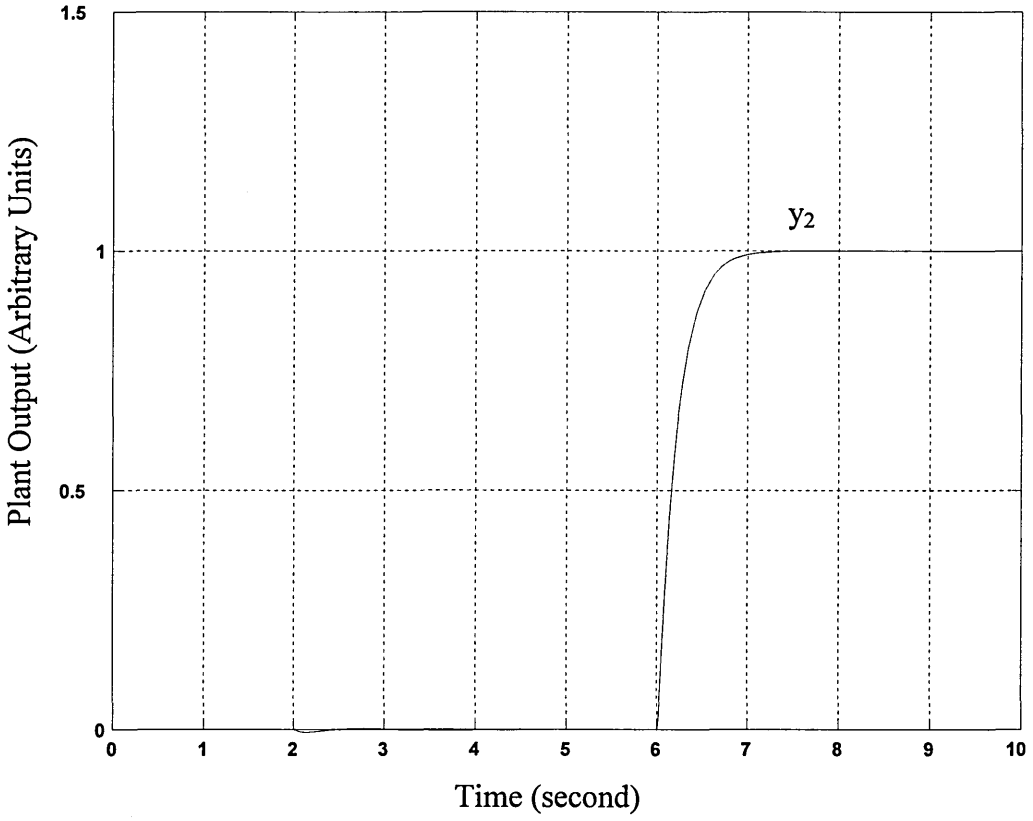

Fig 4.4 Continuous LQG Controller Simulation - Plant Output y_2

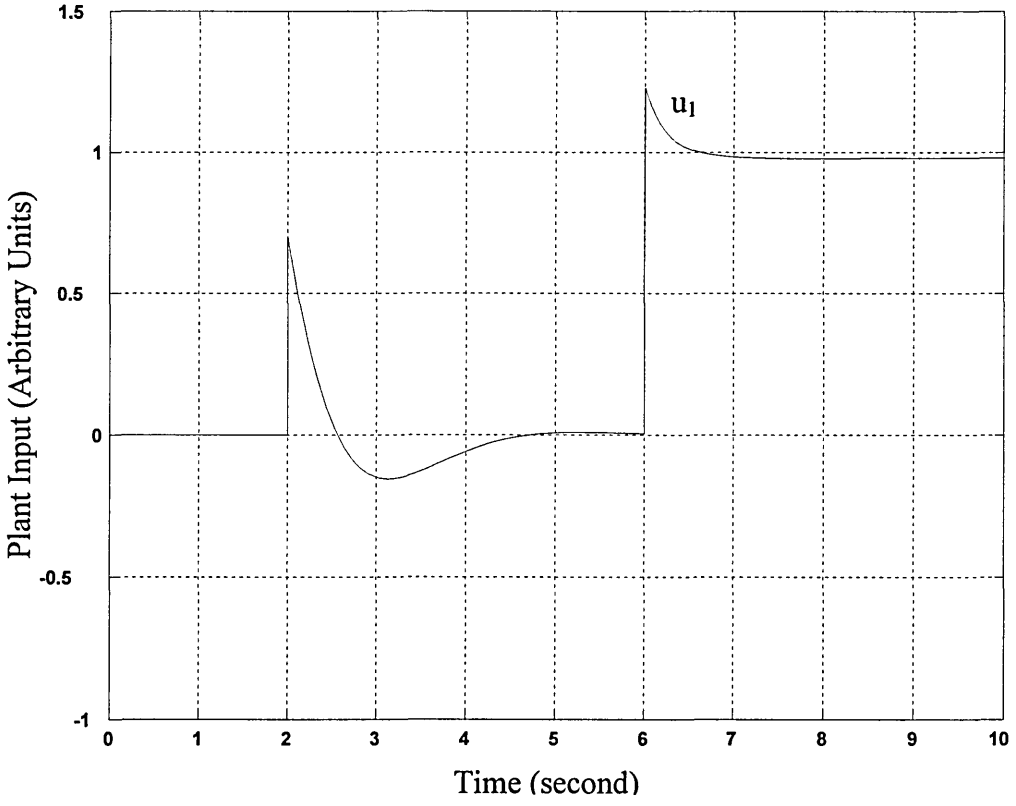

Fig 4.5 Continuous LQG Controller Simulation - Plant Input u_1

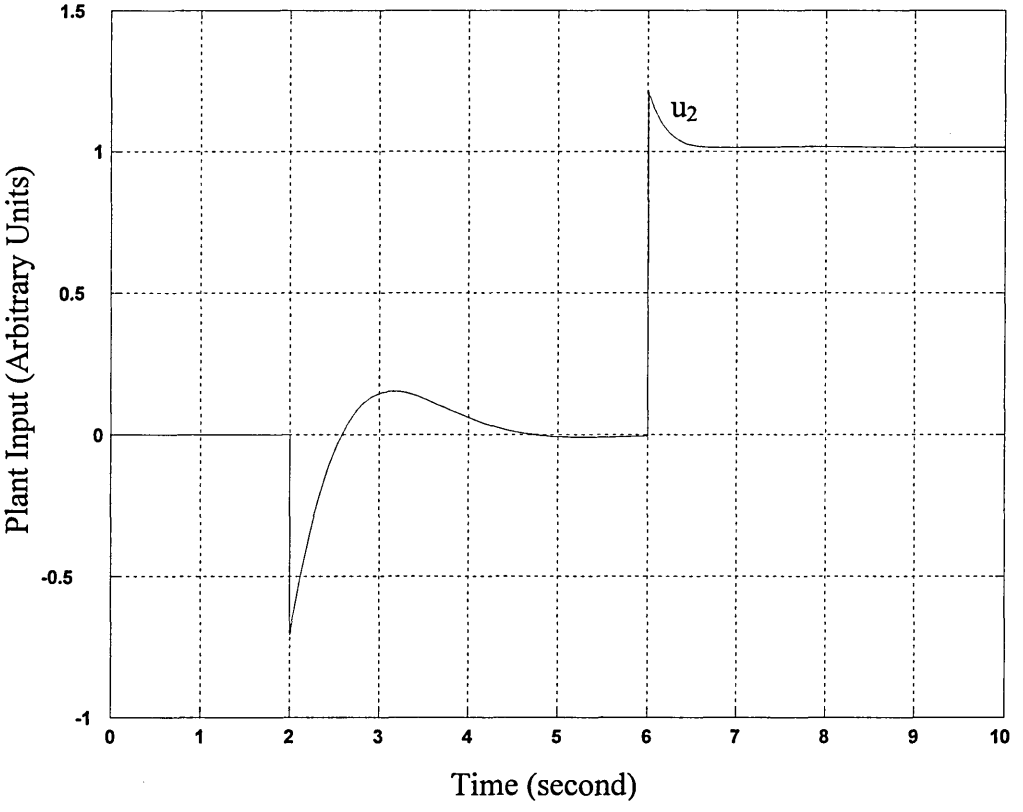

Fig 4.6 Continuous LQG Controller Simulation - Plant Input u_2

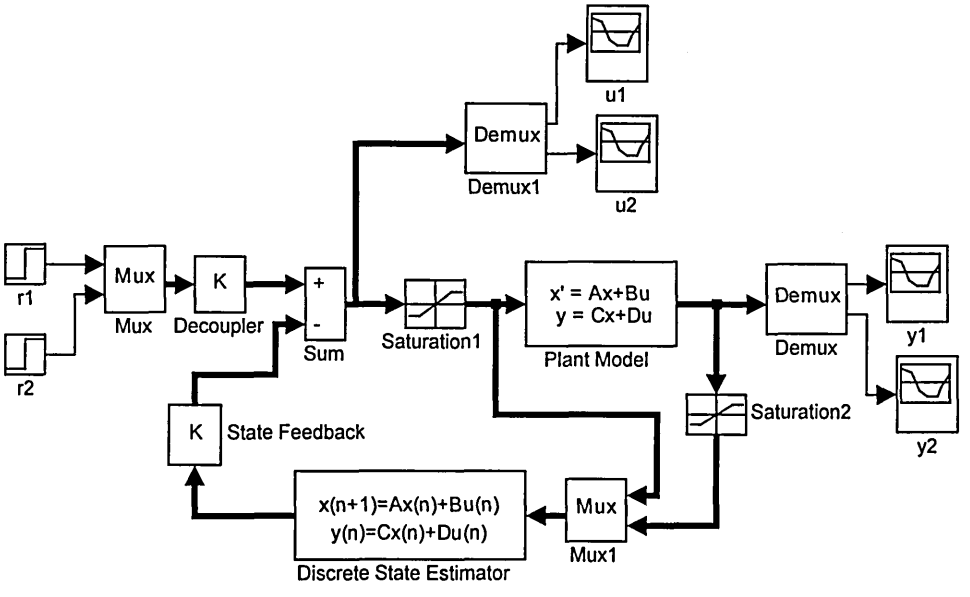

Fig 4.7 Simulink Model for Discrete LQG Controller

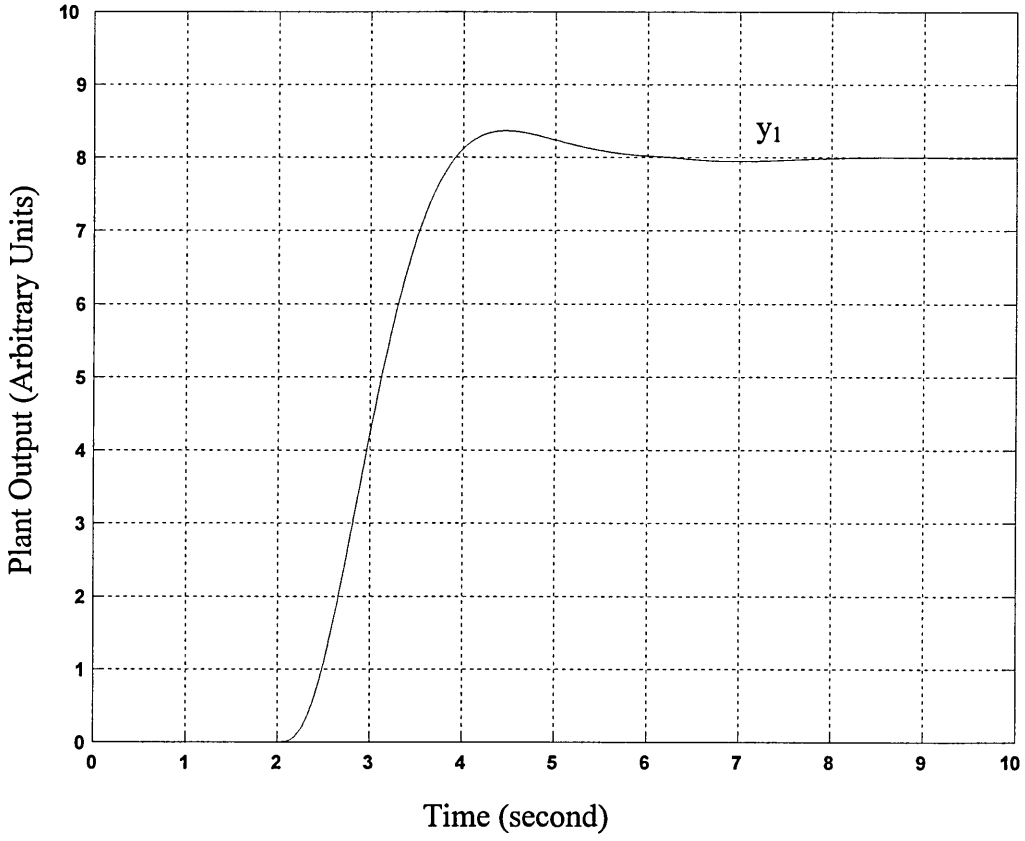

Fig 4.8 Discrete LQG Controller Simulation - Plant Output y_1

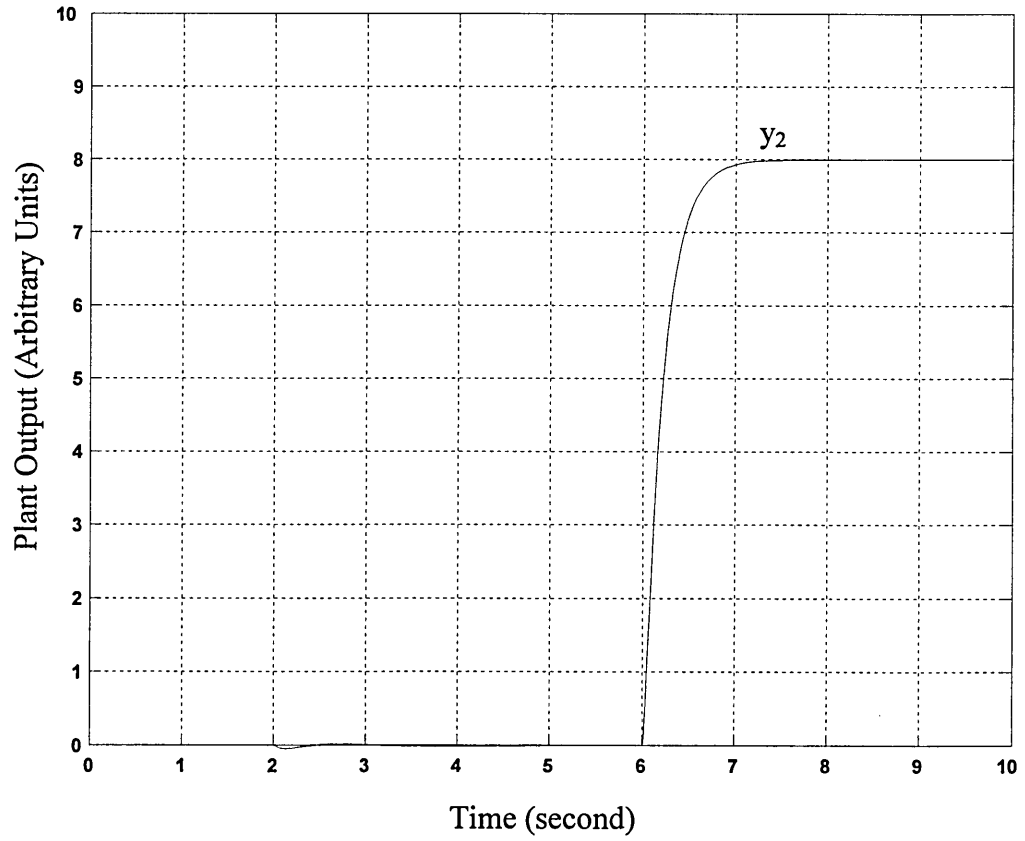

Fig 4.9 Discrete LQG Controller Simulation - Plant Output y_2

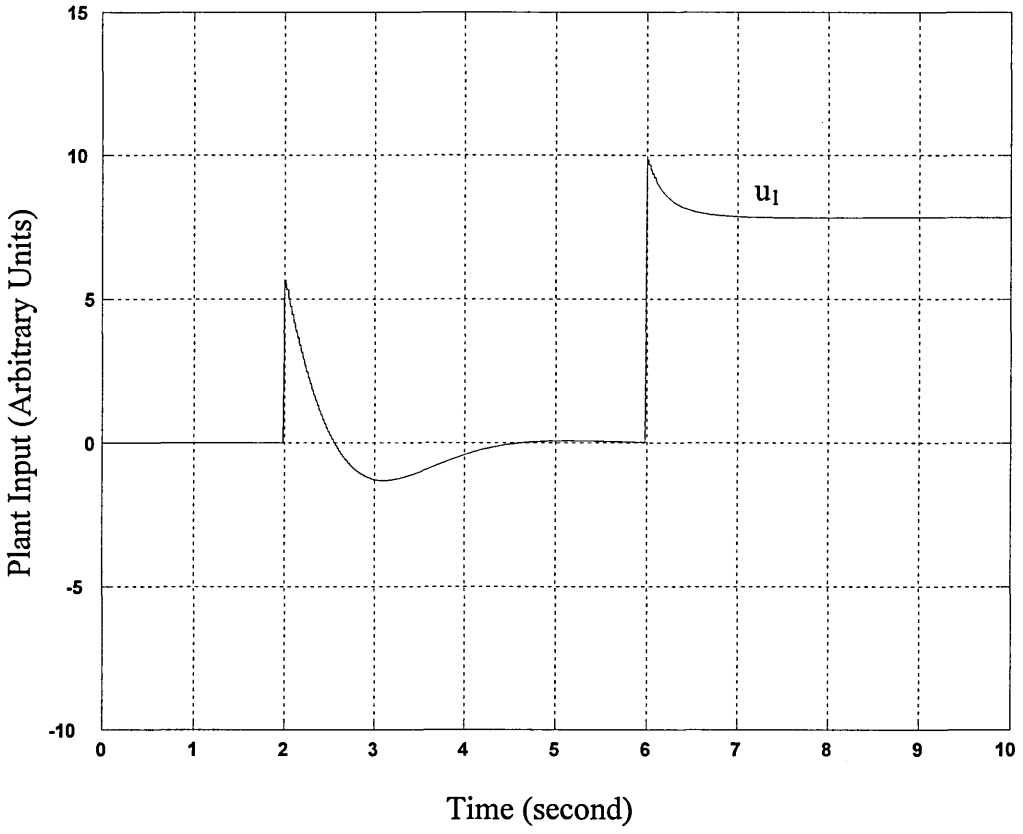

Fig 4.10 Discrete LQG Controller Simulation - Plant Input u_1

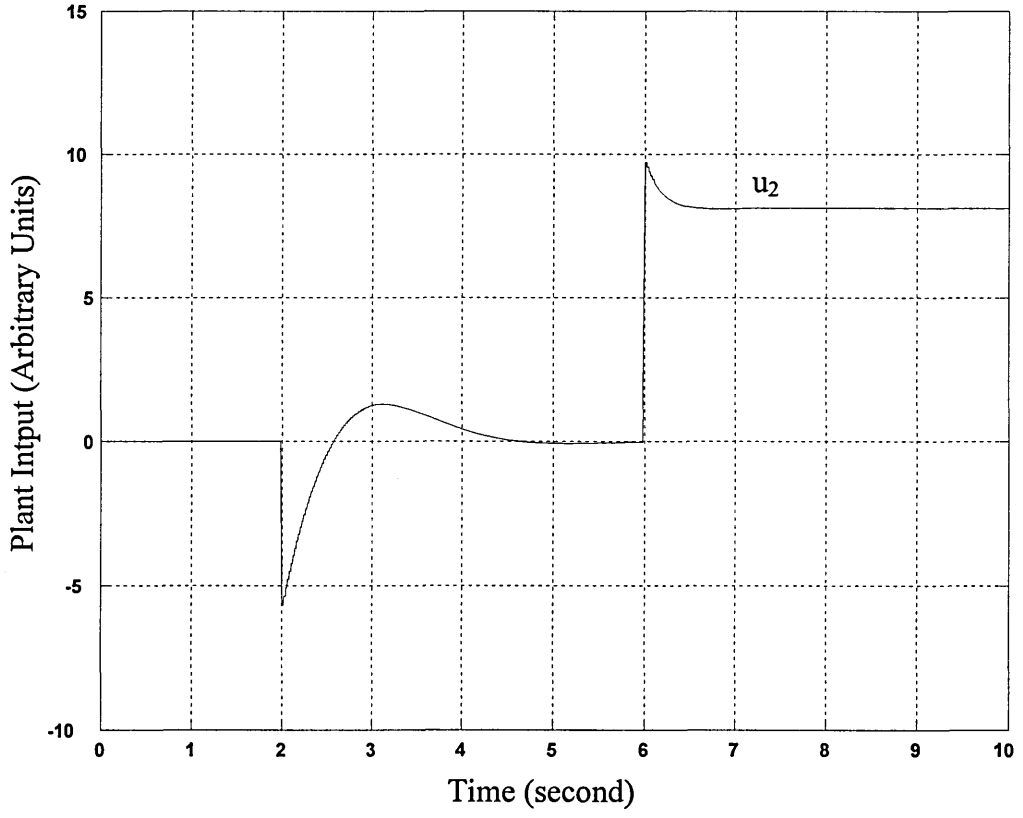

Fig 4.11 Discrete LQG Controller Simulation - Plant Input u_2

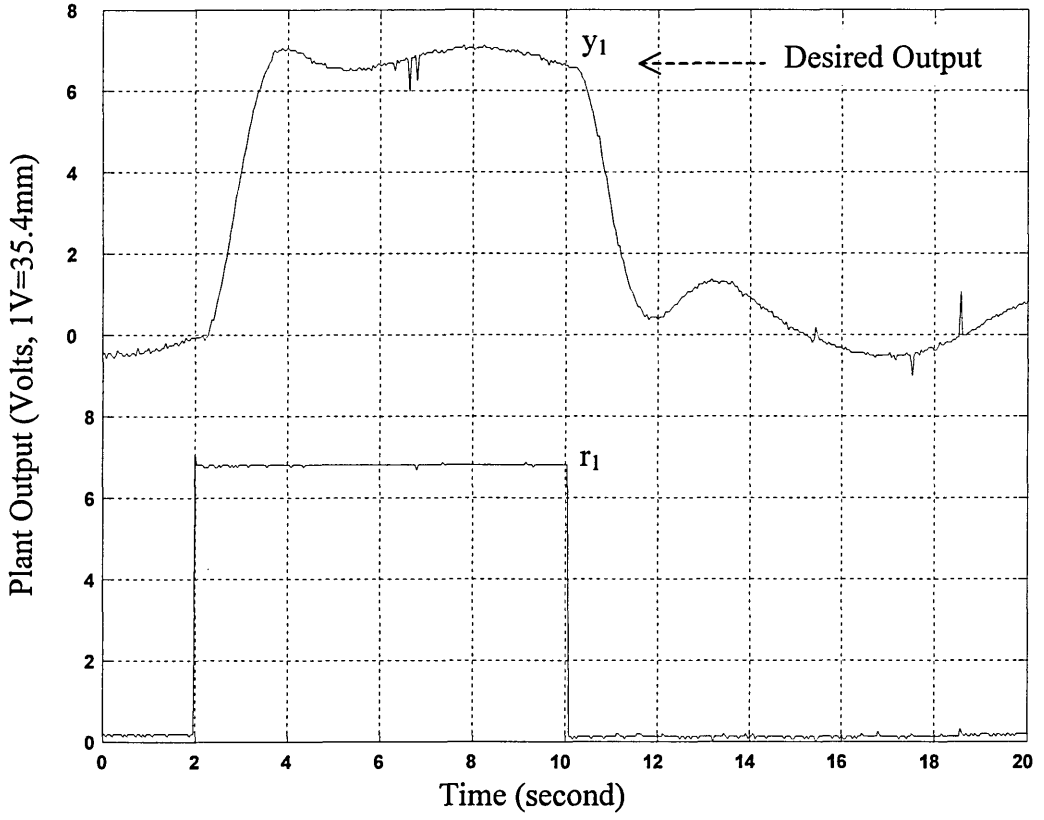

Fig 4.12 LQG Implementation - Plant Output y_1

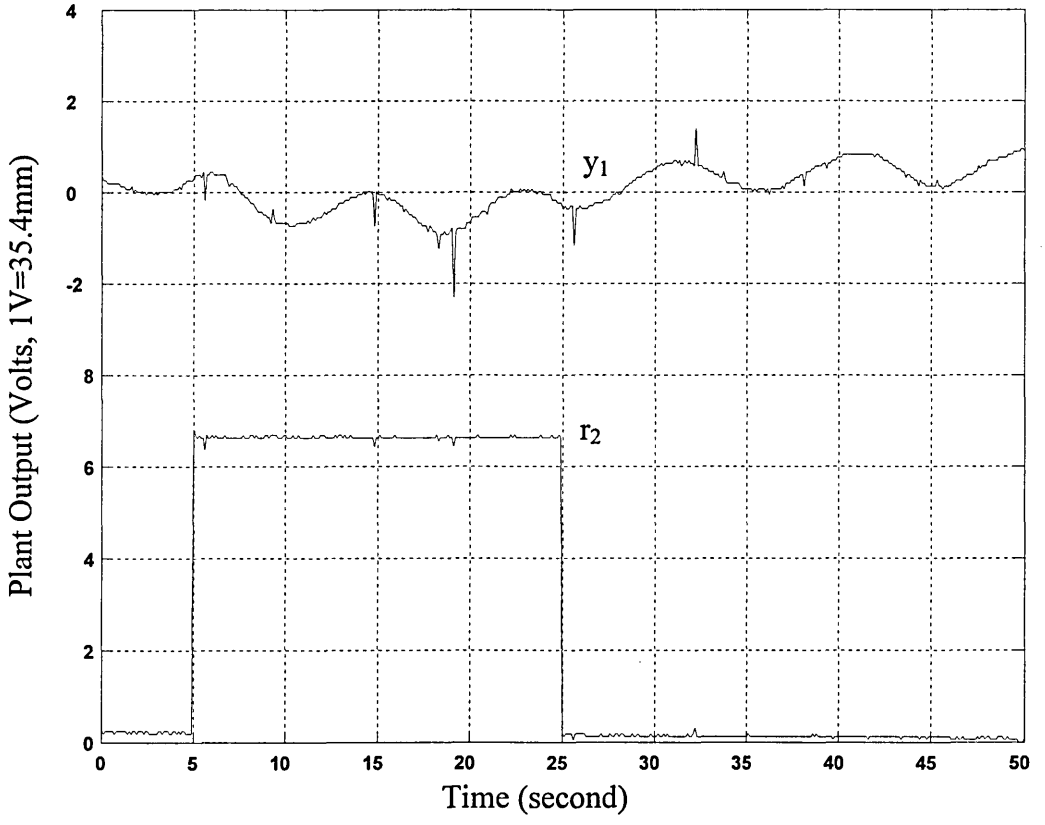

Fig 4.13 LQG Implementation - Plant Output y_1

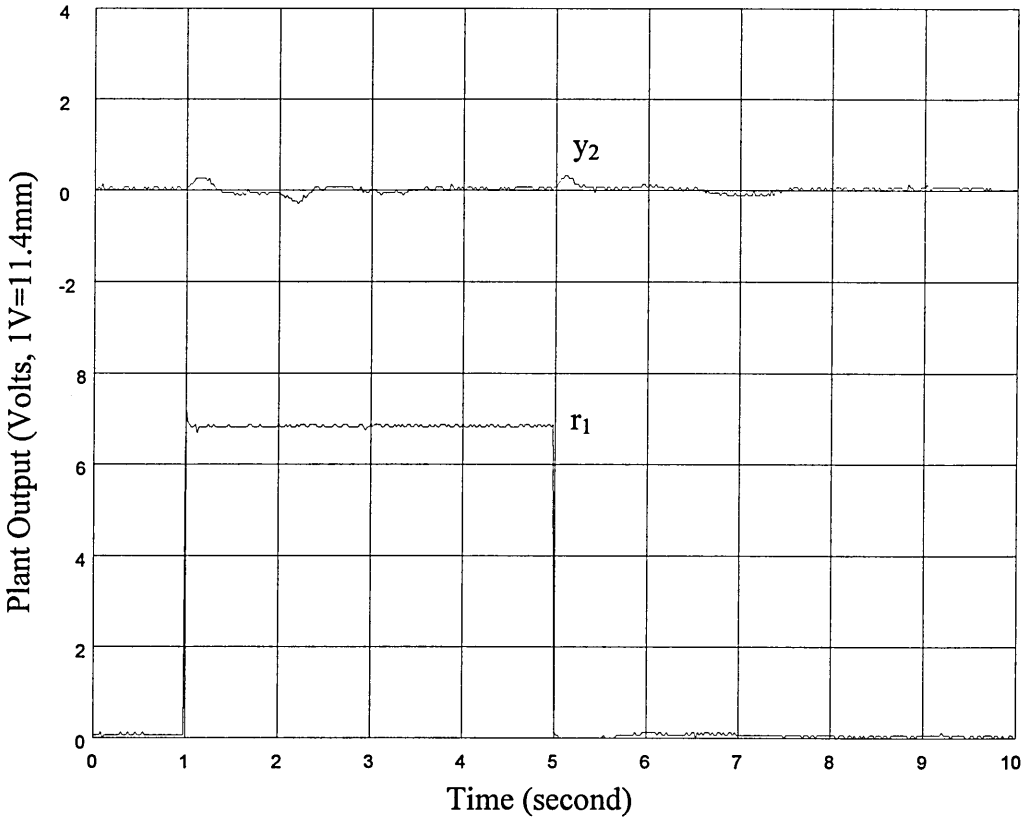

Fig 4.14 LQG Implementation - Plant Output y_2

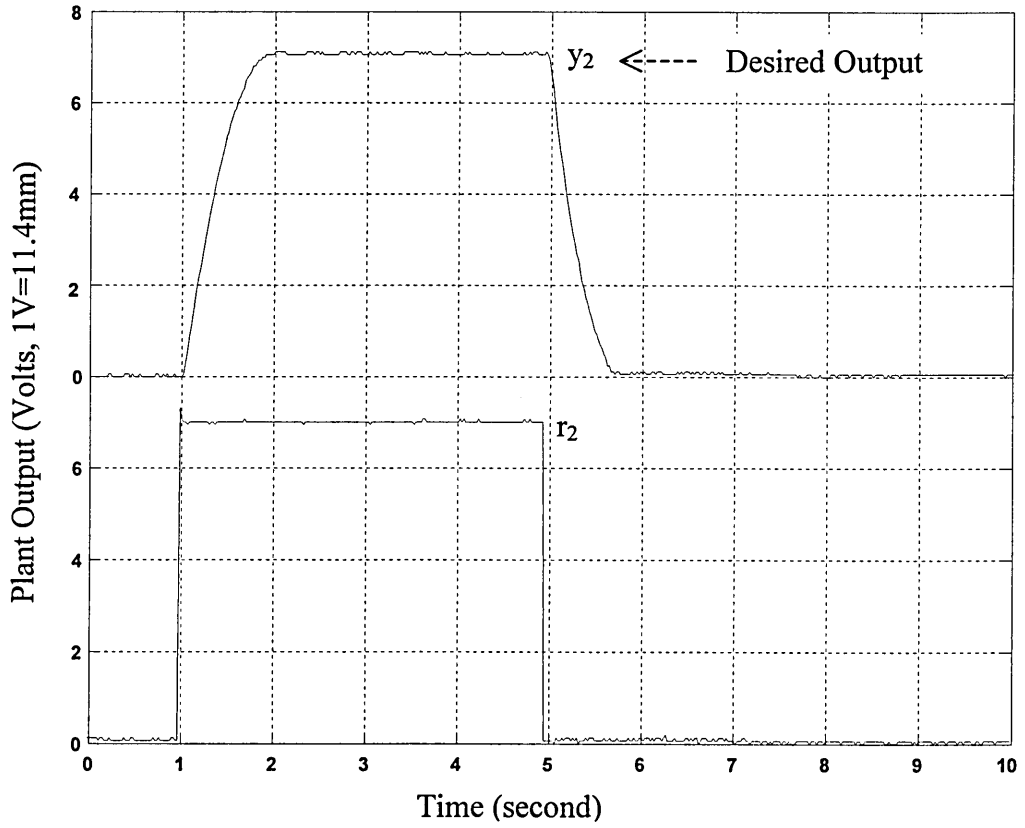

Fig 4.15 LQG Implementation - Plant Output y_2

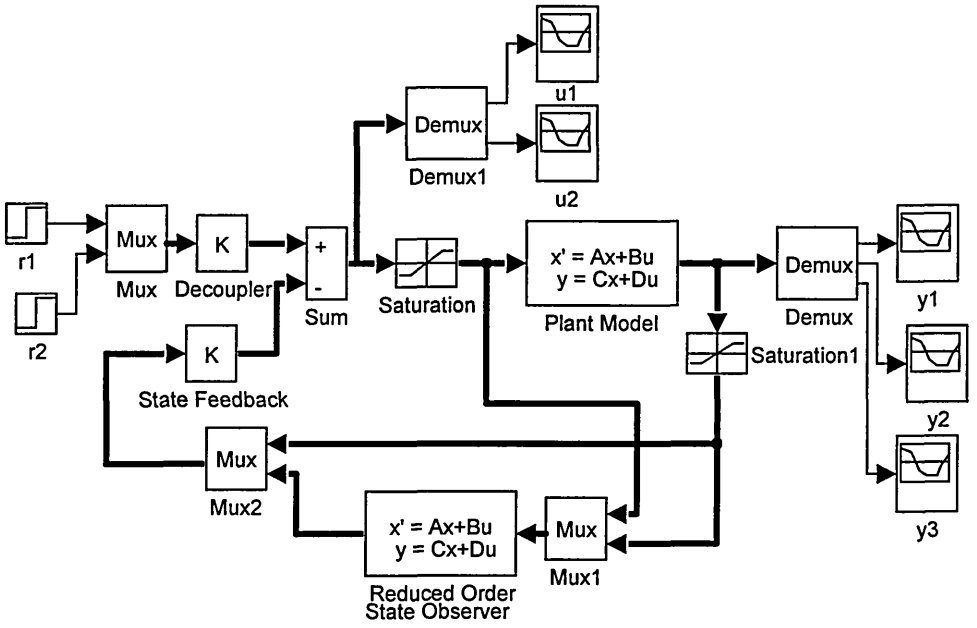

Fig 4.16 Simulink Model for Reduced Order Observer (ROO) Controller

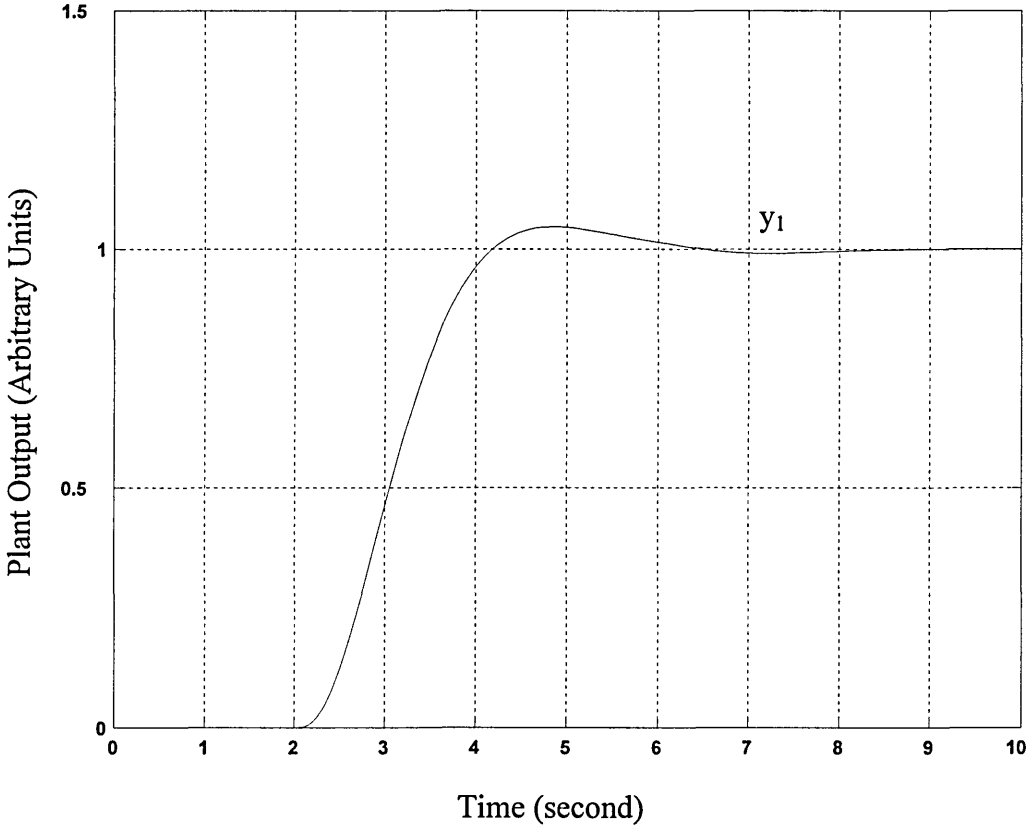

Fig 4.17 Continuous ROO Controller Simulation - Plant Output y_1

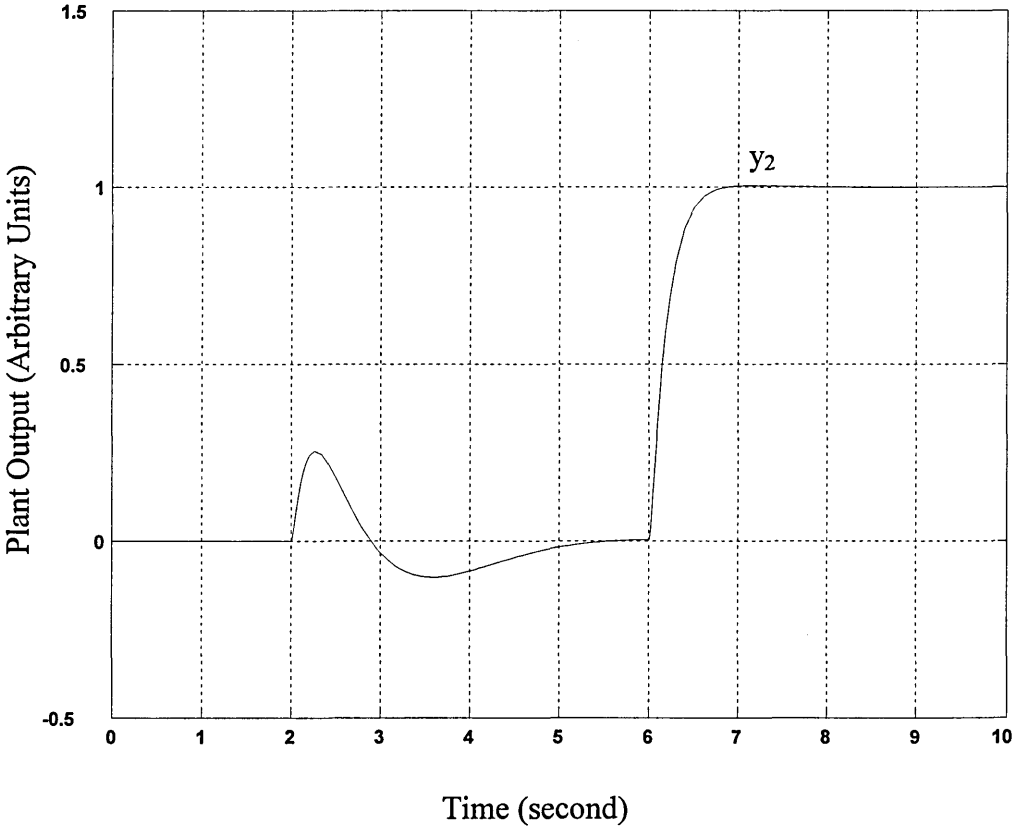

Fig 4.18 Continuous ROO Controller Simulation - Plant Output y_2

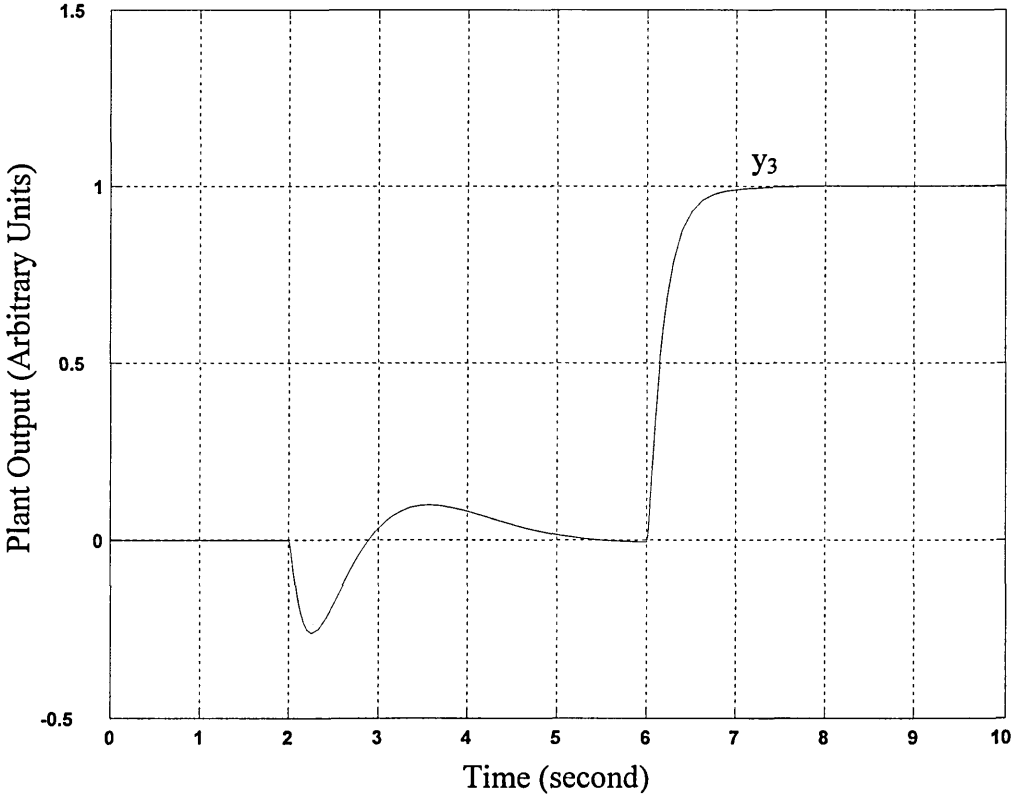

Fig 4.19 Continuous ROO Simulation - Plant Output y_3

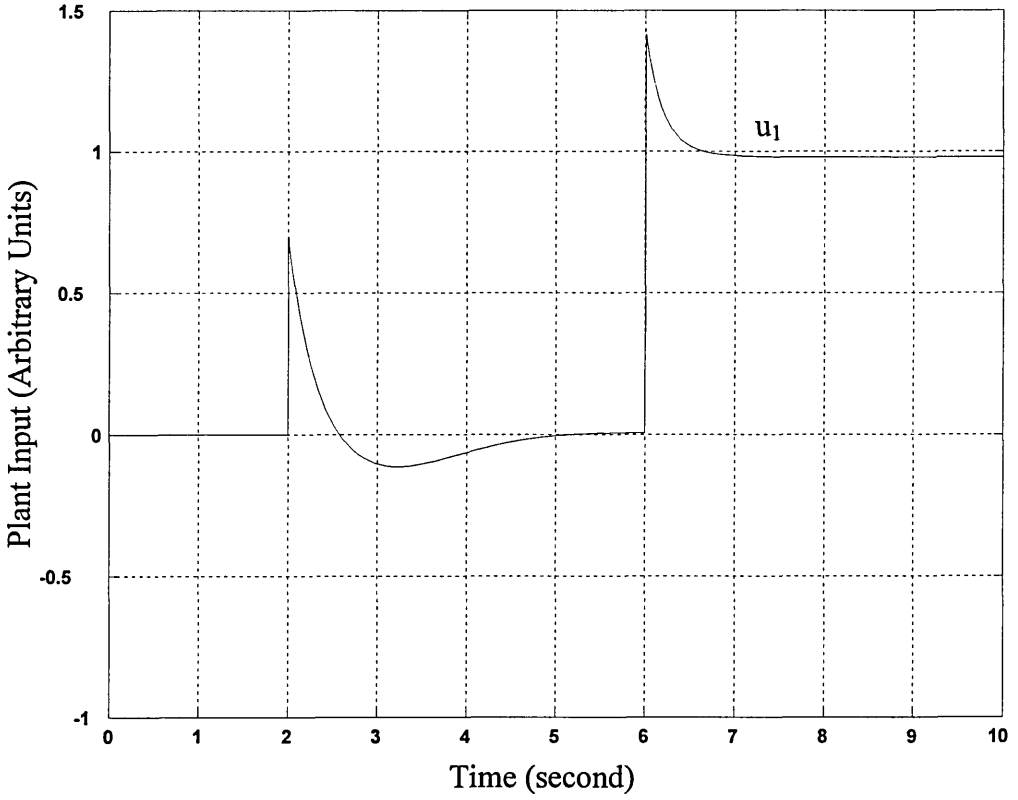

Fig 20 Continuous ROO Controller Simulation - Plant Input u_1

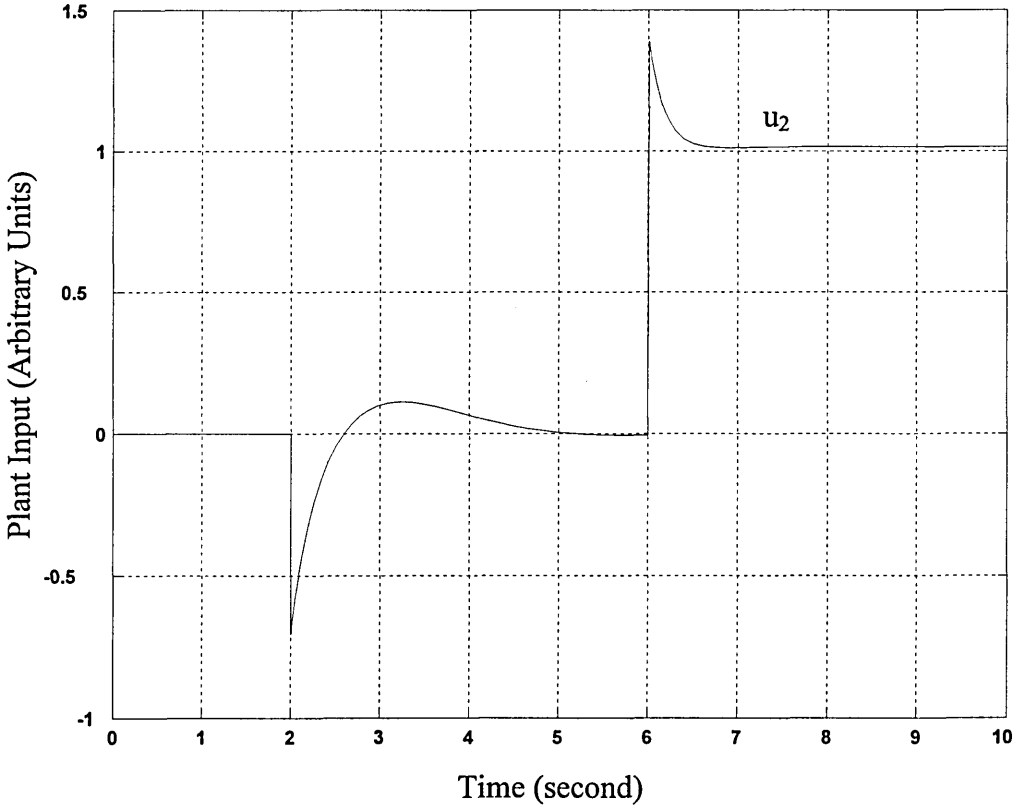

Fig 4.21 Continuous ROO Controller - Plant Input u_2

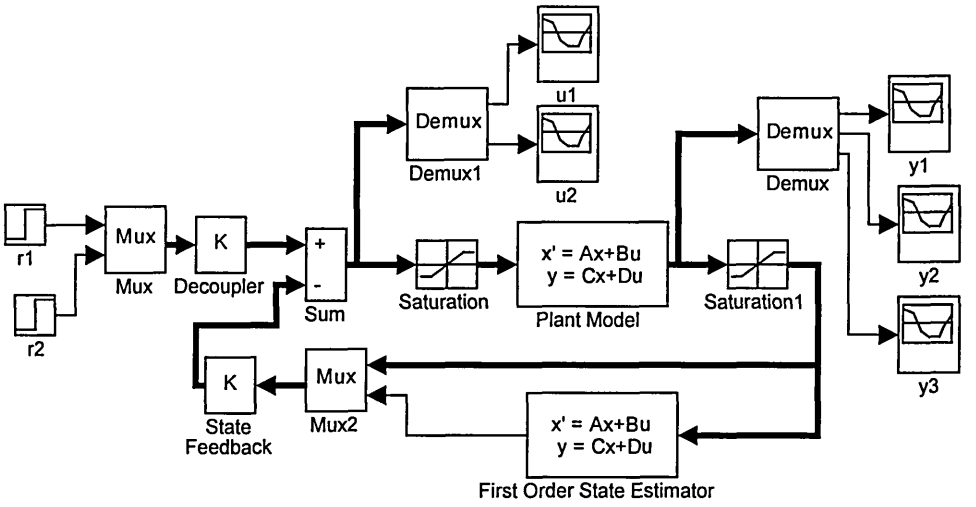

Fig 4.22 Simulink Model for Continuous Simplified ROO Controller

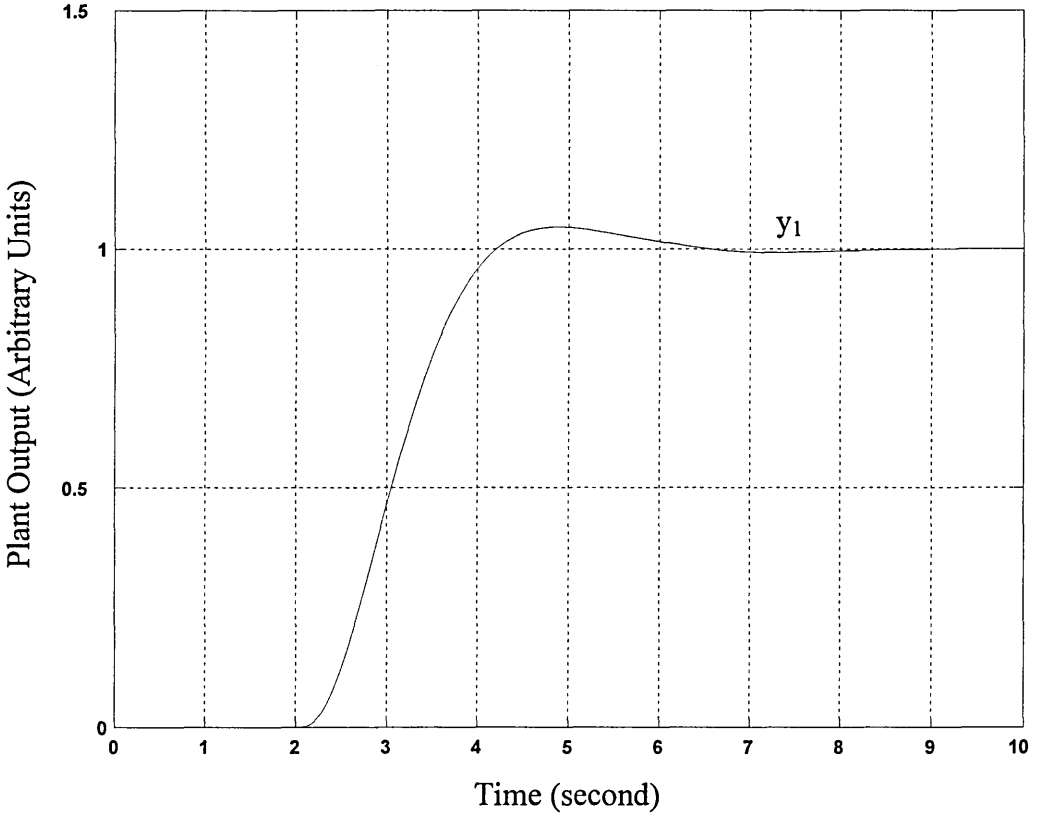

Fig 4.23 Continuous Simplified ROO Controller - Plant Output y_1

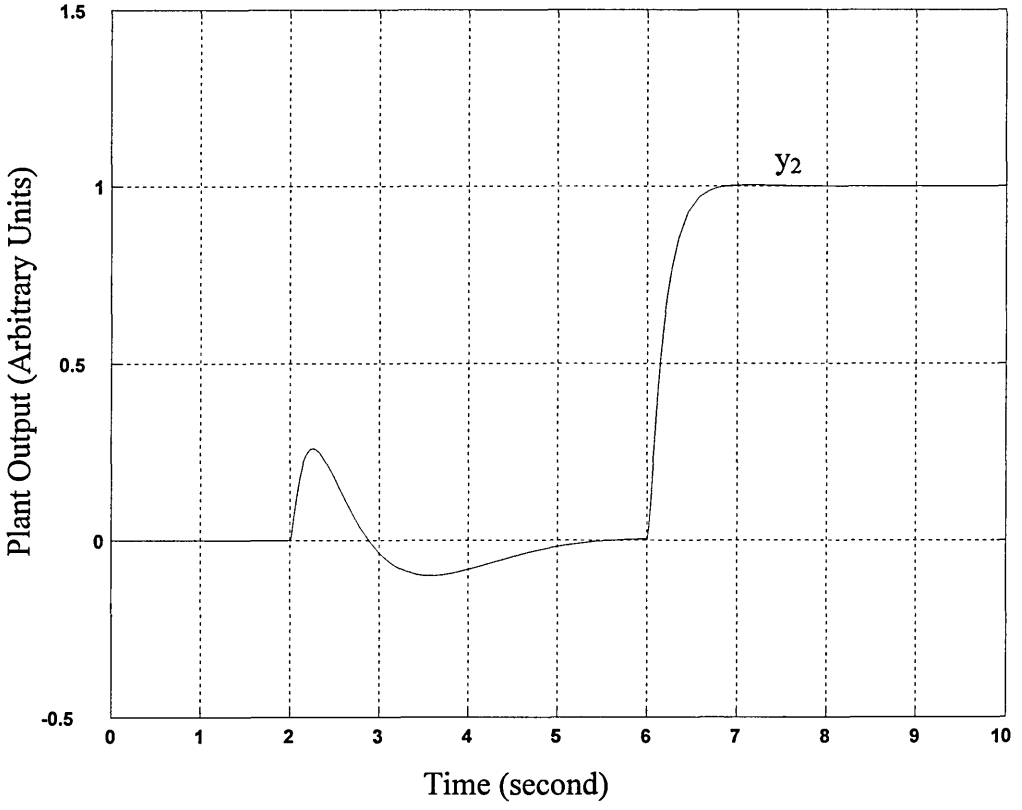

Fig 4.24 Continuous Simplified ROO Controller Simulation - Plant Output y_2

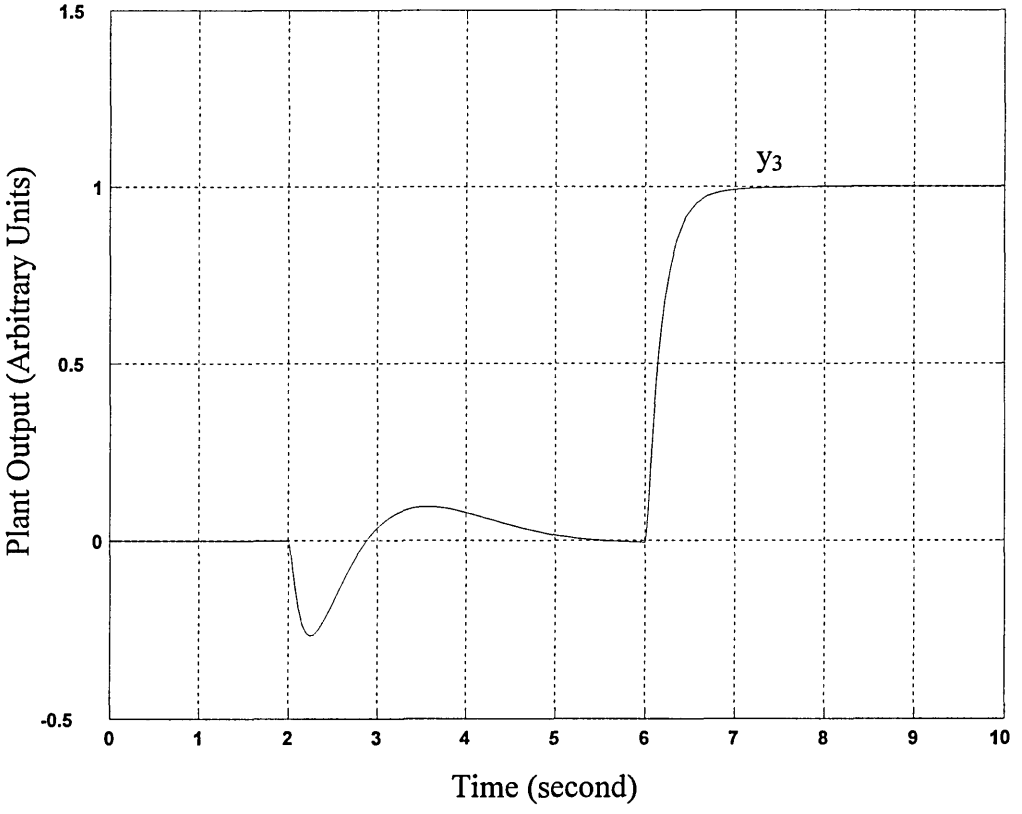

Fig 4.25 Continuous Simplified ROO Controller - Plant Output y_3

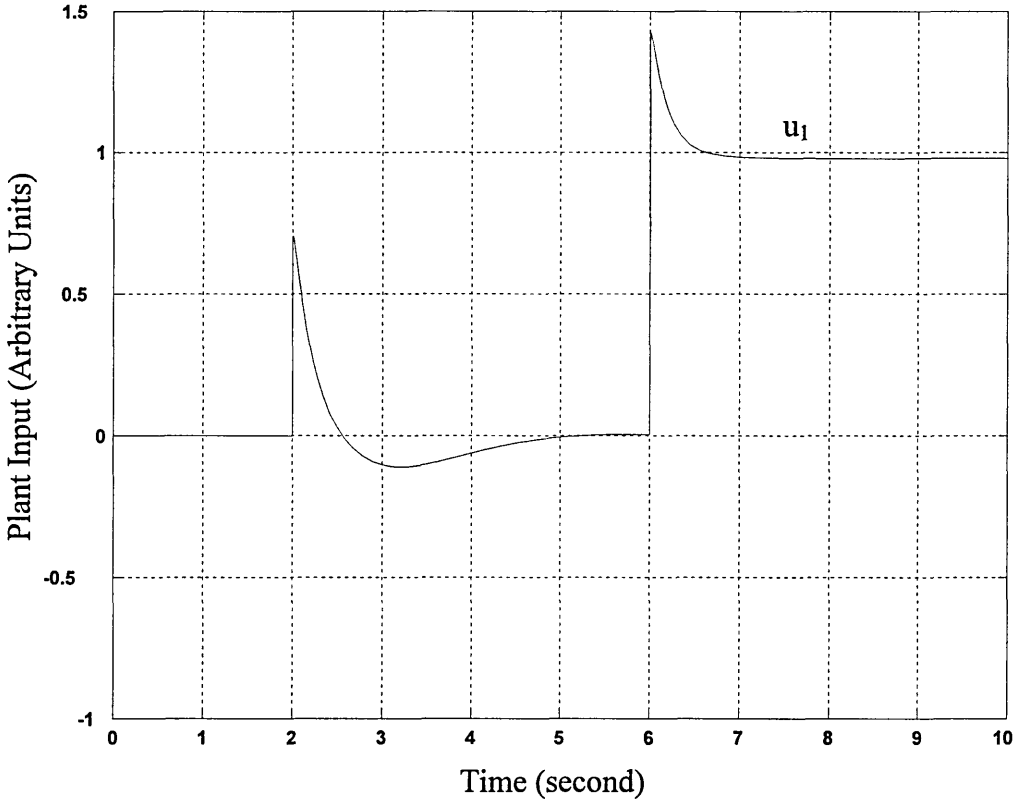

Fig 4.26 Continuous Simplified ROO Controller Simulation - Plant Input u_1

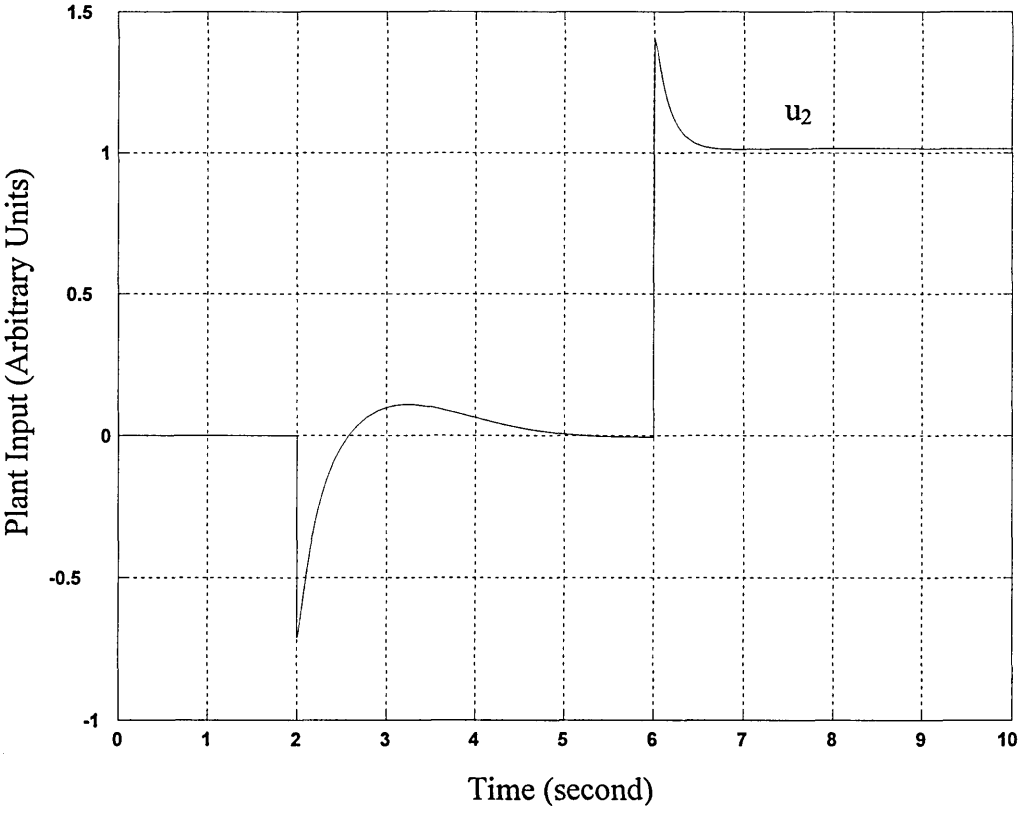

Fig 4.27 Continuous Simplified ROO Controller Simulation - Plant Input u_2

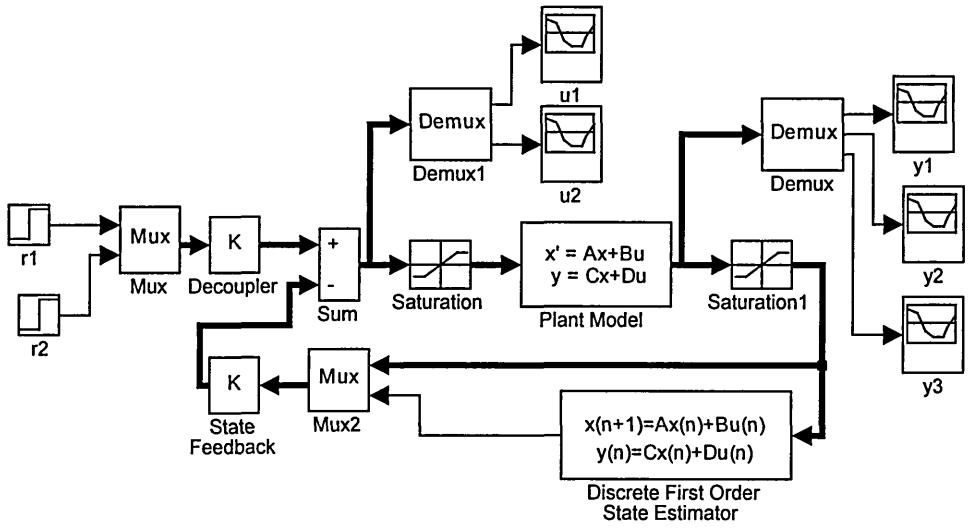

Fig 4.28 Simulink Model for Discrete ROO Controller

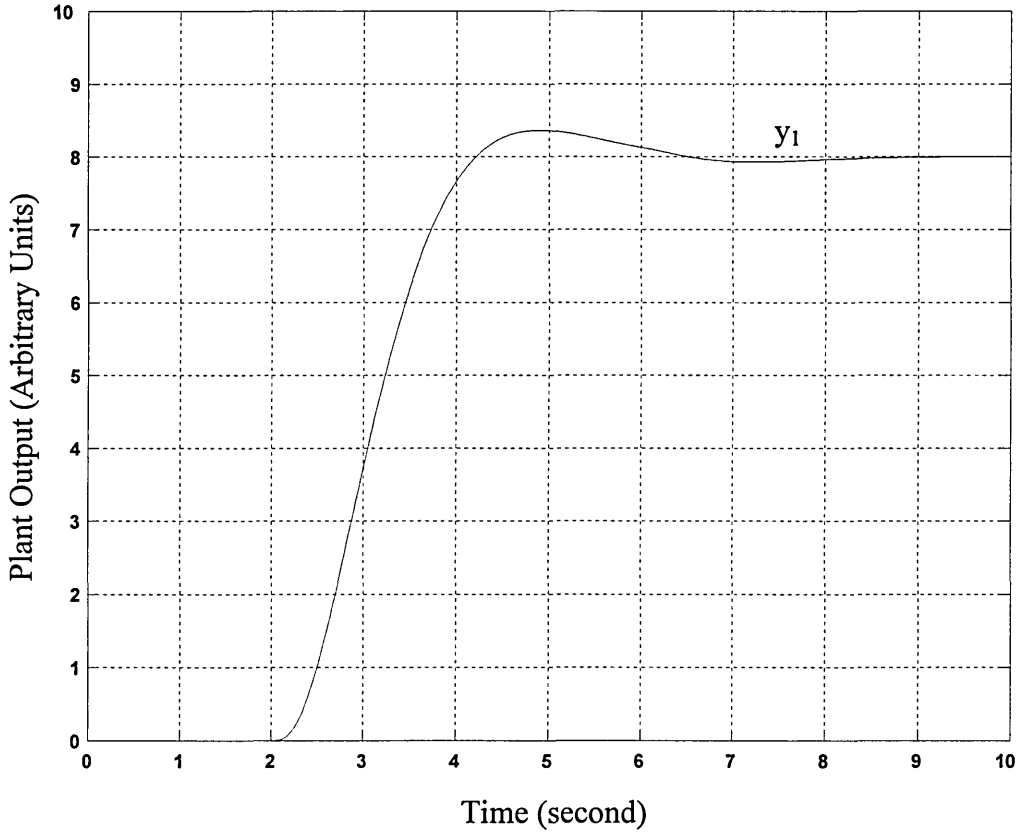

Fig 4.29 Discrete ROO Controller Simulation - Plant Output y_1

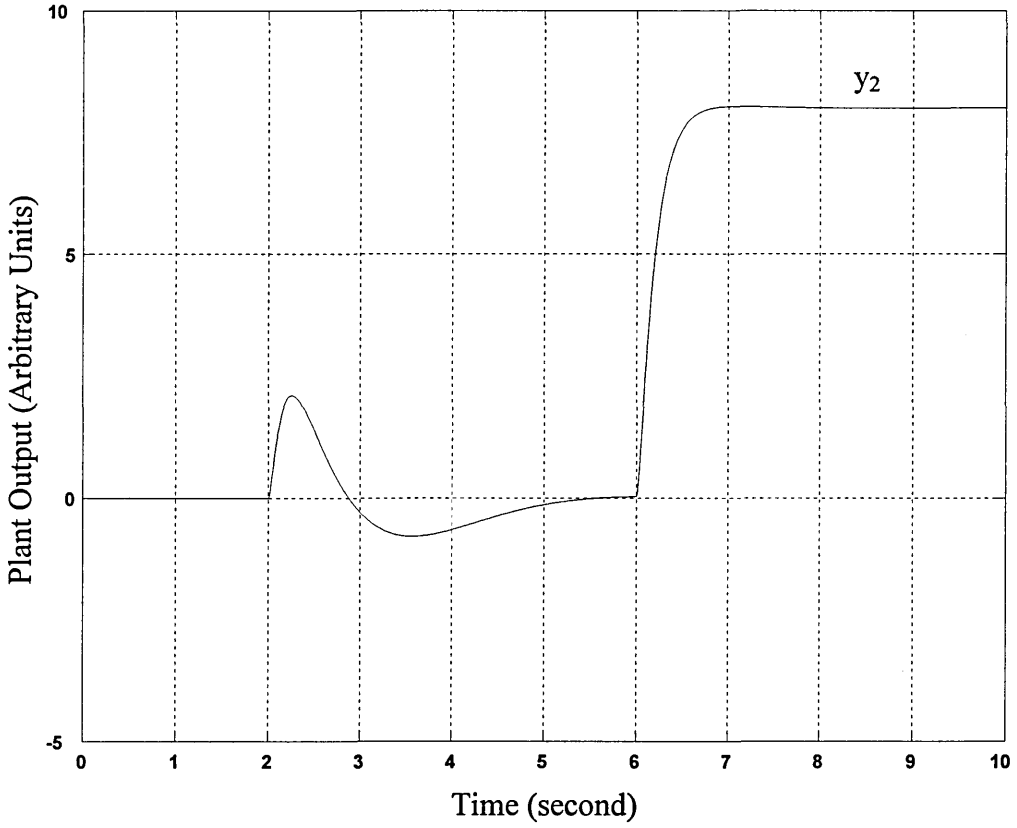

Fig 4.30 Discrete ROO Controller Simulation - Plant Output y_2

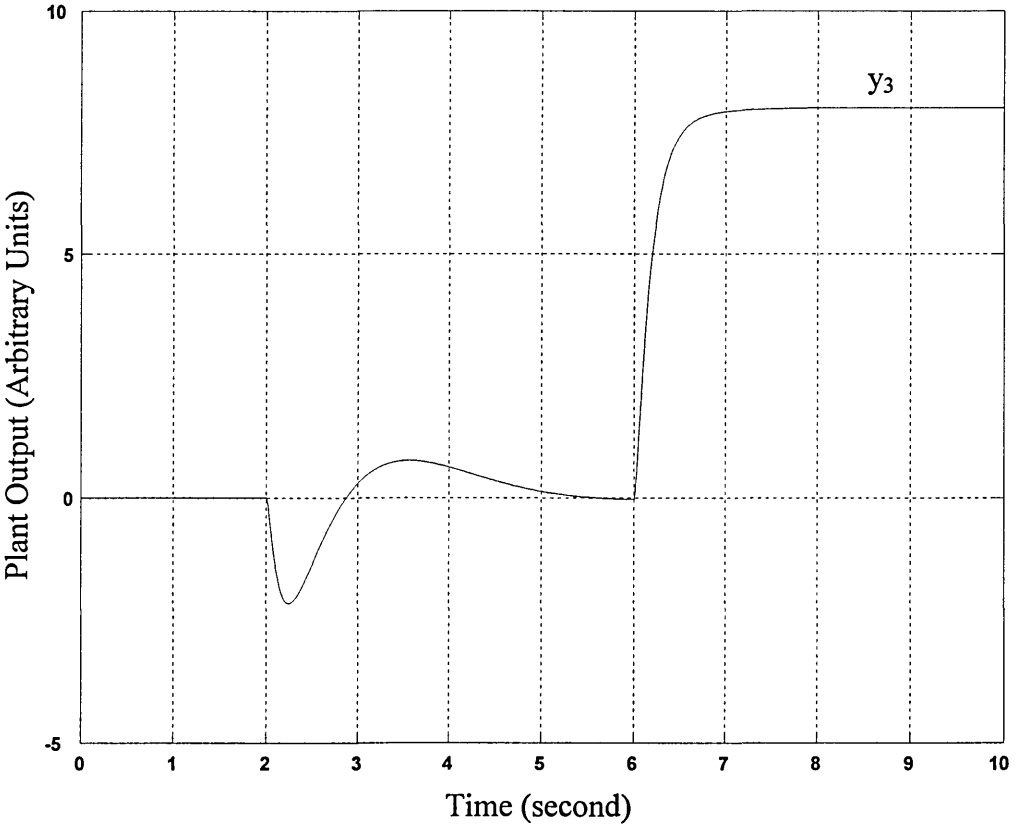

Fig 4.31 Discrete ROO Controller Simulation - Plant Output y_3

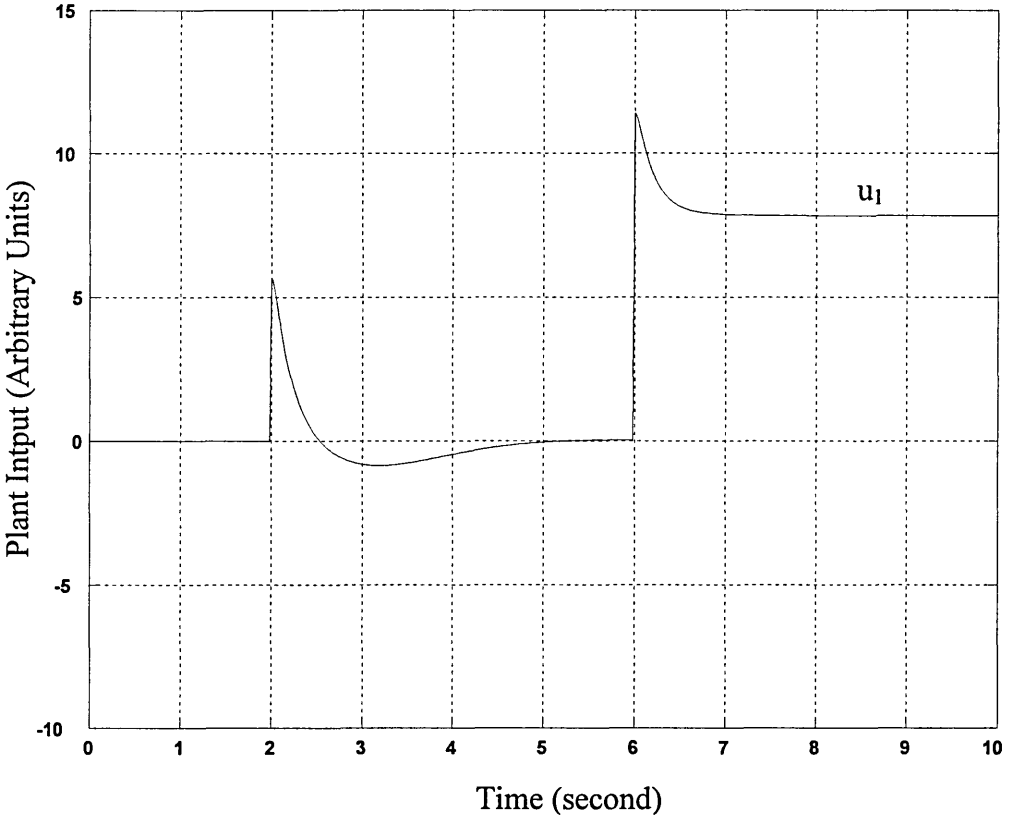

Fig 4.32 Discrete ROO Controller Simulation - Plant Input u_1

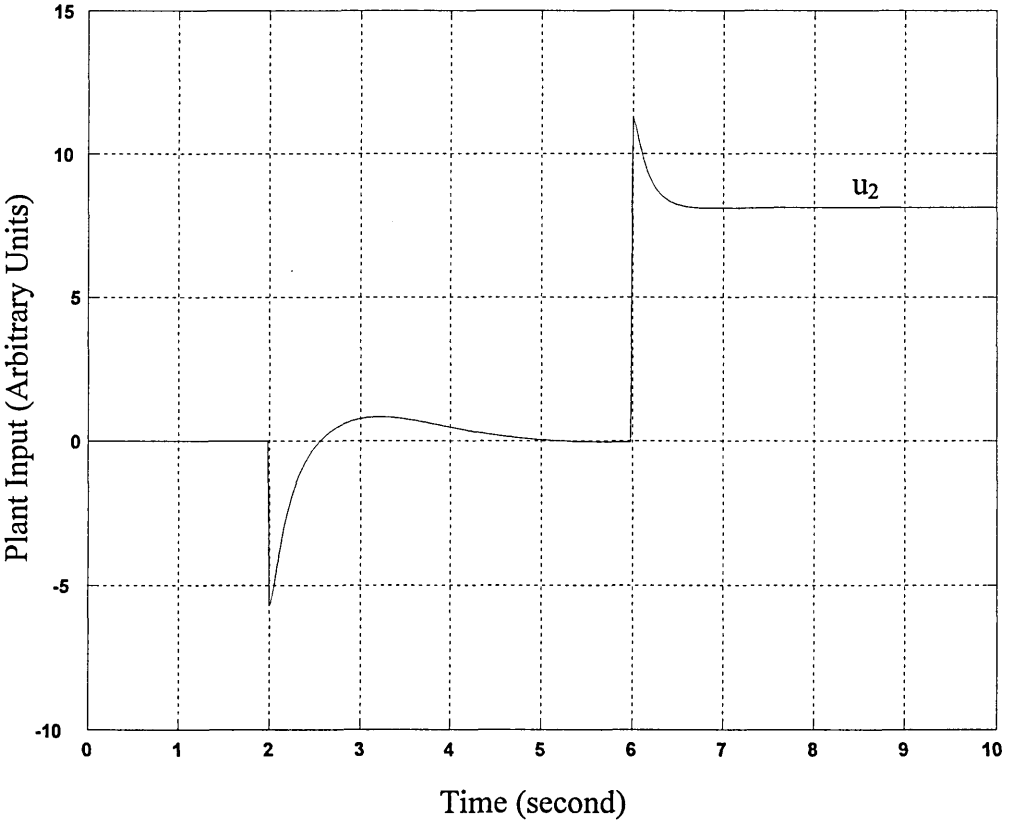

Fig 4.33 Discrete ROO Controller Simulation - Plant Input u_2

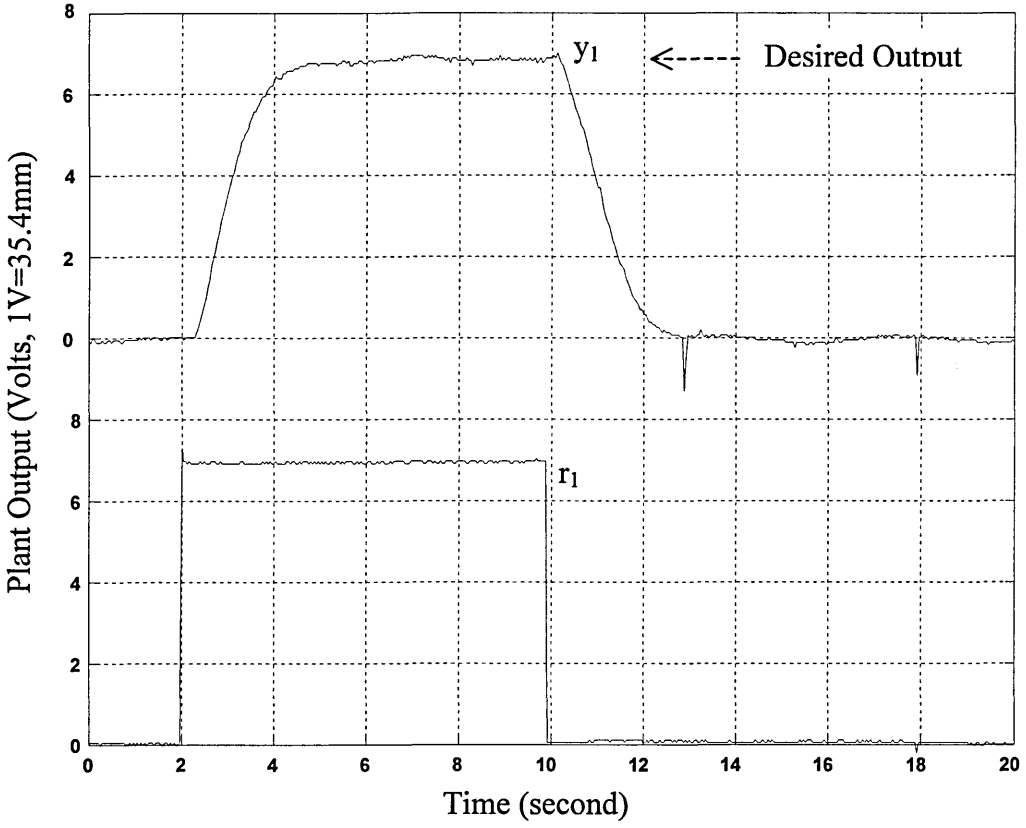

Fig 4.34 Implementation with ROO - Plant Output y_1

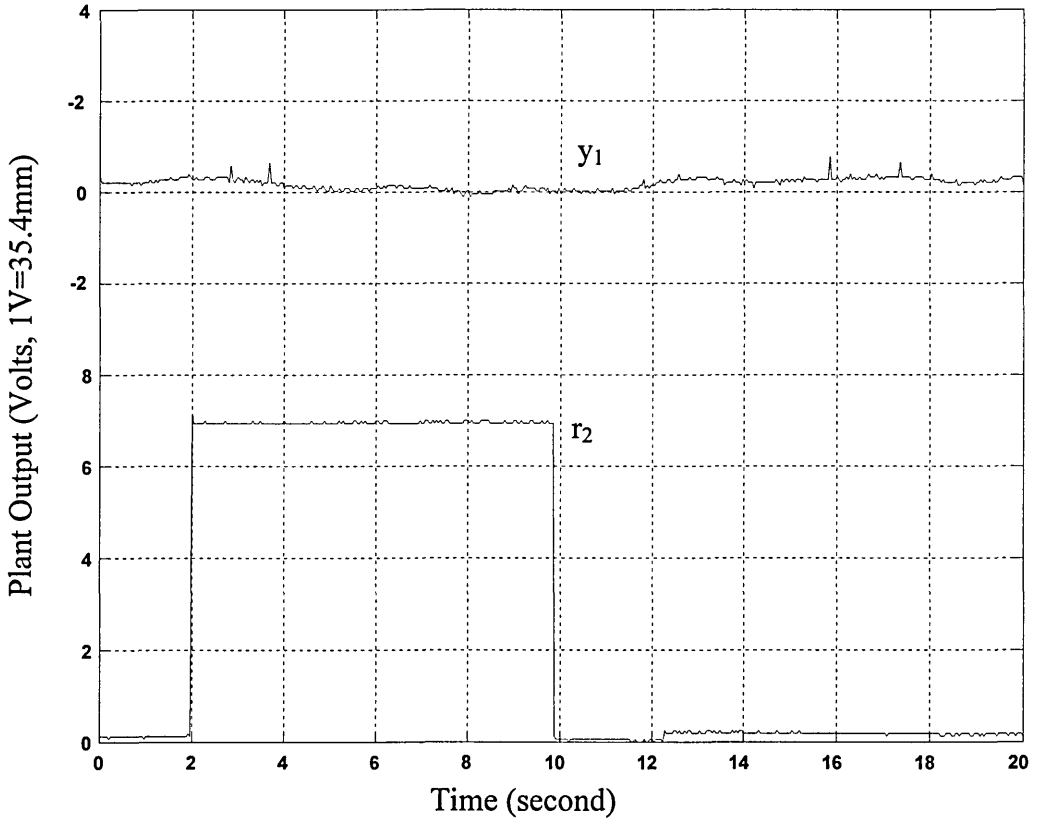

Fig 4.35 Implementation with ROO - Plant Output y_1

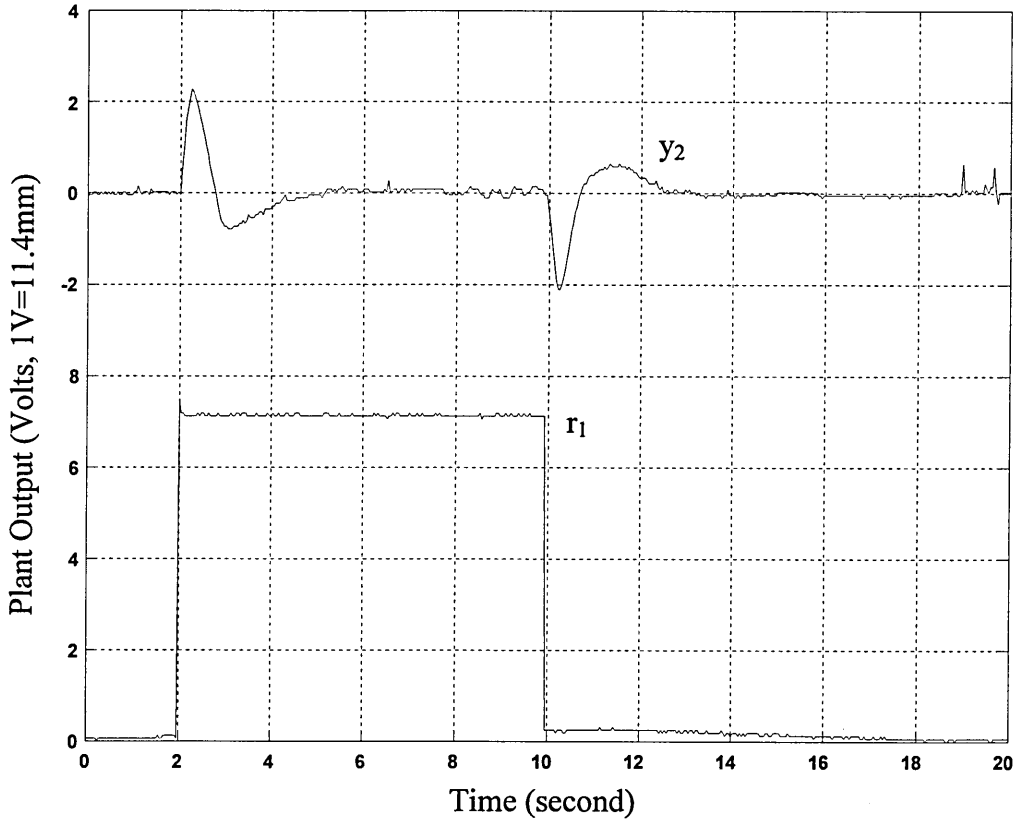

Fig 4.36 Implementation with ROO - Plant Output y_2

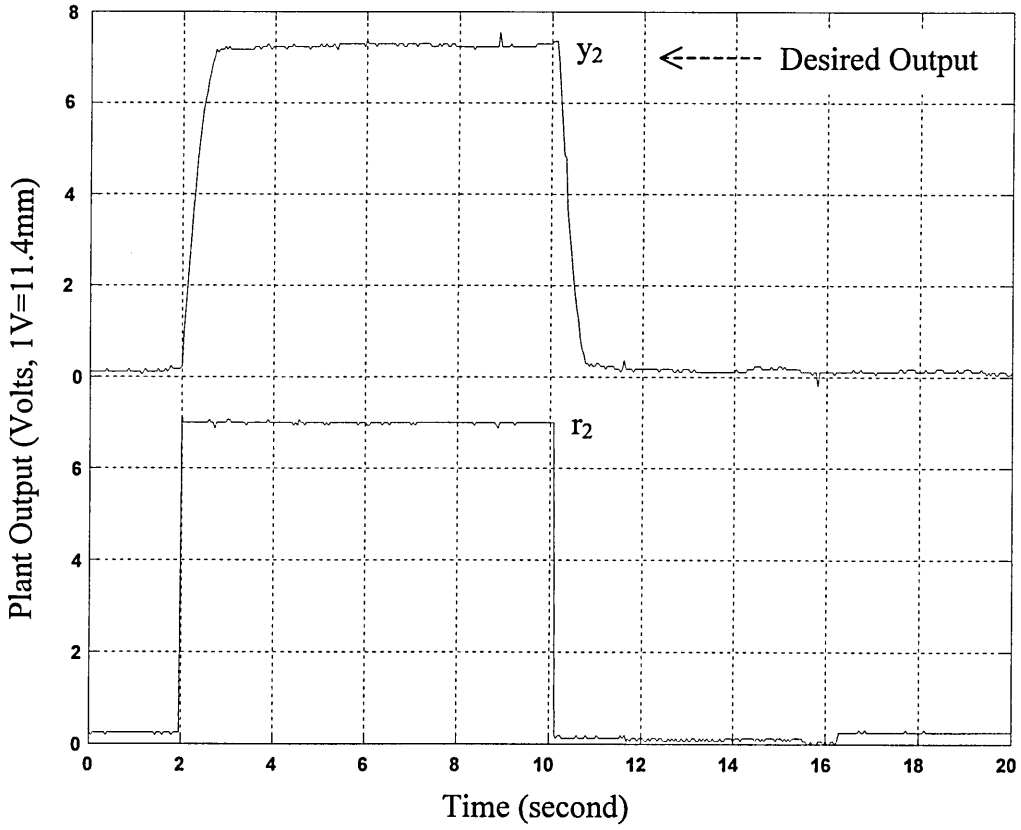

Fig 4.37 Implementation with ROO - Plant Output y_2

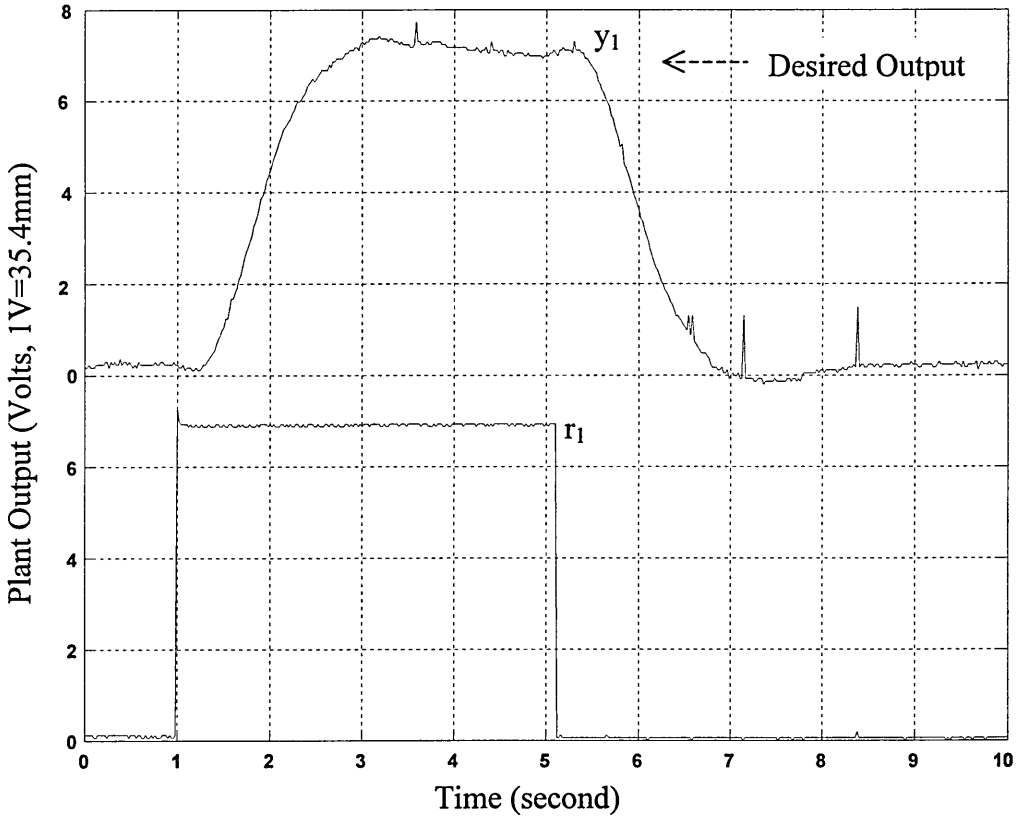

Fig 4.38 Improved LQG Implementation - Plant Output y_1

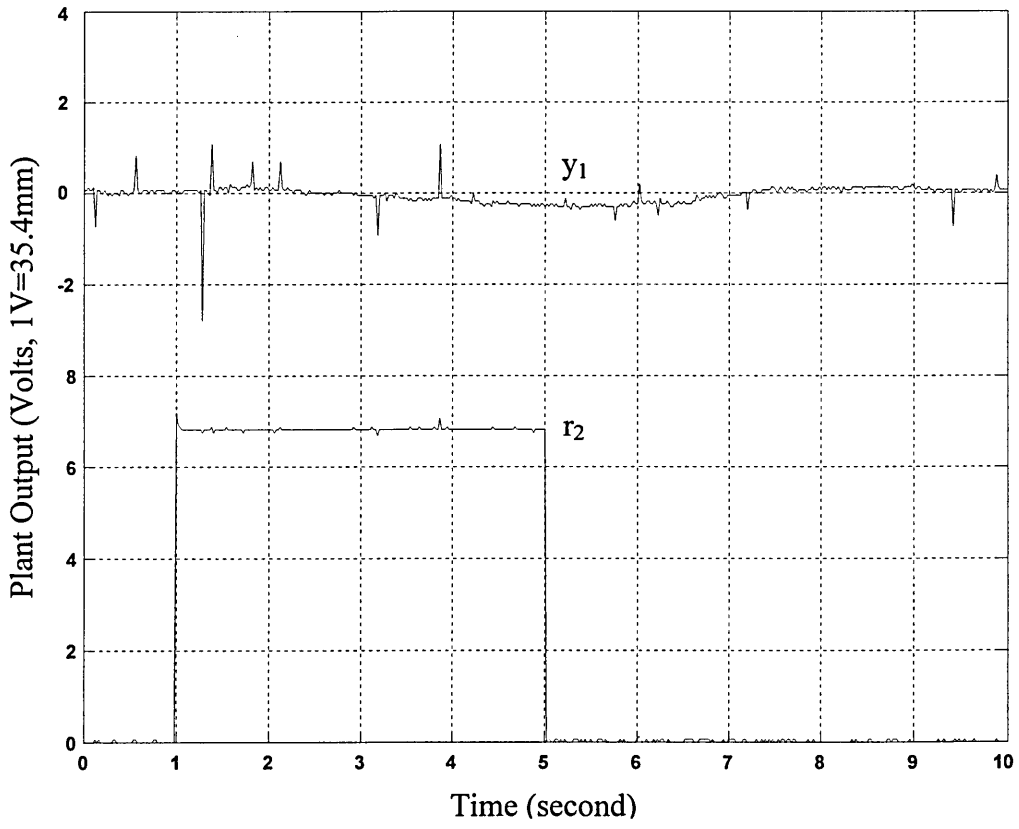

Fig 4.39 Improved LQG Implementation - Plant Output y_1

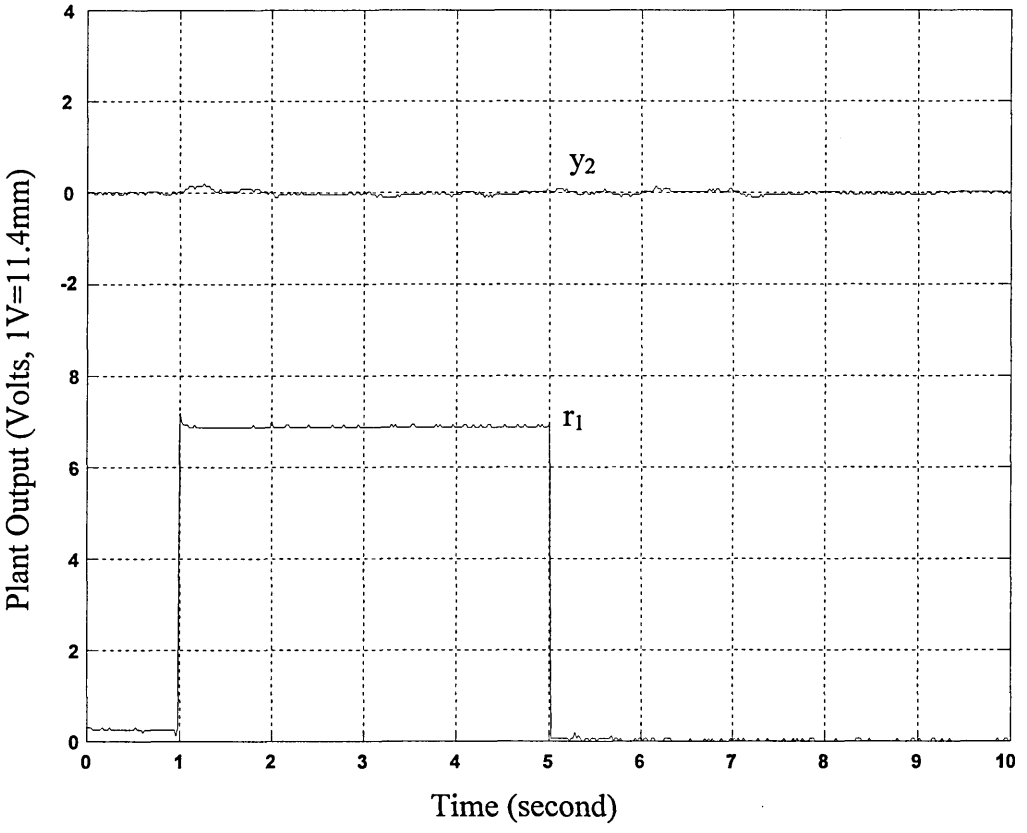

Fig 4.40 Improved LQG Implementation - Output y_2

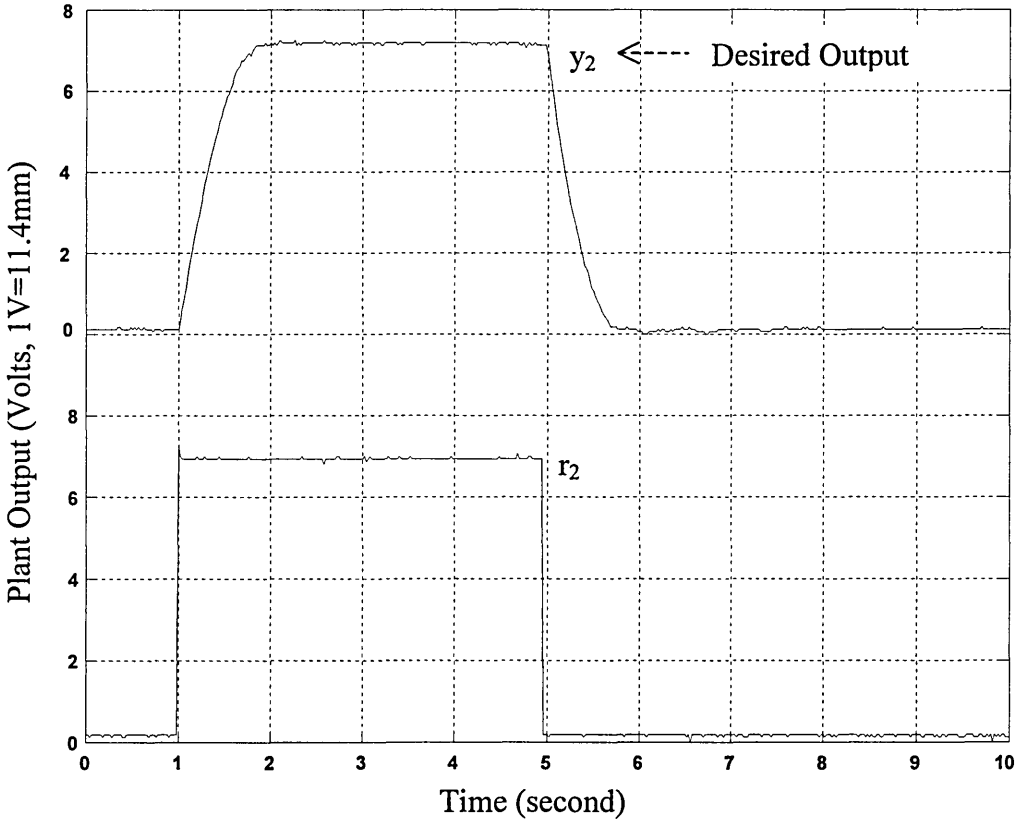

Fig 4.41 Improved LQG Implementation - Plant Output y_2

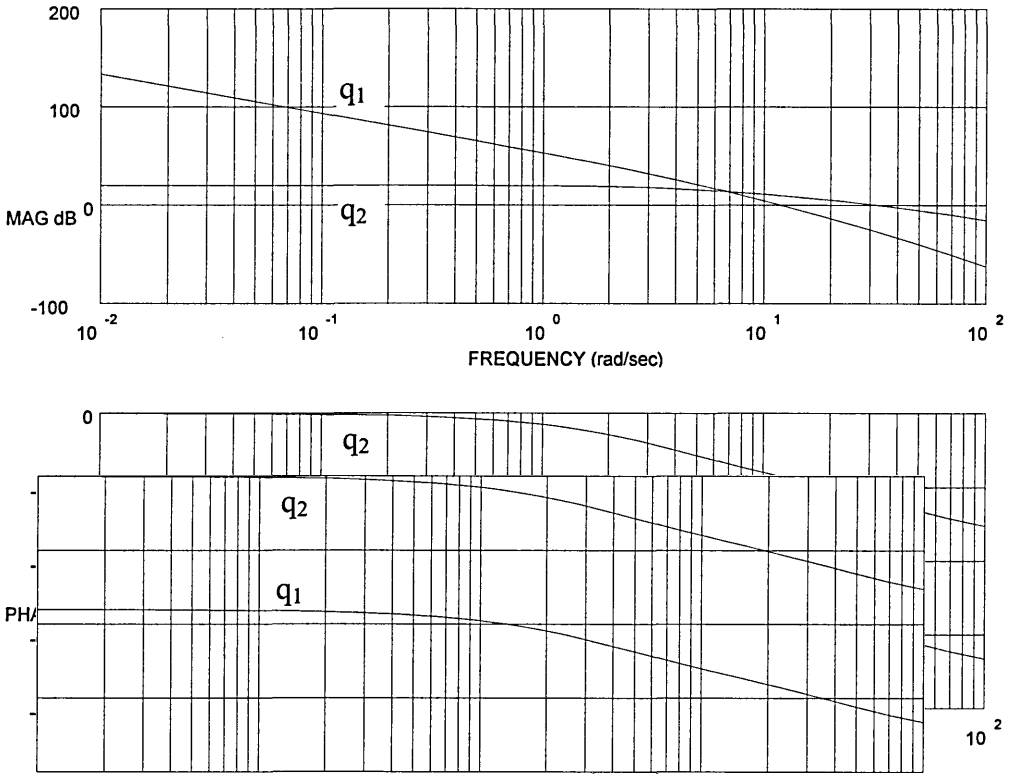

Fig 4.42 Characteristic Loci of GK_h

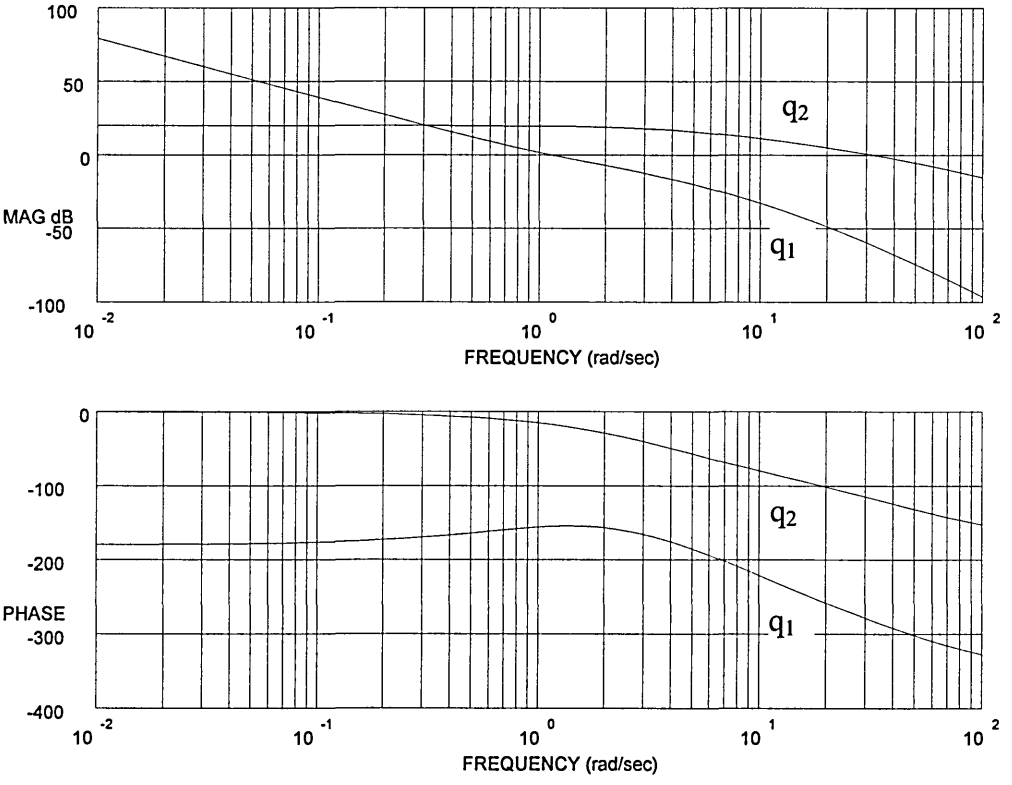

Fig 4.43 Characteristic Loci of GK_hK_m

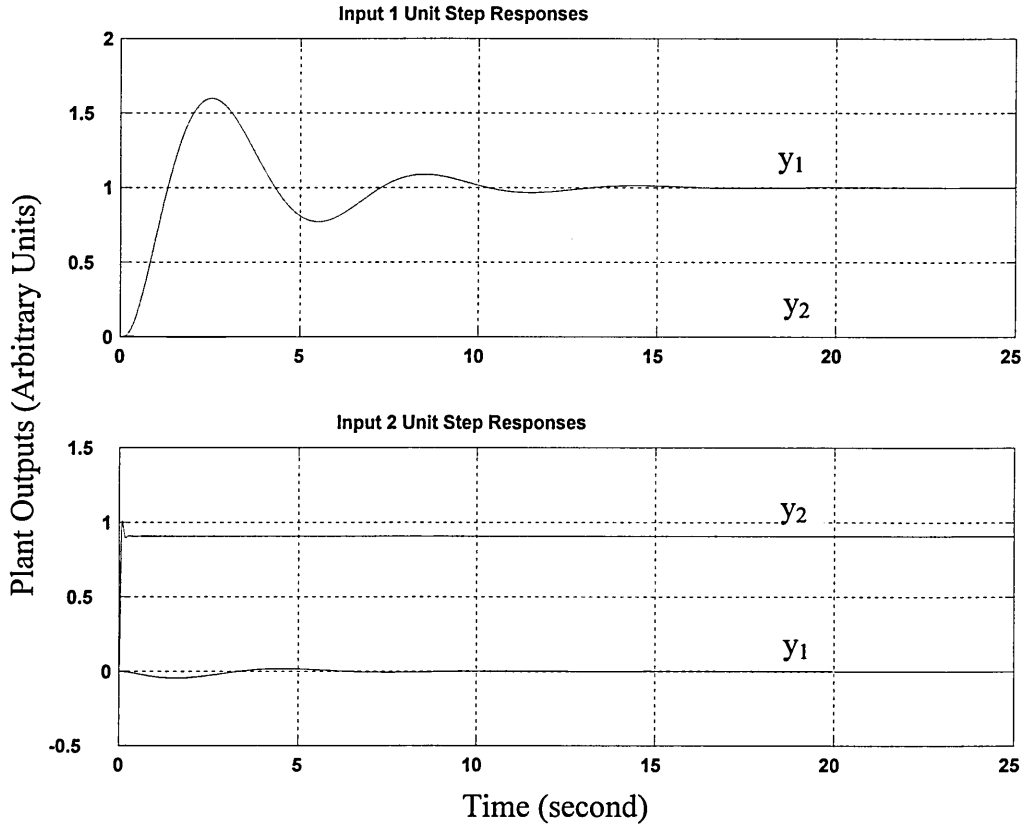

Fig 4.44 Continuous CL Controller Simulation - Plant Outputs with K_h and $K_m(s)$

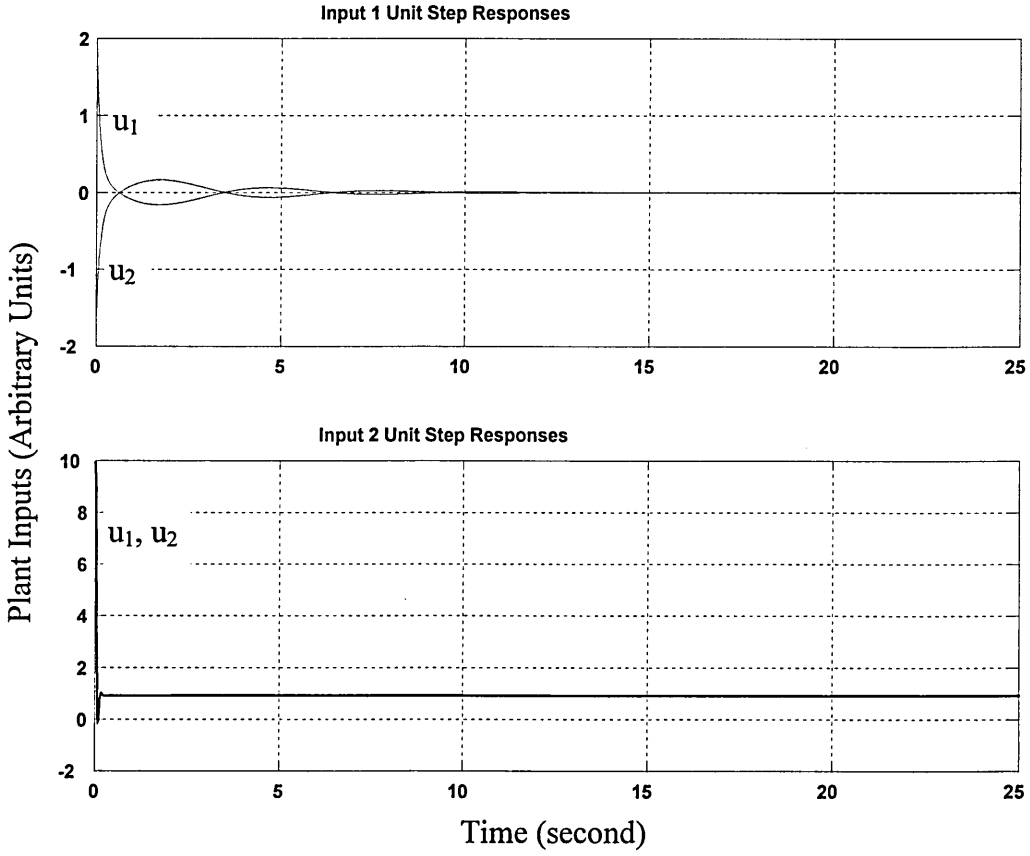

Fig 4.45 Continuous CL Controller Simulation - Plant Inputs with K_h and $K_m(s)$

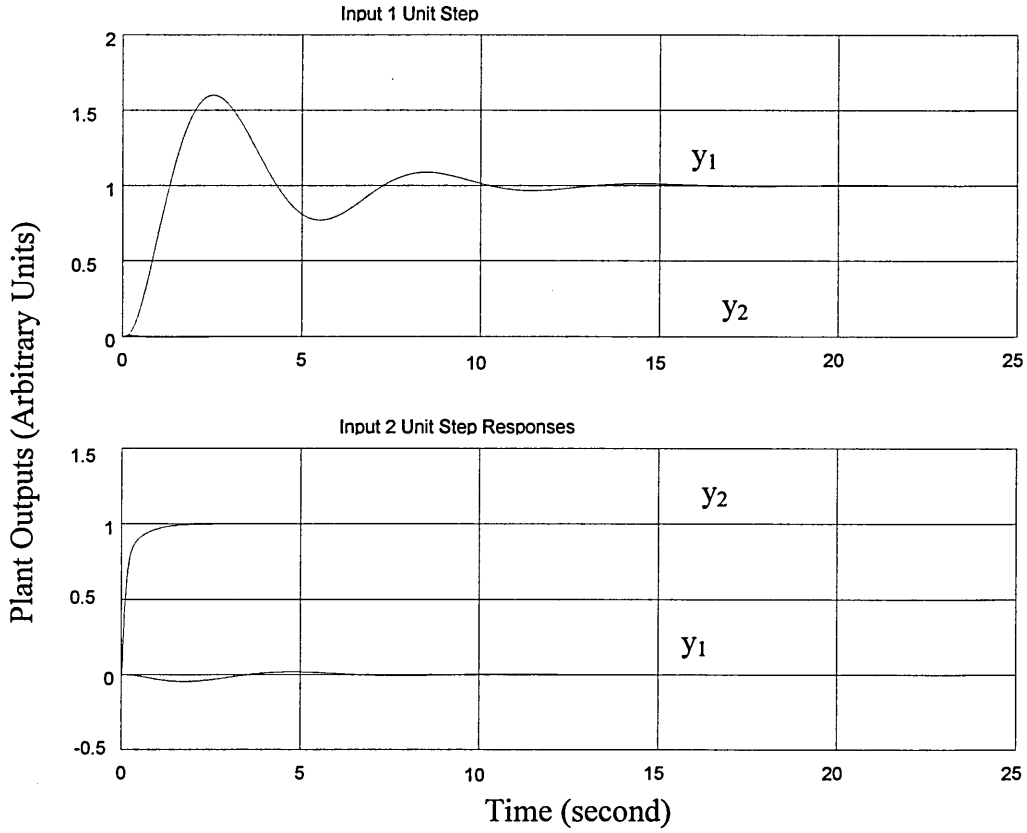

Fig 4.46 Continuous CL Controller Simulation - Plant Outputs

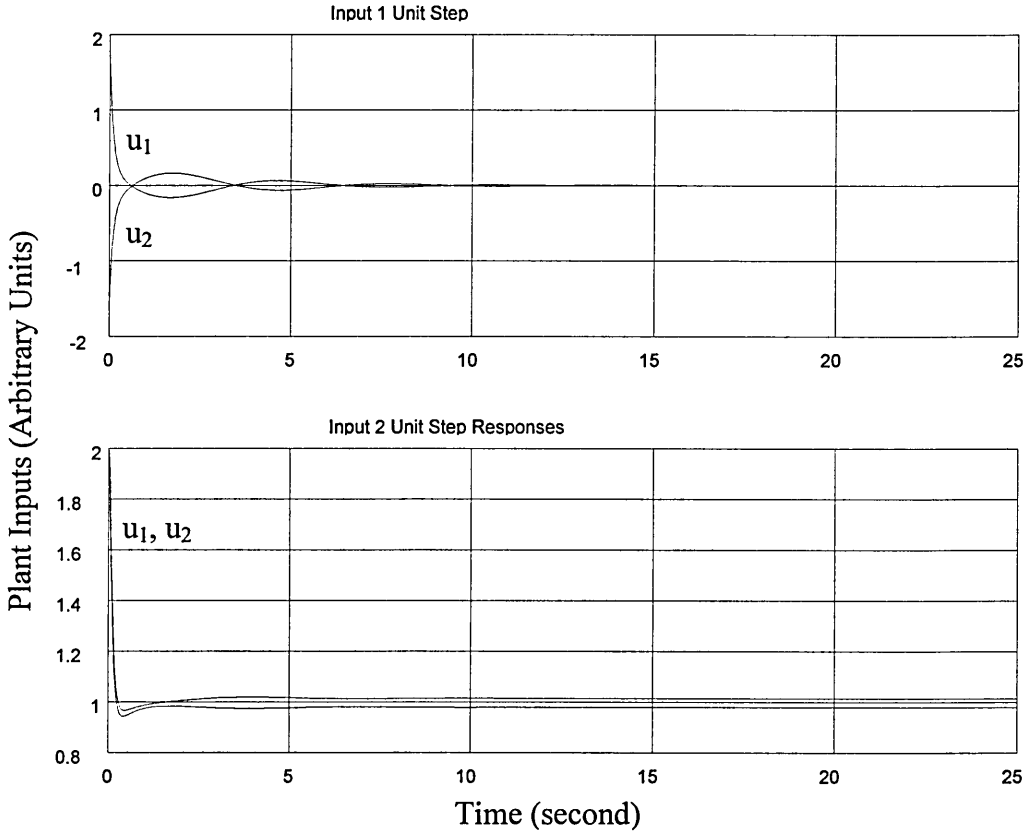

Fig 4.47 Continuous CL Controller Simulation - Plant Inputs

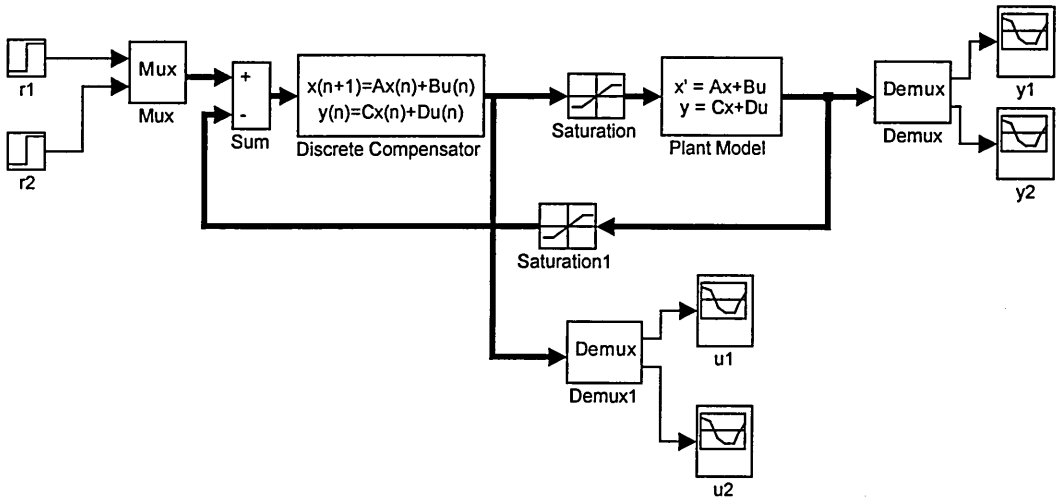

Fig 4.48 Simulink Model for Discrete CL Controller

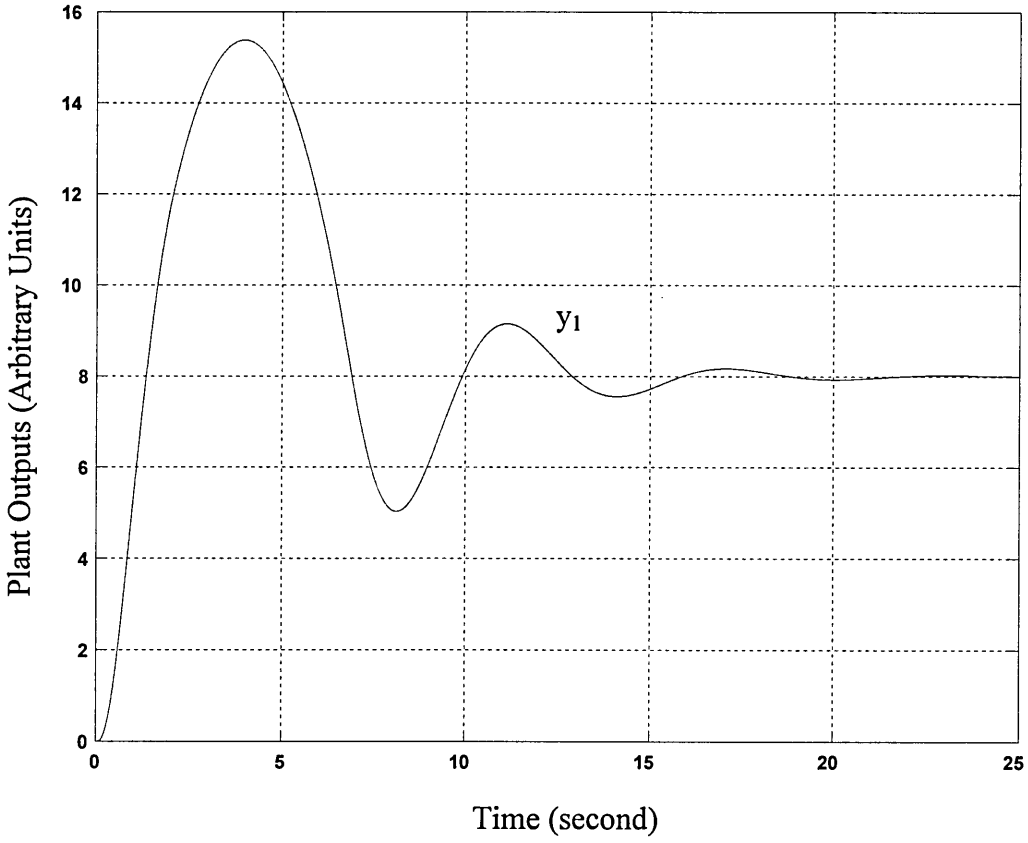

Fig 4.49 Discrete CL Controller Simulation - Plant Output y_1

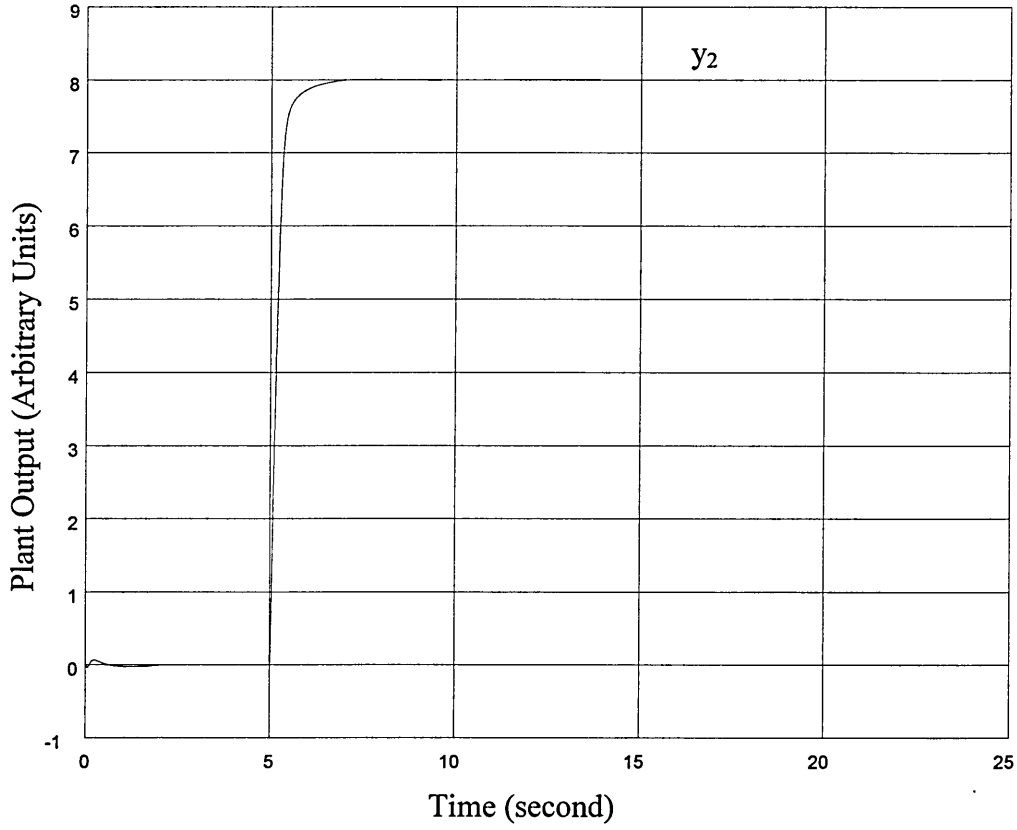

Fig 4.50 Discrete CL Controller Simulation - Plant Output y_2

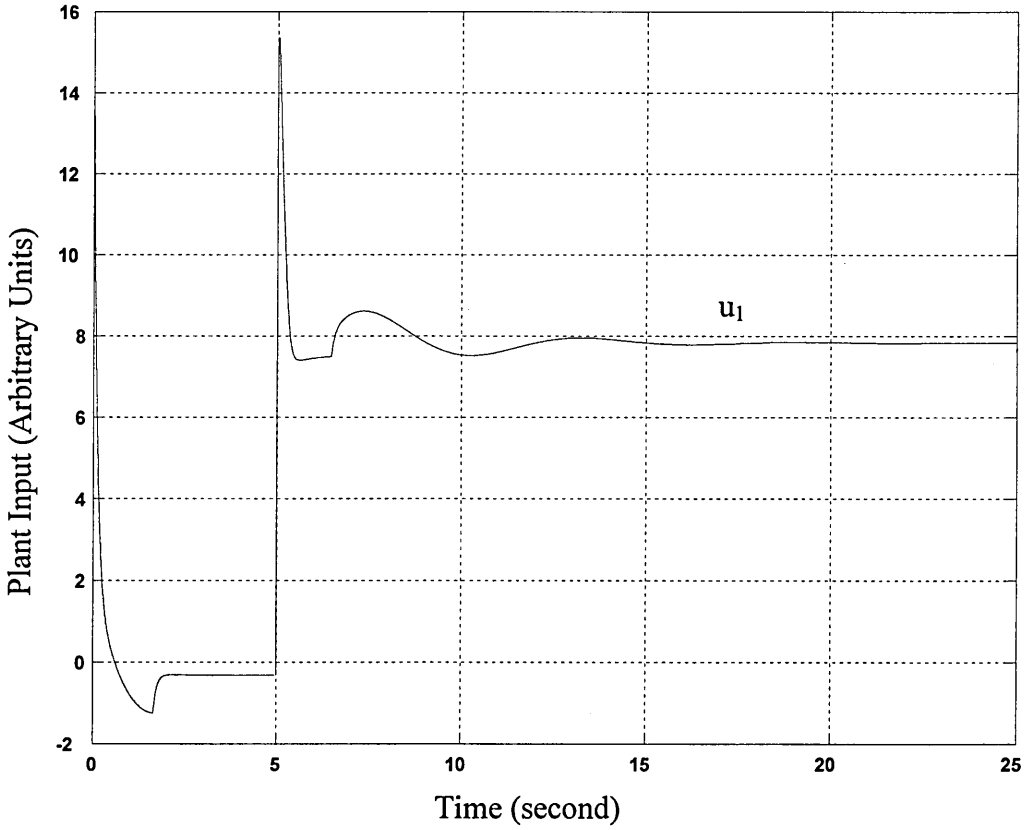

Fig 4.51 Discrete CL Controller Simulation - Plant Input u_1

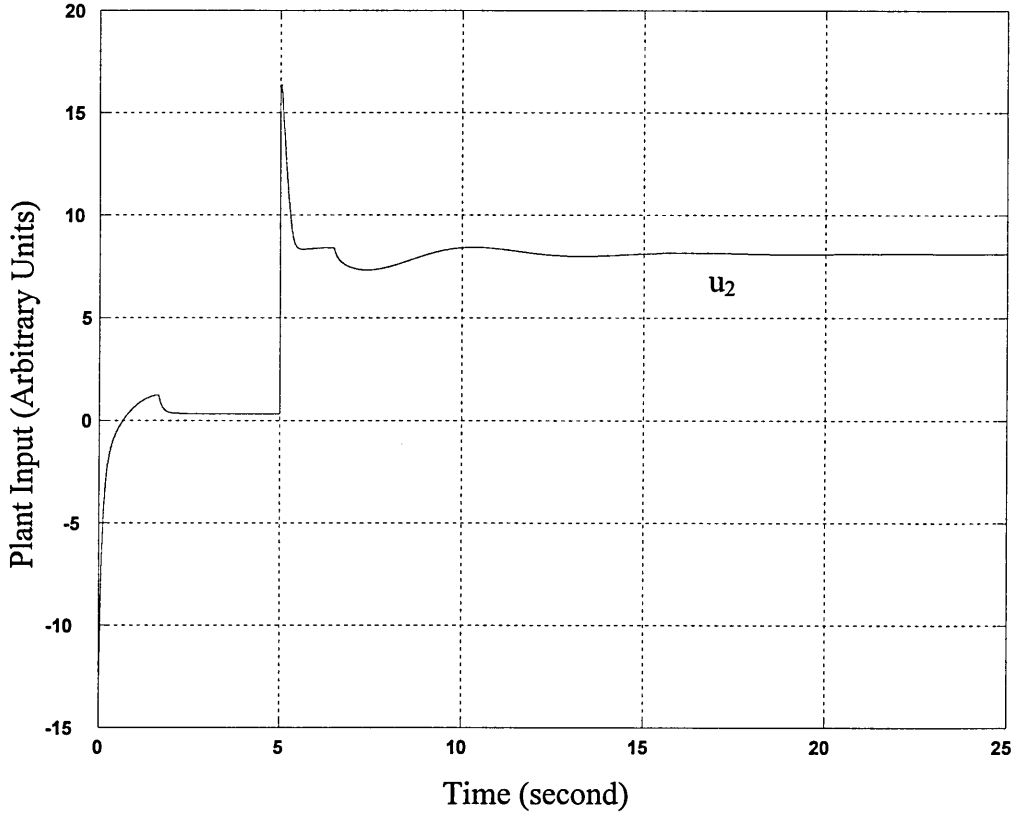

Fig 4.52 Discrete CL Controller Simulation - Plant Input u_2

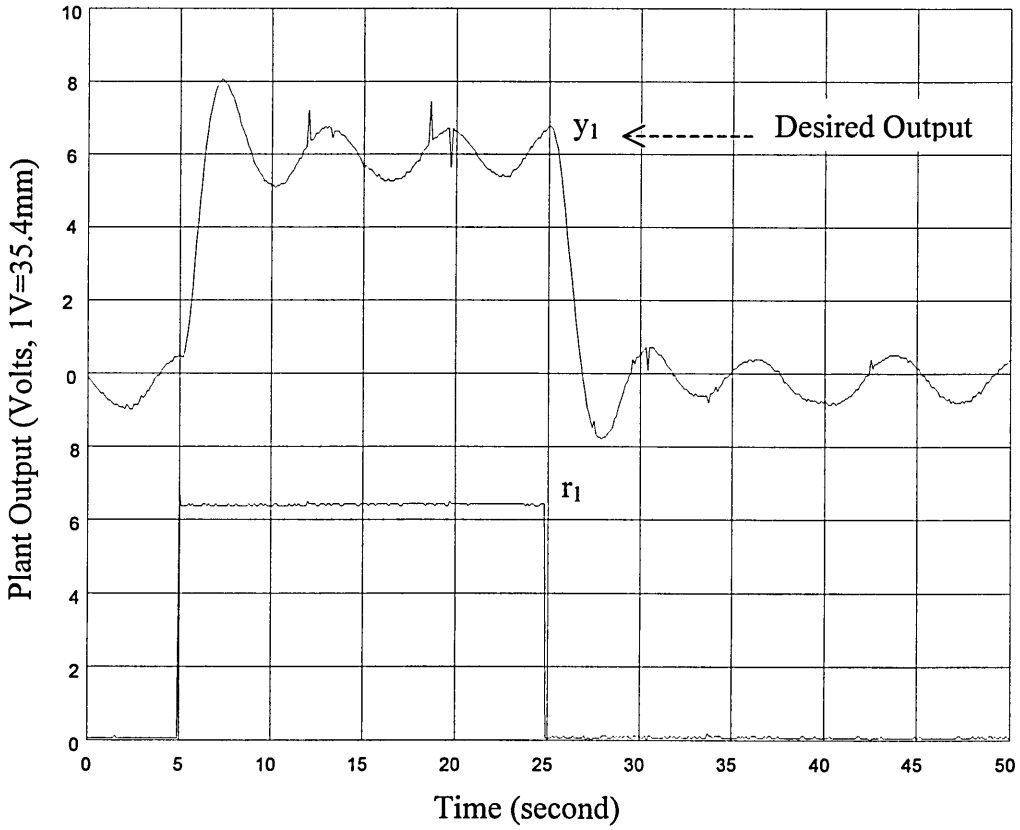

Fig 4.53 Implementation with CL Controller - Plant Output y_1

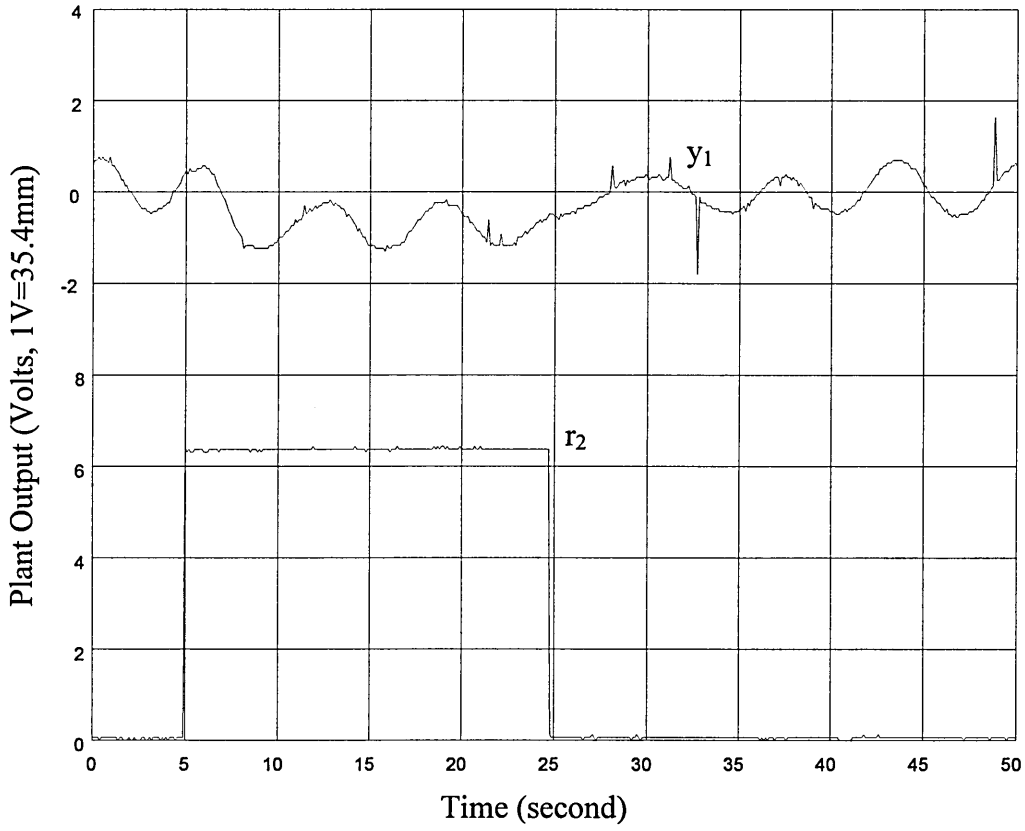

Fig 4.54 Implementation with CL Controller - Plant Output y_1

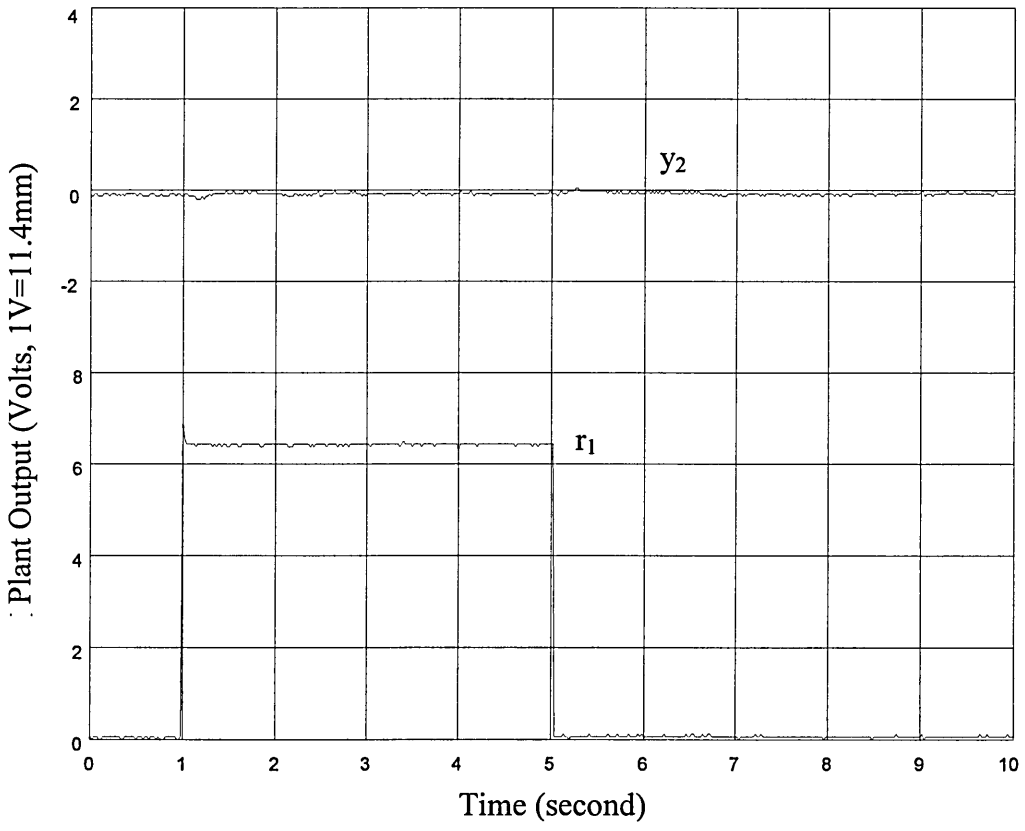

Fig 4.55 Implementation with CL Controller - Plant Output y_2

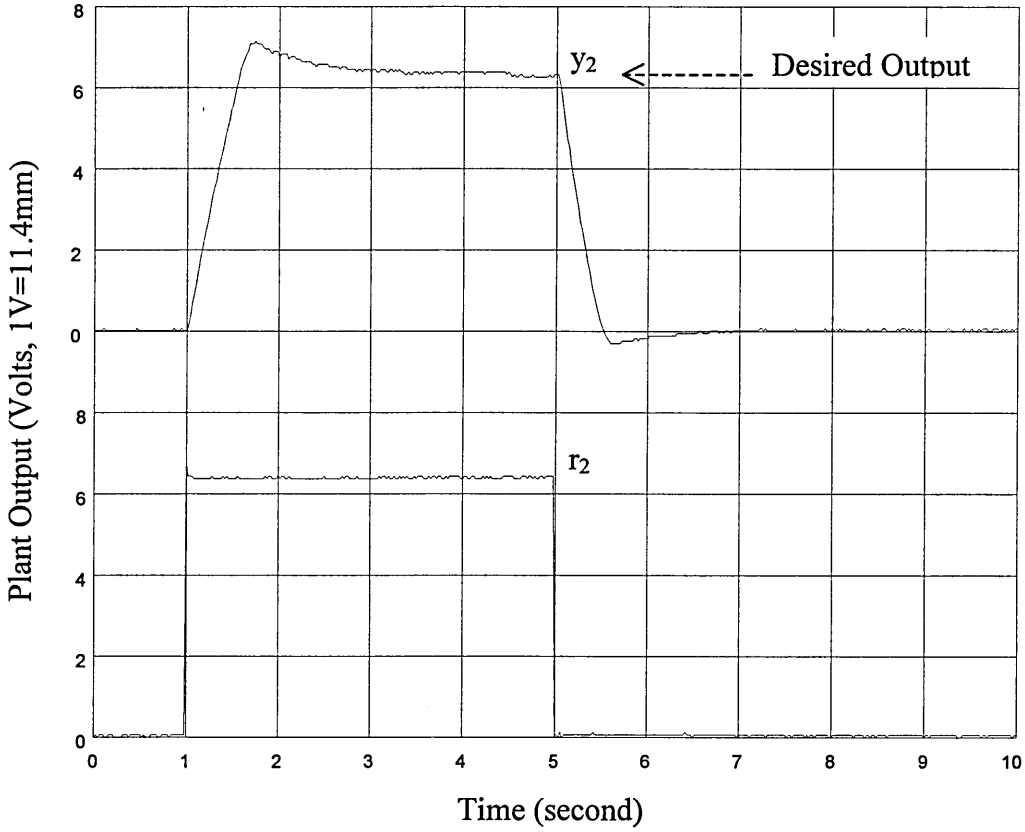

Fig 4.56 Implementation with CL Controller - Plant Output y_2

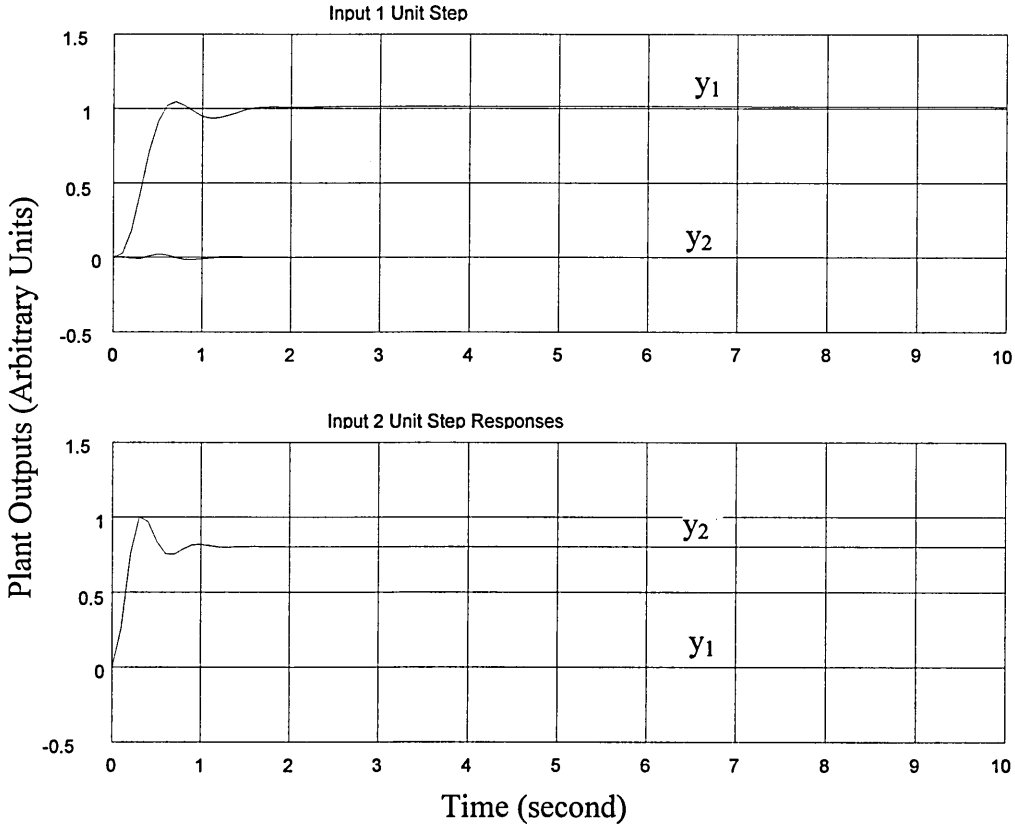

Fig 4.57 Continuous H^{∞} Controller Simulation - Plant Outputs

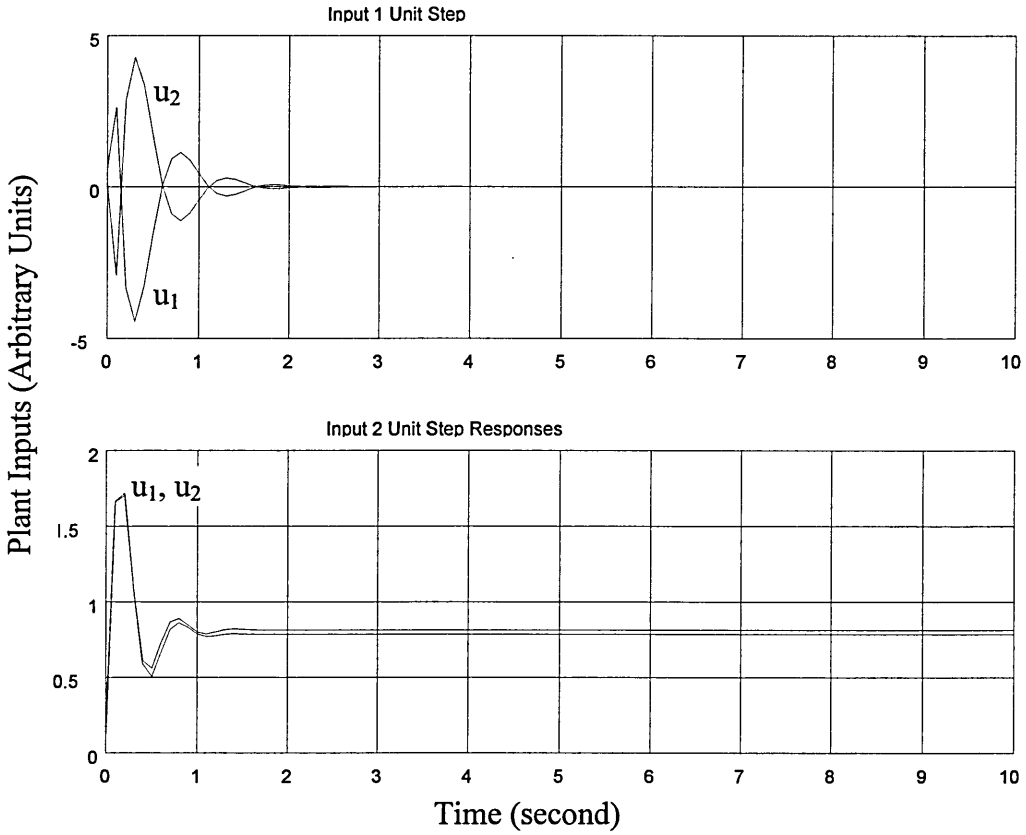

Fig 4.58 Continuous H^{∞} Controller Simulation - Plant Inputs

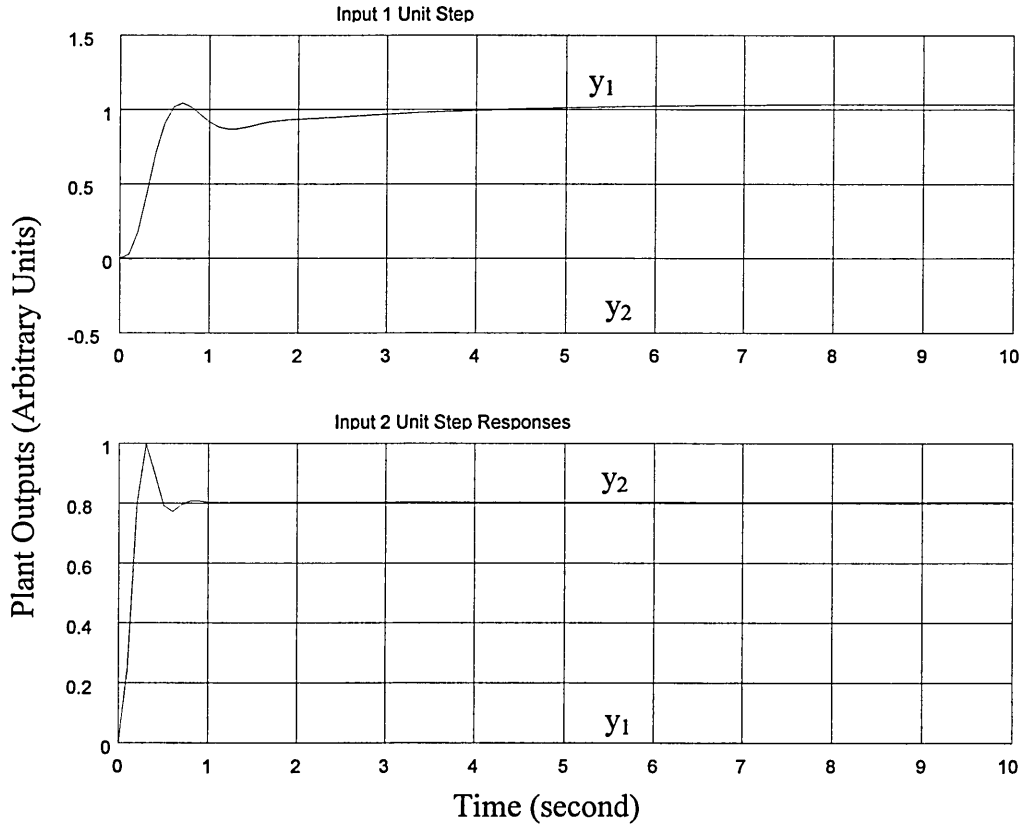

Fig 4.59 Continuous Full-order H^{∞} Controller Simulation - Plant Outputs

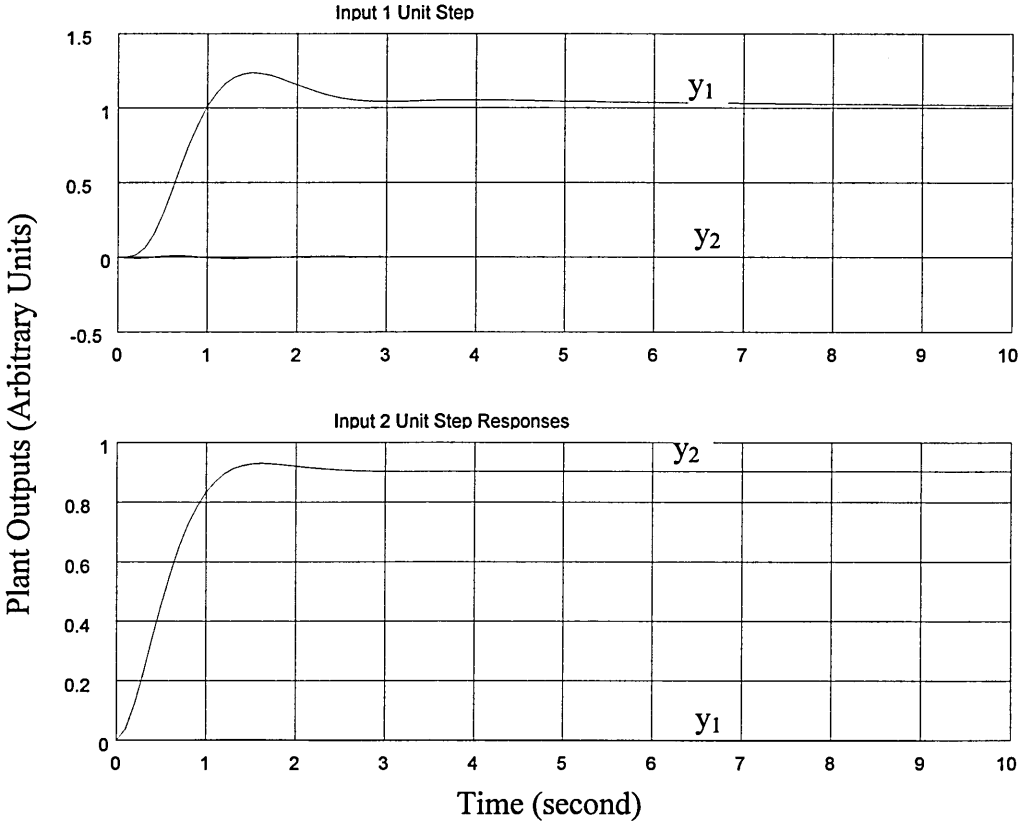

Fig 4.60 Continuous H^{∞} Controller Simulation - Plant Outputs

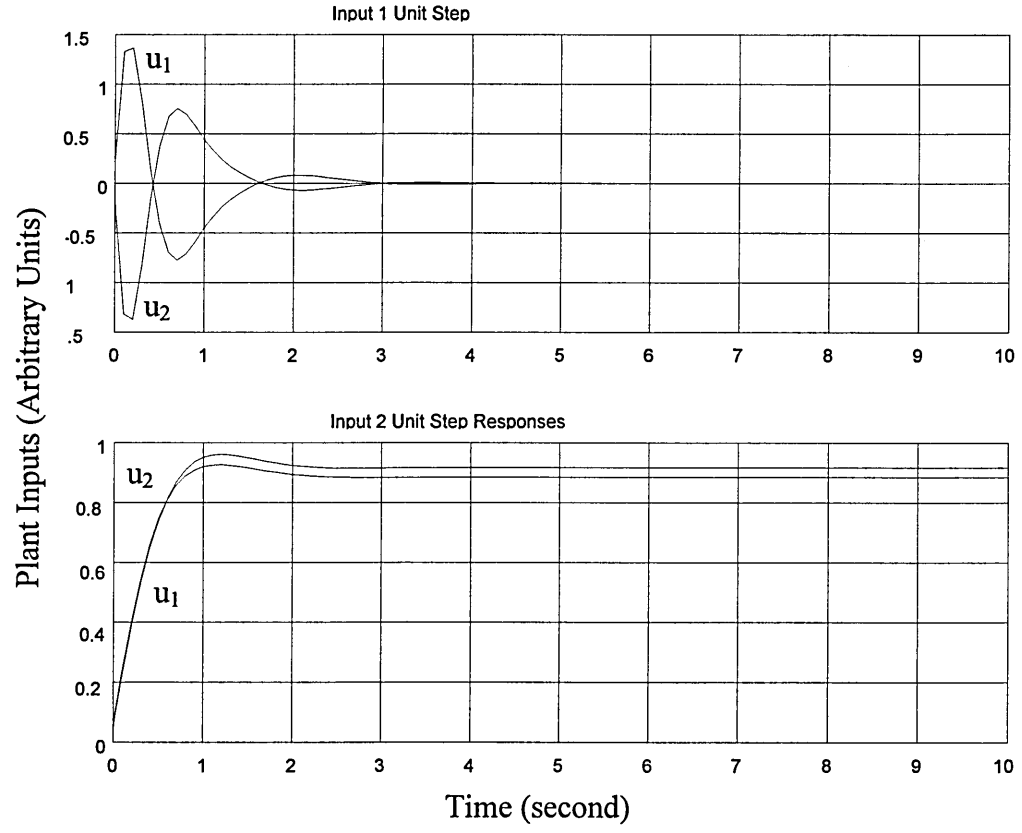

Fig 4.61 Continuous H^{∞} Controller Simulation - Plant Inputs

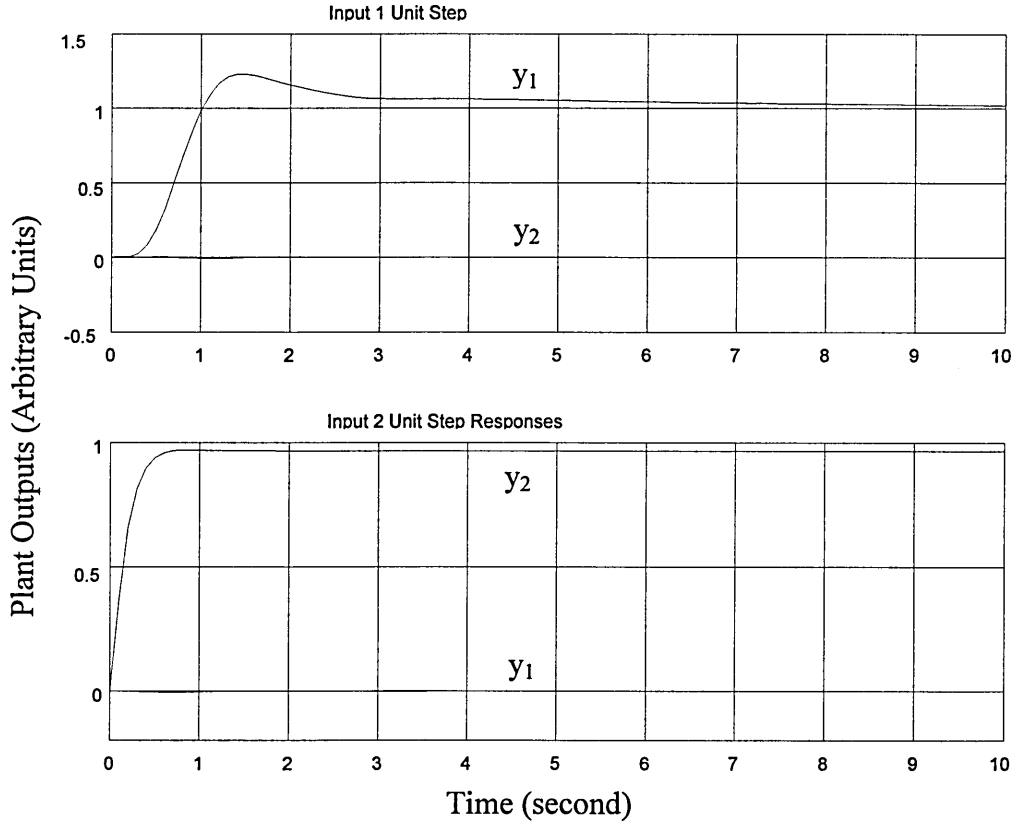

Fig 4.62 Continuous H∞ Controller Simulation - Plant Outputs

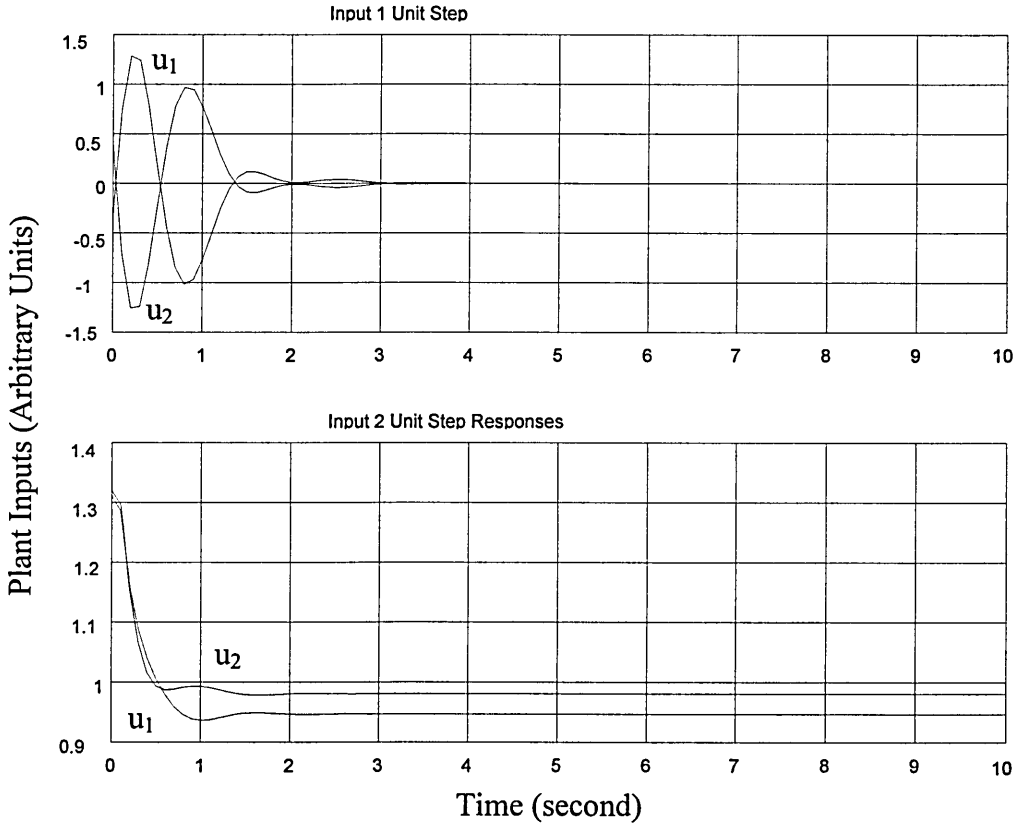

Fig 4.63 Continuous H^{∞} Controller - Plant Inputs

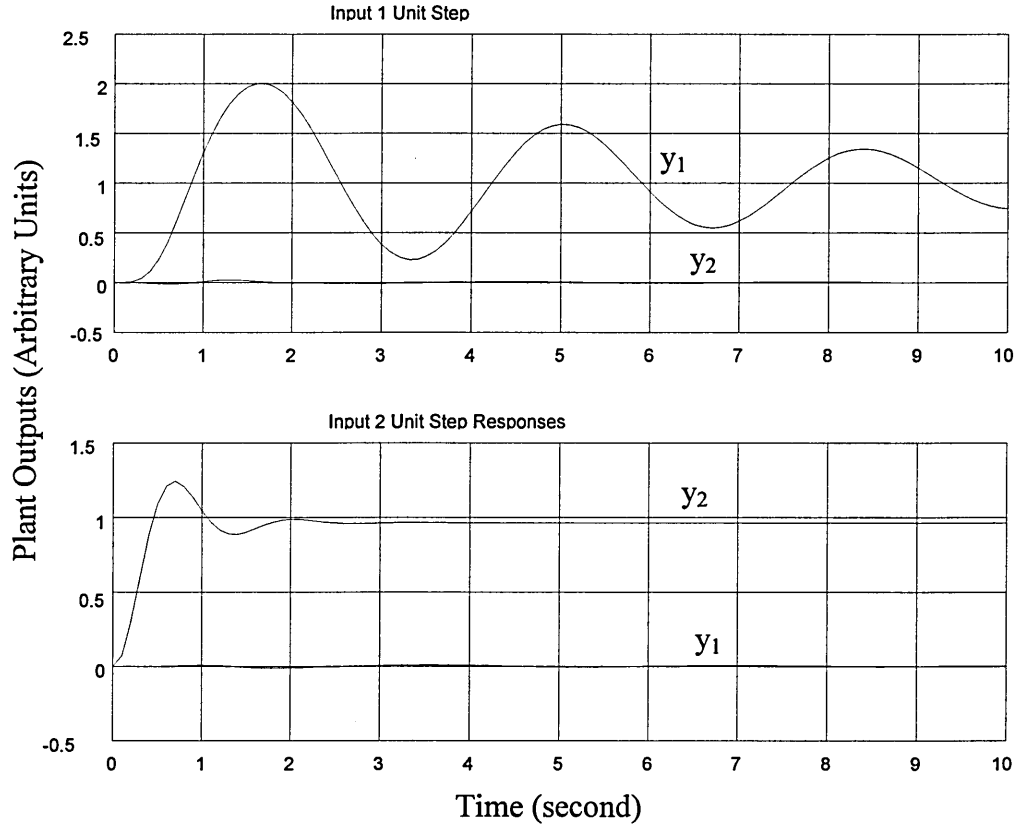

Fig 4.64 Continuous H^{∞} Controller (Reduced by OHMDA) Simulation- Plant Outputs

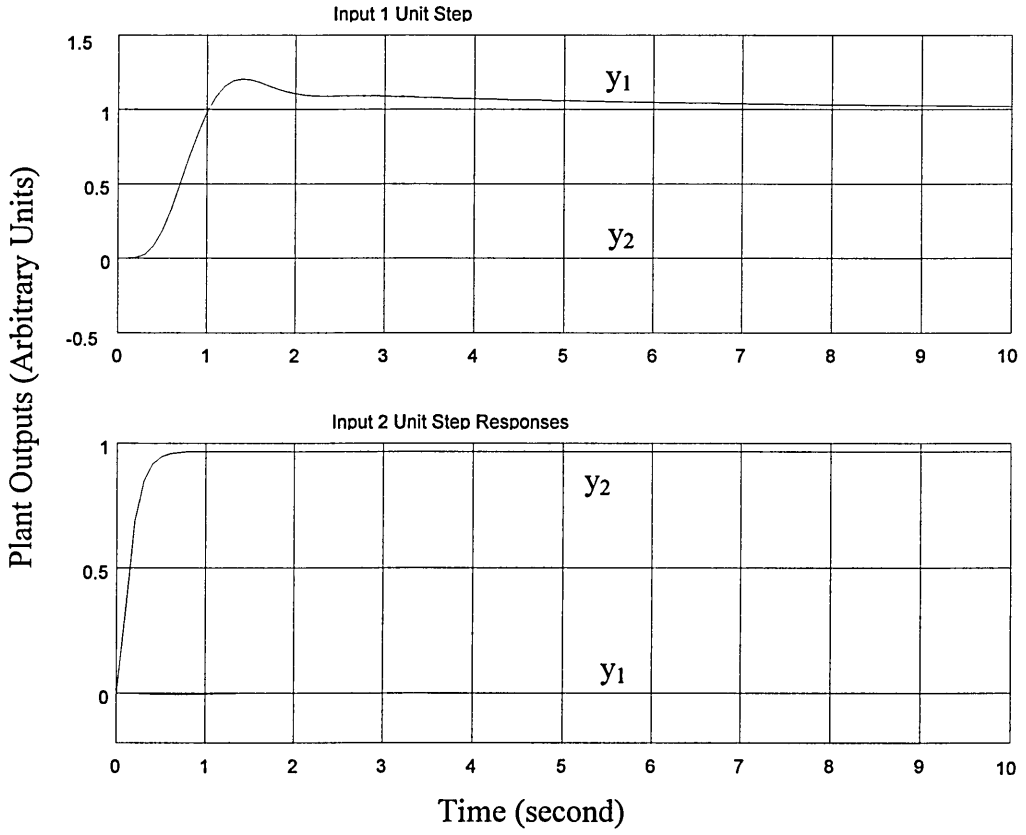

Fig 4.65 Continuous Full-order H^{∞} Controller - Plant Outputs

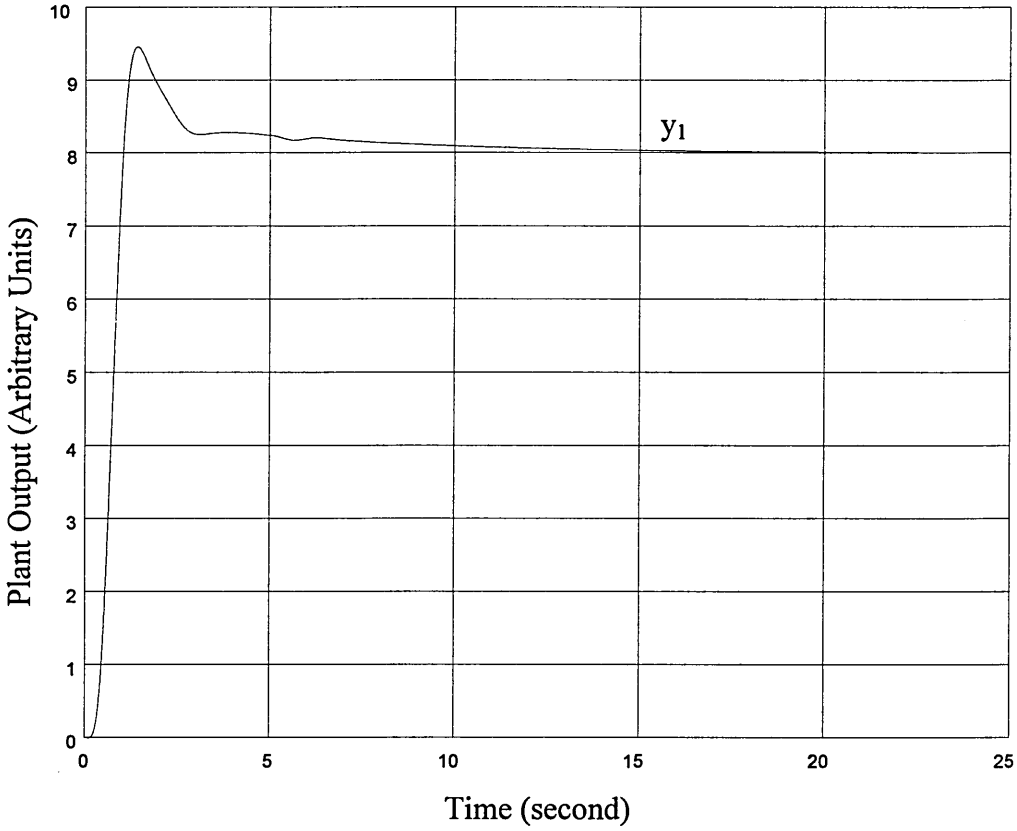

Fig 4.66 Discrete H∞ Controller Simulation - Plant Output y_1

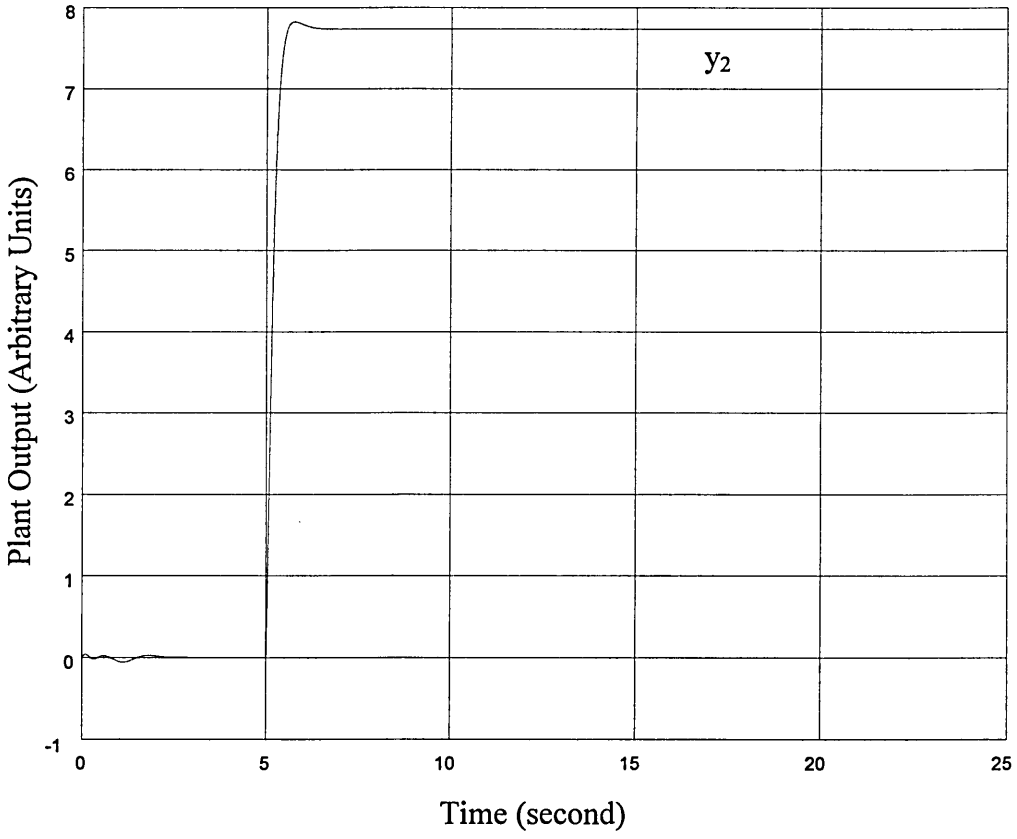

Fig 4.67 Discrete H^{∞} Controller Simulation - Plant Output y_2

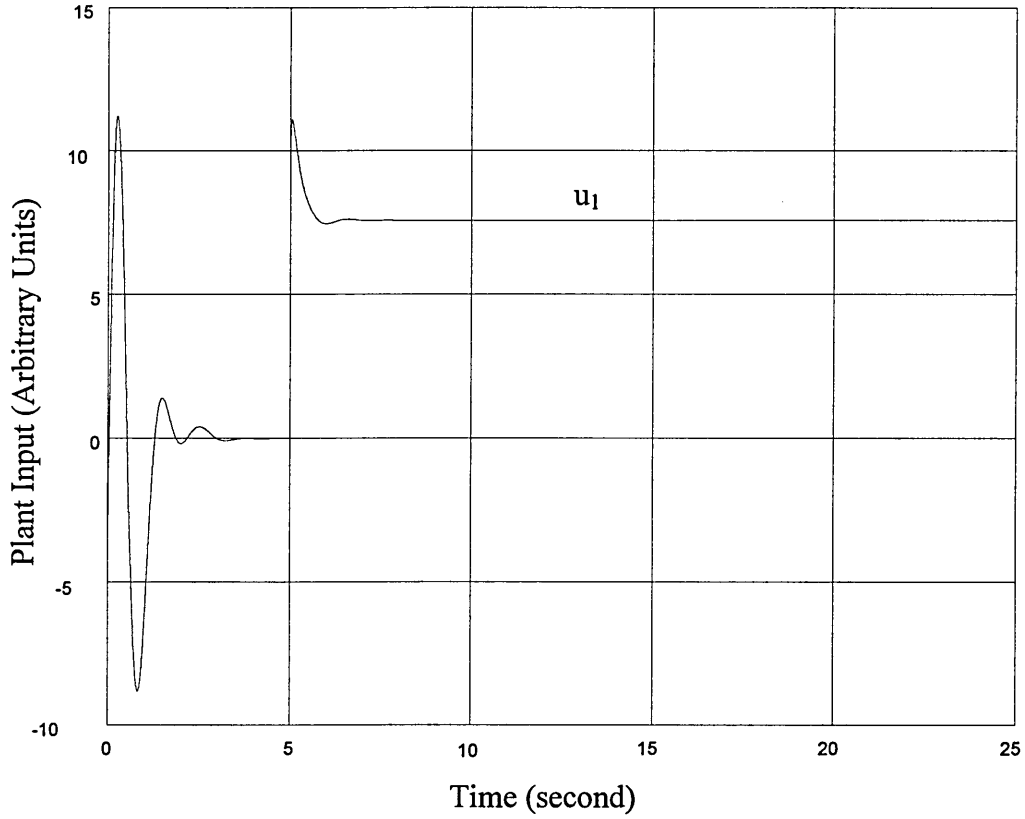

Fig 4.68 Discrete H∞ Controller Simulation - Plant Input u_1

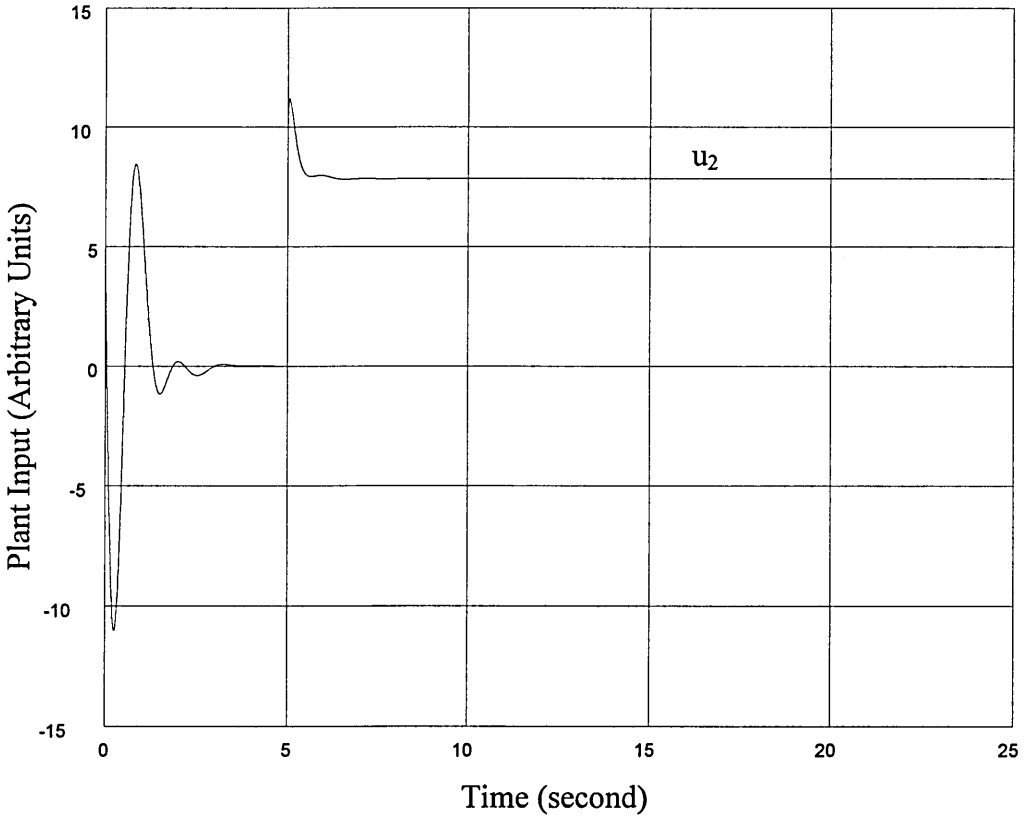

Fig 4.69 Discrete H∞ Controller Simulation - Plant Input u_2

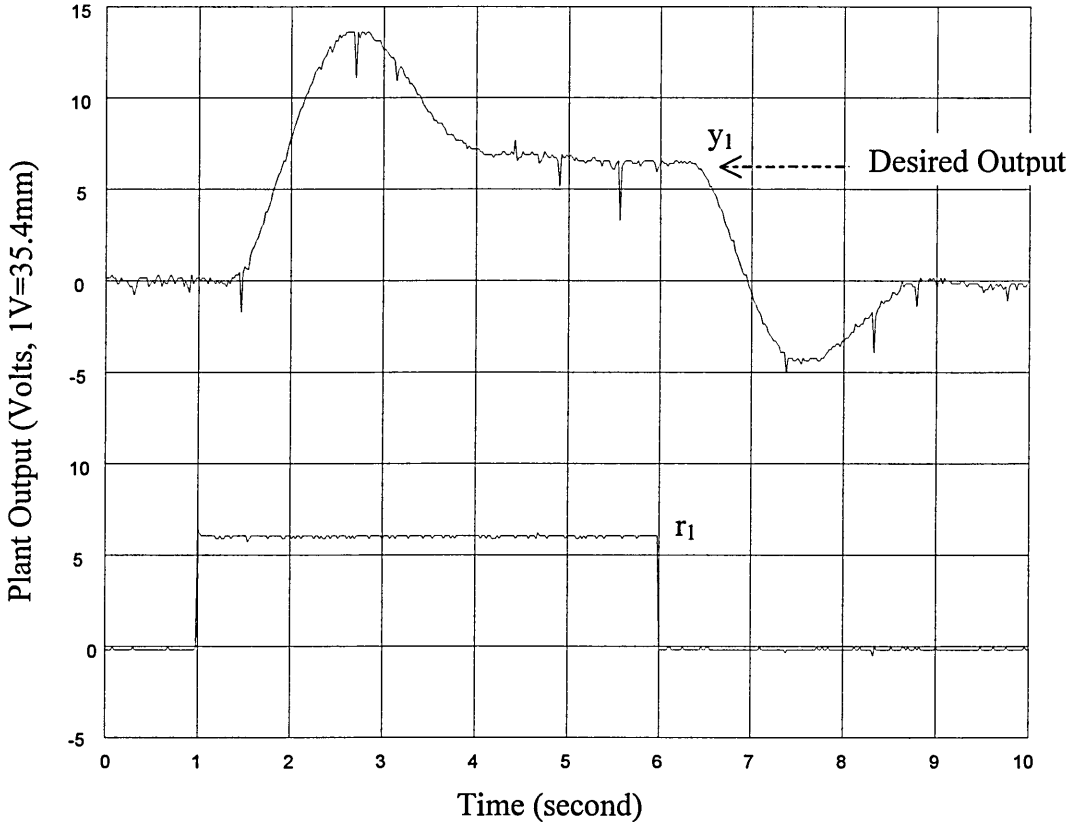

Fig 4.70 H∞ Controller Implementation - Plant Output y_1 for Step on r_1

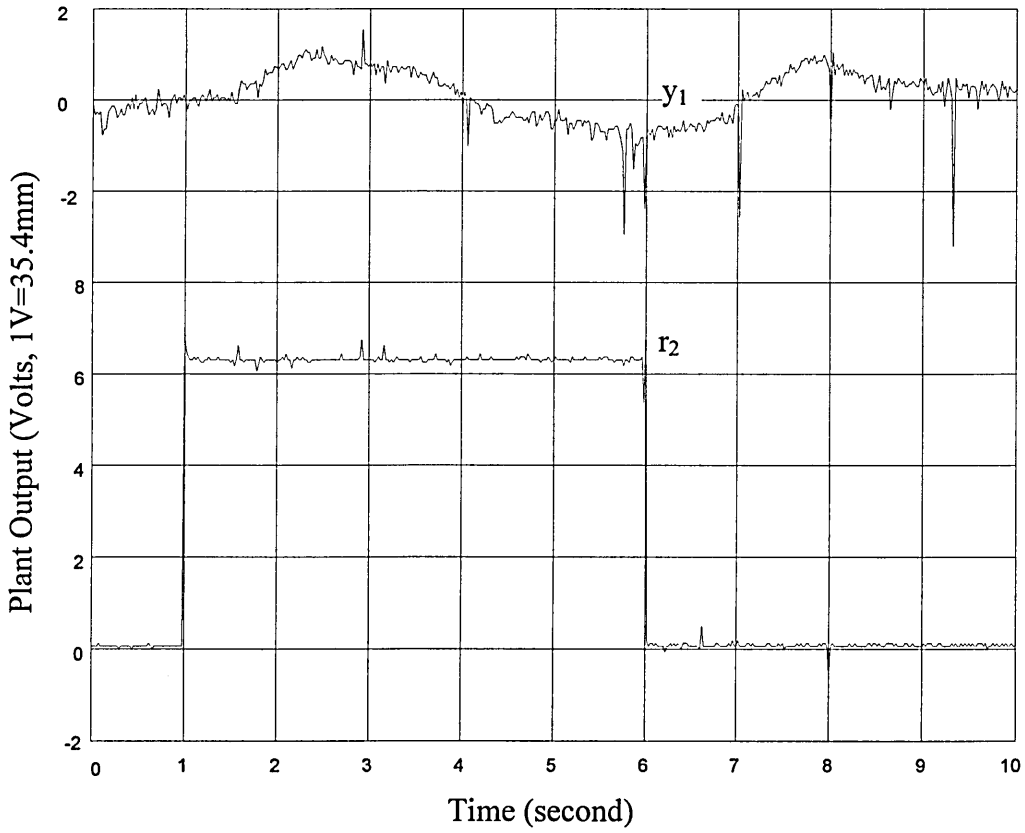

Fig 4.71 . H∞ Controller Implemenatation - Plant Output y_1 for Step on r_2

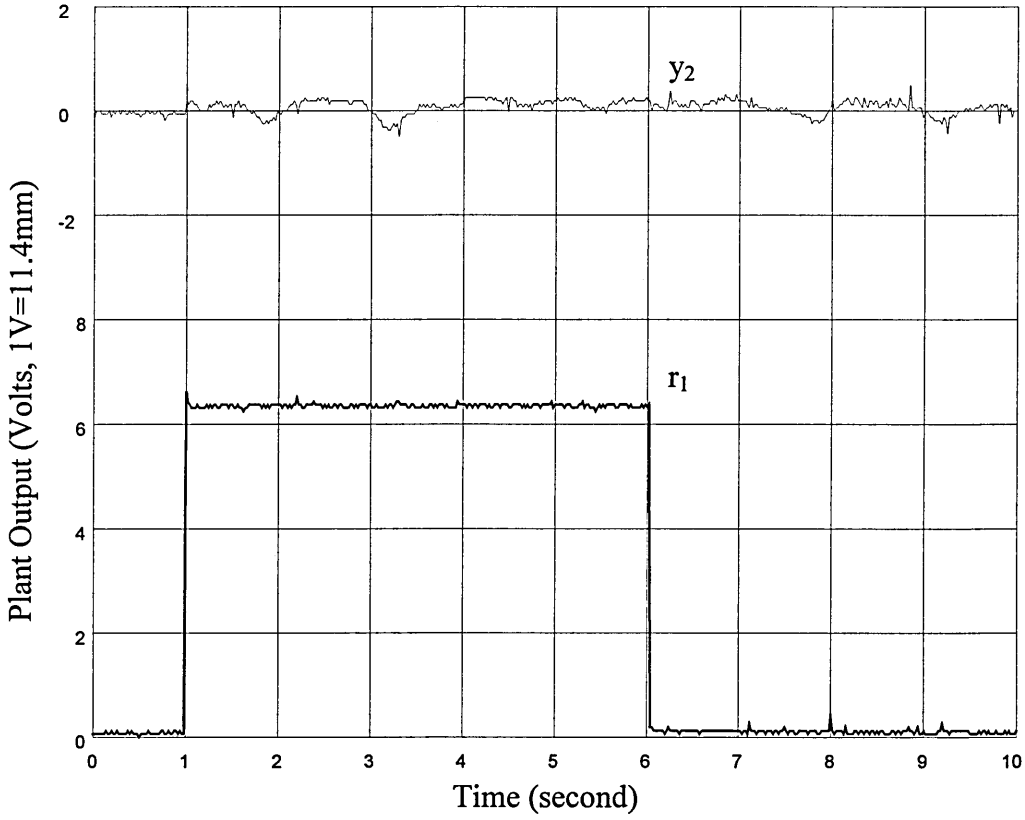

Fig 4.72 H^{∞} Controller Implementation - Plant Output y_2 for Step on r_1

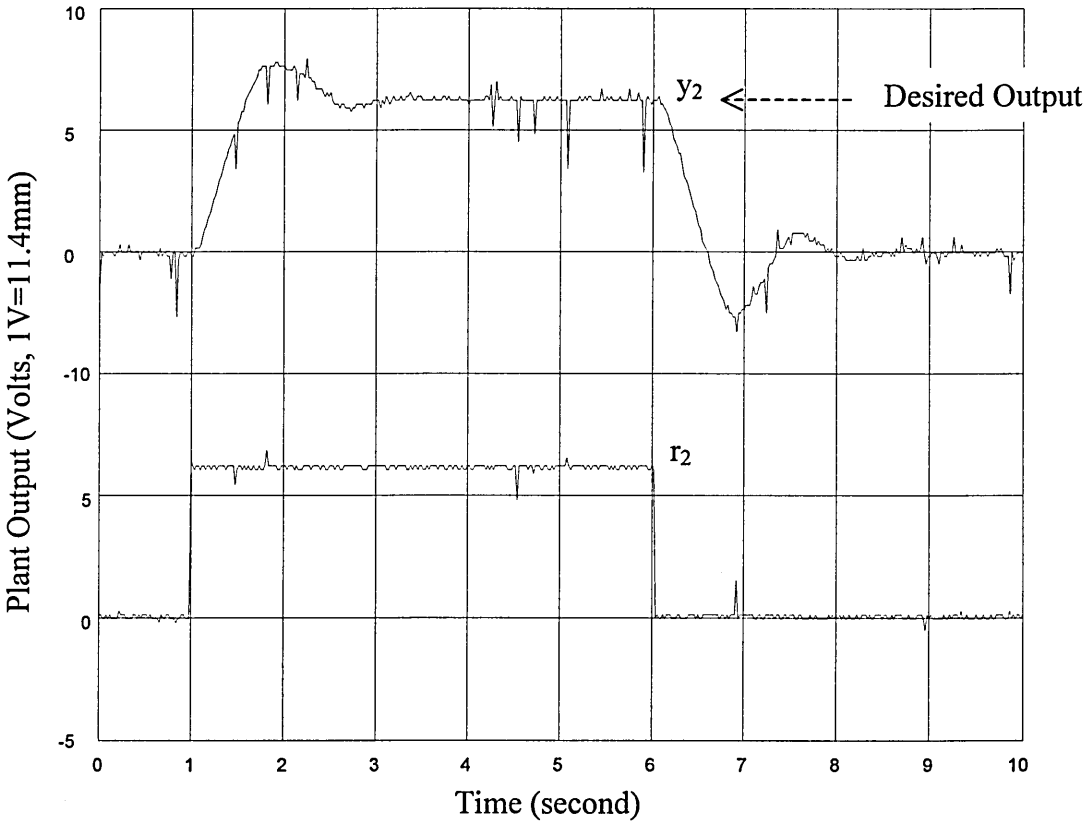

Fig 4.73 H^{∞} Controller Implementation - Plant Output y_2 for Step on r_2

5 Robustness Assessment

In the foregoing work, five distinct controllers were designed and implemented on the beam and carriage equipment. Of these, three were based on state feedback - the original LQG design with full state feedback, the design based on a reduced order observer (using a modified plant model with three outputs) and an improved LQG design. In addition, two controllers with forward path compensation were produced, the designs being based on the Characteristic Locus Method and on H^{∞}/Mixed Sensitivity.

A full and rigorous assessment of the robustness of these controllers was not possible due to the shortage of time available to complete the present work and the complexity of such an assessment. In order to obtain some information on the performance of the controllers with plants deviating significantly from the model used for their designs, the five controller implementations were tested with two modified plants, one plant modification involving a change in carriage dynamics, the other a change in the dynamics of the two rams.

5.1 Plant with Modified Carriage Dynamics

For the plant with modified carriage dynamics, the horizontal separation of the rams, L, was effectively halved to give the carriage equation of motion

$$\ddot{x}_1 = 5.546\,(x_2 - x_3) \qquad (5.1)$$

In order to avoid the need for mechanical modification of the plant, this was achieved by introducing a gain of 2 into the output of the ultrasonic transducer monitoring the carriage horizontal position.

The response of carriage position, y_1, to step inputs of approximately 4V on reference input r_1 are shown in Figs 5.1 to 5.5 for the original LQG controller, the controller based on the reduced order observer (ROO), the improved LQG controller, the characteristic locus (CL) controller and the H^{∞}/mixed sensitivity controller respectively. The LQG and H^{∞} controllers produced highly oscillatory systems. (Simulations based on both the continuous and discrete controllers gave a stable but highly oscillatory result). Comparing the ROO, improved LQG and CL controllers' performance with those using the unperturbed plant (Figs 4.34, 4.38 and 4.53 respectively) and bearing in mind that, due to the rescaling of y_1, the change of carriage position for a given variation in the

transducer signal is halved, these controllers behaved extremely well. The improved LQG design shows some increase in oscillation of the carriage whilst the performance of the ROO controller and the CL controller is comparable to that obtained with the unperturbed plant. The response of the beam height, y_2, was virtually unaffected by the change in carriage dynamics.

In situations where normal plant variations make an increase in the robustness of the system desirable, only the H^∞/mixed sensitivity approach offers the possibility of improvement by the adjustment of parameters explicitly related to robustness. In order to try to improve the H^∞ controller's tolerance to plant perturbations, the design weight $\mathbf{W}_3$ was increased by a factor of 5 to give

$$\mathbf{W}_3 = diag(\frac{s^2}{2}, \frac{s^2}{2}) \qquad (5.2)$$

Fig 5.6 shows the response of y_1 to a step on r_1 using this modified controller with the original plant. Comparison with Fig 4.70 shows that, whilst there is some increase in the low frequency drift or 'hunting' of the carriage using the modified controller, the overshoot is significantly reduced. Fig 5.7 shows the response of y_1 using the modified controller on the plant with modified carriage dynamics. The system, though still oscillatory, is much better behaved than that based on the unmodified controller and, bearing in mind the relatively large change in carriage dynamics, may be considered acceptable in situations where robustness is essential. It is possible to argue that the modified controller performs better with the original plant than the original H^∞ controller, that this is because it is better tuned to the nominal plant model and that this improvement 'stretches' to the modified plant. However, comparison of Figs 5.8 and 4.66 shows no improvement resulting from the modified controller on the nominal plant model at the simulation stage and it could therefore be argued that the overshoot on implementation of the original controller with the original plant (Fig 4.70) is itself a robustness problem (due to discrepancies between the plant and the nominal plant model) and improving robustness to improve performance with the modified plant has inevitably improved performance with the original plant.

5.2 Plant with Modified Ram Dynamics

In an attempt to change the ram dynamics so that the carriage positioning was significantly disturbed, the maximum upward velocity of the left hand ram and the maximum downward velocity of the right hand ram were halved by reducing the corresponding gains on the servoamplifiers. The implementations based on the unmodified controllers with the plant modified in this way showed only a little more low frequency drift of the carriage, presumably because the ram dynamics were in either case fast compared to the carriage. However, the imbalance in the rams' velocities was more marked in producing significant dynamic interaction between reference input, r_2, and carriage position, y_1, as can be seen from Figs 5.9 to 5.13. These show that the worst performers with respect to low frequency drift were the LQG and CL controllers, whilst the worst dynamic interaction was evident using the H^∞ controller. (The interaction is caused by the left hand ram lagging behind the right hand ram when the beam is raised causing the carriage to move leftwards, and the right hand ram lagging the left hand ram when the beam is lowered, again causing the beam to move left).

Finally, the modified H^∞ controller was tried with this plant. The response of y_1 to a step on r_2 is shown in Fig 5.14. This indicates that any improvement in robustness given by the modified controller does not extend to the dynamic interaction problem evident here. The H^∞/mixed sensitivity approach used here is, of course, based (and only loosely based) on an unstructured plant uncertainty model and hence offers no possibility of targetting this specific plant perturbation problem. However, in the steady state, the interaction between r_2 and y_1 can be seen to be of a low order using either H^∞ controller.

This brief study of robustness involved two modifications of the beam and carriage. The improved LQG, CL and ROO controllers performed well with the plant with modified carriage dynamics, whilst the H^∞ and original LQG controllers gave an unstable, oscillatory response. A modified H^∞ controller designed for greater robustness, though a significant improvement on the original, did not perform as well as the ROO controller. The ROO controller again performed best with the modified ram dynamics, though in this case all the controllers gave a stable response.

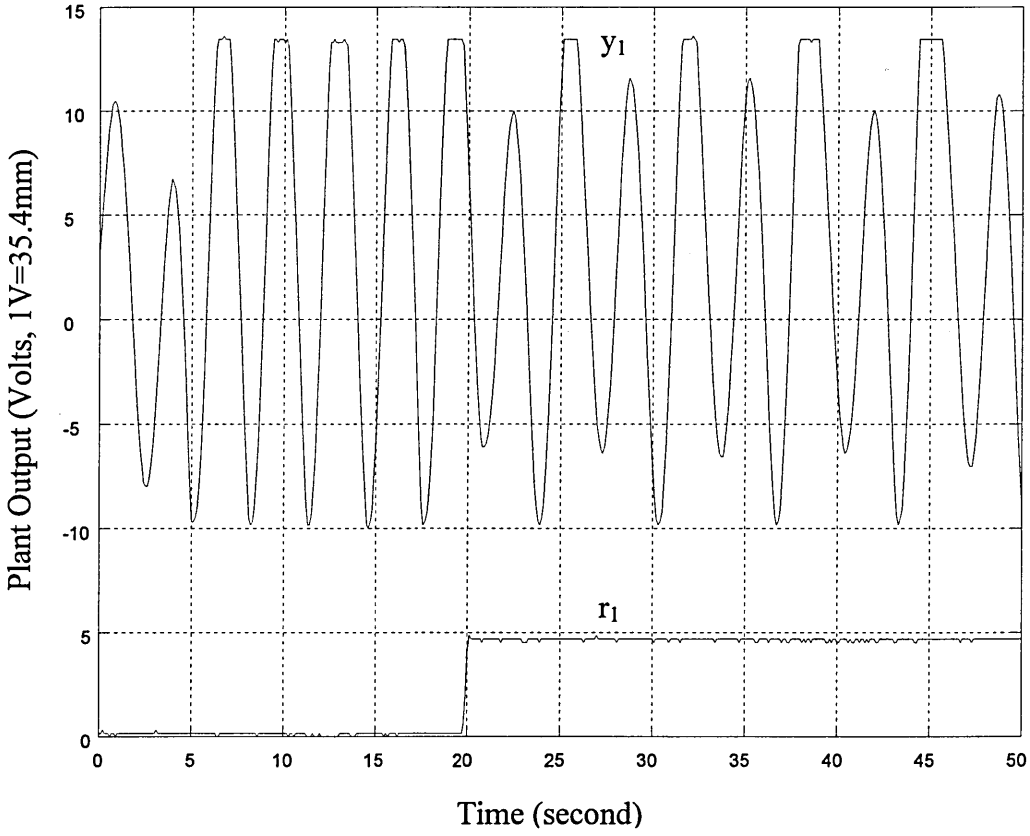

Fig 5.1 LQG Controller, Plant with Modified Carriage Dynamics

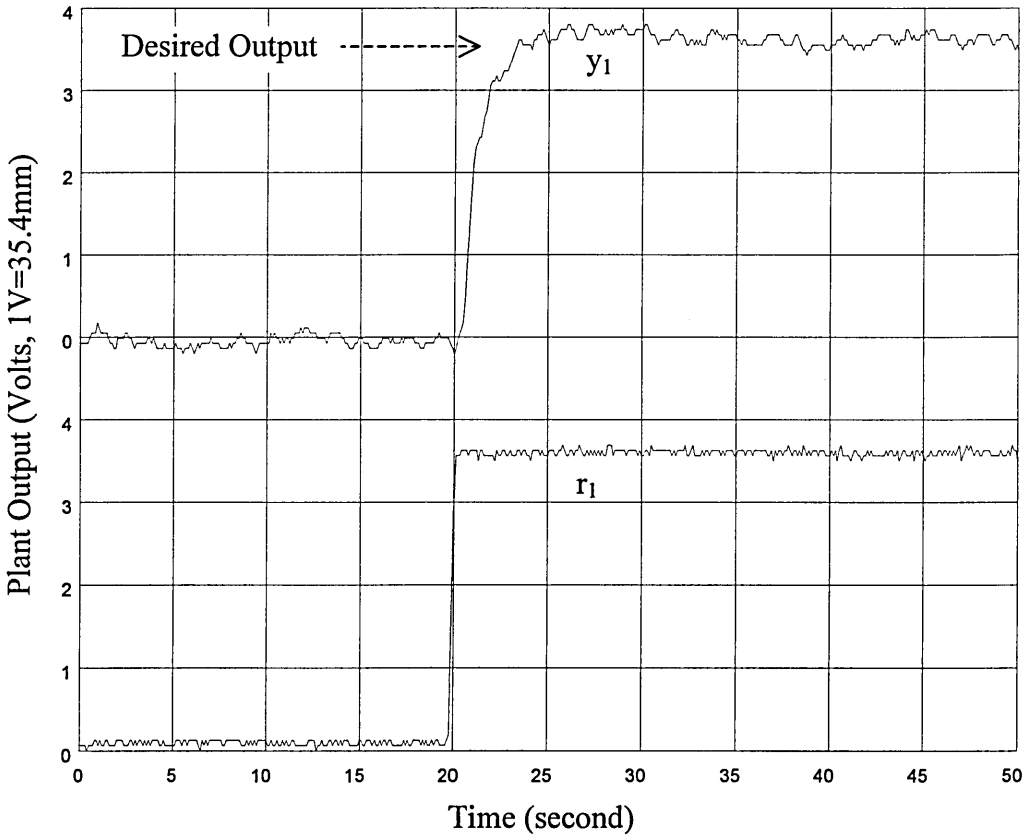

Fig 5.2 ROO Controller, Plant with Modified Carriage Dynamics

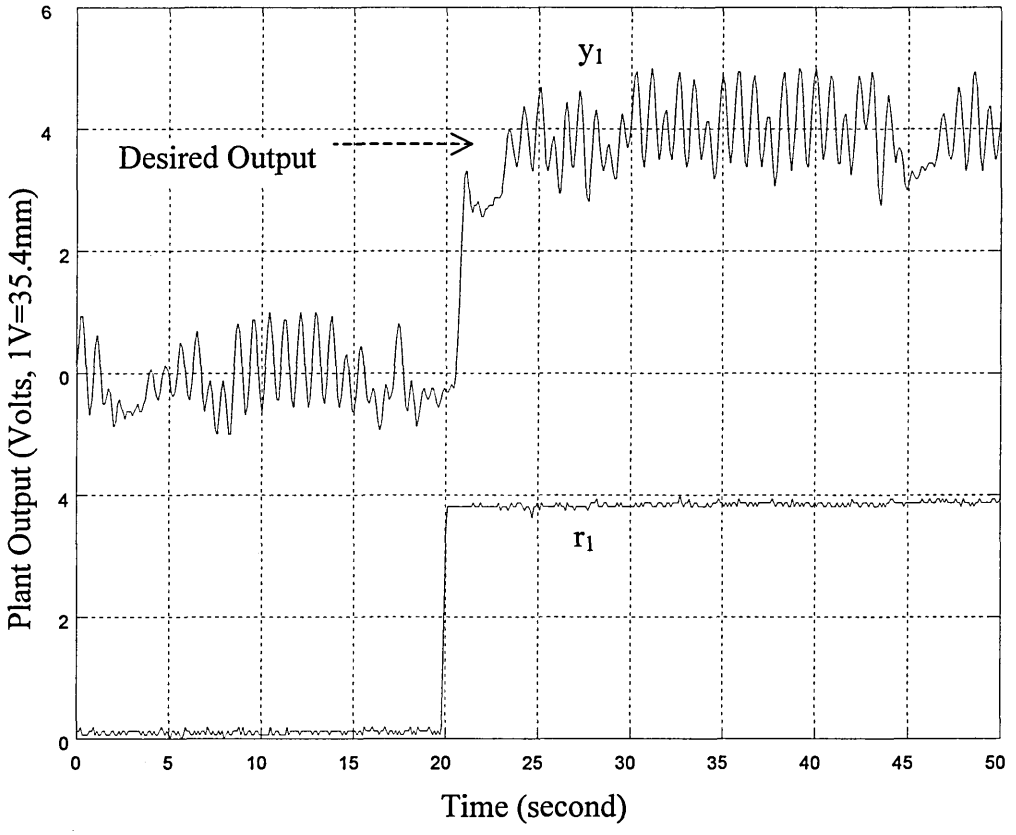

Fig 5.3 Improved LQG Controller, Plant with Modified Carriage Dynamics

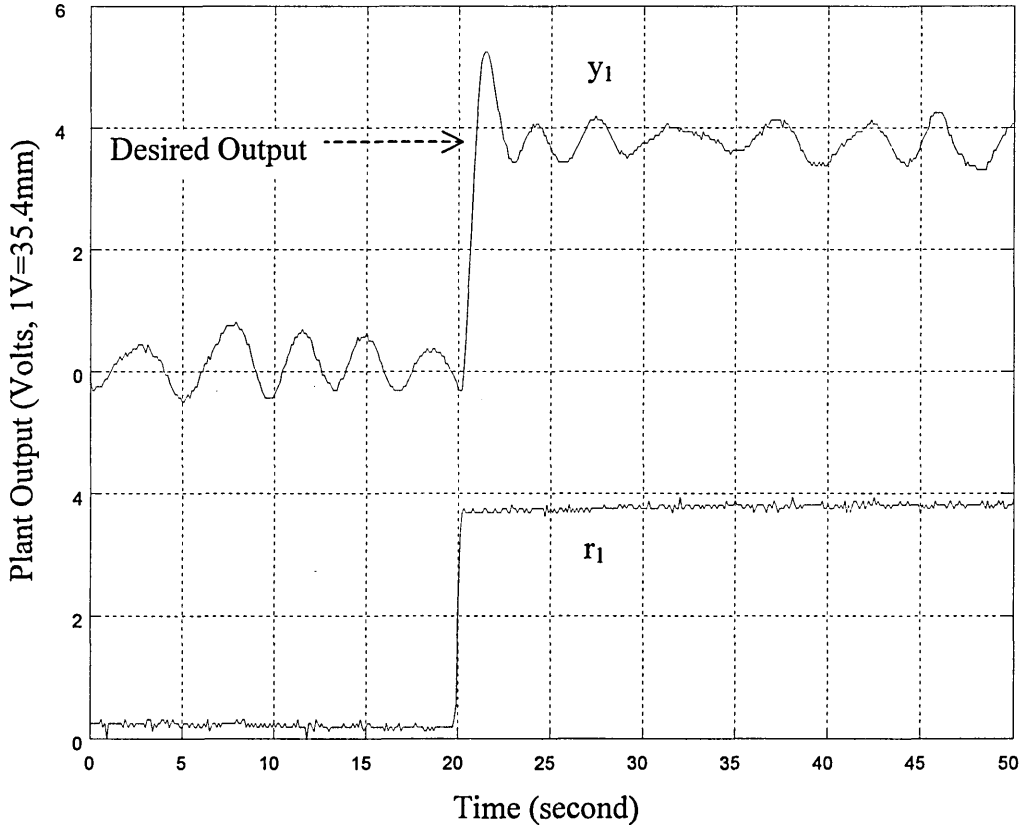

Fig 5.4 CL Controller, Plant with Modified Carriage Dynamics

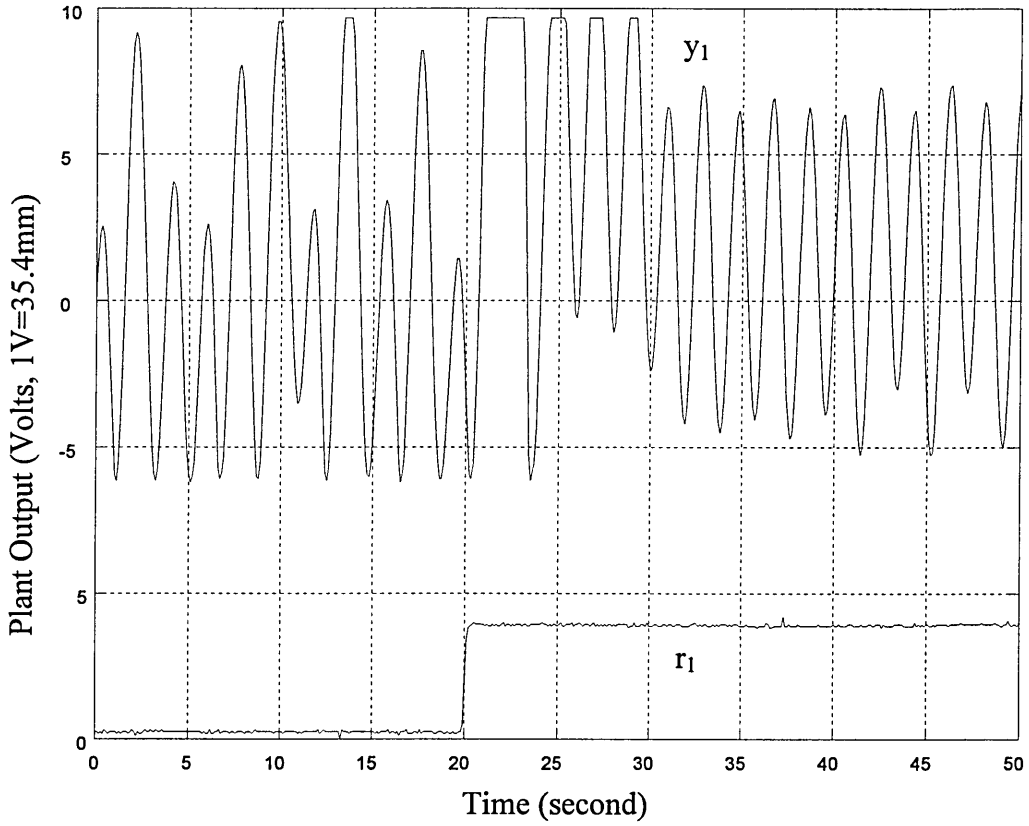

Fig 5.5 H^{∞} Controller, Plant with Modified Carriage Dynamics

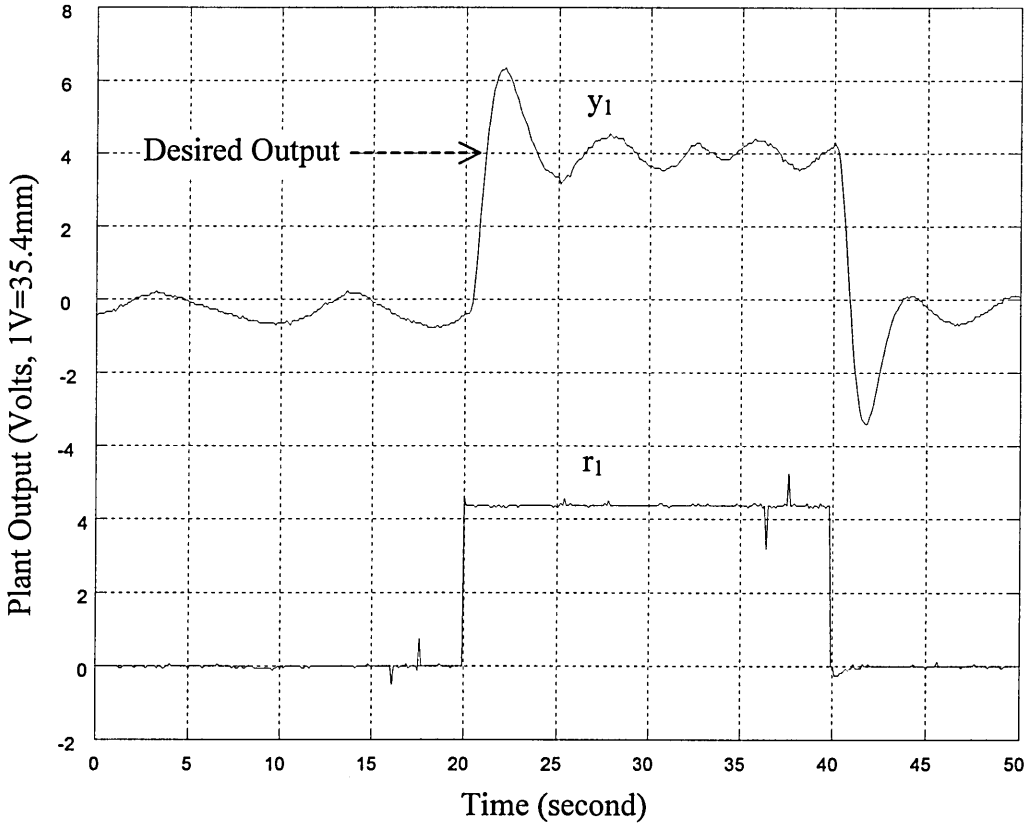

Fig 5.6 Modified H^{∞} Controller, Original Plant

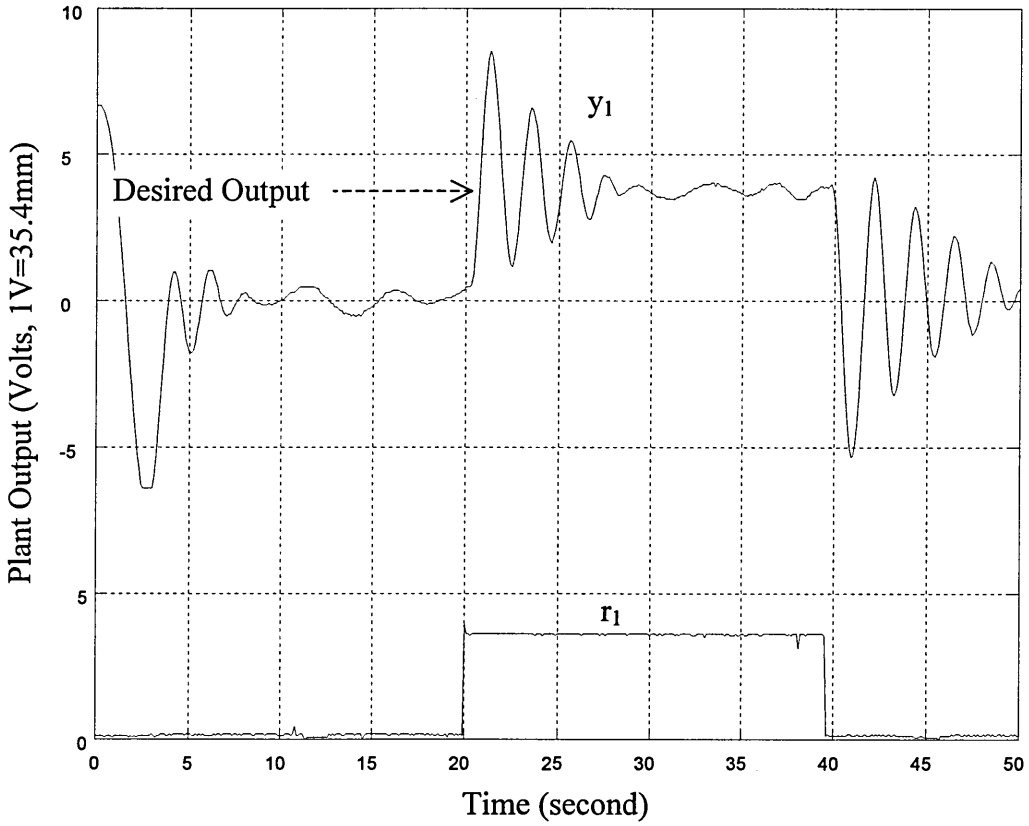

Fig 5.7 Modified H^{∞} Controller, Plant with Modified Carriage Dynamics

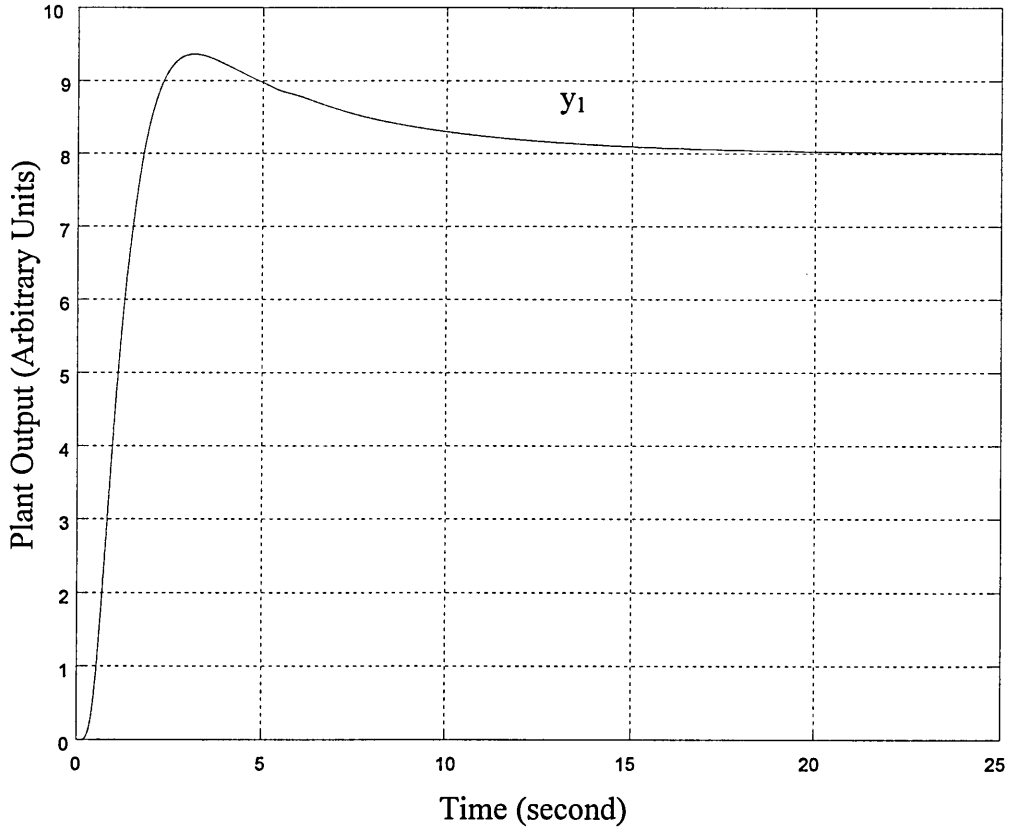

Fig 5.8 Discrete Simulation of Modified H^{∞} Controller with Original Plant

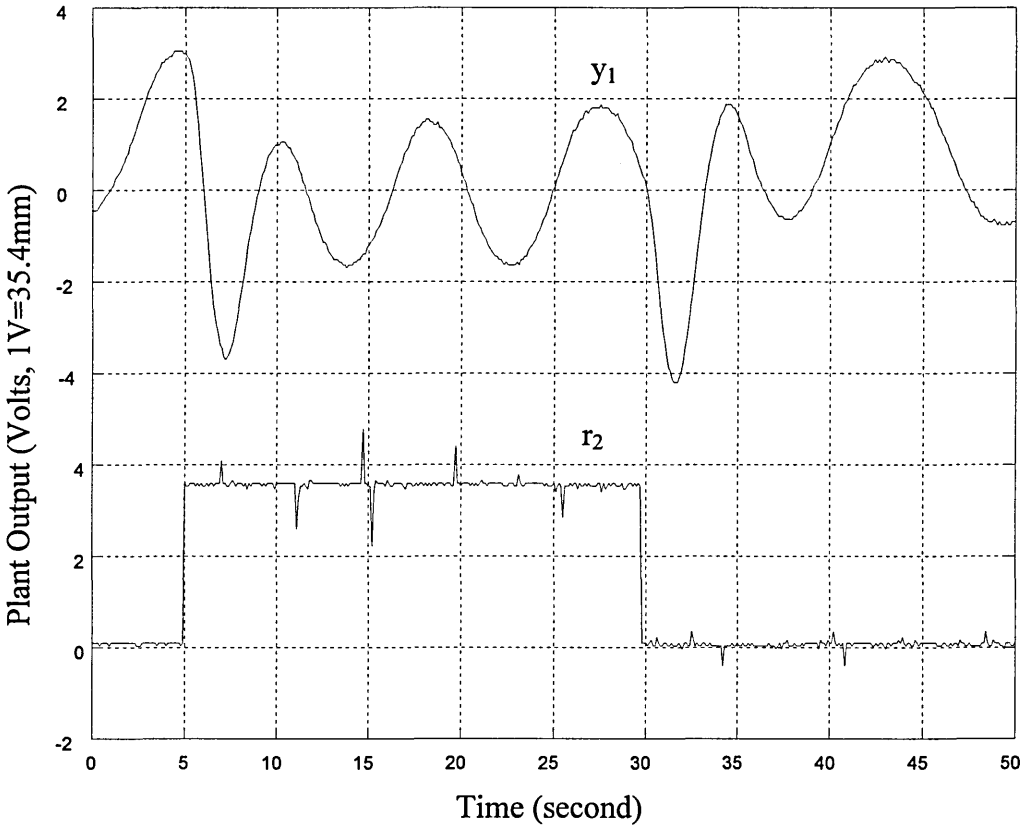

Fig 5.9 LQG Controller, Plant with Modified Ram Dynamics

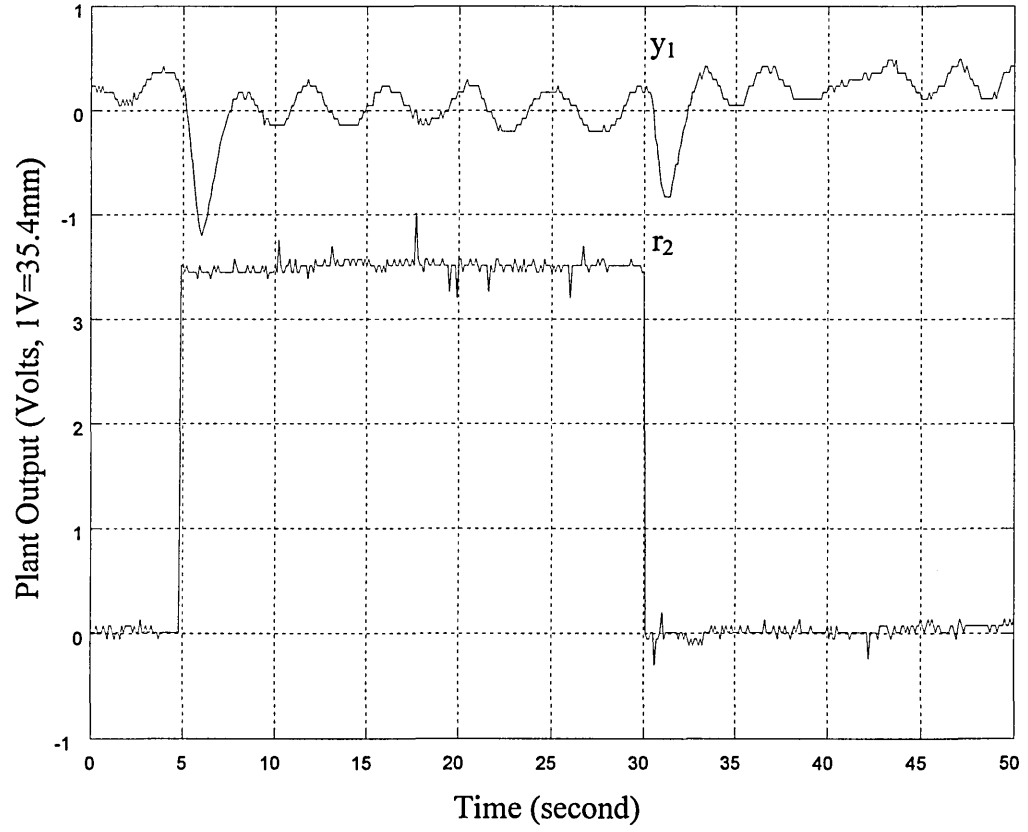

Fig 5.10 ROO Controller, Plant with Modified Ram Dynamics

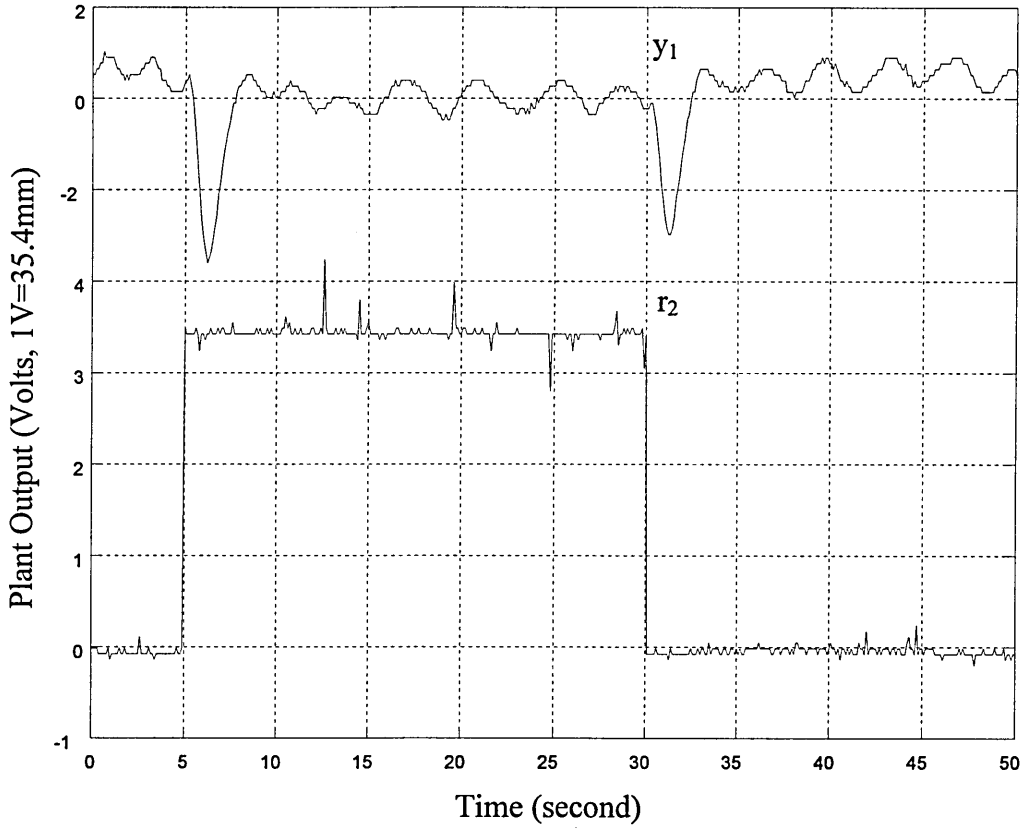

Fig 5.11 Improved LQG Controller, Plant with Modified Ram Dynamics

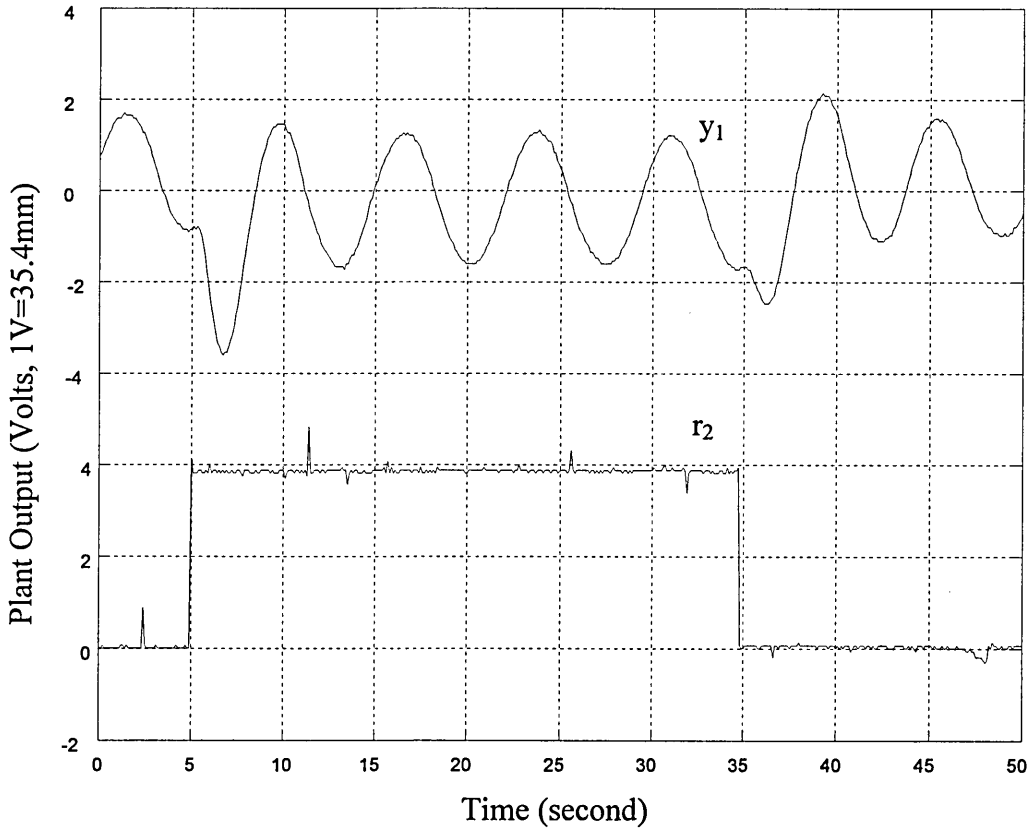

Fig 5.12 CL Controller, Plant with Modified Ram Dynamics

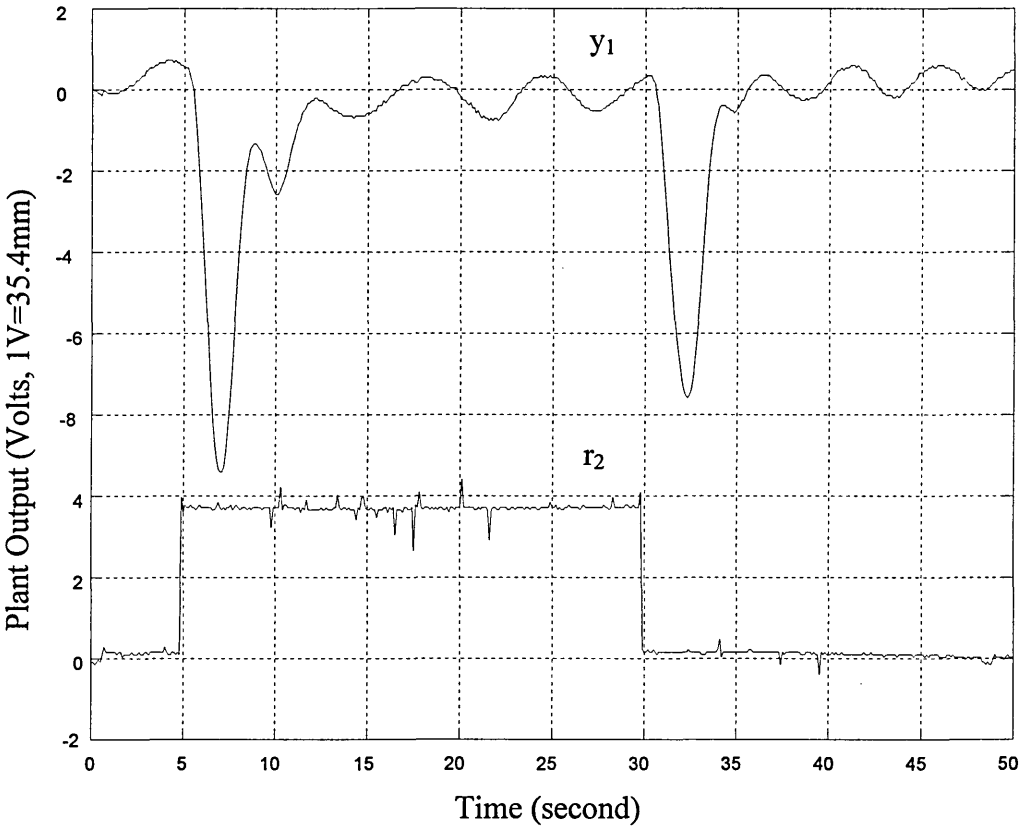

Fig 5.13 Original H^{∞} Controller, Plant with Modified Ram Dynamics

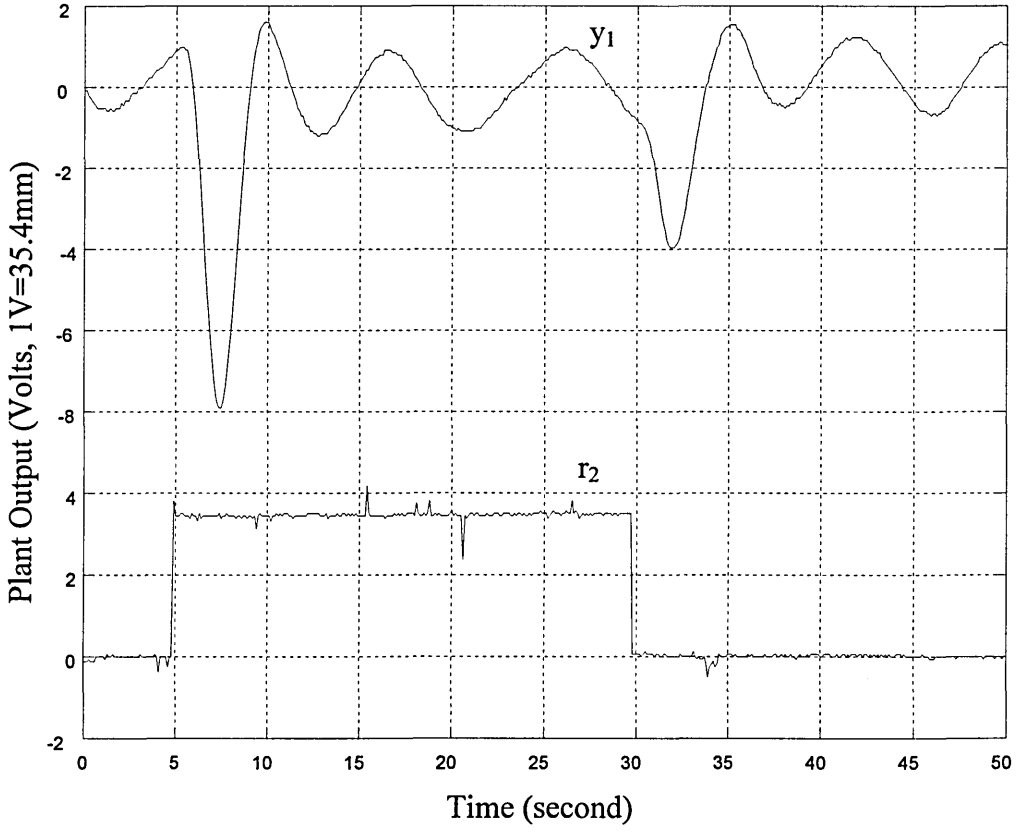

Fig 5.14 Modified H^{∞} Controller, Plant with Modified Ram Dynamics

6 Discussion

The beam and carriage is untypical of mechanical systems in that the carriage dynamics contain a double integrator and the SISO system involving the control of horizontal carriage position by a single ram is inherently unstable. Although, as indicated in Chapter 2, the beam and carriage can be stabilised by a compensator in the form of a constant gain matrix, this leaves no scope for achieving decoupling and satisfactory performance.

The comments which follow may in parts relate to the general applicability of the controller design methods chosen for this work, but it must be borne in mind that the specific design problems encountered and the results obtained may be of a different nature for other types of system.

6.1 General Comments

The process of designing and implementing the five controllers showed the paramount importance of considering the magnitude of control effort, **u**, throughout. Controller designs that achieve satisfactory performance in theory (i.e. at the simulation stage) but only at the expense of large control effort are liable, in practice, to lead to signal saturation and instability. The inclusion of appropriate saturation blocks in the simulation models was invaluable in indicating any occurrence of this problem.

In the present work, no attempt has been made to produce digital controllers directly by z transform methods. The controllers were designed in the s-plane and digitised using Euler's method. Some early work using Tustin[77] showed that stable results could be achieved using larger sampling intervals than those at which Euler became unstable but the sampling intervals available to the implementations used here showed Euler discretisations to be more than adequate.

From a robustness perspective, only plant perturbation has been considered. Process and measurement noise were not considered in the generalised plant model, though estimates of their magnitude were required input for the LQG design procedure.

Generally speaking, it is desirable that a controller for a MIMO system diagonalises the system's transfer function matrix such that the system effectively becomes a set of independent (i.e. uncoupled or non-interacting) SISO control loops. For the controllers

based on state feedback, a steady state decoupler only was attempted, though visual checks showed this to result in little interaction both with the original and the modified plants. For the CL controller, diagonalisation is designed into the system whilst the H^{∞}/mixed sensitivity optimisation punishes interaction via constraints on sensitivity, **S**.

Some discrepancies were found between the discrete simulations and the actual implementations of the controllers. Since only slight errors were anticipated in signal discretisation (A/D and D/A conversions) and implemented sampling times, these inconsistencies are likely to be caused by discrepancies between the nominal plant model and the actual plant. Obviously, problems of this sort would tend to suggest a lack of robustness.

6.2 Comparison of Methods - Application of Methods

The three controllers based on state feedback were arguably much easier to design than the forward path compensators based on the CL and H^{∞} methods. For evaluation of the state feedback coefficients based on LQR design theory, all three controllers used simple identity matrix weighting functions for the weightings of the cost function. The cost function was defined to penalise the plant input vector, **u**, and the plant output vector, **y**. The estimator design required definition of process noise and measurement noise levels for the LQG designs and arbitrary estimator pole placement for the ROO design. Although in theory it would be possible, in a given application, to produce empirically based estimates of process and measurement noise covariance, **W** and **V** respectively, in the present work it was possible and safe to implement designs based on a range of values of **W** and **V** such that these designs, satisfactory or otherwise, could be evaluated in service. The original LQG design was unsatisfactory but, with insight provided by the ROO controller, it was clear that the estimator poles required to be 'speeded up' and this could be achieved by basing the design on expectations of increased process noise and/or decreased measurement noise. For the ROO design, a single estimator pole was required to be chosen and this greatly facilitated the design of a viable controller. (The fact that a satisfactory controller was achieved without the need for estimates of the two ram velocities suggests that the rams could be modelled as first order systems and this would result in a fourth order plant model. Intuitively, this is because the rams are fast compared to the motion of the carriage along the beam. Any further work on the beam and carriage might well use a fourth order model).

The characteristic locus method required the choice of high, mid and low frequencies at which to diagonalise the system and also the choice of dynamic compensation for the mid and low frequency ACC's. Care was required to examine and, if necessary, modify the signs of the columns of the high frequency compensator. This was facilitated in the present work by comparison with the simple decoupling compensator described in Chapter 2. The design of the CL compensator for the beam and carriage proved difficult in that attempts to improve system performance by increasing the order of the compensator showed better performance at the simulation stage but instability at the implementation stage.

The H^{∞}/mixed sensitivity design process was the most difficult conceptually and the most complicated in practice, not least because considerations of robustness were involved. The method required the choice of mixed sensitivity operator, weighting functions for each element of the operator and, since the resulting controller was of a high order, the choice of model reduction method. In addition, the method cannot be applied directly to plants with poles on the imaginary axis and therefore, in the present case, a transformation of the plant was required prior to design and of the resulting controller subsequently. The complexity of the parameters involved in this approach and their manipulation made this design process a difficult one to begin and it was found that the adjustment of weights to improve controller design was far from intuitive.

6.3 Comparison of Methods - Results Obtained

Disregarding the original LQG controller as having been superseded by the improved one, the controllers based on state feedback gave very satisfactory results with the original, unmodified plant. In both cases overshoot and low frequency drift (i.e. hunting) of the carriage were minimal and beam height response and system decoupling excellent. For the CL controller, the control of horizontal carriage position was rather unsatisfactory. There was significant hunting of the carriage and overshoot of approximately 25%. Attempts to improve this situation proved unsuccessful in that the implemented controllers tended to be unstable. The H^{∞} controller produced overshoot of the order of 100%, significant hunting of the carriage and overshoot on beam height of around 30%. This controller gave the least satisfactory performance of all the designs. It was also the only controller to produce such 'soft' control of beam height. Of the two methods of model reduction applied to the H^{∞} controller, OHMDA, though

intended as a more robust technique, proved unsatisfactory and balanced residualisation was used for the final H^{∞} controller.

It is thought that the low frequency drift or hunting of the carriage was due to deadband effects in the amplifier/valve combinations which drive the hydraulic rams. When the carriage began to drift due to finite beam gradient, a threshold change in the controller outputs was required before the rams corrected this tilt angle. The harder, i.e. more responsive, controllers crossed this threshold more quickly than the softer controllers and therefore drift was much reduced with the former. A possible explanation of the difficulty of finding controllers based on forward path compensation which compared with those based on state feedback is that systems containing double integrators are particularly amenable to enhancement via velocity feedback to introduce a coefficient of s in the characteristic equation. In the beam and carriage, the carriage dynamics contained the double integrator and carriage velocity was one of the states fed back in the state feedback controllers. Thus velocity feedback was implemented directly in the state feedback controllers, which was not the case for the CL and H^{∞} controllers.

To some extent the quality of the results obtained with the original plant may reflect the relative ease of application of the methods used to produce the controllers. The ROO and improved LQG designs gave responsive systems whilst the CL controller and particularly the H^{∞} controller were much softer. Although measurement noise was not considered explicitly during the present work, it was noticeable that noise generated at the ultrasonic transducer by escaping air from the hydrostatic carriage bearing produced occasional violent movement of the carriage with the former, hard controllers but this effect was much reduced with the softer CL and H^{∞} controllers. Further investigation of this susceptibility to noise, by short duration (manual) interruption of the ultrasonic transducer's measurement path, showed the improved LQG and particularly the ROO controllers to react violently whilst the CL controller was less sensitive and the original LQG and the H^{∞} controllers well behaved in the presence of this noise. In the case of the original LQG controller, the softness of the controller, both in terms of response to measurement noise and response to control inputs, is due to the more conservative (i.e. larger) estimates of measurement noise and less conservative estimates of process noise.

The rudimentary investigation of robustness showed the ROO controller to be remarkably tolerant of large changes in carriage dynamics whilst the improved LQG

controller still performed adequately. The CL controller's performance appeared to be completely undisturbed but the original LQG and H^{∞} controllers were extremely oscillatory when subjected to this change in the plant. However, the H^{∞}/mixed sensitivity approach does offer a means of directly improving robustness and further work on the controller design produced improved performance with the modified plant without deterioration in performance with the original plant. This improvement, however, was not nearly enough to match the performance of the ROO and improved LQG controllers.

It is possible that further improvements could be made to the CL and H^{∞} controllers but this might require considerable investigation of dynamic compensators in the former case and weighting functions in the latter. Investigation of weights for the H^{∞} controller accounted for easily the greatest part of the total time spent on controller simulations in the present work.

The plant modification involving a change in ram dynamics produced dynamic interaction between the beam height control input and the carriage position with all the controllers, the worst case being the H^{∞} controller, probably because this controller is so soft. In the steady state, however, these modifications did not appear to influence the controller.

7 Concluding Remarks

The work on controller designs described here has been heavily dependent on the support of a computational tool, namely Matlab and its associated toolboxes. To some extent the best results have been obtained using the methods which are easier to apply (although this could be partly a problem of perception - better results suggesting easier methods). The ROO, for instance, made far fewer computational demands than the H^{∞} controller.

General conclusions cannot be drawn from the limited work on robustness assessment. The ROO and improved LQG controllers responded best to plant perturbations, whilst the original LQG and H^{∞} controllers performed least well. The H^{∞}/mixed sensitivity approach gives a means of improving robustness but attempts to match that of the ROO controller were unsuccessful. The indications are, however, that the more responsive state feedback controllers would perform less well in the presence of measurement noise and, where this is significant, a design on the lines of the original LQG controller would be necessary.

The use of step tests for the investigation of controller performance throughout this work might be thought to impose operating conditions of unreasonable severity on the plant. Problems of excessive plant inputs in particular could be much reduced by rate-limiting the reference inputs and generally more satisfactory controller designs might be achieved. However, step testing has been adhered to here as providing a single convenient basis on which to compare controllers designed by the various methods.

8 Further Work

The present work would be enhanced by a detailed study of H^{∞} weight selection. It is also recommended that a thorough and rigorous assessment of robustness be carried out using a plant model extended to include process and measurement noise and that this assessment include, in the case of H^{∞} controllers, the investigation of a variety of model reduction techniques and their effect on robustness.

The beam and carriage apparatus in its final form is a suitable vehicle for the investigation of controller designs based on techniques other than those applied in the present work. For instance, 'soft computing' approaches such as fuzzy logic and neural networks may be investigated and the plant model developed here, possibly reduced to fourth order, will facilitate the design and simulation process.

Finally, it would be advantageous in the application of controllers such as those contained here, to investigate their implementation using more control-oriented technology, such as a modern PLC system (e.g. the Schneider PL7 Pro system) or a graphically programmed data acquisition system (e.g. National Instruments' *Labview*).

References

1. Bode H. W., *Network Analysis and Feedback Amplifier Design*, Van Rostrand, 1945

2. Wiener N., *Generalised Harmonic Analysis*, Acta Math., Vol 55, 1930, pp117-258

3. Nyquist H., *Regeneration Theory*, Bell Systems Technical Journal, Vol 11, 1932, pp126-147

4. Coughanowr D. R. and Koppel L. B., *Process Systems Analysis and Control*, McGraw-Hill Book Company, 1965, pp304-309

5. Povejsil D. J. and Fuchs A. M., *A Method for the Preliminary Synthesis of a Complex Multiloop Control System*, Trans. AIEE, Applications and Industry, No 19, July, 1955, pp129-134

6. Kinnen E. and Liu D. S., *Linear Multivariable Control System Design With Root Loci*, Trans. AIEE, Applications and Industry, No 60, May 1962, pp41-44

7. Kalman R. E., *Contributions to the Theory of Optimal Control*, Bol. Soc. Math. Mex., Vol 5, 1960, pp102-119

8. Luenberger D. G., *Observing the State of a Linear System*, IEEE Trans. Military Electronics, Vol MIL-8, 1964, pp74-80

9. Kalman R. E., *A New Approach to Linear Filtering and Prediction Problems*, Trans. ASME J. of Basic Eng. 82, 1960, pp35-45

10. Kalman R. E. and Bucy R. S., *New Results in Linear Filtering and Prediction*, Trans. ASME J. of Basic Eng. 83, 1961, pp95-108

11. Athans M., *The Role and Use of The Stochastic Linear-Quadratic-Gaussian Problem in Control System Design*, IEEE Trans. Autom. Control Vol AC-16, 1971, pp529-552.

12. Morse A. S. and Wonham W. M., *Status of Noninteracting Control*, IEEE Trans. Automatic Control, Vol AC-16, No 6, Dec. 1971, pp568-581

13. Rosenbrock H. H., *Design of Multivariable Control Systems Using the Inverse Nyquist Array*, Proc. Inst. Elec. Eng., Vol 116, 1969, pp1929-1936

14. Mayne D. Q., *The Design of Linear Multivariable Systems*, Automatica, Vol 9, 1973, pp201-207

15. Rosenbrock H. H., *State Space and Multivariable Theory*, London, Nelson, 1970

16. MacFarlane A. G. J. and Postlethwaite I., *The Generalised Nyquist Criterion and Multivariable Root Loci*, Int. J. Control, Vol 25, No 1, 1977, pp81-127

17. MacFarlane A. G. J. and Kouvaritakis B. A., *A Design Technique for Linear Multivariable Feedback Systems*, Int. J. of Control 25 (1977), pp837-874.

18. MacFarlane A. G. J. and Scott-Jones D. F. A., *Vector Gain*, Int. J. Control, Vol 29, No 1, 1979, pp65-91

19. Zames G., *Feedback and Optimal Sensitivity : Model Reference Transformations, Multiplicative Semi-norms and Approximate Inverses*, IEEE Trans. Automatic Control, Vol ac-28, 1981, pp301-320

20. Doyle J. C., *Analysis of Feedback Systems with Structured Uncertainties*, IEE Proc., Part D Vol 129, No 6, 1982, pp242-250

21. Kwakernaak H., *Robust Control and H^{∞}-Optimization-Tutorial Paper*, Automatica, Vol 29, No 2, 1993, pp255-273

22. Doyle J. C., *Guaranteed Margins for LQG Regulators*, IEEE Trans. Automatic Control, Vol AC-23, 1978, pp756-757

23. Doyle J. C. and Stein G., *Multivariable Feedback Design: Concepts for a Classical / Modern Synthesis*, IEEE Trans. Automatic Control, Vol AC-26, 1981, pp4-16

24. Action Group FM(AG08), *Robust Control Techniques Tutorial Document*, Group for Aeronautical Research and Technology in Europe, Open Report, GARTEUR/TP-088-7, 1997

25. *Matlab Reference Guide*, Math Works Inc., 1994

26. Wellstead P. E., Chrimes V., Fletcher P. R., Moody R. and Robins A. J., *The Ball and Beam Control Experiment*, International Journal of Electrical Engineering Education, Vol 15, 1978, pp21-39

27. Schwarzenbach J. and Gill K. F., *System Modelling and Control*, Edward Arnold, 1978, pp23-26

28. Krauss T. P., Shure L. and Little J. N., *Signal Processing Toolbox User's Guide*, Math Works Inc., 1994

29. Patel R. J. and Munro N., *Multivariable System Theory and Design*, Pergamon Press, 1982, p22

30. See for example Dutton K., Thompson S. and Barraclough B., *The Art of Control Engineering,* Addison-Wesley, 1997, p514

31. Moler C. and Costa P. J., *Symbolic Math Toolbox User's Guide*, Math Works Inc., 1993

32. Patel R. J. et al., op. cit., p38

33. Ibid., p43

34. Patel R. J. et al., op. cit.

35. Skogestad S. and Postlethwaite I., *Multivariable Feedback Control*, John Wiley & Sons, 1997

36. Maciejowski J. M., *Multivariable Feedback Design*, Addison-Wesley Publishing Company, 1989

37. Morari M. and Zafiriou E., *Robust Process Control*, Prentice-Hall International, Inc., 1989

38. Maciejowski J. M., op. cit., p224

39. Ibid.

40. Grace A., Laub A. J., Little J. N. and Thompson C. M., *Control Systems Toolbox User's Guide*, Math Works Inc., 1994, p2-103

41. *Simulink User's Guide*, Math Works Inc., 1993

42. Patel R. J. et al., op. cit., p21

43. Ibid., p29

44. Grace A. et al., op. cit., p2-135

45. Maciejowski J. M., op. cit. p225

46. Franklin G. F., Powell J. D. and Emami-Naeni A., *Feedback Control of Dynamic Systems*, Addison-Wesley Publishing Company, 1994, p516

47. Skogestad S. et al., op. cit., p353

48. Ibid., p355

49. Franklin G. F. et al., p522

50. Ibid., p523

51. Ford M. P., Maciejowski J. M. and Boyle J. M., *Multivariable Frequency Domain Toolbox User's Guide*, Cambridge Control Ltd, 1990

52. Ibid., pMVR-9

53. Ibid., pMVR-25

54. See for example the references cited by Chiang R. Y., and Safonov M. G., *Robust Control Toolbox User's Guide*, Math Works Inc., 1996, p2-52

55. Maciejowski J. M., op. cit., p99

56. Ibid., p100

57. Skogestad S. et al., op. cit., p153

58. Ibid., p307, Remark 2

59. Ibid., p12

60. Ibid., p22

61. Morari M. et al., op. cit., p237

62. Ibid., p236

63. Ibid., pp238-240

64. Ibid., pp265-266

65. Chiang R. Y. and Safonov M. G., *Robust Control Toolbox User's Guide*, Math Works Inc., 1996

66. Skogestad S. et al., p291

67. Grace A. et al., op. cit., p2-117

68. Chiang R. Y. et al., op. cit., p2-88

69. *Turbo Pascal for Windows User's Guide*, Borland International, Inc., 1991

70. *DAS-1600/1400 Series User's Guide*, Keithley Instruments, Inc., 1994

71. Franklin G. F. et al., op. cit., p138

72. Wardman D. and Roddis R., *Design of an Electrohydraulic Multivariable Control System Teaching Facility*, Proceedings of UKACC Conference on Control '96, IEE, Vol 1, 1996, pp36-41

73. Roddis R. and Wardman D., *Implementation of a Digital Controller Based on a Reduced Order Observer for an Inherently Unstable Multivariable System*, International Journal of Mechanical Engineering Education, Vol 6, No 4, 1998, pp327-337

74. Dutton K. et al., op. cit., p486

75. See, for instance, Chiang R. Y. et al., op. cit., p1-56 et seq.

76. Chiang R. Y. et al., op. cit., p1-70,1-71

77. Franklin G. F. et al., op. cit., p617

Appendix I - Glossary of Acronyms

ACC	Approximate Commutative Controller
ARE	Algebraic Riccati Equation
CE	Characteristic Equation
CL	Characteristic Locus
CP	Characteristic Polynomial
CSTB	Control System Toolbox
DSA	Dynamic Signal Analyzer
LQG	Linear Quadratic Gaussian
LQR	Linear Quadratic Regulator
LTR	Loop Transfer Recovery
MIMO	Multiple Input, Multiple Output
MVFDTB	Multivariable Frequency Domain Toolbox
MVFR	Multivariable Frequency Response
OHMDA	Optimum Hankel Minimum Degree Approximation
RCTB	Robust Control Toolbox
ROO	Reduced Order Observer
RP	Robust Performance
RS	Robust Stability
SISO	Single Input, Single Output
TFM	Transfer Function Matrix
UNF	Unity Negative Feedback

Appendix II - M-files

Lqg

```
% LQG Controller Design
clear
load nsymmod
% Compute State Feedback Matrix
[k,s,eigvalsys]=lqry(a,b,c,d,eye(2),eye(2));
% Compute Estimator Gain Matrix
q=0.001*b*b';
%q=b*b';
r=0.01*eye(2);
%r=0.0001*eye(2);
[l,p,eigvalest]=lqe(a,eye(6),c,q,r);
% Compute Estimator State Space Equations
[ae,be,cexy,dexy]=estim(a,b,c,d,l,1:2,1:2);
k
eigvalsys
%k(:,5:6)=zeros(2,2)
l
eigvalest
ae
be
% Remove Estimates of y
ce=cexy(3:8,:); % =eye(n)
de=dexy(3:8,:); % =zeros(n,n)
% Compute TFM of Closed-loop System
af=a-b*k;
[num1,den1]=ss2tf(af,b,c,d,1);
[num2,den2]=ss2tf(af,b,c,d,2);
% Compute DC Gain Matrix of Closed-loop System
g11=num1(1,7)/den1(7);
g12=num2(1,7)/den2(7);
g21=num1(2,7)/den1(7);
g22=num2(2,7)/den2(7);
g0=[g11 g12;g21 g22];
% and Invert it
invg0=inv(g0)
```

Redest

```
% Reduced Order Observer Feedback Matrix Design
% Assumes 6th Order Plant, 3 Measured States
clear
load nsym2x3
% Compute State Feedback Matrix
[k,s,eigvalsys]=lqry(a,b,c,d,eye(3),eye(2));
k
eigvalsys
% Compute Matrix Partitions
Aaa=a(1:3,1:3);
Aab=a(1:3,4:6);
Aba=a(4:6,1:3);
Abb=a(4:6,4:6);
Ba=b(1:3,:);
Bb=b(4:6,:);
% Specify Observer Poles
p=[-10;-10+10i;-10-10i];
% Compute Observer Gain Matrix
L=(place(Abb',Aab',p))'
% Compute the State Space Description of the
% Reduced Order Observer
Ae=Abb-L*Aab
Be=[Bb-L*Ba Aba-L*Aaa+Abb*L-L*Aab*L]
Ce=eye(3)
De=[zeros(3,2) L]
% Compute the State Space Description of the
% Simplified Reduced Order Observer
Aes=Ae(1,1)
Bes=Be(1,3:5)
Ces=Ce(1,1)
Des=De(1,3:5)
% Compute TFM of the Closed-loop System
af=a-b*k;
[num1,den1]=ss2tf(af,b,c,d,1);
[num2,den2]=ss2tf(af,b,c,d,2);
% Compute DC Gain Matrix for the Closed-loop System
g11=num1(1,7)/den1(7);
g12=num2(1,7)/den2(7);
g21=num1(2,7)/den1(7);
g22=num2(2,7)/den2(7);
g0=[g11 g12;g21 g22];
% and Invert it
invg0=inv(g0)
```

Charloc

```
% M-file to Compute CL's and Closed Loop Eigenvalues
% with HF, MF and LF Compensation

% load data
clear
load c:\matlab\arr\nsymmod
ap=a;bp=b;cp=c;dp=d;
% specify frequency vector
w=logspace(-2,2);

% compute MVFR matrix
f=mv2fr(ap,bp,cp,dp,w);

% get index to freq for action of HF compensator, Kh
index=min(find(w>=30));

% align eigenvectors at this freq
[f30,w30]=fgetf(w,f,index);
kh=align(f30);

% adjust signs of compensator's columns
kh=kh*[1 0;0 -1] % Sign change for stability

% and compute MVFR of HF compensated plant
fh=fmul(w,f,kh);

% Check alignment
misalg=fmisalg(w,fh)
index
wh=w(index)

% examine resulting CL's
clh=feig(w,fh);
clhs=csort(clh);
figure(1)
plotbode(w,clhs)
disp('Press a key.....')
pause

% Define kd for MF facc
% kd=[1/50*(s+1)/(s+10) 0;0 1]
snum=[1 1;1 0];
sden=[50*[1 10];1 0];
% kd=[1/50*(s+1)^2/(s+3)^2 0;0 1]
% This gives tighter performance than the above with the
% nonsymmetrical model but is unstable with the symmetrical
% model and with the actual plant. Stability margin low?
%snum=[1 2 1;0 1 0];
```

```
%sden=[50*[1 6 9];0 1 0];

% Get index to freq at which MF ACC is to act
index=min(find(w>=0.1));

% Design ACC
[am,bm,cm,dm]=facc(w,fh,index,snum,sden);
[Kmnum,Kmden]=mvss2tf(am,bm,cm,dm)
% To reduce order of Km
[am,bm,cm,dm]=minreal(am,bm,cm,dm);
[Kmnum,Kmden]=mvss2tf(am,bm,cm,dm)


% Obtain MVFR of Km
fm=mv2fr(am,bm,cm,dm,w);

% and compute MVFR with HF and MF compensation
fmh=fmulf(w,fh,fm);

% Check alignment
misalg=fmisalg(w,fmh)
index
wm=w(index)

% Examine resulting CLs
clmh=feig(w,fmh);
clmhs=csort(clmh);
figure(2)
plotbode(w,clmhs)
disp('Press a key.....')
pause

% Examine closed loop step response of system so far
[ahp,bhp,chp,dhp]=mvser([],[],[],kh,ap,bp,cp,dp);
[amhp,bmhp,cmhp,dmhp]=mvser(am,bm,cm,dm,ahp,bhp,chp,dhp);
[a,b,c,d]=mvfb(amhp,bmhp,cmhp,dmhp,[],[],[],eye(2));
eigvals=eig(a)
t=[0:.01:25];
figure(3)
mv2stepr
disp('Press a key.....')
pause

% Examine Control Inputs
[ak,bk,ck,dk]=mvser(am,bm,cm,dm,[],[],[],kh);
[a,b,c,d]=feedback(ak,bk,ck,dk,ap,bp,cp,dp,-1);
figure(4);
mv2stepr
disp('Press a key.....')
pause
```

```
% Define Kd for LF facc
% kd=[1 0;0 0.2+0.5/s]
snum=[1 0;.2 0.5];
sden=[1 0;1 0];

% Get index to freq at which ACC is to act
index=min(find(w>=0.01));

% Design ACC
[al,bl,cl,dl]=facc(w,fmh,index,snum,sden);
[Klnum,Klden]=mvss2tf(al,bl,cl,dl)
% To reduce order of Kl
[al,bl,cl,dl]=minreal(al,bl,cl,dl);
% Display Kl
[Klnum,Klden]=mvss2tf(al,bl,cl,dl)

% Obtain MVFR of Kl
fl=mv2fr(al,bl,cl,dl,w);

% and compute MVFR with HF, MF and LF compensation
flmh=fmulf(w,fmh,fl);

% Check alignment
misalg=fmisalg(w,flmh)
index
wl=w(index)

% Examine resulting CLs
cllmh=feig(w,flmh);
cllmhs=csort(cllmh);
figure(5)
plotbode(w,cllmhs)
disp('Press a key.....')
pause

% Examine closed loop step response of complete system
[almhp,blmhp,clmhp,dlmhp]=mvser(al,bl,cl,dl,amhp,bmhp,cmhp,dmhp);
[a,b,c,d]=mvfb(almhp,blmhp,clmhp,dlmhp,[],[],[],eye(2));
eigvals=eig(a)
t=[0:.01:25];
figure(6)
mv2stepr
disp('Press a key.....')
pause

% Examine Control Inputs
[ak,bk,ck,dk]=mvser(al,bl,cl,dl,am,bm,cm,dm);
[ak,bk,ck,dk]=mvser(ak,bk,ck,dk,[],[],[],kh);
[a,b,c,d]=feedback(ak,bk,ck,dk,ap,bp,cp,dp,-1);
```

```
figure(7);
mv2stepr
disp('Press a key.....')
pause

% Compute TFM of Compensator
[num,comden]=mvss2tf(ak,bk,ck,dk)

%Name compensator state mats. for simulink model
acp1=ak
bcp1=bk
ccp1=ck
dcp1=dk
```

Hinfinit

```
% Program to Design Mixed Sensitivity H-Infinity Controller
% For Beam and Carriage

% Define Plant in SS
clear
load nsymmod
ap=a; bp=b; cp=c; dp=d;

% Shift imag. axis left (ie plant poles right) by 0.1
a0=a+0.1*eye(size(a));
% and Make into Tree
ss_g=mksys(a0,b,c,d);

% Define weights on S(s), KS(s) and T(s)
%w1=[0.0004 0.04 1;0.01*[0.25 1 1];0.0001 0.02 1;0.01*[0.0625 0.5 1]];
%w1=[0 10;10 1;0 10;10 1];
w1=[0 10;10 1;0 50;10 1];
%w2=[1;1;1;1];
%w2=[0.1*[0.2 1];0.002 1;0.1*[0.2 1];0.002 1];
w2=[0.05*[0.2 1];0.002 1;0.05*[0.2 1];0.002 1];
%w3=[1 0 0;0 0 4;1 0 0;0 0 16];
w3=[1 0;0 10;1 0;0 10];

% Generate augmented plant in 2-port tree format
tss_p=augtf(ss_g,w1,w2,w3);

% Choose design method
method=menu('Choose Design Method','Standard H-Infinity Control','H-Infinity
Optimal Control');

% Compute 'central' controller (ie. U(s)=0)
if method==1
  [ss_cp,ss_cl,hinfo,tss_k]=hinf(tss_p);
else
  start_row=1; stop_row=6;
  [gamopt,ss_cp,ss_cl]=hinfopt(tss_p,[start_row:stop_row]);
  fprintf('gamopt = %f\n',gamopt)
end

% Return Tzw in SS form ( for cost function)
% NB. This Tzw is for pole-shifted plant and, if 'hinfopt' is
% selected, the weightings specified include gamopt as a factor
[acl,bcl,ccl,dcl]=branch(ss_cl);
[acl,bcl,ccl,dcl]=minreal(acl,bcl,ccl,dcl);

% Calculate Tzw by alternative route to check understanding)
% NB. If hinfopt used, gamopt assumed to multiply all rows of Tzw
if method==2
```

```
  w1(1,:)=gamopt*w1(1,:);
  w1(3,:)=gamopt*w1(3,:);
  w2(1,:)=gamopt*w2(1,:);
  w2(3,:)=gamopt*w2(3,:);
  w3(1,:)=gamopt*w3(1,:);
  w3(3,:)=gamopt*w3(3,:);
  tss_p=augtf(ss_g,w1,w2,w3);
end
[ss_cl1]=lftf(tss_p,ss_cp);
[acl1,bcl1,ccl1,dcl1]=branch(ss_cl1);
[acl1,bcl1,ccl1,dcl1]=minreal(acl1,bcl1,ccl1,dcl1);

% Return Compensator in SS Form
[acp,bcp,ccp,dcp]=branch(ss_cp);

% Shift Imag. Axis of Controller Right (ie poles left) by 0.1
acp=acp-.1*eye(size(acp));

% Reduce order of Compensator
% Model Reduction by Balanced Residualization
[acp1,bcp1,ccp1,g,t]=balreal(acp,bcp,ccp);
g
[acp1,bcp1,ccp1,dcp1]=modred(acp1,bcp1,ccp1,dcp,[4:size(acp,1)])

% Model Reduction by Hankel Norm Optimisation
[acp2,bcp2,ccp2,dcp2]=ohkapp(acp,bcp,ccp,dcp,1,3);;

% Plot step responses using compensator
[af,bf,cf,df]=series(acp,bcp,ccp,dcp,ap,bp,cp,dp);
[af1,bf1,cf1,df1]=series(acp1,bcp1,ccp1,dcp1,ap,bp,cp,dp);
[af2,bf2,cf2,df2]=series(acp2,bcp2,ccp2,dcp2,ap,bp,cp,dp);

% Calculate CLTF of Compensated Plant, Tyr, and Plot Step Response
%[a,b,c,d]=cloop(af,bf,cf,df,-1);
[a,b,c,d]=cloop(af1,bf1,cf1,df1,-1);
%[a,b,c,d]=cloop(af2,bf2,cf2,df2,-1);
t=[0:0.1:10];
figure(1)
mv2stepr
disp('Type any key to Continue')
pause

% Plot Control Inputs for Above, Tur
%[a,b,c,d]=feedback(acp,bcp,ccp,dcp,ap,bp,cp,dp,-1);
[a,b,c,d]=feedback(acp1,bcp1,ccp1,dcp1,ap,bp,cp,dp,-1);
%[a,b,c,d]=feedback(acp2,bcp2,ccp2,dcp2,ap,bp,cp,dp,-1);
figure(2)
mv2stepr
disp('Type any key to Continue')
pause
```